P-07-232

Oskarshamn site investigation

Stress measurements with hydraulic methods in borehole KLX12A

Daniel Ask, Vattenfall Power Consultant AB

Francois Cornet, Christophe Brunet
Institut de Physique du Globe de Paris

Frederic Fontbonne, Geostress Co

December 2007

Svensk Kärnbränslehantering AB
Swedish Nuclear Fuel
and Waste Management Co
Box 250, SE-101 24 Stockholm
Tel +46 8 459 84 00

ISSN 1651-4416
SKB P-07-232

Oskarshamn site investigation

Stress measurements with hydraulic methods in borehole KLX12A

Daniel Ask, Vattenfall Power Consultant AB

Francois Cornet, Christophe Brunet
Institut de Physique du Globe de Paris

Frederic Fontbonne, Geostress Co

December 2007

Keywords: AP PS 400-06-067, MKW wireline unit, Mosnier tool, Straddle packer system, Cluster approach, Stress determination, Hydraulic fracturing (HF-tests), Hydraulic tests on pre-existing fractures (HTPF-tests), En echelon fractures, Boremap, Injection tests, Re-opening tests, Hydraulic jacking, Normal stress, Horizontal and vertical stresses.

Summary

Hydraulic rock stress measurements were performed in borehole KLX12A at the Oskarshamn candidate area, Sweden. The measurements were carried out in two separate campaigns and a total of 17 hydraulic fracturing tests and hydraulic tests on pre-existing fractures were conducted between the 20th of July to the 11th of August, 2006.

The work involved cooperation between Vattenfall Power Consultant AB (Contractor), Institut de Physique du Globe de Paris (IPGP), and Geostress Co (both Sub-contractors). Vattenfall Power Consultant AB provided an MKW wireline system and field personnel, whereas IPGP supplied downhole equipment, data acquisition system, and field personnel. Finally, Geostress contributed with field personnel.

This report presents scope, objectives and performance of the stress measurements in borehole KLX12A. Further, a description is given of the employed test equipment, quality assurance, testing methodology (the so called cluster approach /Ask and Cornet 2006, 2007/), and results of stress interpretation at the Oskarshamn site. A more detailed account for instrument calibration, data collection, experiences of and observations made during the field work is outlined in Appendix I.

The results of the stress calculations indicate a non-linear stress distribution along the borehole. Yet, the state of stress could be resolved satisfactory using the cluster approach /Ask and Cornet 2006, 2007/ at the depth of a planned future repository of nuclear waste. The best solutions at 400–440 and 490–540 m vertical depth (mvd) are as follows:

400–440 mvd	**490–540 mvd**
σ_h = 12.6 ± 1.4 MPa	σ_h = 15.1 ± 0.2 MPa
σ_H = 17.4 ± 2.8 MPa	σ_H less than 30 MPa assuming tensile strength of 5 MPa and neglect of pore pressure
σ_v = 11.0 MPa	σ_v = 13.4 MPa
Orientation of σ_H = 132 ± 4°N	Orientation of σ_H = 161 ± 5°N

Sammanfattning

Hydrauliska bergspänningsmätningar har utförts i borrhål KLX12A i Oskarshamn. Totalt gjordes 17 hydrauliska bergspänningsmätningar i två separata kampanjer mellan den 20:e juli och den 11:e augusti, 2006.

Aktiviteten var ett samarbetsprojekt mellan Vattenfall Power Consultant AB (huvudkonsult), Institute de Physique du Globe de Paris (IPGP), och Geostress Co (båda dessa organisationer underkonsulter). Vattenfall Power Consultant AB tillhandahöll ett MKW wireline-system samt fältpersonal, IPGP stod för borrhålsutrustning, datainsamlingssystem och fältpersonal, medan Geostress bidrog med fältpersonal.

Denna rapport presenterar syfte, omfattning och utförande av bergspänningsmätningarna i borrhål KLX12A. Vidare beskrivs utrustning, kvalitetssäkringsaspekter, testmetodik (den s k klustermetoden /Ask och Cornet 2006, 2007/) samt tolkningen av bergspänningarna i Oskarshamn. I bilaga I ges en mer detaljerad redogörelse för exempelvis instrumentkalibrering, datainsamling samt allmänna erfarenheter av och observationer gjorda under fältarbetet.

Denna rapport beskriver utrustningen, kvalitetssäkring av data, testmetodik (dvs klustermetoden) och resultat av spänningstolkning i borrhål KLX12A. En mer ingående beskrivning av fältresultat och observationer återfinns i Appendix I.

Resultaten från spänningsberäkningarna visar att spänningarna är olinjära längs borrhålet. Trots detta kunde spänningssituationen kring planerat förvarsdjup bestämmas med hjälp av klustermetodiken. De bästa lösningarna vid intervallen 400–440 respektive 490–540 m vertikalt djup (mvd) är enligt följande:

400–440 mvd	**490–540 mvd**
σ_h = 12,6 ± 1,4 MPa	σ_h = 15,1 ± 0,2 MPa
σ_H = 17,4 ± 2,8 MPa	σ_H mindre än 30 MPa baserat på en antagen draghållfasthet om 5 MPa och försumbar portryckseffekt
σ_v = 11,0 MPa	σ_v = 13,4 MPa
Orientering av σ_H = 132 ± 4°N	Orientering av σ_H = 161 ± 5°N

Contents

1 Introduction

This report describes the objectives, scope, and performance of hydraulic stress measurements in borehole KLX12A at the Oskarshamn candidate site, Sweden. The hydraulic tests involved Hydraulic Fracturing (HF) and Hydraulic Tests on Pre-existing Fractures (HTPF). The measurements are a part of the activities within the investigation program at the Oskarshamn site. The work was carried out in compliance with the Activity Plan AP PS 400-06-067.

The investigated borehole is located within the Oskarshamn candidate area and is visualized in Figure 1-1.

Controlling documents for performance of the activities are listed in Table 1-1. Both Activity Plans and Method Descriptions are SKB's internal controlling documents. To this should be added extensive internal quality operational procedures of Vattenfall Power Consultant AB, including a general Manual for testing and Quality Operating Procedures, seven Checklists, four Quality Assurance Report forms, and an object specific Quality plan.

Figure 1-1. *Location of core hole KLX12A within the Laxemar area, as of April, 2006.*

Table 1-1. Controlling documents for performance of the activities.

Activity Plan	Number	Version
Rock stress measurements with hydraulic fracturing (HF) and hydraulic testing of pre-existing fractures (HTPF) in borehole KLX12A	AP PS 400-06-067	1.0
Rock stress measurements with hydraulic methods	SKB MD 182.003e	2.0
Instructions for cleaning borehole equipment and certain surface equipment	SKB MD 600.004e	1.0

Borehole KLX12A extends to 602.29 mbl (metres borehole length) and is at ground surface directed 315.92° (clock-wise from North) and has a dip of 75.07° from the horizontal. The inclination entails that the total vertical depth reached is about 555.92 mvd (metres vertical depth). The numbers of different tests performed in borehole KLX12A is presented in Table 1-2.

The work involved cooperation between Vattenfall Power Consultant AB (Contractor), Institut de Physique du Globe de Paris (IPGP), and Geostress Co (both sub-contractors). Vattenfall Power Consultant AB provided an MKW wireline system and field personnel, IPGP supplied downhole equipment, data acquisition system, and field personnel, and finally, Geostress contributed with field personnel.

The methodology of testing and analysis, which is based on the ISRM suggested methods for rock stress estimation by hydraulic fracturing and hydraulic tests on pre-existing fractures /Haimson and Cornet 2003/, is outlined in Chapter 5.

Table 1-2. Tests conducted in borehole KLX12A.

Test no. [–]	Bh length [m]	Vert. depth [m]	Test type
1	590.1	547.0	HTPF
2	579.4	536.0	HF
3	574.2	531.0	HTPF
4	572.0	529.0	HF
5	564.4	522.0	HF
6	536.0	496.0	HTPF
7	532.0	491.0	HTPF
8	529.6	488.0	HTPF
9	491.2	453.0	HF
10	484.6	446.0	HF
11	481.4	443.0	HTPF
12	472.9	436.0	HF
13	470.0	433.0	HTPF
14	451.0	414.0	HTPF
15	438.1	402.5	HTPF
16	236.7	210.0	HF (failed)
17	222.2	196.0	HF

2 Scope, objectives, and structure of presentation

Large scale stress determination measurements using hydraulic stress measurement techniques have been undertaken during the summer and autumn of year 2006 for the Oskarshamn (Laxemar) candidate site (one borehole) and another campaign at the Forsmark candidate site (5 boreholes on three different drill sites). This report presents scope, objectives and performance of the stress measurements in borehole KLX12A at the Oskarshamn site. Further, a description is given of the employed test equipment, quality assurance, testing methodology (the so called cluster approach /Ask and Cornet 2006, 2007/), and results of stress interpretation at the Oskarshamn site. A more detailed account for instrument calibration, data collection, experiences of and observations made during the field work is outlined in Appendix I.

The hydraulic rock stress measurements in borehole KLX12A were conducted in two separate campaigns between the 20th and 26th of July and between the 7th and the 11th of August. In total, 17 hydraulic fracturing tests and hydraulic tests on pre-existing fractures were performed.

The objectives of the hydraulic stress measurements at drill site 12 were to (i) decrease uncertainty in data on in situ state of stress, (ii) increase the understanding of how local geological site conditions may affect the state of stress, and (iii) provide input for site descriptive modelling on the state of stress at the site.

The borehole specific objectives involved:

- Identify what types of fractures that seem feasible for HTPF.
- Identify possible decoupling zones along the borehole.
- Determine the state of stress at the borehole location, from 100 m depth and down to the well bottom.

The results of the stress determination involve presentation in clusters. The presentation of results is restricted to the work done and the raw data results obtained. No attempts are made to put the data into a geological/tectonic context nor to discuss similarities/deviations observed with other types of stress data.

3 Description of the testing equipment

3.1 Overwiew of equipment components

The surface equipment is based on an upgraded MKW (MessKabelWinde) wireline unit of Vattenfall Power Consultant AB, with which the downhole tool is moved within the borehole on a seven conductor geophysical logging cable and a winch system (Figure 3-1). The downhole tool involves a combined straddle packer and HTPF electrical imaging tool of Institut de Physique du Globe de Paris (IPGP).

The suggested wireline system, together with the HTPF tool of IPGP for fracture orientation and characterization, optimizes the testing performance. A schematic view of the system is given in Figure 3-2.

3.2 Pump equipment

The high-pressure water pump is a three-plunger Hermetic (type AH30) with a maximum pressure of 100 MPa. The pump delivers 17 l/min at a pressure of 75 MPa. The pump is remotely controlled by revolutions per minute, which enables a very large interval of flows at high pressures that are required for reliable quasi-static re-opening and hydraulic jacking (step-pressure) tests.

Figure 3-1. *Photo of the upgraded MKW wireline unit of Vattenfall Power Consultant AB during operation in borehole KLX12A.*

3.3 Wireline system/tube system

The wireline system (Figure 3-1) is driven by a Hatz diesel engine (type 3 L30S), which through the Mannesmann-Rexroth hydraulic pump system (type HS-17-G 905-3-0) drives the high-pressure water pump (see above) and the winch (upgraded to MKW-1500).

The logging cable is a seven-conductor Rochester 3/8" (type 7-H-375A) with a breaking strength of 5.8 tons.

The coiled tubings, one for the straddle packer (OD 1/4", service pressure 100 MPa) and one for the test section (OD 3/8", service pressure 50 MPa), are made of seamless stainless steel. Although not determined at the time of this report, the suggested system is known to have a high stiffness (compressibility of the order 10^{-11} m^3/Pa).

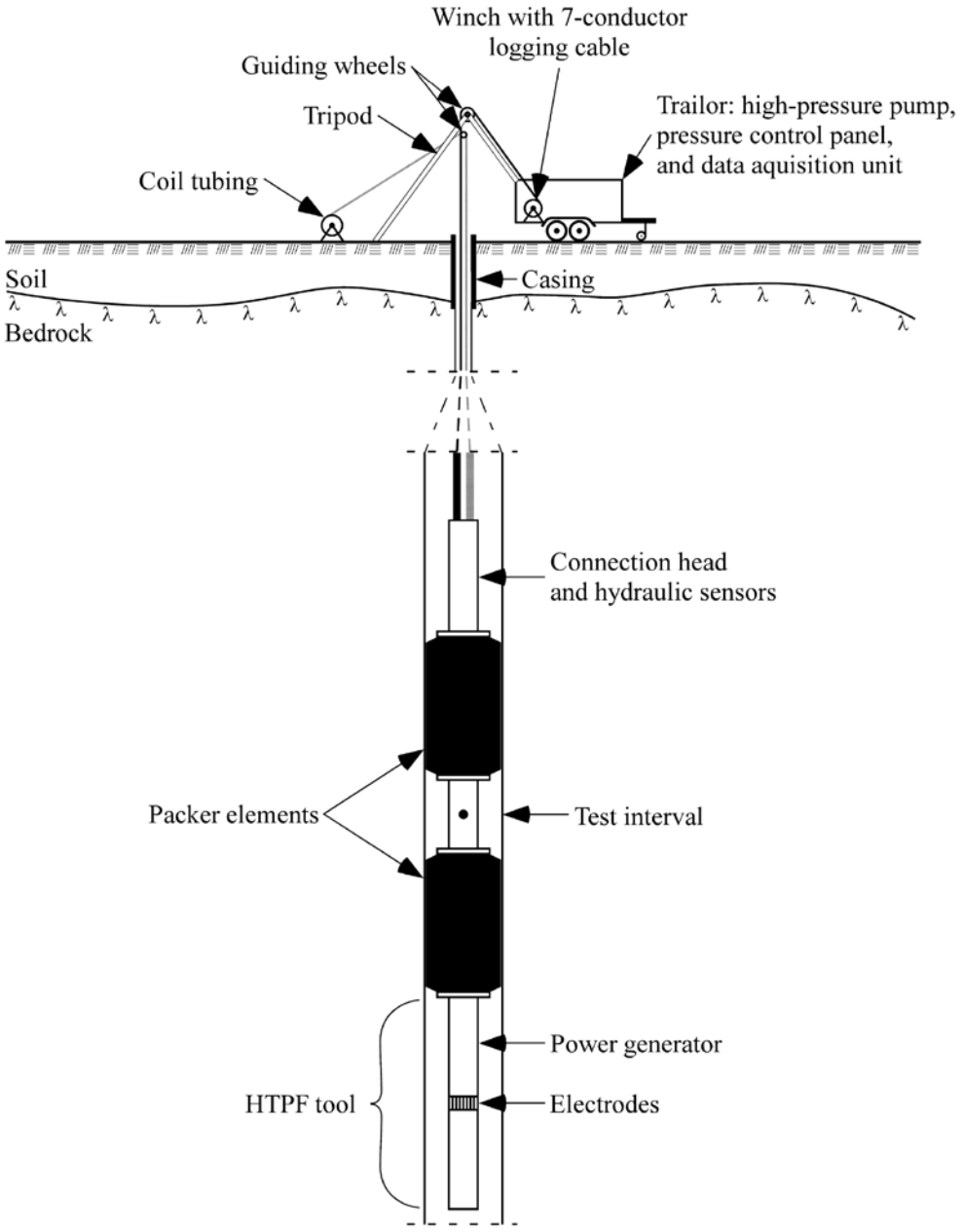

Figure 3-2. *Schematic overview of the wireline equipment with straddle packer and HTPF tool.*

3.4 Packer system

The straddle packer is equipped with steel-reinforced packer elements (TAM, OD = 67 mm; Figure 3-3). The sealing length is about 1 m, the length of the test section about 1.0 m in a 76 mm borehole, and the maximum service differential pressure is 33 MPa (burst pressure close to 50 MPa).

Figure 3-3. *The straddled packer system showing its large deformability implying that it may operate in wells with very variable diameters.*

Figure 3-4. *The straddle packer and the HTPF tool. The top of the downhole assembly is shown in the lower, left corner and terminates with the upper packer element. The second and third parts include the lower packer element and a weight used in inclined boreholes (mounted below the HTPF tool), respectively. The fourth part is the HTPF tool where the thicker central part contains the electrodes.*

3.5 Equipment used to determine and document position in the borehole and orientation of fractures

The fracture orientation data are collected using the HTPF tool /Mosnier and Cornet 1989/, which combines the possibility of running tests through a wireline activated straddle packer with that of obtaining electrical images of the fractures intersecting the borehole (Figure 3-4). The electrical imaging technique has been adopted from Mosnier's azimuthal laterolog /Mosnier 1982/. During measurement, an alternating electric voltage is applied between a distant electrode (the armour of the logging cable) and a number of electrodes set in various azimuths on a ring placed at the centre of the tool. The electric current emitted (or received) by each of the electrodes on the central ring is proportional to the conductance of that part of the borehole wall facing the electrode. Focusing electrodes located on both sides of the electrode ring ensure that electric current lines are normal to the borehole wall. The results can be displayed either as polar diagrams or graphically as horizontal bands made by juxtaposed squares (one square per electrode). Because the intersection of a plane with a cylinder is an ellipse, planar fractures are easily detected by their sinusoidal shape. As the tool orientation is known, with the aid of two tilt meters (accuracy of 0.5°) and 3 magnetometers (accuracy of 3° to 4°) inside the tool, both dip and strike of the fractures can be determined /Cornet 1993/. As the tool is run at least twice over a test section, the repeatability can be used to determine the fracture orientation within half a degree for dip and 5 degrees for azimuth. Because the intensity of the injected electrical current can be adapted, it is possible either to highlight very tiny fractures, or to work on very conductive fractures. This provides a dynamic view that is not accessible to direct core examination as shown on Figure 3-5 below.

A very strong benefit of the HTPF tool is the ability to make differential plots of the test section before and after the injection test, which clearly demonstrates which fracture has been stimulated. However, the methodology was not necessary in borehole KLX12A.

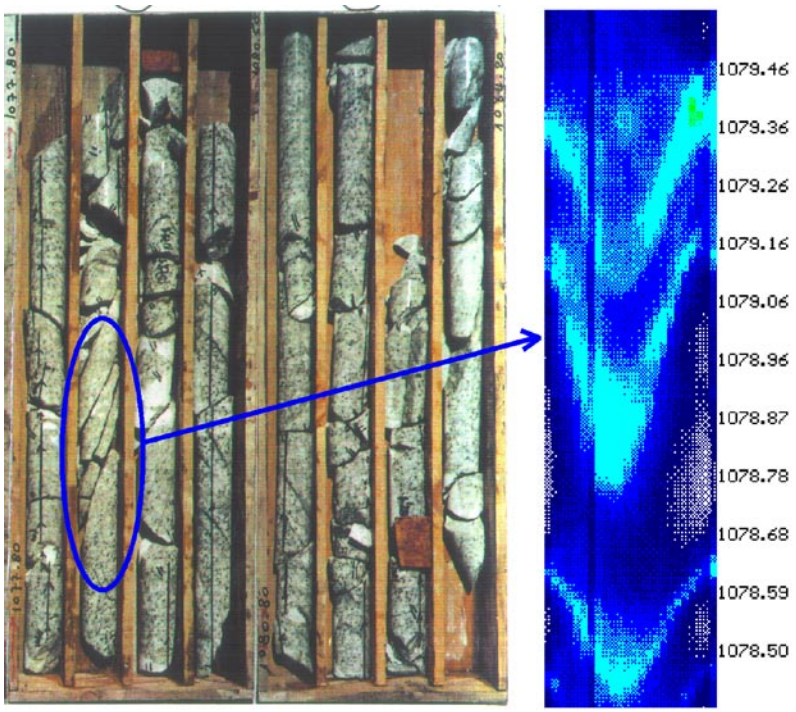

Figure 3-5. *Comparison between cores and fractures. Cores appear very broken while electrical images show that the fractures are in fact quite tight in situ. The tightness of fractures is established during permeability tests.*

3.6 Data recording

The data were collected using a data acquisition system (PC and DQPad6020E, 16-channels, 12 bit resolution) that integrates simultaneously the surface data (injection flow rate, injection pressure, depth of test as provided by depth reader of logging cable) and downhole data (electrical images, downhole pressure for both interval and packers, plus tool orientation). Furthermore, a backup system was also brought to the field (PC and 2 Intab PC-loggers 3150, 8-channels, 12 bit resolution). This provided an excellent redundancy that ensured retrieving data.

Packer and interval pressures were monitored at ground surface by pressure gauges (EFE pressure transducers, type P925R, 0–40 MPa, precision 0.03%) and downhole (EFE, type P922A, 0–50 MPa). The flow was measured at surface with a high precision mass flow meter (Micro Motion Rosemount D12 with max 5 l/m, 39 MPa, and precision 0.004 g/cc).

4 Quality assurance and equipment calibrations

4.1 General

To ensure that data are collected with an optimum quality, a number of quality assurance measures are undertaken prior to, during, and after field work (Figure 4-1).

Prior to departure for the field, all system components are systematically tested for functionality and key components for data collection are calibrated (Table 4-1). Once all components have been approved, all equipment is carefully packed according to pre-established packing lists.

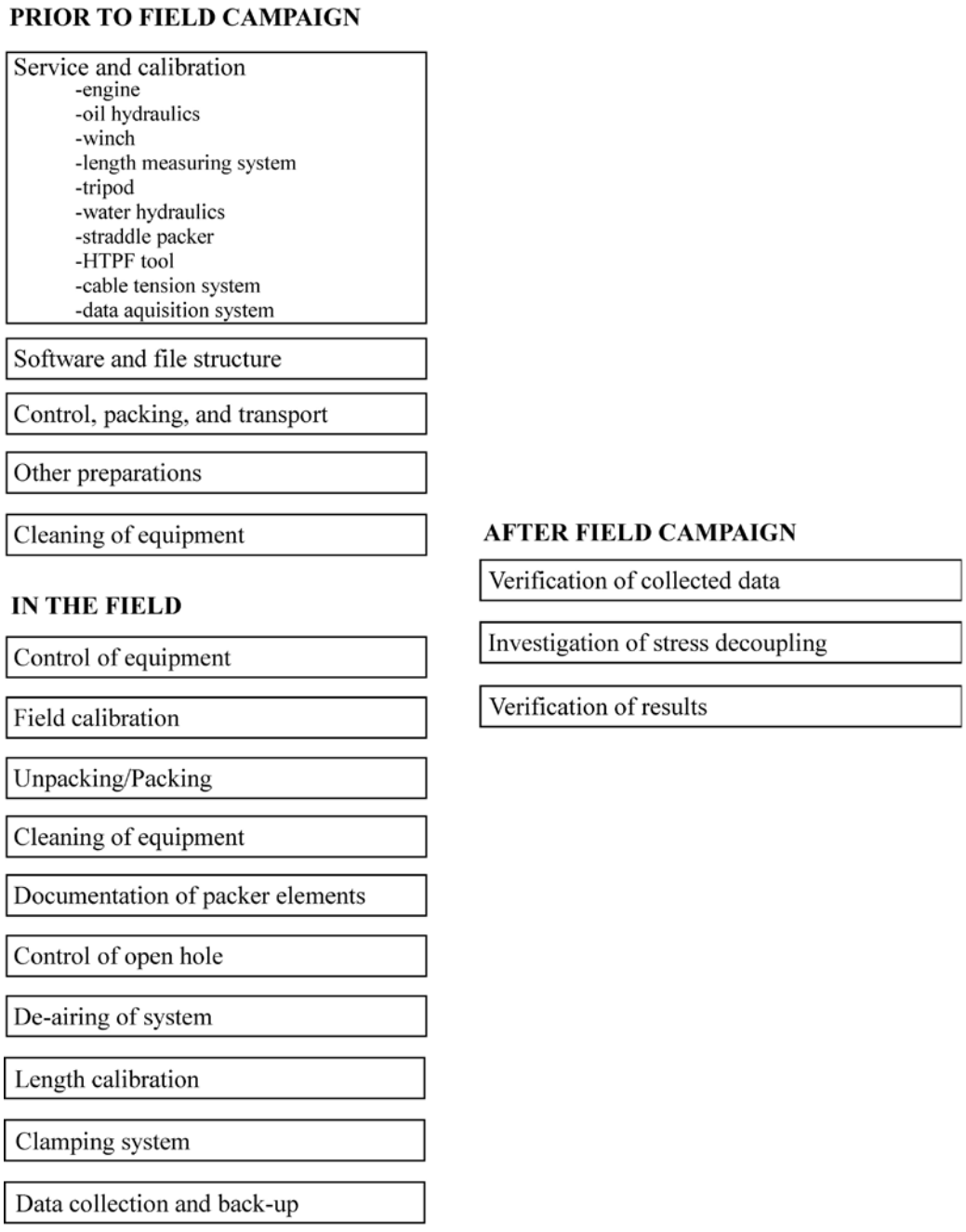

Figure 4-1. *Schematic overview of quality assurance procedures during hydraulic stress measurements.*

Table 4-1. Calibration list of key components.

Calibration item	Prior to field campaign	During field campaign	After field campaign
Downhole pressure gauge	Yes	Optional	Yes
Surface pressure gauges	Yes	Optional	–
Flow meter	Yes	Optional	–
Tilt meters	Yes	Yes	Yes
Magnetometers	Yes	Yes	Yes
Length system	–	Yes	–
Cable tension system	Yes	Yes	–

In the field, the functionality and the packing is once again verified. Field calibrations of pressure and flow gauges are also undertaken at drill site 12.

After field work, the functionality of key components is once again verified. The most important steps of the quality assurance procedures are outlined below. A more detailed description can be found in /Ask 2006a/ and /Ask 2006b/.

4.2 Calibration of equipment

4.2.1 Overall quality of data recording

There are a few independent means to verify that the overall data recording has been successful. This involves readings of orientation devices and of downhole pressures as the tool is lowered and hoisted in the borehole.

The values of the magnetic field inclination, as determined from magnetometers, offer a completely independent check on the digitization procedure used for the downhole data acquisition and surface data recording. The quality procedure has identified a 50 Hz electrical noise affecting the downhole sensors as a result of ground currents (we measured 14 Volts and 50 Hz at ground surface). Interestingly, the noise is smaller during the second campaign, during which two nuclear reactors were shut down.

The electrical noise is a site specific phenomenon which has never been observed in any of our previous field campaigns, except at the Forsmark site, where similar problems were encountered. The noise (ground currents) results in a digitization problem close to the surface, causing the timer that samples the data to be slightly off phase, and a small error is introduced. This noise affects all downhole sensors. This implied that, for tests above 250 m, collected data were given special attention.

The results from the magnetometers and inclinometers may also be used to verify reproducibility. This involves comparisons of derived fracture orientations with those of the BIPS, but more importantly, we compare our determination of magnetic field inclination (angle with vertical) with that of the Uppsala magnetic field observatory (Appendix I). For borehole KLX12A, we are always within 2° below 100 mbl with the Uppsala observatory results. Above this depth, noise is disturbing all downhole sensors.

The reproducibility of well orientation (comparison between pre- and post-logs) is always better than 2° for dip and azimuth and the average difference between the Maxibor results are 3.6°. Note, however, that the well orientation of the HTPF tool refers to the magnetic North, whereas the Maxibor refers to the geographical North. Thus, we have established that our orientation determination for the tool is reliable and reproducible and well within expected errors.

The other independent control of successful data recording is correlated with the observed variations in downhole pressure during lowering and hoisting in the borehole. These variations, which were investigated after completed field campaign, can be compared with the theoretical weight of the water column in the borehole and indicate that no discrepancies were found during measurements in borehole KLX12A.

4.2.2 Pressure transducers, flow meter, tilt meters, and magnetometers

For the measurements in borehole KLX12A, the pressure transducers are calibrated against a reference load cell and the flow meters by volume (mass) determination per time unit prior to field measurements. The results from the calibrations are given in Appendix I, which include the following items:

- Calibration of downhole pressure transducer in the test section (five calibrations).
- Calibration of pressure transducer in the packers.
- Calibration of surface transducers.
- Calibration of flow meter.
- Calibration of orientation devices. These components were checked for functionality and calibrated several times during the campaign: prior to departure to the field, before entering each borehole, and after completed measurements. Moreover, after the field campaign, the electrical imaging logs are used to provide independent data on dip and azimuth of the well (see Chapter 4.2.1 above).

The orientation devices were checked for functionality and calibrated during the campaign. Moreover, after the field campaign, the electrical imaging logs were used to provide independent data on dip and azimuth of the well (Appendix I).

4.2.3 Length measurement

For the sake of stress determination, the knowledge of absolute depth to within a few metres is quite sufficient. But because the objective is to relate images of features on the HTPF logs with those observed on cores, an adjustment to some decimetres is necessary.

During the measurements in KLX12A, the reference marks could not be detected with the HTPF tool. Instead, the length was calibrated using detailed comparisons with images, cores, and the BIPS for unique features at three locations, of which the two deepest located involved detailed mapping of fractures for about 15–20 m. Once identified, by interpolation, an equivalence is proposed between HTPF logs and BIPS/Boremap depths for the complete borehole length. Thereafter, each pre-existing fracture tested was correlated with the equivalent fracture observed on the cores. In addition, the tested fracture was photo documented in the core boxes. This comparison entails that the length calibration between the two systems is within 3 dm for KLX12A.

The results of the length calibration yielded the following approximation:

BIPS mbl = 1.000 · electrical imaging depths –1 (± 0.2) mbl.

4.2.4 Cable tension measurement

The cable tension (or weight) measuring device, which is a safety measure to prevent pulling off the geophysical cable by mistake if stuck in the borehole, has an accuracy of 10 kg and its functionality was tested prior to departure and in the field by attaching a weight.

4.2.5 Fracture orientation methods

In principle, the fracture orientations (here expressed as the normal to the fracture plane) can in this specific assignment be determined with three different methods:

- Based on magnetometers and inclinometers of the HTPF tool
- Based on SKB's deviation measurements of the well (the optical Maxibor method or the magnetic Flexit method) together with tool face (inclinometers) of the HTPF tool
- Based on SKB's Boremap system (Maxibor or Flexit deviation measurements) and tool face of the BIPS tool.

In the result files (Appendix I), the results using method 2 are displayed (based on the Maxibor method). The reason for this choice of method is primarily twofold: (i) the well deviation data from SKB were judged more reliable than those of the magnetometers of the Mosnier tool; (ii) the Boremap system cannot be used for induced fractures and at the time of this report, the Boremap system was not proven to yield more reliable results than that of method 2. In addition, it is not recommended to use different systems for fracture orientation determinations as the different methods likely yield different uncertainties in the fracture orientation. If employed, this would introduce a weighting factor in the data during stress inversion, i.e. induced fractures are given higher or lower weight during inversion as compared with pre-existing fractures.

Regrettably, after this study was commenced, a decision was taken to update SKB's well deviation measurements, entailing that for many boreholes Maxibor measurement would be exchanged to Flexit measurements as the official deviation measurement files in SKB's database Sicada. This update affects the fracture orientations of both the HTPF tool and in Boremap as they are based on deviation data. As a result of this, a study was initiated attempting to quantify the corresponding error for the HTPF tool. The result is presented in Appendix I and indicates that the error is very small and, in practice, negligible for the sake of stress determination. Note that in Appendix I, the Boremap orientations based on the new Flexit well deviation data are presented, whereas the orientations of the HTPF tool is based on Maxibor.

4.3 Verification of indata for stress calculation

4.3.1 Fracture orientations

The reliability of the fracture orientation determination rests on three features:

- The proper recording of all parameters that characterize the position of the tool in the well (borehole length, and azimuth and dip values from 3 magnetometers, and 2 inclinometers).
- The good understanding of tool manufacturing and its consistency with data processing routines.
- The repeatability of orientations during comparisons of multiple scans of the same fracture.

The reliability of orienting sensors (inclinometers and magnetometers) is provided by the repeatability of observations. Further comparison with independent data provides evaluation of accuracy of tool orientation (see Chapter 4.2.1).

Note that all orientations represent the normal to the fracture plane, positive downwards, and are given with respect to geographic North according to coordinate system RT90 2.5 gon W 0: –15 for x and y and RHB70 for z, using a right-hand rule notation.

Unambiguous fracture orientation data involve proper recording of tool positioning, repeatability of different logs, and clearly visible fracture traces.

4.3.2 Normal stresses

The normal stress determination is based on shut-in pressure determinations, because /Cornet et al. 2003/ observed that the normal stress may be overestimated during the opening phase of a hydraulic jacking test. The normal stress is determined using two methods suggested by ISRM /Haimson and Cornet 2003/ and involves only cycles where the injected volume is in the range of 2 to 5 litres into the formation.

Quasi-static reopening pressure tests have been conducted, but their primary purpose is to minimize chances of creating new fractures as well as of rotations of the fracture planes. The value of the reopening pressure is also an interesting source of "qualitative" information. When it is equal to the shut-in pressure value, it suggests that the fracture is sub-parallel to the borehole axis. This is later verified by the fracture imaging. In this case the quasi-static reopening measurement provides a useful complementary measurement of the normal stress. However, in many an instance, this quasi-static reopening pressure has been found significantly larger than the shut-in pressure. When this occurs, it suggests that the fracture is inclined with respect to the borehole axis. This is later verified by the post-frac image. Accuracy of the pressure transducers is provided both by initial and field calibrations and by the pressure recorded in the well, when packers are deflated.

Specific to the Oskarshamn site (as for the Forsmark site), two additional quality assurance features have been introduced. The first one refers to the influence of fractures generated by the packers, at the interface between the packers and the pressurized interval. During some tests (also occurring at the Forsmark site), these fractures remain opened by the packer, when pressure drops in the interval and prevents proper shut-in measurements. The other quality assurance aspect considered was related to fluid percolating to the borehole, below the straddle packer. This results in a progressive increase in the shut-in pressure that is not linked to the fracture extension but to the change in stress close to the well, through the coupling imposed by the packers. Significance of "back-up pressure" can be evaluated from cable tension variations recorded during testing.

Note that normal stresses are denoted using a geomechanical sign convention with compressive stresses taken as positive.

Unambiguous normal stress data involve repeatable and clearly defined shut-in values from tests involving 2 to 5 litres of injected water volume and that show a pronounced flow-back after completed testing.

5 Methodology for data collection in borehole KLX12A

5.1 General line of work

The general line of work in borehole KLX12A involved the following steps:

1. Mobilization
2. Verification of open hole, i.e. logging with dummy
3. Reconnaissance log of entire borehole
4. Length calibration
5. Selection of suitable test sections
6. Injection testing
7. Post-logging of test section
8. Demobilization

In this chapter, the most important steps, items 3 and 6, of the work are outlined.

5.2 Reconnaissance log and selection of suitable test sections

Because the notion of rock stress is a concept of continuum mechanics, it is necessary to identify volumes where the continuity hypothesis is verified. In other words, bodies that may be approximated by a continuum need to be identified. Moreover, because the stress at a specific point involves six components, the determination of the regional stress field includes determination of six functions for the domain under consideration. This requires integrating measurements conducted at points that sample properly the continuum volume of interest.

The first interpretation of the continuity hypothesis is given by the reconnaissance log with the HTPF tool (Appendix I). During the reconnaissance log, the intensity of the injected electrical current is adjusted to highlight very tiny fractures (which are suitable for hydraulic injection testing), which means that very conductive fractures, i.e. potential stress decoupling zones, are clearly outlined by a significant change of resistivity. The first evaluation provided by the HTPF tool is used for selection of suitable test sections. In Appendix I, each test section is marked on the length calibrated reconnaissance log.

Given the non-linear and scattered stress profiles derived from previous overcoring stress data in the region, application of a standard profiling approach would be hampered by the non-linearity. Instead, the methodology chosen for the tests in borehole KLX12A involved the cluster approach /e.g. Ask and Cornet 2006, 2007/. This implies that measurements are grouped in clusters with the aim of determination of the full stress tensor. The objective of each individual cluster is to collect sufficient HF and HTPF data in a small enough volume to permit complete stress determination without considering stress gradients. This results in a minimum of parameters at each cluster but also has the benefit of that the continuity hypothesis may be more easily evaluated by comparisons of full tensors from multiple clusters along a borehole. The adopted methodology thus includes three steps:

- Identification of domains where the continuity hypothesis is validated preliminary.
- Combination of HF and HTPF measurements in a clustered procedure so that each cluster corresponds to a small enough volume to permit complete stress determination without considering stress gradients. These clusters were, when possible, located at the very depth of existing overcoring measurements.

- Integration of results from all clusters so as to establish the validity of the continuity hypothesis and determine the complete stress field within the domain of interest with proper attention to decoupling zones.

It is important to identify the depth where the stress determination is desired: one objective has therefore been to focus on placing clusters at planned repository depth at the Oskarshamn site.

5.3 Injection testing

5.3.1 General

The applied injection tests were a combination of hydraulic fracturing (HF) and hydraulic testing on pre-existing fractures (HTPF), which are described below. We emphasize that the execution and interpretation of the two methods are consistent with the ISRM recommendations /Haimson and Cornet 2003/.

In wells that are inclined with respect to a principal stress direction, hydraulic fracturing will not yield axial fractures, but fractures of en echelon type. /Peska and Zoback 1995/ have shown that such tests are very useful for constraining the maximum horizontal principal stress magnitude.

HTPF measurements are commonly used to constrain the magnitude of primarily σ_H but also σ_v, once σ_h has been solved with hydraulic fracturing technique. However, because of the limitations in the HF technique in inclined wells, the cluster approach will depend very much on the success rate of the HTPF technique.

5.3.2 Hydraulic fracturing (HF) tests

The overall purpose of the hydraulic fracturing test, in case of a vertical borehole aligned with a principal stress direction, is to determine the horizontal stress magnitudes and orientations. However, in thrust regimes, the fracture plane rotates during propagation, giving an estimate of the vertical stress component. If the minimum horizontal stress can be determined by other means, the HF test provides an estimate of the maximum horizontal stress based on the breakdown pressure, rock tensile strength, and a hypothesis of the pore pressure effect.

We have adopted the following scheme to conduct HF tests:

- Permeability test involving a rapid pressurization of the test section up to between 1–3 MPa and subsequent monitoring of the pressure decay for about 5 to 10 minutes. Release of test section pressure.
- Rapid pressurization of the test section so that peak pressure is obtained in 1–3 min. When breakdown is reached, the pumping is stopped and the pressure decline is monitored. About 5 minutes after fracture closure (shut-in), the test section is vented. In the beginning of the venting, the test interval is closed back and the rise in pressure is monitored. When the initial permeability test has shown that the rock is fairly impervious, this action provides a means to verify that the fluid pressure has been injected into the rock mass and that no significant by-passing to the borehole has occurred.
- Standard quasi static slow re-opening test (hydraulic jacking/step-rate pressure test) with about 5 pressure steps, starting way below the previous shut-in reading and going up in 2 MPa steps, until the fracture is clearly open. This is followed by a standard shut-in test. We consequently have not adopted fast flow rate re-opening tests for evaluating the maximum horizontal principal stress magnitude, because it is difficult to ascertain that the pore pressure has reached its original value and because theories based on the re-opening pressure are associated with great uncertainties /e.g. Ratigan 1992, Ito et al. 1999, Rutqvist et al. 2000/.

- Hydraulic jacking followed by shut-in until repeatable normal stresses are produced.
- If the normal stresses are not self consistent (repeatable), a cyclic jacking /e.g. Rutqvist 1995/ and thereafter a rapid re-opening followed by shut-in is conducted (not necessary in borehole KLX12A).

Some estimate of the maximum horizontal stress may be retrieved from the breakdown pressure reading when the rock tensile strength has been determined with some confidence.

5.3.3 Hydraulic tests on pre-existing fractures (HTPF)

Generally, HTPF measurements are used to constrain the magnitude of primarily σ_H, but also σ_v, once σ_h has been solved with hydraulic fracturing technique. The HTPF tests aim at opening and stimulating pre-existing planes of weakness with, preferably, a large range of fracture directions and inclinations /Cornet 1993/.

We have adopted the same testing procedure as for the HF tests, but with one major difference: the flow rate during the opening phase should be chosen much smaller to enhance the possibility of re-opening as the fluid has time to penetrate the fracture plane and add an additional stress component.

For the HTPF technique, the choice of suitable fractures for HTPF testing is crucial. Generally, for this type of test, isolated fractures are sought, implying that the nearest neighbouring fracture should be at least 1 m above or below the tested fracture. Moreover, individual tests should be separated by c 2 m to avoid the local stress change caused by the neighbouring test as a result of the mechanical opening of a fracture. The chosen fractures for HTPF testing should also be distributed with a large variety of dip and dip directions for a reliable resolution of all stress components during stress inversion. The objective is to take advantage of optimally oriented pre-existing fractures, even if they are in a very limited quantity. If more directions are available, the resolution of proposed methodology will be improved. Preferably, the chosen fractures should be at least partially opened or coated with weak fracture minerals, which, using a low flow rate test, enhances the possibility for re-opening as the fluid has time to penetrate the fracture plane and add an additional stress component. In this respect, the HTPF tool has great benefits, as it directly outlines the fractures suitable for testing. What remain to ascertain is that the fractures are isolated and that the full stress tensor can be solved in each cluster.

With the HTPF method, the stress tensor is evaluated so as to fit best all measured data according to a misfit function that characterizes the quality of the fit. The misfit function is a non-dimensional feature that describes the discrepancy between observed and computed values as determined with a calculated stress model. The misfit must include errors associated with all measured parameters, i.e. errors in both normal stress and in fracture orientation. The solution is defined as the stress model that minimizes the misfit function, i.e. the model that is closest to all the measurements.

If HTPF tests are close enough to HF tests, integration of HF and HTPF data is conducted on the hypothesis of a uniform stress field.

When tests have been run at large distances from one another, the solution requires a parameterization of the stress field in the rock mass. The choice of parameterization for stress calculation depends on the number of measurement points and the range of orientations of the tested fractures. A commonly applied parameterization of the stress field involves the assumption of linear stress variation along the borehole axis, i.e. the stress at point X_m is expressed as a linear function of the stress at point X_o with a stress gradient, α, along the borehole axis according to:

$$\sigma(X_m) = \sigma(X_O) + (X_m - X_O) \cdot \alpha \qquad 5\text{-}1$$

In its general form, it involves 12 model parameters and requires a minimum of 14–15 tests for its solution (because measurements are never exact and always involve some uncertainty, it is always desirable to conduct more tests than there are unknown model parameters). It is to be noted here that if the borehole is inclined to a principal stress direction by more than 15 to 20°, en echelon fractures result from HF tests. /Peska and Zoback 1995/ have shown that such tests are very useful for constraining the maximum horizontal principal stress magnitude. In /Ask et al. 2007/, a similar but new approach for packer induced fractures is presented.

When the borehole is vertical and there are no lateral stress variations, the vertical stress remains principal at all depths and the system involves only 10 unknown model parameters /Haimson and Cornet 2003/ (the theory is outlined in more detail in Chapter 6.2). HF tests, in vertical wells, provide directly six parameters: principle directions and their variation with depth and the minimum horizontal stress component and its gradient (in strike-slip regimes) or the vertical component and its gradient (in thrust regimes). The remaining parameters are subsequently solved by HTPF technique.

5.4 Observed problems during injection testing

During the very first test in borehole KLX12A, the tool was displaced during injection testing as a result of pressure build-up behind the downhole tool. The reason for this pressure build-up is not fully understood but it is probably a combination of several factors. First of all, the bedrock is completely impervious (i.e. all pre-existing fractures are sealed) and pressure cannot escape if trapped below the tool. Hence, already the inflation of the packer would increase the pressure behind the tool, although not to such a degree that the tool would move. During injection in to the test section, additional pressure build-up behind the tool could result from: (i) short-circuiting through fractures so that the injected water to pass through these fractures and below the tool; and (ii) leakage though the packer. The displacement of the downhole tool damaged the 20 m hydraulic hoses and the bridle immediately above the tool, forcing a break in measurements for repair of equipment. The second phase of measurements did not encounter problems, but similar problems appeared at several tests during the subsequent measurements in borehole KFM08A at the Forsmark site /Ask et al. 2007/. Continuous monitoring of cable tension helped keep the displacement of the tool, when it occurred, at an acceptable minimum value.

Similar to what was discovered at the Forsmark site, but not at all as frequent, a number of sub-horizontal fractures were induced. The physical explanation for the observed induced sub-horizontal fractures is presently unknown, but they may be en echelon type of fractures. The fractures were analyzed in more detail in /Ask et al. 2007/.

6 Results from stress inversion

6.1 General about the line of work

The general line of work included a run-through of all tests to identify the tests that are judged most reliable. Indeed, some tests are associated with features that reduce their reliability as estimates of the state of stress at the site. Factors that reduce the reliability of the tests involve primarily multiple fractures in the test section, non-optimal fracture orientation (poorly resolved fracture orientation or unclear image of the fracture), and poor flow-back after completed testing.

One observed problem in the collected data involves the existence of fractures induced by the packer, even though a very careful pressurizing procedure had been adopted. These packer-induced fractures raise some difficulty for some of the tests but, at the same time, provide an independent means to validate the stress field that has been determined. These fractures are outside the scope of the present report but the methodology is presented in /Ask et al. 2007/ with application on drill site 7 at the Forsmark site.

Normal stresses are denoted using a geomechanical sign convention with compressive stresses taken as positive. All orientations represent the normal to the fracture plane, positive downwards, and are given with respect to geographic North according to coordinate system RT90 2.5 gon W 0: –15 for x and y and RHB70 for z, using a right-hand rule notation. Measurement positions are given as the borehole length of the centre of the test section as well as converted to corresponding vertical depth.

In Appendix I, we outline those data that have been considered as reliable for the sake of stress determination, which we denominate “unambiguous data”. Unambiguous data implies that the test involves reliable fracture orientation and normal stress determination. Hence, the fracture orientation data involve proper recording of tool positioning, repeatability of different logs, and clearly visible fracture traces. Unambiguous normal stress data involve repeatable and clearly defined shut-in values from tests involving 2 to 5 litres of injected water volume and show a pronounced flow-back after completed testing.

All stress determinations are based on unambiguous stress data. The inversions involved testing different fracture alternatives (if present) to derive the most reliable solution.

6.2 Method for inversion

The inversion procedure is based on a least squares measure of misfit and the Tarantola-Valette gradient algorithm /Tarantola and Valette 1982, Cornet and Valette 1984/. It assumes a linear variation of the stress field throughout the volume sampled by the tests considered for the inversion.

When tests have been run at large distances from one another, the solution requires a parameterization of the stress field in the rock mass. The choice of parameterization for stress calculation depends on the number of measurement points and the range of orientations of the tested fractures. A commonly applied parameterization of the stress field involves the assumption of linear stress variation along the borehole axis, i.e. the stress at point X_m is expressed as a linear function of the stress at point X_o with a stress gradient, α, along the borehole axis according to Equation 5-1:

In its general form, it involves 12 model parameters (Equation 6-1) and requires a minimum of 14–15 tests for its solution (because measurements are never exact and always involve some uncertainty, it is always desirable to use more tests than there are unknown model parameters). If a lateral stress gradient can be neglected, the stress field is characterized by 12 parameters according to:

$$\sigma\left(X^m\right)=\sigma\left(X\right)+\left(z^m-z\right)\alpha^{[z]} \qquad 6\text{-}1$$

For hydraulic fracturing/HTPF data, the fracture normal stress can be expressed as:

$$\left[\sigma\left(X^m\right)\vec{n}^m\right]\vec{n}^m=\sigma^m_{normal} \qquad 6\text{-}2$$

where n^m is the normal of the m^{th} fracture plane and includes the dip direction ϕ^m and the dip φ^m of the normal to the m^{th} fracture plane with respect to the vertical direction. With these definitions, Equation 6-2 can be formulated in matrix form according to:

$$\sigma^m_n=\left(\left[SB\cdot S^o\cdot SB^T+\left(z^m-z\right)\cdot AB\cdot A^o\cdot AB^T\right]\vec{n}^m\right)\vec{n}^m \qquad 6\text{-}3$$

where matrices S^0 and A^0 represent the stress and gradient tensors, SB includes the Euler angles E_1 to E_3, which describe S^0 in the geographical frame of reference, AB includes Euler angles E_4 to E_6, which describe A^0 in the S^0 frame of reference, z^m is the depth of the m^{th} fracture, and z is the chosen calculation depth (normally the average depth of the data set; /Ask 2004/.

The inversion is performed using a method developed by /Cornet 1993/, based on the least squares criterion /Tarantola and Valette 1982, Cornet and Valette 1984/. In this method, *a priori* knowledge of the unknown model parameters is assumed to exist, which can be formulated in terms of expected value, variance and covariances. In practice, large error bars are placed on assumed central values for the unknown parameters. The hydraulic fracturing and HTPF data consist of four components: the depth, z^m, of the m^{th} fracture plane, the dip direction, ϕ^m, and the dip, φ^m, of the normal to the m^{th} fracture plane with respect to the vertical direction, and the fracture normal stress, σ_n^m. Thus, for a 12-parameter problem, hydraulic fracturing and HTPF data involve 4m+12 = M components for m measurements.

A vector π_o can be created which includes *a priori* values according to:

$$\pi_0=col\begin{bmatrix}\left(z_o,\phi_o,\varphi_o,\sigma_{no}\right)^1,...,\left(z_o,\phi_o,\varphi_o,\sigma_{no}\right)^M,\\ E_1,E_2,E_3,E_4,E_5,E_6,S_1,S_2,S_3,\alpha_1,\alpha_2,\alpha_3\end{bmatrix} \qquad 6\text{-}4$$

The corresponding covariance matrix is denominated C_o and is diagonal, because measurements and unknown parameters are assumed independent /Cornet 1993/. The correspondingly computed, or *a posteriori,* vector is of the form:

$$\pi=col\begin{bmatrix}\left(z,\phi,\varphi,\sigma_n\right)^1,...,\left(z,\phi,\varphi,\sigma_n\right)^M,\\ E_1,E_2,E_3,E_4,E_5,E_6,S_1,S_2,S_3,\alpha_1,\alpha_2,\alpha_3\end{bmatrix} \qquad 6\text{-}5$$

A vector function $f(\pi)$ may be introduced in which the m^{th} component is defined by:

$$f^m\left(\pi\right)=\sigma^m_n-\left(\left[SB\cdot S^o\cdot SB^T+\left(z^m-z\right)\cdot AB\cdot A^o\cdot AB^T\right]n^m\right)n^m \qquad 6\text{-}6$$

The solution of the inverse problem is defined by the minimum of:

$$\left(\pi-\pi_o\right)^T C_o^{-1}\left(\pi-\pi_o\right) \qquad 6\text{-}7$$

The problem is a conditional least square, i.e. the minimum of Equation 6-7 is sought as to satisfy the condition $f(\pi) = 0$. /Tarantola and Valette 1982/ demonstrated that this can be solved using the iterative algorithm based on the fixed-point method:

$$\pi_{n+1}=\pi_o+C_oF_n^T\left(F_n\,C_o\,F_n^T\right)^{-1}\left[F_n\left(\pi_n-\pi_o\right)-f\left(\pi_n\right)\right] \qquad 6\text{-}8$$

where F is a matrix of partial derivatives of $f(\pi)$ valued at point π.

6.3 Results of hydraulic fracturing in borehole KLX12A

In borehole KLX12A, four of the seven hydraulic fracturing tests failed and resulted in sub-horizontal fractures (Appendix I), similar to the boreholes investigated in Forsmark /Ask et al. 2007/. In addition, two of the remaining three tests with induced axial fractures also have induced sub-horizontal fractures. This result was unexpected in the near-vertical borehole KLX12A, but it was also encountered in borehole KFM07C at the Forsmark site /Ask et al. 2007/. However, also a hydraulic test on pre-existing fractures resulted in inducement of axial fractures. Hence, in total, four tests with axial fractures were collected in borehole KLX12A (Table 6-1). These fractures constrain the orientation of the horizontal stresses effectively; σ_h is oriented 71±5°N (i.e. σ_H is oriented 161±5°N).

However, only Test 4 involves axial fractures within the test section area, whereas the other axial fractures extend or are located underneath the packer elements. Thus, this test should be used for stress evaluation. On the other hand, during the first pressurization cycle in Test 4, a very non-linear behaviour of the borehole pressure is noted (noticeable also on Test 2 and pronounced in Test 5). This demonstrates progressive fracture extension with correlative fluid penetration, way before breakdown is reached.

If the stress at the borehole wall is tensile, but lower than the tensile strength, the fluid percolation will not be axisymmetric but rather a preferential percolation within the zone of tensile stress so that the classical hydraulic fracturing is simply not valid as it will underestimate the breakdown pressure. /Cornet 1989/ demonstrated this at the Moodus site in Conneticut.

Yet, we proceed with the classical hydraulic fracturing equation to obtain a maximum value of the maximum horizontal stress:

$$\sigma_H = 3\sigma_h - P_b + T - a \cdot P_p \qquad 6\text{-}9$$

where σ_h and σ_H are the minimum and maximum horizontal stresses, P_b is the breakdown pressure, T is the tensile strength, P_p is pore pressure, and a is an unknown constant between 0 and 1.

The pore pressure is unknown because the permeability, in the extension zone close to the borehole before failure occurs, is stress dependent. The extreme values occur for (1) a = 0, P_p value arbitrary; and (2) a = 1 and $P_p = P_b$, giving the maximum and minimum magnitudes for σ_H, respectively. In the following, we assume that pore pressure effects may be neglected, i.e. we will estimate the upper limit for the magnitude of σ_H.

Tensile strength measurements have not been determined using minifrac tests on cores in connection to the campaign. A rough indication of the in situ tensile strength can be evaluated by the difference in breakdown pressure and shut-in/re-opening. Table 6-1 indicates that the tensile strength is of the order 3 MPa, which can be regarded as a lower limit. /Lindfors 2004/ made two successful minifrac tests on cores from KSH01A, which resulted in an average tensile strength of about 15 MPa. However, /Schmitt and Zoback 1992/ showed that the minifrac tests

Table 6-1. Hydraulic fracturing tests in borehole KLX12A with induced axial fractures.

Bh length [mbl]	Vert. depth [mvd]	Test no.	$P_{b,A}$ [MPa]	$P_{b,B}$ [MPa]	σ_n [MPa]	Azimuth [°N]	Dip [°]
579.4	536.0	2	18.7	**20.2**	15.7	56[1]	84[1]
572.0	529.0	4	**15.7–16.7**	16.7–17.7	15.1	85	77
564.4	522.0	5	16.3	**17.3**	14.7	72[1]	80[1]
532.0	491.0	7	12.8–13.2	**13.5–13.9**	10.4	71[1,2]	80[1,2]

Note: P_b and σ_n are the breakdown pressure and normal stress, respectively ($P_{b,A}$ and $P_{b,B}$ denote maximum pressure in test section and packer, respectively, where bold font denote the most proper pressure); Azimuth and Dip refer to the normal of the fracture plane; [1] denote tests with also sub-horizontal fracture/fractures; and [2] denote HTFP test.

result in increasing tensile strength (and Young's modulus) and related it to that the associated pore pressure perturbation cannot reach equilibrium over the time scale of a minifrac test. The increase of tensile strength is a result of assuming that the initial pore pressure is uniformly maintained for the duration of the test. Hence, the tensile strength obtained from minifrac tests should be regarded as an upper limit of the true value. Moreover, the limited amount of tested samples and the unknown scale factor between the lab and in situ scales renders the result of the KSH01A tests somewhat inconclusive. /Lindfors 2004/ suggested a scale factor of 0.6, giving an in situ tensile strength estimate of about 9 MPa, which again should be regarded as the upper value. Thus, the in situ tensile strength is in the range 3–9 MPa, but cannot be pinpointed exactly. In the following, it is assumed that the tensile strength is 5 MPa. Note that the magnitude of σ_H is directly proportional to the tensile strength, i.e. an increasing tensile strength implies an increasing magnitude of σ_H and vice versa.

Using the σ_h estimate from Test 4 and an assumed tensile strength of 5.0 MPa yields:

Test 2:

$\sigma_{H,\,max} = 3 \cdot 15.1 – 20.2 + 5.0 = 30.1 \pm 0.8$ MPa (plus the uncertainty in tensile strength)

Test 4:

$\sigma_{H,\,max} = 3 \cdot 15.1 – 16.2 + 5.0 = 34.1 \pm 1.0$ MPa (plus the uncertainty in tensile strength)

Test 5:

$\sigma_{H,\,max} = 3 \cdot 15.1 – 17.3 + 5.0 = 33.0 \pm 0.8$ MPa (plus the uncertainty in tensile strength)

Test 7:

$\sigma_{H,\,max} = 3 \cdot 15.1 – 13.7 + 5.0 = 36.6 \pm 0.9$ MPa (plus the uncertainty in tensile strength)

Because all these equations are judged as overestimates of σ_H, the minimum value is regarded as the most realistic upper bound of σ_H. Hence, σ_H is less than 30 MPa in the interval 490 to 540 mvd.

6.4 Results of stress determination and inversion in borehole KLX12A

6.4.1 Section 490 to 540 mvd (Tests 1 to 8)

For stress determination, Test 1 is not considered unambiguous given the displacement of the tool during testing. Moreover, Test 7 yields a fracture that extends within the packer interval and therefore is not considered reliable for the evaluation of σ_h.

Test 8 corresponds to a fracture with relatively shallow dip and does not bring any significant constraint on principal stress magnitudes but would require consideration on the vertical stress gradient if they were to be included in the inversion. They have not been considered in order to keep a small enough depth interval so that vertical gradients may be neglected. The vertical stress gradient was assumed to 0.026 MPa/m, which is verified by that the tests with fractures dipping 25° or less from the horizontal plane display an average vertical gradient of 0.0255 MPa/m. Hence, the solution for the interval 490 to 540 mvd is based on the hydraulic fracturing data in the previous chapter:

$\sigma_h = 15.1 \pm 0.2$ MPa

σ_H less than 30 MPa

$\sigma_v = 13.4$ MPa (assumed to equal the theoretical weight of the overburden)

Orientation $\sigma_H = 161 \pm 5$°N (based on induced axial fractures).

6.4.2 Section 400 to 440 mvd (Tests 9 to 15)

The attention has focused on Tests 11, 12, 13, 14 and 15 (all unambiguous tests), that have been run between 443 m and 402 mvd. But for Test 13, three different fractures have been observed in the pressurized interval and the test was as a result not included in the inversion. This leaves four tests for two unknowns, if we assume that the maximum horizontal stress direction is that defined between 490 m and 540 m and a vertical stress gradient of 0.026 MPa/m.

Tests 9, 10, and 14 correspond to fractures with relatively shallow dip. As such, they do not bring any significant constraint on principal stress magnitudes but would require consideration on the vertical stress gradient if they were to be included in the inversion. Thus, in order to keep a small enough depth interval so that vertical gradients may be neglected, Tests 9, 10, and 14 were discarded.

In Table 6-2, the values considered for the determination of σ_H and σ_h between 402 m and 443 m is given. As a first attempt, an inversion was run with assumed mean standard deviation on azimuth of 5°, 3° for dip, and 0.4 MPa on normal stress determination. The *a priori* orientation of the maximum horizontal principal stress was imposed to be N160°E.

Table 6-2. Table of values considered for determination of horizontal

Depth [mvd]	Test no	Azimuth [°N]	Dip [°N]	σ_n [MPa]
443.0	11	298	63	13.8
436.0	12	248	24	9.7
414.0	14	91	34	14.1
402.5	15	31	87	12.7

At 425 m this yields solution 1:

Depth [mvd]	Parameter	σ_H [MPa]	σ_h [MPa]	σ_v[1] [MPa]	Orient σ_H [°N]
425	Magnitude	30.5	4.5	11.0	156
	Std	3.7	1.8	–	2.5
	95% conf. int.	23.1–37.9	0.9–8.1	–	151–161

[1] Vertical stress gradient assumed to correspond to 0.026 MPa/m.

For all data, differences between *a posteriori* and *a priori* are within 2 standard deviations.

Then a new solution has been searched with a 0.2 MPa standard deviation on normal stress and keeping 5° and 3° standard deviation for azimuth and dip, respectively. This yields solution 2:

Depth [mvd]	Parameter	σ_H [MPa]	σ_h [MPa]	σ_v[1] [MPa]	Orient σ_H [°N]
425	Magnitude	32.4	3.3	11.0	156
	Std	3.6	1.5	–	2.4
	95% conf. int.	25.2–39.6	0.3–6.3	–	151.2–160.8

[1] Vertical stress gradient assumed to correspond to 0.026 MPa/m.

For all data, differences between *a posteriori* and *a priori* are within 2 standard deviations.

Then, attempts where made to impose the real, measured standard deviations on orientations but no convergence of the iterative procedure was observed. Solutions 1 and 2 are however not acceptable for, with such stress magnitudes, the minimum tangential stress at the borehole wall is roughly –20 MPa, a value that would have resulted in tensile fractures, when none have been observed.

As a result, a new solution was searched around the direction 140°N and the following result was obtained:

Depth [mvd]	Parameter	σ_H [MPa]	σ_h [MPa]	σ_v[1] [MPa]	Orient σ_H [°N]
425	Magnitude	17.4	12.6	11.0	132
	Std	2.8	1.4	–	4.0
	95% conf. int.	11.8–23.0	9.8–15.4	–	124–140

[1] Vertical stress gradient assumed to correspond to 0.026 MPa/m.

For most data, differences between *a posteriori* and *a priori* are within 2 standard deviations (Table 6-3).

While the erroneous solutions 1 and 2 are fairly similar, solution 3 is very different from the two first solutions. Solution 3 also provides a much improved fit of measured and calculated fracture orientations, although the fit of measured and calculated normal stresses are slightly lower. This demonstrates the importance of the accuracy on fracture orientations when too few tests are available for constraining the solution.

The inversion attempts in borehole KLX12A, as at the Forsmark site /Ask et al. 2007/, indicate that the stress field variation with depth is non-linear. This is for KLX12A manifested in the failure to determine a stress profile over longer depth intervals and by relatively pronounced uncertainties of the solved parameters. However, the cluster approach has been fruitfully applied.

In order to obtain a better constraint on stress magnitudes, it is proposed to integrate these results with constraints imposed by the dip and azimuth of packer induced fractures /see Ask et al. 2007/.

Table 6-3. A priori and a posteriori data in best solution for borehole KLX12A in the interval 400–440 mvd.

Depth [mvd]	Test no	Az_{meas} [°N]	Az_{calc} [°N]	Error [°N]	STD_{Az}	Dip_{meas} [°N]	Dip_{calc} [°N]	Error [°N]	STD_{Dip}	$\sigma_{n,meas}$ [MPa]	$\sigma_{n,calc}$ [MPa]	Error [MPa]	$STD_{\sigma n}$ [MPa]
443.0	11	298	295.1	2.8	4.5	63	52.8	10.2	2.5	13.8	14.8	1.0	0.5
436.0	12	248	245.7	2.3	5.5	24	17.0	7.0	2.5	9.7	10.8	1.1	0.3
414.0	14	91	101.4	10.4	6.5	34	48.6	14.6	3.0	14.1	13.4	0.7	0.2
402.5	15	31	31.0	0.0	2.0	87	87.0	0.0	1.0	12.7	12.7	0.0	0.2

7 Discussion and summary

7.1 General

Hydraulic rock stress measurements were performed in borehole KLX12A at the Oskarshamn candidate area. Of the 17 tests conducted in KLX12A, thirteen tests involve completely unambiguous data, i.e. have a reliable normal stress and a well defined fracture geometry, of which 9 involve a single fracture geometry (Appendix I).

In a few cases, sub-horizontal fractures were induced. These fractures sometimes appear in the test section, although they are more commonly located at the end of the test section (i.e. at the packer ends) and underneath the packers. Hence, a majority of the fractures are packer induced. The sub-horizontal fractures were induced when the pressure in the test section was just moderately higher (a few bars) than the theoretical weight of the overburden rock mass. These fractures are more thoroughly discussed in /Ask et al. 2007/ and will not be commented further here.

The results of the stress inversions indicate a non-linear stress distribution (Figure 7-1). In the interval 490 to 540 mvd, minimum horizontal stress is well constrained and reaches 15.1 ± 0.2 MPa and is oriented 71 ± 5°N. Because most axial fractures are located underneath the packer elements and because the only tests where the axial fractures are within the test section (Test 4) displays a non-linear borehole pressure during pressurization, maximum horizontal stress cannot be determined. Instead, the tests were used to derive an upper bound of σ_H; σ_H is less than 30 MPa in the interval 490 to 540 mvd.

In the interval 400 to 440 mvd, the tests were chosen as to minimize the number of unknowns to be determined. As a result, four tests were used to constrain the horizontal stresses. These were found to be 12.6 ± 1.4 and 17.4 ± 2.8 MPa, respectively, and the orientation of σ_H was found to be 132 ± 4.0°N.

The vertical stress gradient was in both intervals assumed to correspond to the theoretical weight of the overburden rock mass (i.e. 0.026 MPa/m). This is verified by that the tests with fractures dipping 25° or less from the horizontal plane display an average vertical gradient of 0.0255 MPa/m.

The results thus demonstrate that, as at the Forsmark site, the stress field variation with depth is non-linear and interpolation of results over long depths interval is not warranted. For borehole KLX12A, the cluster approach has been fruitfully applied.

In order to obtain a better constraint on stress magnitudes, it is proposed to integrate these results with constraints imposed by the dip and azimuth of packer induced fractures /see Ask et al. 2007/. However, this is outside the scope of the present report.

Because of local disturbances, such as fractures and fracture zones, larger σ_H-magnitudes may be observed, implying that it is smaller in adjacent domains, in order to maintain equilibrium, when integration is made on larger rock mass volumes. As a result of this, an important question to discuss is the origin of the stress heterogeneity, e.g. a block effect, water circulation and correlated alteration, or temperature disturbances. This is though outside the scope of the present report.

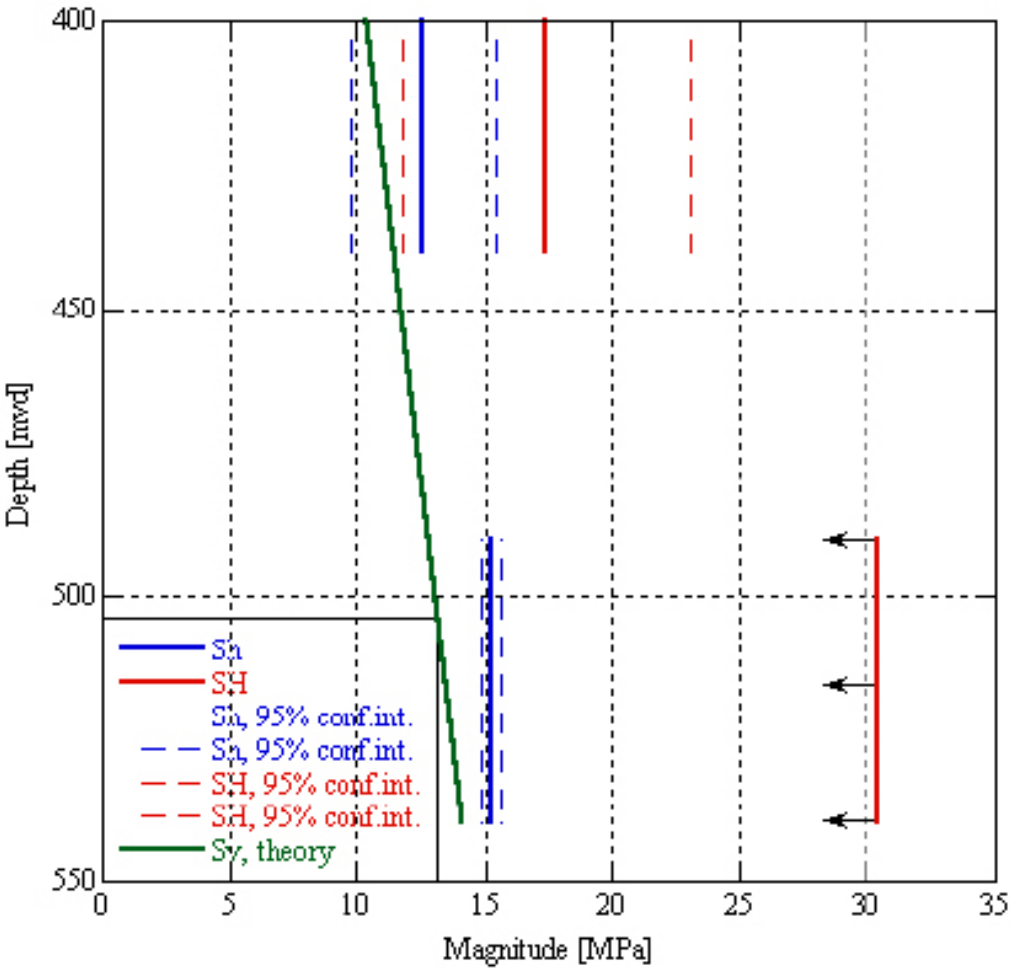

Figure 7-1. *Best inversion solutions obtained for borehole KLX12A between 400 and 540 mvd.*

7.2 Uncertainties in stress determination results

The uncertainties in the stress determination results may be divided into two categories; those associated with the collected data used for stress determination and those associated with the parameterization/mathematical model used to describe the stress field.

7.2.1 Uncertainties associated with collected data

The uncertainties in collected data are visualized in Appendix I and for e.g. normal stresses it involves an uncertainty of a few bars. These uncertainties are completely normal in hydraulic stress measurement campaigns and do not pose a problem for stress determination. Of the 17 tests conducted, 13 involve unambiguous data, i.e. have a reliable normal stress and a well-defined fracture geometry (but only nine of these exhibit one single fracture plane). Note that the stress determinations are based on entirely unambiguous data. The reasons for the ambiguity in the data are described below in decreasing order or importance.

During the injection testing in borehole KLX12A, it became clear that in some tests, sub-horizontal fractures were induced at pressures just moderately higher than the corresponding theoretical vertical stress at the location in question. Hence, unless the chosen pre-existing fracture could be re-activated before reaching the level of the theoretical vertical stress (a few bars), sub-horizontal fractures would be induced. This implies that a constraint for injection testing prevailed and that sub-horizontal fractures were induced in all cases where the fracture did not re-activate before reaching this critical pressure. The physical explanation for these fractures is yet to be determined (although one attempt is presented in /Ask et al. 2007/). Often, these tests also resulted in a poor

flow-back after completed testing, which in many cases is explained by that the fractures are located underneath the packer elements. Although the sub-horizontal fractures reduced the number of unambiguous tests, they contain very useful information as described in /Ask et al. 2007/.

Two additional problems existed during the field measurements; noise in the HTPF tool and tool displacement during testing.

A noise in the HTPF tool was outlined in the quality procedure and consisted of a systematic magnetic discrepancy above about 250 m depth at the Oskarshamn site. This discrepancy is due to a 50 Hz electrical noise that is collected by our HTPF tool resulting from ground currents. Hence, for tests conducted above 250 m, collected data were given special attention.

The tool displacement during injection testing appeared in the deepest test in borehole KLX12A (Appendix I; but also at in borehole KFM08A /Ask et al. 2007/) as a result of pressure build-up behind the downhole tool. The reason for this pressure build-up is not fully understood but it is probably a combination of several factors. First of all, the bedrock is completely impervious (i.e. all pre-existing fracture are sealed) and pressure cannot escape if trapped below the tool. Hence, already the inflation of the packer would increase the pressure behind the tool, although not to such a degree that the tool would move. During injection in to the test section, additional pressure build-up behind the tool could result from: (i) short-circuiting through fractures, which are dominatingly sub-vertical respectively sub-horizontal; and (ii) leakage through the packer.

7.2.2 Uncertainties associated with the parameterization and determination of the stress field

As previously noted, the difficulties during data collection in the borehole reduced the number of unambiguous data. However, they were not as severe as preventing a proper stress determination.

Because the notion of rock stress is a concept of continuum mechanics, it is necessary to identify volumes where the continuity hypothesis is verified. In other words, bodies that may be approximated by a continuum need to be identified. Moreover, because the stress at a specific point involves six components, the determination of the regional stress field includes determination of six functions for the domain under consideration. This requires integrating measurements conducted at points that sample properly the continuum volume of interest.

In the methodology of Vattenfall Power Consultant AB, the first interpretation of the continuity hypothesis is given by the reconnaissance log with the HTPF tool (Appendix I). The first evaluation provided by the HTPF tool is also used for selection of suitable test sections.

Given the non-linear and scattered stress profiles derived from previous overcoring stress data in the region, application of a standard profiling approach was believed to be hampered by the non-linearity. Instead, the methodology chosen for the tests in borehole KLX12A involved the cluster approach /e.g. Ask and Cornet 2006, 2007/. This implies that measurements are grouped in clusters with the aim of collecting a sufficient number of HF and HTPF data in a small enough volume to permit complete stress determination without considering stress gradients. Such an approach would result in a minimum of parameters at each cluster but also have the benefit of that the continuity hypothesis would be more easily evaluated by comparisons of full tensors from multiple clusters along a borehole.

This proposed strategy was, as opposed to the results at the Forsmark site /Ask et al. 2007/ where a larger number of ambiguous data were collected, successful for borehole KLX12A /Ask et al. 2007/. However, the results of the deeper cluster are not completely satisfactory due to unfortunate and un-controllable circumstances in the injection tests. The tests yielding sub-axial fractures are indeed optimal for determination of stress orientations, but regrettably, the location of the fractures with respect to the downhole tool prevented normal analysis of stress magnitudes. In fact, of the four tests with axial fractures between 491 and 536 mvd, only one was located completely within the sealed off section. This drawback results in a reduced resolution of maximum horizontal stress and only an upper limit could be determined.

Similar to the Forsmark site /Ask et al. 2007/, the stresses in borehole KLX12A are clearly non-linear when comparing the result of the two clusters and when investigating the variation of the normal stress with depth of any fracture of given orientation. During stress inversion, the non-linear stress distribution is directly visualized in the resolution of the unknown parameters and by convergence problems. In other words, interpolation of stress data over long depth intervals may not be warranted. If the packer-induced fractures would be used, the results may be improved.

8 References

Aamodt R L, Kuriyagawa M, 1981. Measurements of instantaneous shut-in pressure in crystalline rock. Proc. Workshop on Hydraulic Fracture Stress Measurements (Eds. Zoback M D, Haimson B C), Monterey, USA. USGS, p. 139–42.

Ask D, 2004. New developments of the Integrated Stress Determination Method and application to the Äspö Hard Rock Laboratory, Sweden. Doctoral Thesis, Royal Institute of Technology, Stockholm.

Ask D, Cornet F H, 2006. Strategy for in situ rock stress measurements. Proc. 4th Asian Rock Mechanics Symposium (Eds. Leung CF, Zhou YX), Singapore. B & JO Enterprice, p. 99–107.

Ask D, 2006a. Manual for hydraulic rock stress measurements, version 1.32. Internal report, Vattenfall Power Consultant AB.

Ask D, 2006b. Quality operating procedures, hydraulic rock stress measurements, version 3. Internal report, Vattenfall Power Consultant AB.

Ask D, Cornet FH, 2007. The integrated stress determination method and suggested measurement strategy. ISRM News Journal, 3:9, p. 24–27.

Ask D, Cornet F H, Fontbonne F, Brunet C, 2007. Forsmark site investigation. Stress measurements with hydraulic methods in boreholes KFM07A, KFM07C, KFM08A, KFM09A, and KFM09B. SKB P-report in print, Svensk Kärnbränslehantering AB.

Brudy M, Zoback M D, 1993. Compressive and tensile failure of boreholes arbitrary inclined to principal stress axis: application to the KTB boreholes, Germany. Int. J. Rock. Mech. Min. Sci., 30, p. 1035–8.

Cornet F H, Valette B, 1984. In situ determination from hydraulic injection test data. J. Geophys. Res., 89, p. 11527–37.

Cornet, F H, 1989. Material presented at the AGU meeting in 1989.

Cornet, F H, 1993. The HTPF and the integrated stress determination methods. Comprehensive Rock Engineering, 3, (J. Hudson, Ed.). Pergamon Press, Oxford, p. 413–432.

Cornet F H, Li L, Hulin J P, Ippolito I, Kurowski P, 2003. The hydromechanical behaviour of a fracture: an in situ experimental case study. Int. J. Rock Mech. Min. Sci., 40, p. 1257–70.

Enever J, Chopra P N, 1989. Experience with hydraulic fracturing stress measurements in granites. Proc. Int. Conf. On Rock Stress and Rock Stress Measurements (Ed. Stephansson O), Stockholm. Centek Publisher, Luleå, p. 411–20.

Haimson B C, Cornet F H, 2003. ISRM Suggested Methods for rock stress estimation – Part 3: hydraulic fracturing (HF) and/or hydraulic testing of pre-existing fractures (HTPF). Int. J. Rock Mech. Min. Sci., 40, p. 1011–20.

Hayashi K, Haimson B C, 1991. Characteristics of shut-in curves in hydraulic fracturing stress measurements and determination of in situ minimum compressive stress. J. Geophys. Res., 96, p. 18311–21.

Ito T, Evans K, Kawai K, Hayashi K, 1999. Hydraulic fracturing reopening pressure and the estimation of maximum horizontal stress. Int. J. Rock Mech. & Geomech. Abstr., 36, p. 811–26.

Lindfors U, 2004. Oskarshamn site investigation. Hydraulic fracturing and HTPF rock stress measurements in borehole KSH01A. SKB P-report in print, Svensk Kärnbränslehantering AB.

Mosnier J, 1982. Détection électric des fractures naturelles ou artificielles dans un forage. Ann. Géophs., 38, p. 537–40.

Mosnier J, Cornet F H, 1989. Apparatus to provide an image of the wall of a borehole during hydraulic fracturing experiments. Proc. 4th Europ. Gepth. Update – Int- Sem., Florence, Kluwer, Dordrecht, p. 205–12.

Peska P, Zoback M D, 1995. Compressive and tensile failure of inclined well bores and determination of in situ stress and rock strength. J. Geohys. Res., 100, p. 12791–811.

Ratigan J L, 1992. The use of the fracture reopening pressure in hydraulic fracturing stress measurements. Rock Mech. Rock Eng., 25, p. 125–136.

Rutqvist J, 1995. Coupled stress-flow properties of rock joints from hydraulic field testing. Doctoral Thesis, Royal Institute of Technology, Stockholm.

Rutqvist J, Tsang C-F, Stephansson O, 2000. Uncertainty in the principal stress estimated from hydraulic fracturing measurements due to the presence of the induced fracture. Int. J. Rock Mech. & Geomech. Abstr., 37, p. 107–20.

Schmitt D R, Zoback M D, 1992. Diminished pore pressure in low-porosity crystalline rock under tensional failure. Apperent strengthening by dilatancy. *J. Geophys. Res.*, 97, pp. 273–288.

Tarantola A, Valette B, 1982. Generalized non-linear inverse problem solved using the least square criterion. Rev. Geophys. Space Phys., 20, p. 219–32.

Zoback M D, Barton C A, Brudy M, Castillo D A, Finkbeiner T, Grollimund B R, Moos D B, Peska P, Ward C D, Wiprut D J, 2003. Determination of stress orientation and magnitude in deep wells. Int. J. Rock. Mech. Min. Sci., 40, p. 1049–76.

APPENDIX I

OSKARSHAMN SITE INVESTIGATION. COLLECTION OF HYDRAULIC ROCK STRESS DATA IN BOREHOLE KLX12A

Oskarshamn site investigation

Collection of hydraulic rock stress data in borehole KLX12A

Daniel Ask, Vattenfall Power Consultant AB

Francois Cornet, Institut de Physique du Globe de Paris

Frederic Fontbonne, Geostress Co.

Christophe Brunet, Institut de Physique du Globe de Paris

November, 2007

SUMMARY

Hydraulic rock stress measurements were performed in borehole KLX12A at the Oskarshamn candidate area, Sweden. The measurements were carried out in two separate campaigns and a total of 17 hydraulic fracturing tests and hydraulic tests on pre-existing fractures were conducted between the 20th of July to the 11th of August, 2006.

The work involved cooperation between Vattenfall Power Consultant AB (Contractor), Institut de Physique du Globe de Paris (IPGP), and Geostress Co (both Sub-contractors). Vattenfall Power Consultant AB provided an MKW wireline system and field personnel, whereas IPGP supplied downhole equipment, data acquisition system, and field personnel. Finally, Geostress contributed with field personnel.

This document includes a detailed description of the observations made in the field, and results.

Of the 17 tests conducted in borehole KLX12A, thirteen involve completely unambiguous data, i.e. have a reliable normal stress and a well-defined fracture geometry of which nine involve a single fracture geometry. Another three tests involve axial fractures indicating the direction of σ_H, as well as stating that one principal stress is vertical. The success rate of testing was hence somewhat lower than expected for this type of hydraulic stress measurement equipment. The primary reason for the reduced success rate was that multiple fractures were opened or induced. In some cases, sub-horizontal fractures were created when the pressure in the test section was just moderately larger (a few bars) than the theoretical weight of the overburden rock mass. The physical explanation for these fractures is yet to be determined although an attempt is made in Ask et al. (2007). We would like to emphasize that the observed sub-horizontal fractures contain very useful information. If a failure criterion for these fractures has been derived, they will probably contribute much to the knowledge of the present state of stress at the Oskarshamn site.

The hydraulic fracturing data indicate a relatively large span for the direction of σ_H (between 146 and 175°N), which averages 161°N.

SAMMANFATTNING

Hydrauliska bergspänningsmätningar har utförts i borrhål KLX12A i Oskarshamn. Totalt gjordes således 17 tester i under två kampanjer mellan den 20:e juli och 11:e augusti, 2006.

Aktiviteten var ett samarbetsprojekt mellan Vattenfall Power Consultant AB (huvudkonsult), Institute de Physique du Globe de Paris (IPGP), och Geostress Co (båda dessa organisationer underkonsulter). Vattenfall Power Consultant AB tillhandahöll ett MKW wireline-system samt fältpersonal, IPGP stod för borrhålsutrustning, datainsamlingssystem och fältpersonal, medan Geostress bidrog med fältpersonal.

Detta dokument innehåller en detaljerad beskrivning av fältobservationer och resultat.

Av de 17 utförda injektionstesterna i borrhål KLX12A bedöms tretton som helt otvetydiga, dvs uppvisar tillförlitlig normalspänning och välbestämd sprickorientering av vilka nio uppvisar en enskild sprickgeometri. Ytterligare tre tester ger information of riktningen på största horisontalspänning, liksom att en huvudspänning är vertikal. Andelen lyckade tester är därför något lägre än normalt för metoden och är en följd av att flera sprickor öppnats eller inducerats vid ett flera tester. I vissa fall inducerades sub-horisontella sprickor redan vid ett pålagt tryck endast måttligt överstigande den teoretiska vertikalspänningen och innebar därför en stark begränsning av metodens möjligheter. De bakomliggande fysikaliska orsakerna till uppkomsten av dessa sprickor återstår att förklara, även om en ansats till detta gjorts i Ask m fl (2007). Vi vill dock betona att om ett brottkriterium för dessa sprickor kan härledas, kan en systematisk analys av den datamängd som dessa sprickor representerar sannolikt ge ett mycket värdefullt bidrag till beskrivningen av det rådande spänningsfältet i Oskarshamn.

Resultaten från de lyckade hydrauliska spräckningarna påvisar en relativt stor spridning i riktningen för σ_H (mellan 146 and 175^{o}N), med ett medel kring 161^{o}N.

Contents

1 Collected data in borehole KLX12A

The collected data comprise numerous parameters for determination of the stress field but also for verification of the data recording quality, which are described below.

1.1 Fracture orientation and groundwater pressure data

The three alternative means of determining fracture orientations available in this activity are described in Chapter 4.3.1 of the main report. Regarding fracture orientation by using the Mosnier tool the reliability of the fracture orientation determination rests on three features:

- The proper recording of all parameters that characterize the position of the tool in the well (borehole length, and readings from 3 magnetometers and 2 inclinometers).
- The good understanding of tool manufacturing and its consistency with data processing routines.
- The repeatability of orientations during comparisons of multiple scans of the same fracture.

There are a few independent means to verify that the overall data recording has been successful. One involves readings of orientation devices as the Mosnier tool is lowered and hoisted in the borehole. The values of the magnetic field inclination, as determined from magnetometers, offer a completely independent check on the digitization procedure used for the downhole data acquisition and surface data recording. The quality procedure has outlined a 50 Hz electrical noise affecting the downhole sensors as a result of ground currents (we measured 14 Volts and 50 Hz at ground surface). Interestingly, the noise is smaller during the second campaign, during which two nuclear reactors were shut down. The noise is site specific, although it was also found at the Forsmark site, and results in a digitization problem close to the surface, causing the timer that samples the data to be slightly off phase, and a small error is introduced. This noise affects all downhole sensors.

The results from the magnetometers and inclinometers may also be used to verify reproducibility. This involves comparisons of derived fracture orientations with those of the BIPS, but more importantly, we compare our determination of magnetic field inclination (angle with vertical) with the Uppsala magnetic field observatory (Appendix 1). For borehole KLX12A, we are always within 2° below 100 mbl with the Uppsala observatory results. Above this depth, noise is disturbing all downhole sensors.

Moreover, the measurements of well orientation are reproducible (comparison between pre- and post-logs) and it is always better than 2° for dip and azimuth and the average difference between the Maxibor results are 3.6°. Note, however, that the well orientation of the HTPF tool refers to the magnetic North, whereas the Maxibor refers to the geographical North. Thus, we have established that our orientation determination for the tool is reliable and reproducible and well within expected errors.

The other independent control of successful data recording is correlated with the observed variations in downhole pressure during lowering and hoisting in the borehole. These variations, which were investigated after completed field campaign, can be compared with the theoretical weight of the water column in the borehole and indicate that no discrepancies were found during measurements at drill site 12.

1.2 Calibration of equipment

1.2.1 Pressure transducers and flow meter

Prior to the measurements, the pressure transducers were calibrated against a reference load cell and the flow meters by volume (mass) determination per time unit prior to field measurements (Appendix 2). Note that response remains linear with time and that the calibration factor has not changed during the complete duration of all tests at the Forsmark site (calibrations were run in May, early June, late July, and in October, 2006). The apparent noise comes from the time response of the testing system, not from the transducers. If data would have been plotted with respect to time, all sensors would have been very stable. Also note that nowhere in the stress determination procedure do we require flow rate measurements. These are only used to control the re-opening of fractures, and the normal stress measurements are only based on shut-in.

1.2.2 Tilt meters and magnetometers

The orientation devices were checked for functionality and calibrated several times during the campaign: prior to departure to the field, before entering each borehole, and after completed measurements.

The calibration prior to descent in the well consists of two phases. In the first phase, the orientation device is placed in a special calibration support and both inclinometers and the three magnetometers are tested for various inclinations and orientations so that the readings are not saturated for any inclination/orientation.

In phase two, the orientation device is placed inside the HTPF tool (Mosnier, 1982; Mosnier and Cornet, 1989). Using a special calibration plate, the tool is first placed vertically and orientations are checked for every 20^{o} of rotation around the tool axis. Thereafter, the HTPF tool is inclined about 45^{o} towards the North, followed by verification of readings for every 20^{o} rotation around the tool axis. The latter is then repeated with the tool inclined 45^{o} towards East, South, and West. Finally, the HTPF tool is placed horizontally and is rotated around a vertical axis during which the output of the axial magnetometer is sampled. When the tool is fixed in the N, E, S, and W, the output of the perpendicular magnetometers is sampled during the corresponding rotation around the tool axis.

Phases one and two of the calibration before descent are repeated when the work in the well has been completed, to verify that the readings are systematic. Moreover, after the field campaign, the electrical imaging logs are used to provide independent data on dip and azimuth of the well (see Chapter 1.1 above).

1.2.3 Length measurement

For the sake of stress determination, the knowledge of absolute depth to within a few metres is quite sufficient. But because the objective is to relate images of features on the HTPF logs with those observed on cores, an adjustment to some decimetre is necessary.

Initially, the reference grooves were intended to be identified with the HTPF tool. However, the grooves proved to be too small for identification and a different strategy had to be adopted.

Instead, we compared the electrical imaging log with the cores and the BIPS images for a few unique features in the well. Once identified, by interpolation, an equivalence is proposed between HTPF logs and BIPS/Boremap depths for the complete borehole length. Thereafter, each pre-existing fracture tested was correlated with the equivalent fracture observed on the cores. In addition, the tested fracture was photo documented in the core boxes. This comparison entails that the length calibration between the two systems is within 2 dm.

During the measurements in KLX12A, the reference marks could not be detected with the HTPF tool. Instead, the length was calibrated using detailed comparisons with images, cores, and the BIPS for unique features at three locations, of which the two deepest located involved detailed mapping of fractures for about 15-20 m.

The first depth correspondence is the bottom of the borehole cone at about 100 mbl (97.4 to 102.1 m). The second mark involves characteristic veins at 272.2 and 283.5 on the electrical log (271.0 and 282.4 on the BIPS, respectively). The third reference mark corresponds to a unique fracture at about 438.97 mbl on the electric log, which is 438.07 mbl on the BIPS.

A gradient for the borehole was determined and the correspondence between the HTPF log and the length calibrated BIPS was within 2 dm. Together, these allowed exact determination of the fracture tested in each test section. This leads us to propose the following approximation:

BIPS mbl = 1.000 * electrical imaging depths – 1 (± 0.2) mbl.

1.3 Reconnaissance logs

Because the notion of rock stress is a concept of continuum mechanics, it is necessary to identify volumes where the continuity hypothesis is verified. The first interpretation of the continuity hypothesis is given by the reconnaissance log with the HTPF tool (Appendix 3). During the reconnaissance log, the intensity of the injected electrical current is adjusted to highlight very tiny fractures (which are suitable for hydraulic injection testing), which means that very conductive fractures, i.e. potential stress decoupling zones, are clearly outlined by a significant change of resistivity. The first evaluation provided by the HTPF tool is used for selection of suitable test sections.

Note that the borehole lengths as displayed in the reconnaissance log may be somewhat shifted as compared with the lengths given in the various tables of this document. This is a length calibration problem with no significance for the interpretation of data.

1.4 Testing results

The results of testing are presented in Appendix 3. For each test the following is presented:

- The downhole pressures in the chamber (test section) and in the packers versus time are displayed and below, in a separate plot, the fluid flow rate versus time.

- Blow-ups of the shut-in curves for each cycle are presented on the second page.
- The third page displays the pressure versus flow rate during the jacking tests for all cycles (if conducted).
- The fourth and fifth pages include the post-frac log with the test section marked. Note that this log starts at the bottom and moves upwards, implying that the fracture is "up-side down" compared to the following detailed plots.
- The next pages include detailed plots of the test section with: (i) results of the reconnaissance log; (ii) results of the post-log, which may be multiple when different electrical gains have been applied to enhance visibility and/or when the fracture is located underneath the packers; (iii) interpretation of fracture one; (iv) interpretation of fracture two; etc.

The borehole lengths as displayed in the reconnaissance log and in the post-log may be somewhat shifted as compared with the lengths given in the various tables of this document. This is a length calibration problem with no significance for the interpretation of data. The correct borehole length and vertical depth for each test are found in the tables.

1.5 Interpreted data

The analysis of data is based on the ISRM suggested methods for rock stress estimation by hydraulic fracturing and hydraulic tests on pre-existing fractures (Haimson and Cornet, 2003).

The interpreted data in Appendix 4 are presented in tabular form so that full traceability is achieved. This means that the appendices cover the collected raw data, the first interpretation of the data (e.g. normal stresses for each cycle in the injection testing), and the final interpretation of e.g. the normal stress acting on the fracture.

Normal stresses are denoted using a geomechanical sign convention with compressive stresses taken as positive. Measurement positions are given as the borehole length of the center of the test section. The corresponding vertical depth is based on recalculation of the borehole length using the deviation file delivered from Sicada. All orientation data represent the normal of the fracture plane, positive downwards, and are given with respect to geographic North according to coordinate system RT90 2.5 gon W 0:-15 for x and y and RHB70 for z, using a right-hand rule notation.

1.5.1 Fracture orientation data

In principle, the fracture orientations (i.e. the normal to the fracture plane) can in this specific assignment be determined with three different methods:

- Based on magnetometers and inclinometers of the HTPF tool
- Based on SKB´s deviation measurements of the well (the optical Maxibor method or the magnetic Flexit method) and tool face (inclinometers) of the HTPF tool
- Based on SKB´s Boremap system (Maxibor or Flexit deviation measurements) and tool face of the BIPS tool.

However, it must be pointed out that the third method is not available for fractures induced during the HF-/HTPF-campaign, because they were induced after the logging with the BIPS tool.

In the result files (Appendix 4), the results using method 2 are displayed (based on the Maxibor method).

Fracture orientation determined with the HTPF tool is obtained by fitting a sinusoid to the electrical image seen on the log. Special zooming techniques are used to identify more precisely the fracture. Two sinuoids are fitted to the image so as to identify domains of uncertainty. The central value is taken as the dip and azimuth values and the width of the interval on the values is selected as the 90% confidence level (to be compared with 99% confidence interval for pressure data).

1.5.2 Normal stresses

Because Cornet et al. (2003) observed that the normal stress may be overestimated when based on opening phases of hydraulic jacking tests, only shut-in values have been used. The shut-in pressure determinations have been made using two methods: (i) an overestimate of the shut-in pressure is provided by the Hayashi and Haimson procedure (1991) that indicates when the fracture stops being "opened"; and (ii) an underestimate is provided by the Aamodt and Kuriyagawa procedure (1981) that indicates the first pressure for which the fracture may be regarded as "closed". The normal stress, or shut-in value, is taken equal to the mean of these methods, i.e.

$$\sigma_n = \frac{\sigma_{n,Aa\,\mathrm{mod}\,t,\min} + \sigma_{n,Aa\,\mathrm{mod}\,t,\max} + \sigma_{n,Hayashi,\min} + \sigma_{n,Hayashi,\max}}{4} \quad (1)$$

Moreover, the tangent method of Enever and Chopra (1989) is used to allow comparisons (Appendix 4). The extreme values for the Hayashi and Haimson (1991) and the Aamodt and Kuriyagawa procedure (1981) are taken as bounds of the 99% confidence interval.

1.6 Comparison of fracture orientations determined with different methods

In Appendix 5, the fracture orientations as observed in the Boremap-system are compared with those of the electrical imaging system. Note that this appendix presents the truly tested fractures, as opposed to the fractures aimed for testing presented in Chapter 1.9. After this comparative study was initiated, a decision was taken to up-date SKB´s well deviation measurements, entailing that for many boreholes Maxibor measurement will be exchanged to Flexit measurements as the official deviation measurement files in SKB´s database Sicada. This up-date also affects the fracture orientations in Boremap as they are based on deviation data. In Appendix 5, the Boremap orientations based on the new Flexit well deviation data are presented.

For borehole KLX12A, the correspondence between methods yields an average deviation for azimuth and dip of the normal to the fracture plane of 13.3 and 3.7 degrees, respectively. One test reduces the agreement with respect to azimuth (at 481.4 mbl) and when excluded, the average difference between methods is reduced to 8.2 degrees.

1.7 Analysis of errors in well orientation data on fracture orientation determination

Because the results of the electrical imaging system is dependent upon the well deviation data, the up-date of deviation data from Maxibor to Flexit introduce errors in the fracture orientation data of the electrical imaging system. As a result of this, a study was initiated attempting to quantify this error. The result is presented in Appendix 6 and indicates that the error is small and negligible for the sake of stress determination. Hence, HTPF orientations were not updated with the new Flexit well deviation data.

1.8 General trends in collected data

The normal stresses of the tests in borehole KLX12A indicate that quite a few measurements are fairly close, or even below, the corresponding theoretical weight of the overburden rock mass (0.026 MPa/m; Figure 1-1 and Figure 1-2). However, given the variations in normal stresses and orientations (Figure 1-3), the data are promising for the subsequent stress determination. The result will be discussed in more detail in Chapter 1.9.

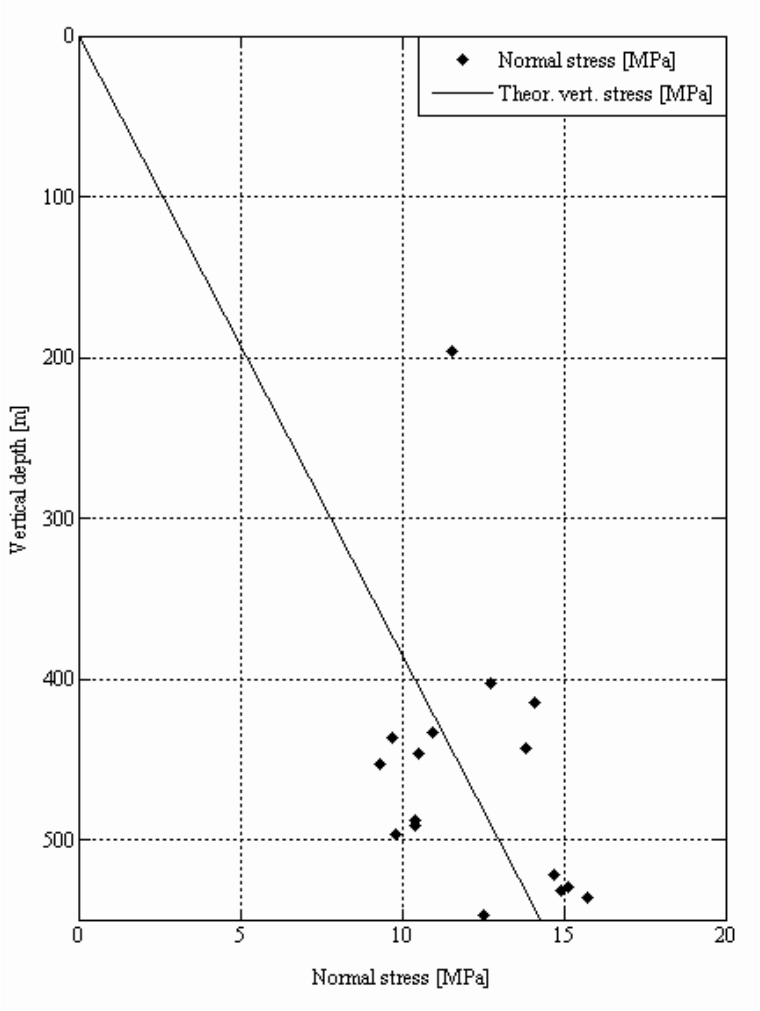

Figure 1-1. *Normal stresses versus depth in borehole KLX12A.*

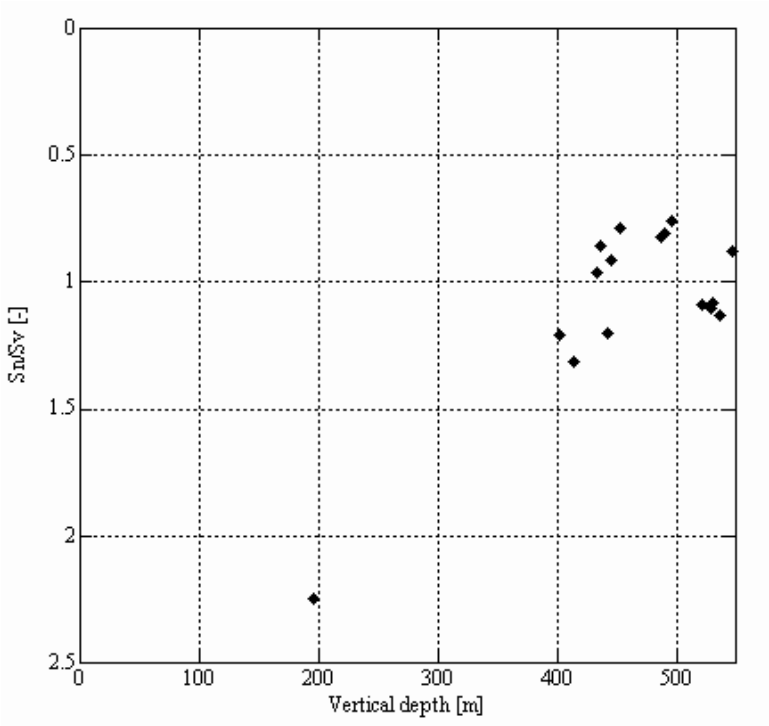

Figure 1-2. *Normal stresses divided by theoretical vertical stress versus depth in borehole KLX12A.*

Polar plots of the fractures aimed for testing versus the observed distribution of the normal to the tested fractures are presented in Figure 1-3. The result indicates that a large number of sub-horizontal fractures have been tested.

A **B**

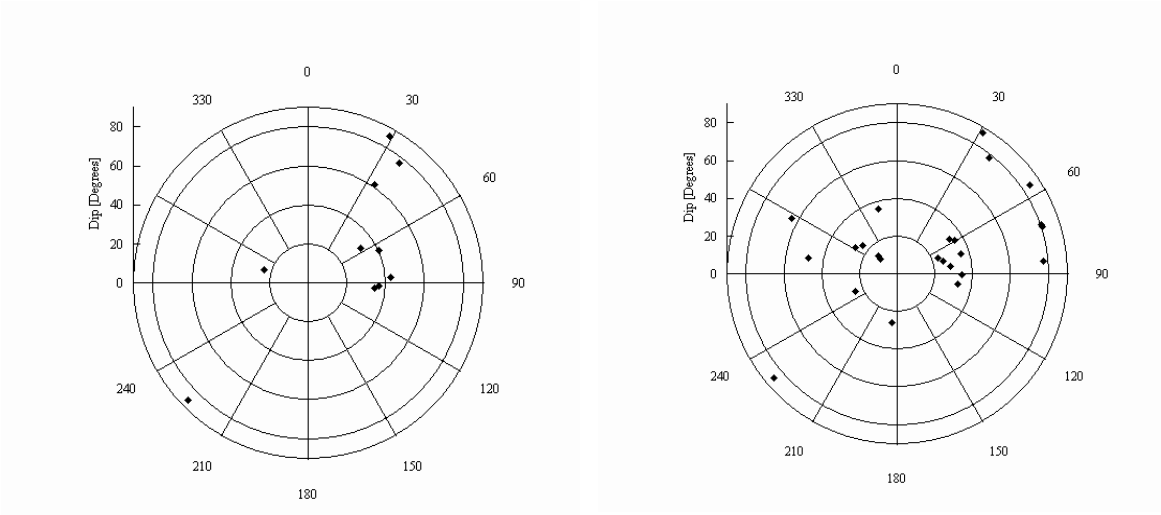

Figure 1-3. *Polar plot of normal to the fracture planes in borehole KLX12A: A) Fractures aimed for testing; B) Resulting fracture orientations.*

1.9 Individual tests

The individual tests results for borehole KLX12A are presented in Table 1-1 and indicate that a large number of sub-horizontal fractures have been tested. These fractures sometimes appear in the test section, at the end of the test section (i.e. at the packer ends) and sometimes underneath the packers. Hence, some of the fractures have been induced by the packers.

The induced sub-horizontal fractures cause a significant problem in the evaluation of the tests. The reason for this is that the opening of a fracture changes the stress field locally, but leaves the normal stress unaffected. Hence, for multiple fractures in the test section, the fracture normal stresses can be unambiguously determined only when the fractures are parallel.

Of the hydraulic fracturing tests, three tests were successful in inducing an axial fracture; at 579.4, 572.0, and 564.4 mbl. These fractures suggest an orientation of σ_H around 146, 175, and 162^{o}N, respectively. In two cases, the axial fractures were induced by the upper (579.4 mbl) or lower packer (564.4 mbl). Moreover, an axial fracture was induced by the upper packer during the HTPF test at 532.0 mbl, indicating an orientation of σ_H around 161^{o}N. The attempt at 236.7 mbl failed completely as a result of a short-circuit around the packer and the remaining three tests induced or re-opened sub-horizontal fractures.

Because the effect of the sub-horizontal fractures on the stress calculations has not been investigated fully at this stage, HTPF tests that have changed the resistivity image of the aimed pre-existing fracture but that also include sub-horizontal fractures, have been assigned “potentially successful re-opening” in Table 1-1 below.

Table 1-1. Results from individual injection tests in borehole KLX12A.

			Aimed fracture (BOREMAP)					
Test [No]	**Bh length [m]**	**Depth [m]**	**Azimuth [°N]**	**Dip [°]**	**σ_n [Bar]**	**$\sigma_{v,theory}$ [Bar]**	**Successful re-opening**	**Additional fractures**
1	590.1	547.0	226	86	125	142	Yes	No
2*	579.4	536.0	-	-	157	139	HF with axial fracture	Sub-horizontal fractures^{UP,TS}
3*	574.2	531.0	54	32	149	138	Yes	No
4*	572.0	529.0	-	-	151	138	HF with axial fracture	No
5	564.4	522.0	-	-	147	136	HF with axial fracture	Sub-horizontal fracture^{EoP}
6*	536.0	496.0	65	40	98	129	Yes	No
7*	532.0	491.0	93	34	104	128	Potentially	Axial fracture in lower packer position
8*	529.6	488.0	92	36	104	127	Yes	No
9*	491.2	453.0	-	-	93	118	Failed HF	Sub-horizontal fracture^{EoP}
10*	484.6	446.0	290	24	105	116	Potentially	Sub-horizontal fracture^{TS}
11*	481.4	443.0	39	61	138	115	Yes	No
12*	472.9	436.0	-	-	97	113	Failed HF	Sub-horizontal fracture^{TS}
13*	470.0	433.0	56	75	109	113	Potentially	Sub-horizontal fractures^{TS,EoP}
14*	451.0	414.0	93	43	141	108	Yes	No
15*	438.1	402.5	27	87	127	105	Yes	No
16	236.7	210.0	-	-	-	55	Failed HF	-
17	222.2	196.0	-	-	115	51	Failed HF	Sub-horizontal fracture^{EoP}

Note: “TS”, “EoP”, and “BP” denote sub-horizontal fracture in the Test Section, at the End of the Packer, and Underneath the Packer, respectively. Theoretical vertical stress based on a vertical gradient of 0.026 MPa/m. Unambiguous data are marked with “*” in the first column.

2 Discussion and summary

2.1 General

Hydraulic rock stress measurements were performed in borehole KLX12A at the Oskarshamn candidate area. Of the 17 tests conducted in KLX12A, thirteen involve completely unambiguous data, i.e. have a reliable normal stress and a well-defined fracture geometry, of which nine involve a single fracture geometry. Another three tests involve an axial fracture indicating the direction of σ_H, as well as stating that one principal stress is vertical. The success rate of testing was hence somewhat lower than expected for this type of hydraulic stress measurement equipment.

The primary reason for the reduced success rate was that multiple fractures were opened or induced. In some cases, sub-horizontal fractures were created when the pressure in the test section was just moderately larger (a few bars) than the theoretical weight of the overburden rock mass. The physical explanation for these fractures is not yet to be determined. We would like to emphasize that the observed sub-horizontal fractures contain very useful information. If a failure criterion for these fractures has been derived, they will probably contribute much to the knowledge of the present state of stress at the Oskarshamn site.

The hydraulic fracturing data indicate a relatively large span for the direction of σ_H (between 146 and 175^{o}N), which averages 161^{o}N.

The induced sub-horizontal fractures as well as the other test sections with multiple fractures cause a significant problem in the normal evaluation of the injection tests. The reason for this is that the opening of a fracture changes the stress field locally, but leaves the normal stress unaffected. Hence, for multiple fractures in the test section, the fracture normal stresses can be unambiguously determined only when the fractures are parallel.

By the appearance of the sub-horizontal fractures on the electrical imaging logs, many fractures seem to have experienced no or very limited propagation fluid percolation, although visual inspection is a somewhat speculative approach. This would imply that, similar to drilling induced fractures (Brudy and Zoback, 1993; Peska and Zoback, 1995; Zoback et al., 2003) or fractures induced by sleeve fracturing technique (Stephansson, 1983a; b), they do not extend far into the rock. If this would be true, they would not distort the stress field as much as fully propagated fractures. Because the effect of the sub-horizontal fractures has not been investigated fully at this stage, HTPF tests that have changed the resistivity image of the aimed pre-existing fracture but that also include sub-horizontal fractures, have been assigned “potentially successful re-opening” in Table 1-1 below. This denomination has also been given the tests with multiple pre-existing fractures in the test section.

For the somewhat surprising result of normal stresses lower than the theoretical vertical stress (Figure 1-1 and Figure 1-2), the most reasonable explanation is that the normal stress corresponds to a sub-horizontal fracture located near the end of the packer element. The fracture is thereby prevented from closing when pressure drops in the interval and affects the shut-in measurement. This is manifested by poor flow back tests that help detect this difficulty. In practice, flow back tests are part of the quality

assurance procedure for selecting completely unambiguous tests. This phenomenon has, as far as we know, not been found elsewhere. This means that it is either specific to the Oskarshamn site (as well as the Forsmark site), or perhaps more likely, it has not been detected before due to limitations in fracture determination methods (which normally involve impression packer technique).

2.2 Borehole specific objectives

The objectives of the hydraulic stress measurements in borehole KLX12A were to (i) decrease uncertainty in data on in-situ state of stress, (ii) increase the understanding of how local geological site conditions may affect the state of stress, and (iii) provide input for site descriptive modelling on the state of stress at the site.

The borehole specific objectives involved:

- Identify what types of fractures that seem feasible for HTPF.
- Identify possible decoupling zones along the borehole.
- Determine the state of stress at the borehole location, from 100 m depth and down to the well bottom.

These objectives and how they have been fulfilled are described below.

2.2.1 Identification of fractures suitable for HTPF testing

The effectiveness of the HTPF tool is clear when looking at the result of the reconnaissance and post-logs. A large number of electrically conductive features exist in the boreholes, and they are repeated for each new log performed, which implied that they may be opened using a suitable injection testing strategy. The HTPF tool was also successful with respect to post-log images, which also include the entire packer sections. Indeed, this feature has proven most valuable given the very common observation of packer induced fractures.

2.2.2 Identify possible decoupling zones along the borehole.

The electrical imaging tool is very useful for identification of possible decoupling zones. Such zones are clearly displayed as electrical anomalies (red coloured in the logs).

2.2.3 Determine the state of stress from c. 100-1000 mbl

The stress determination are undertaken in the main report.

APPENDIX 1

WELL AZIMUTH, WELL INCLINATION, AND MAGNETIC INCLINATION IN KLX12A

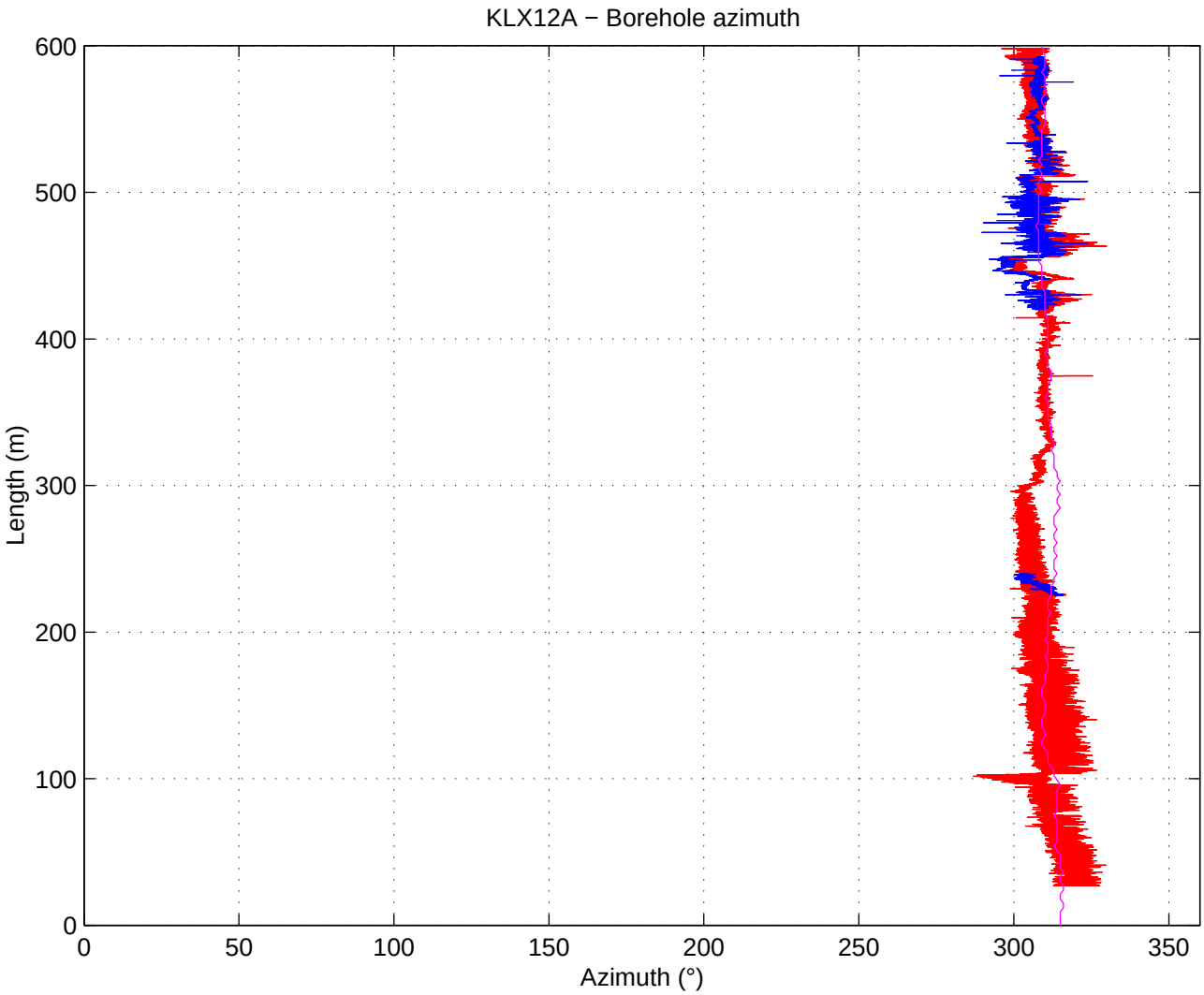
KLX12A − Borehole azimuth
Length (m)
Azimuth (°)
0
100
200
300
400
500
600
0
50
100
150
200
250
300
350

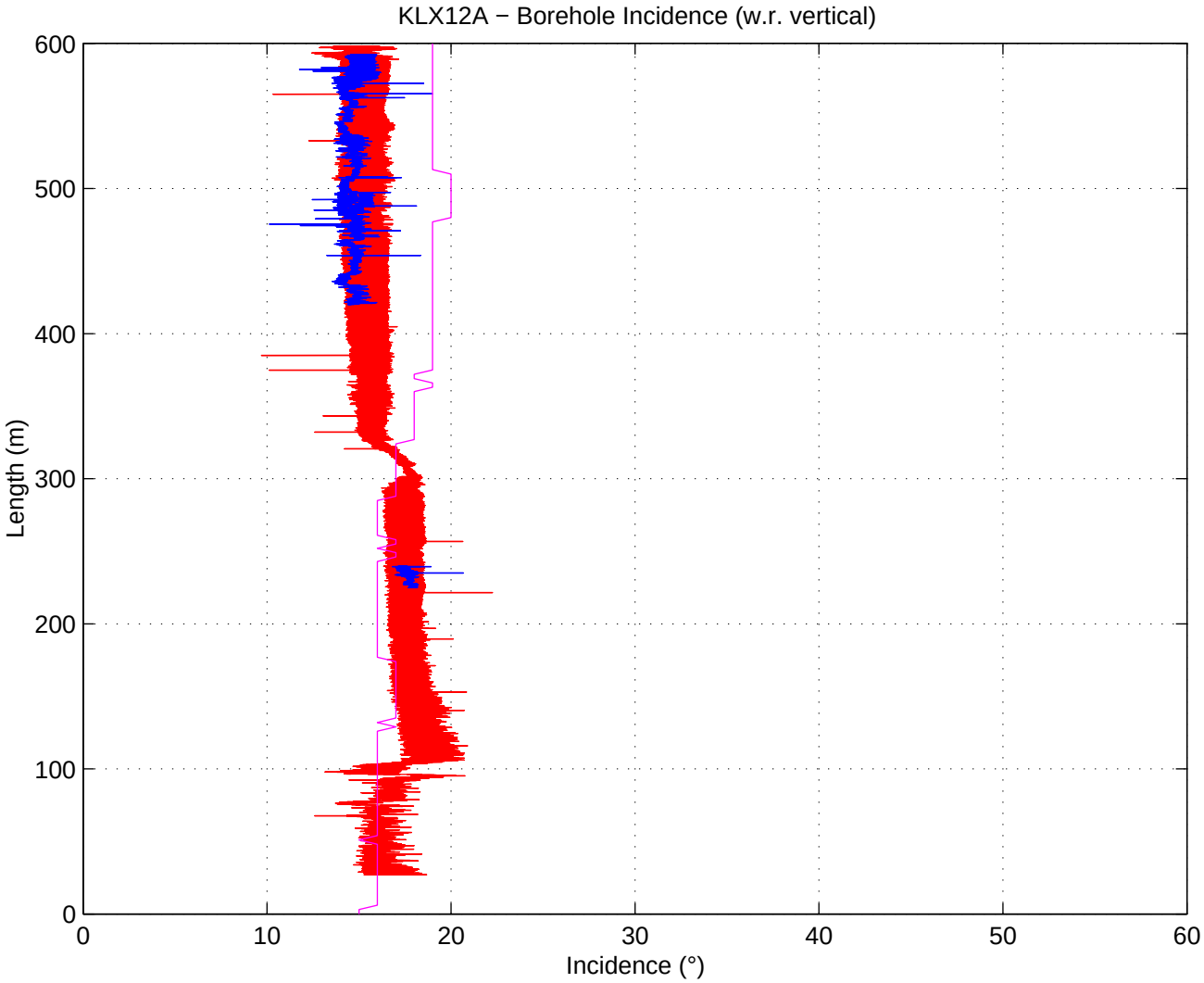
KLX12A − Borehole Incidence (w.r. vertical)
Length (m)
Incidence (°)
0
100
200
300
400
500
600
0
10
20
30
40
50
60

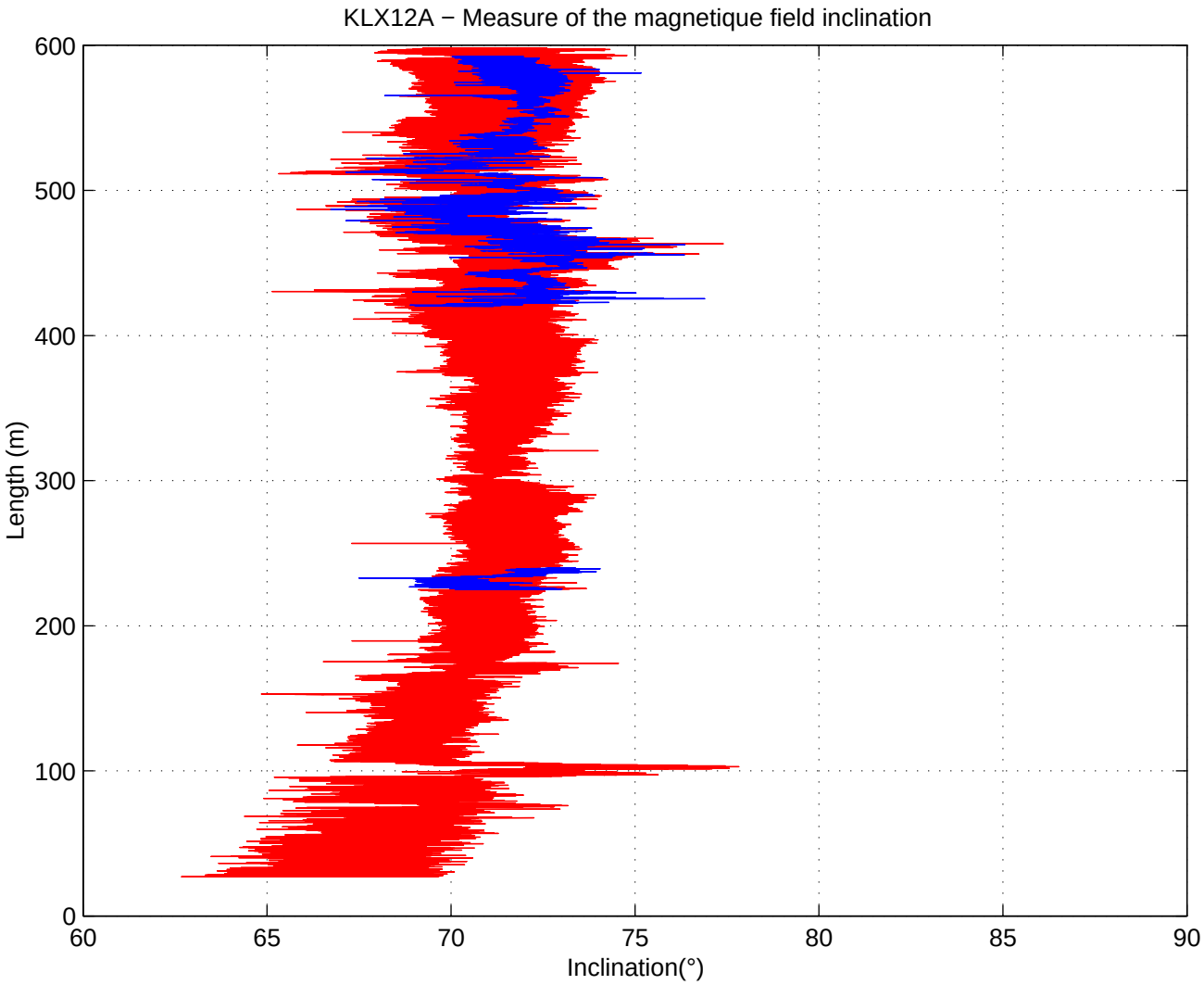
KLX12A − Measure of the magnetique field inclination
Length (m)
Inclination(°)
0
100
200
300
400
500
600
60
65
70
75
80
85
90

APPENDIX 2

CALIBRATION CURVES FOR PRESSURE TRANSDUCERS AND FLOW METER

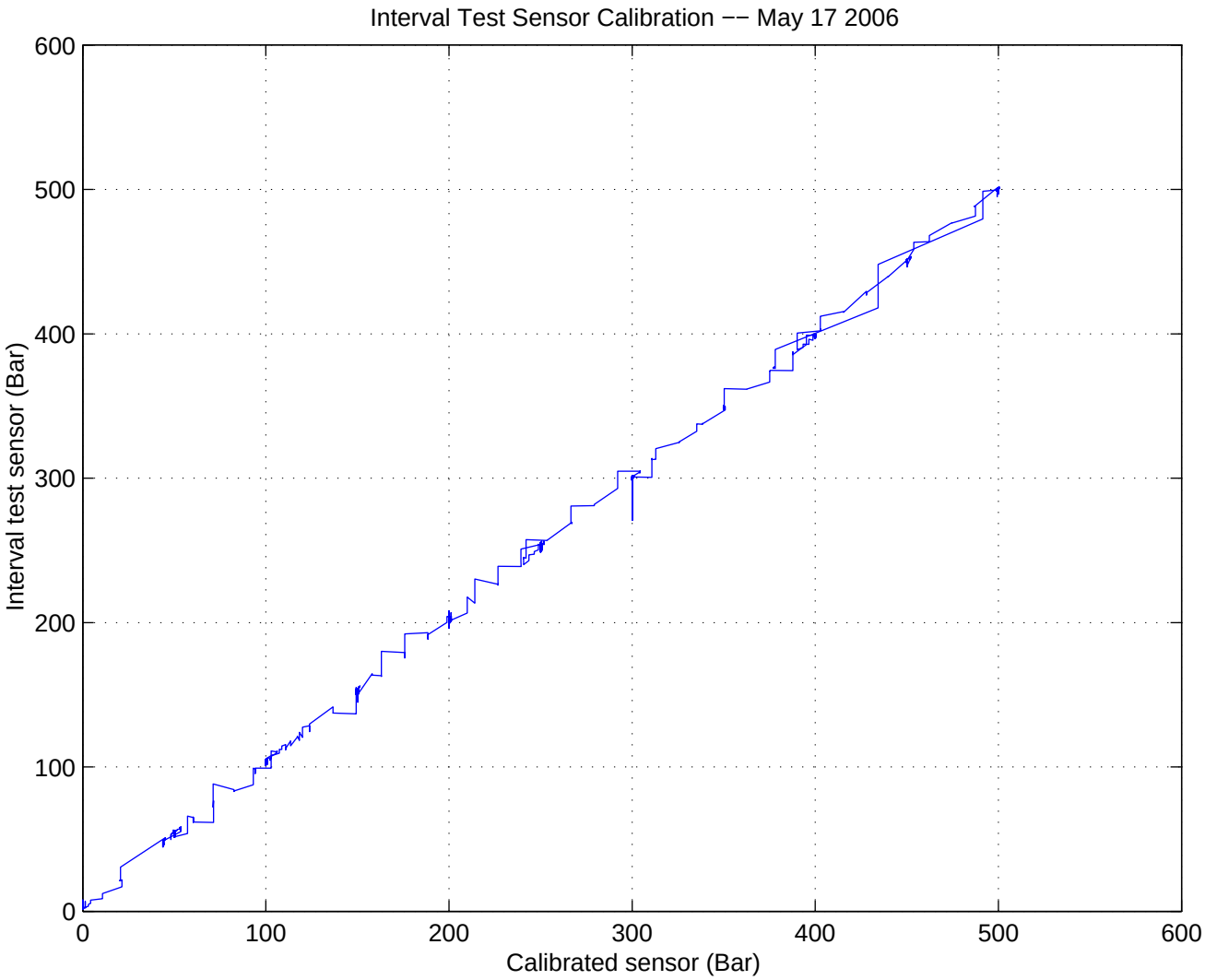
Interval Test Sensor Calibration −− May 17 2006
Interval test sensor (Bar)
Calibrated sensor (Bar)
0
100
200
300
400
500
600

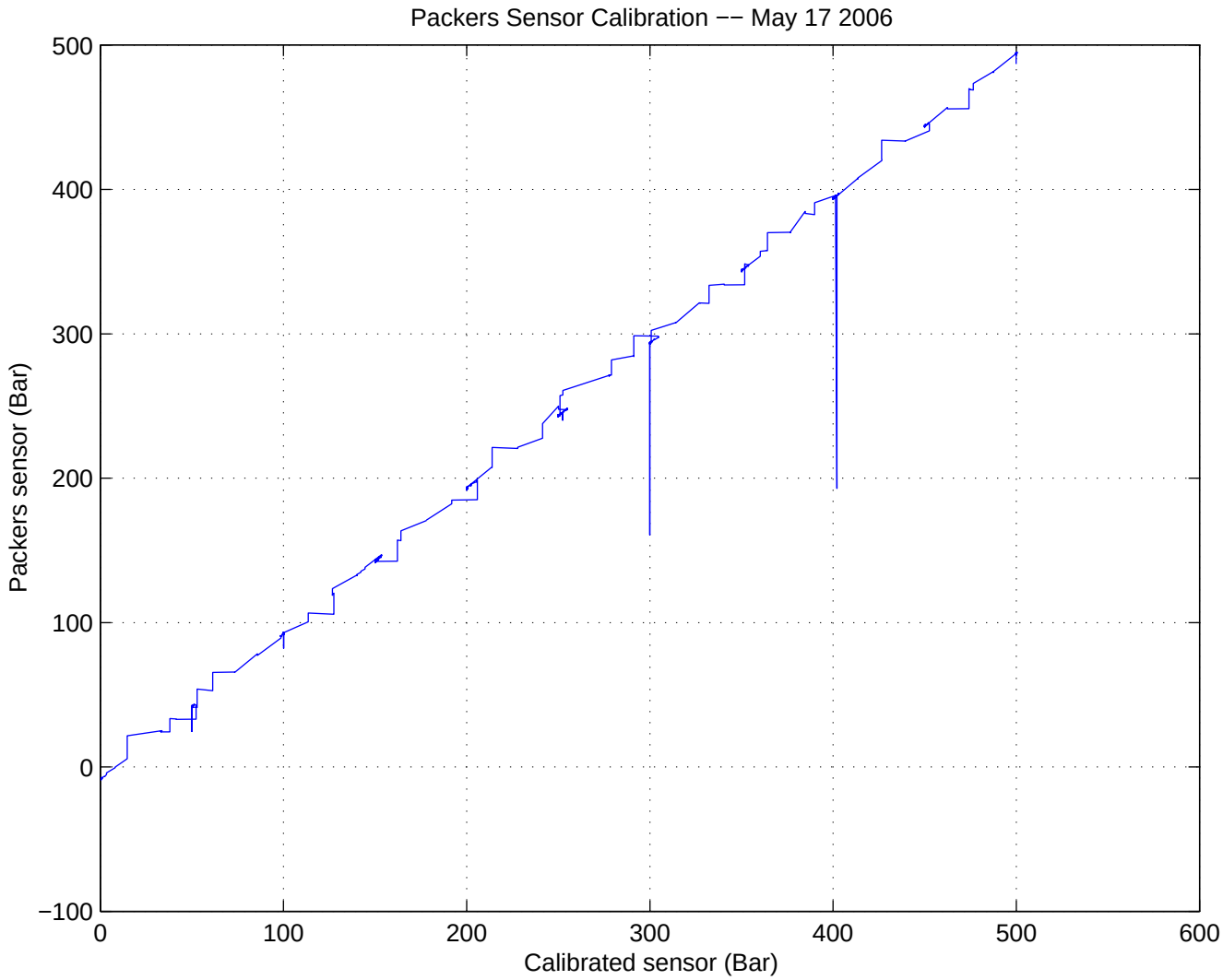
Packers Sensor Calibration −− May 17 2006
Packers sensor (Bar)
Calibrated sensor (Bar)
500
400
300
200
100
0
−100
0
100
200
300
400
500
600

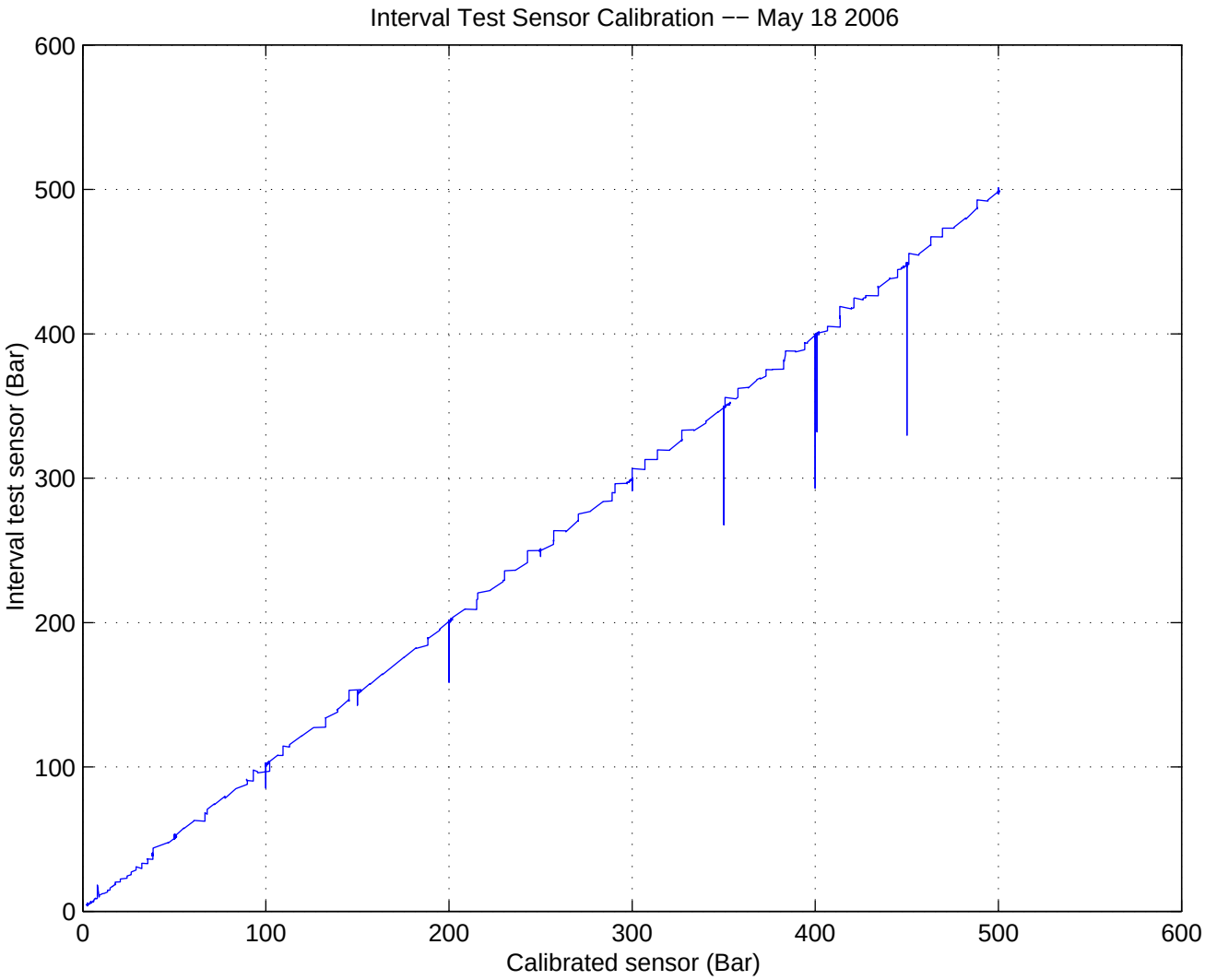
Interval Test Sensor Calibration −− May 18 2006
Interval test sensor (Bar)
Calibrated sensor (Bar)
0
100
200
300
400
500
600

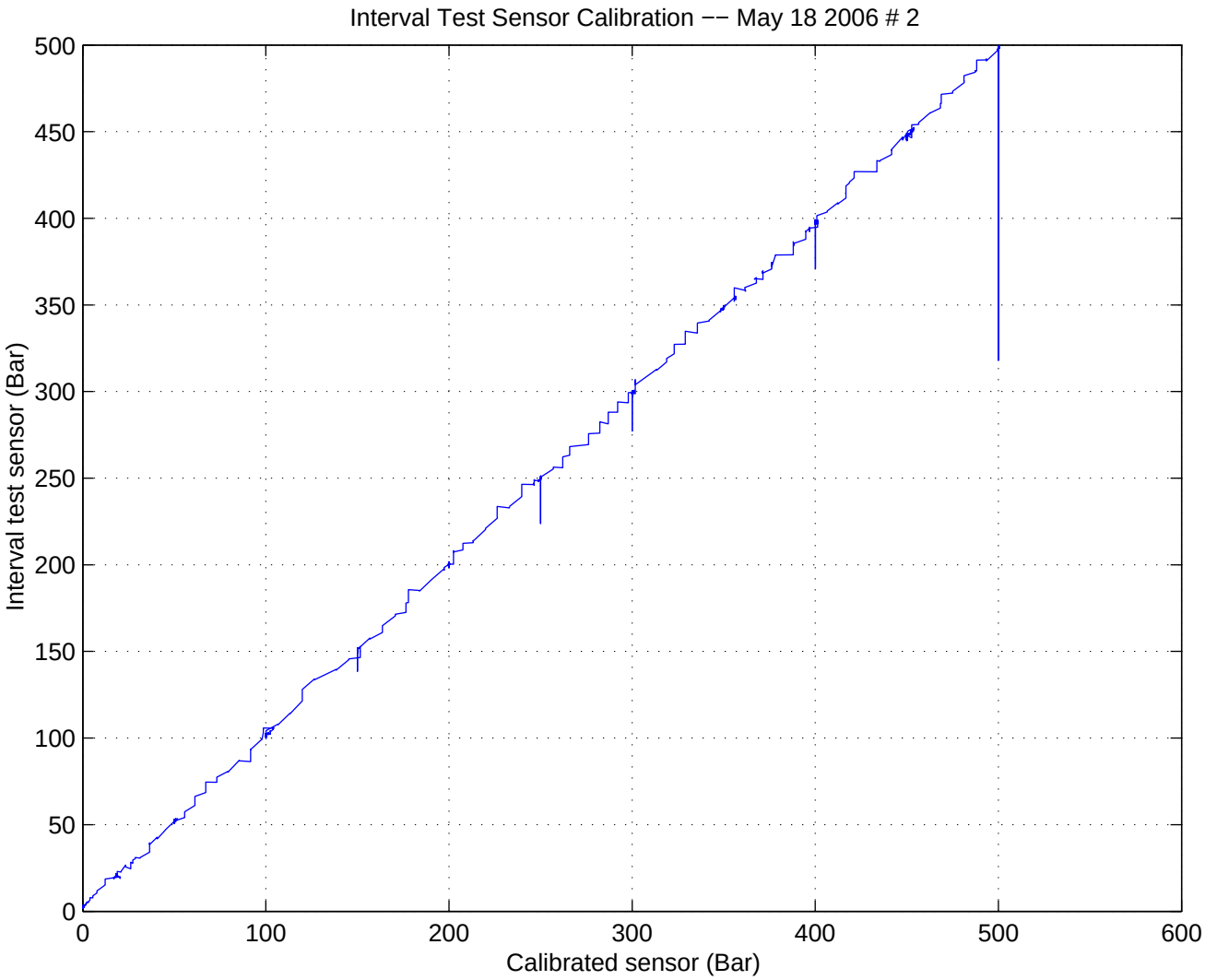
Interval Test Sensor Calibration −− May 18 2006 # 2
Interval test sensor (Bar)
Calibrated sensor (Bar)
0
50
100
150
200
250
300
350
400
450
500
0
100
200
300
400
500
600

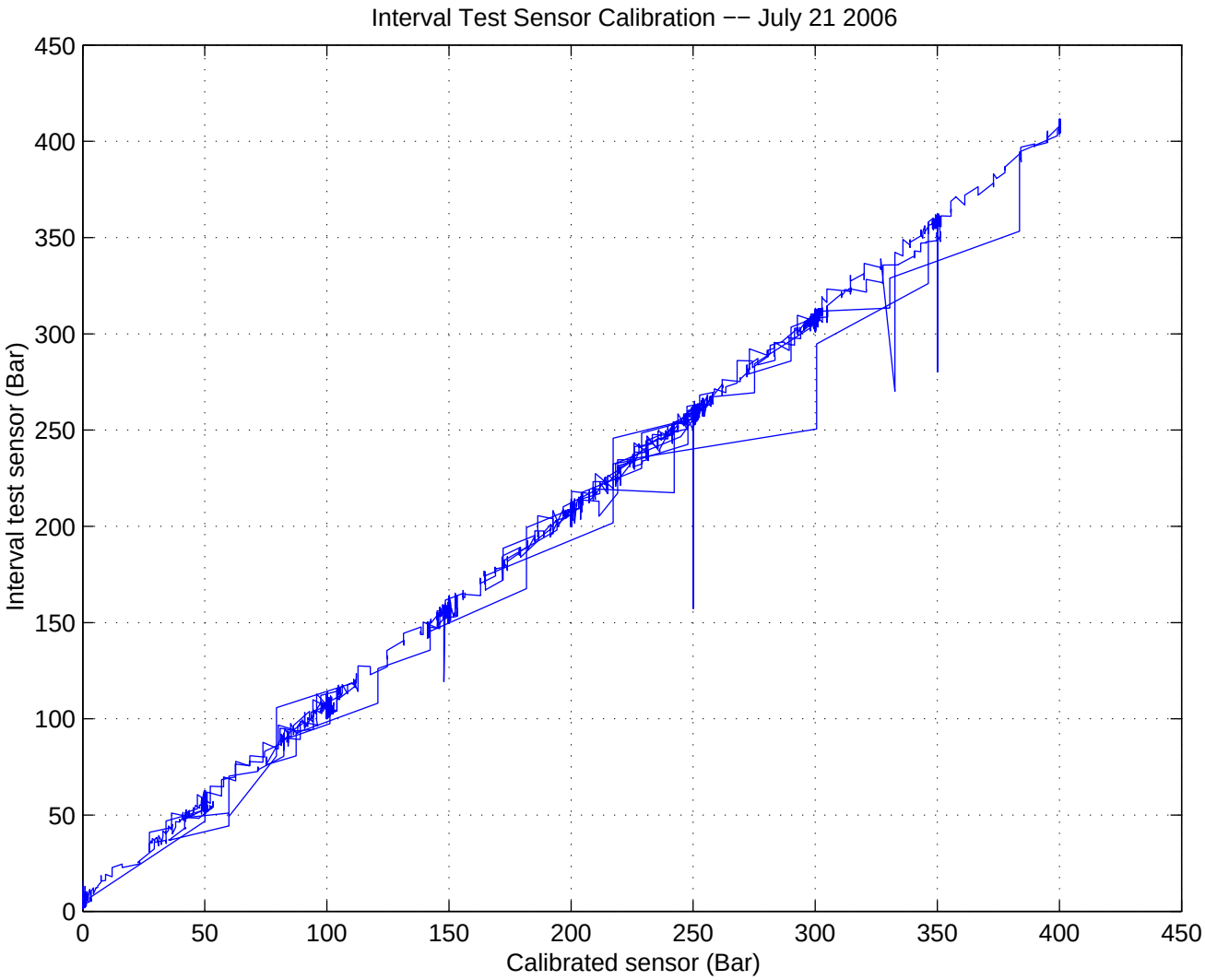
Interval Test Sensor Calibration −− July 21 2006
Interval test sensor (Bar)
Calibrated sensor (Bar)
0
50
100
150
200
250
300
350
400
450

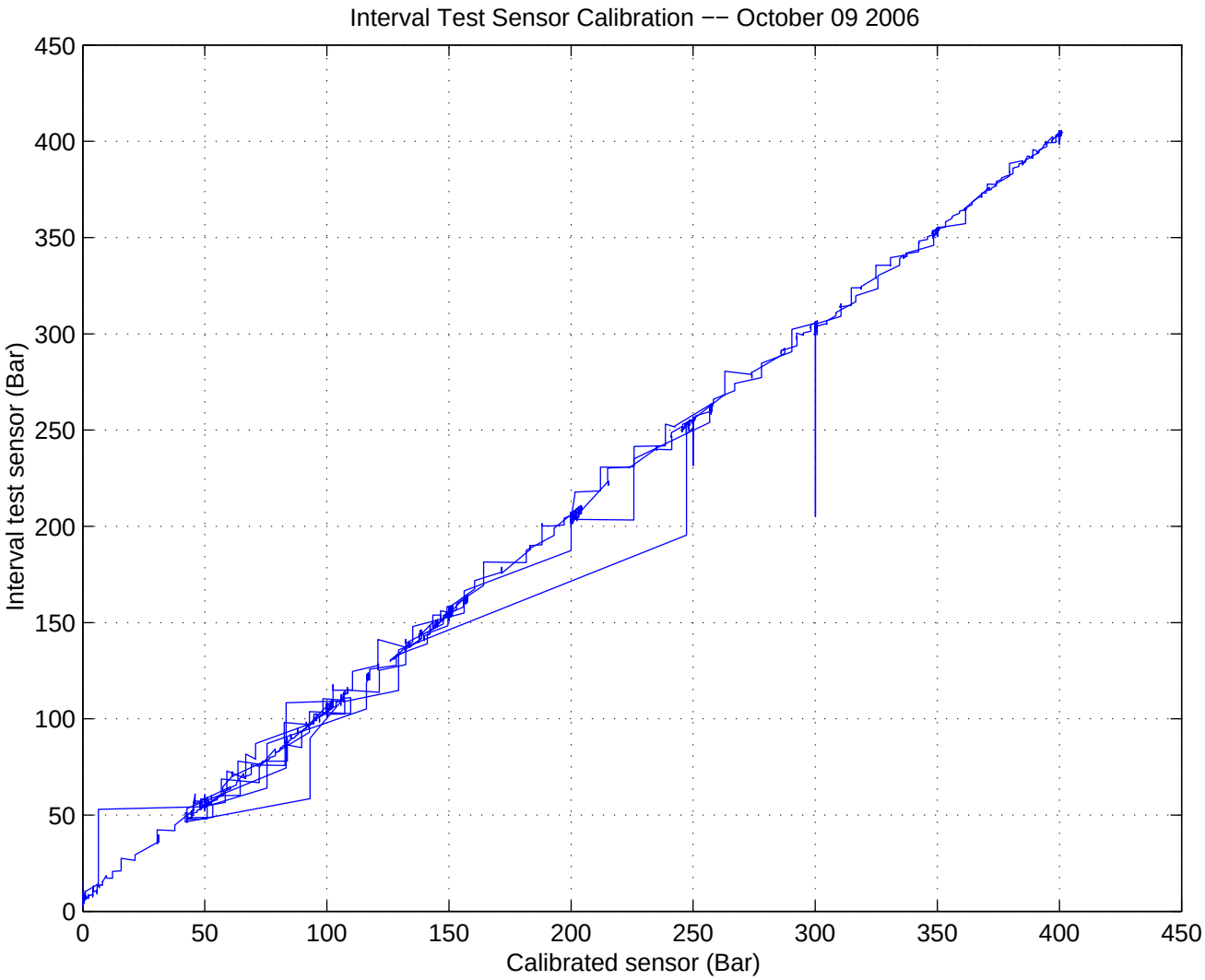
Interval Test Sensor Calibration −− October 09 2006
Interval test sensor (Bar)
Calibrated sensor (Bar)
0
50
100
150
200
250
300
350
400
450

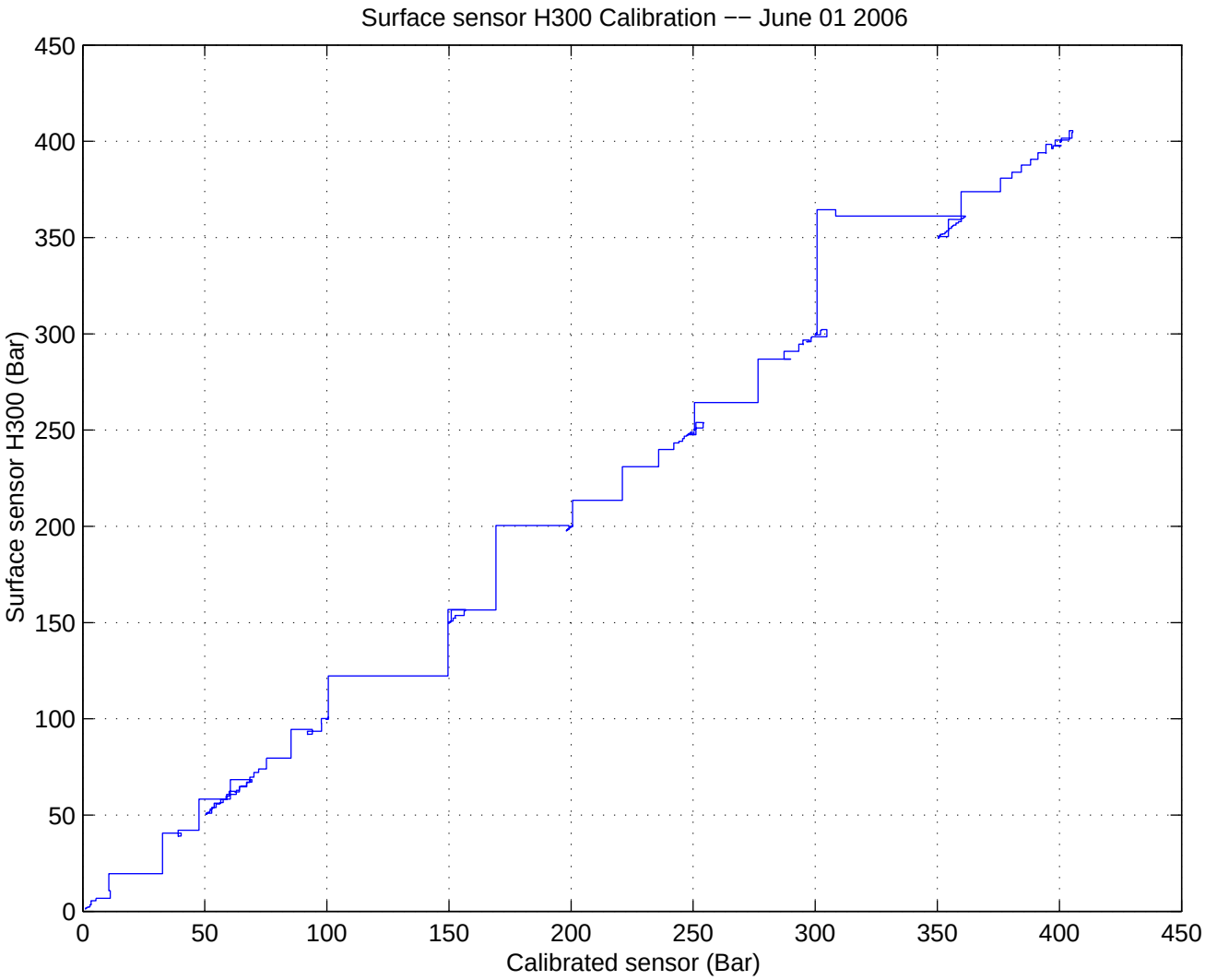
Surface sensor H300 Calibration −− June 01 2006
Surface sensor H300 (Bar)
Calibrated sensor (Bar)
0
50
100
150
200
250
300
350
400
450

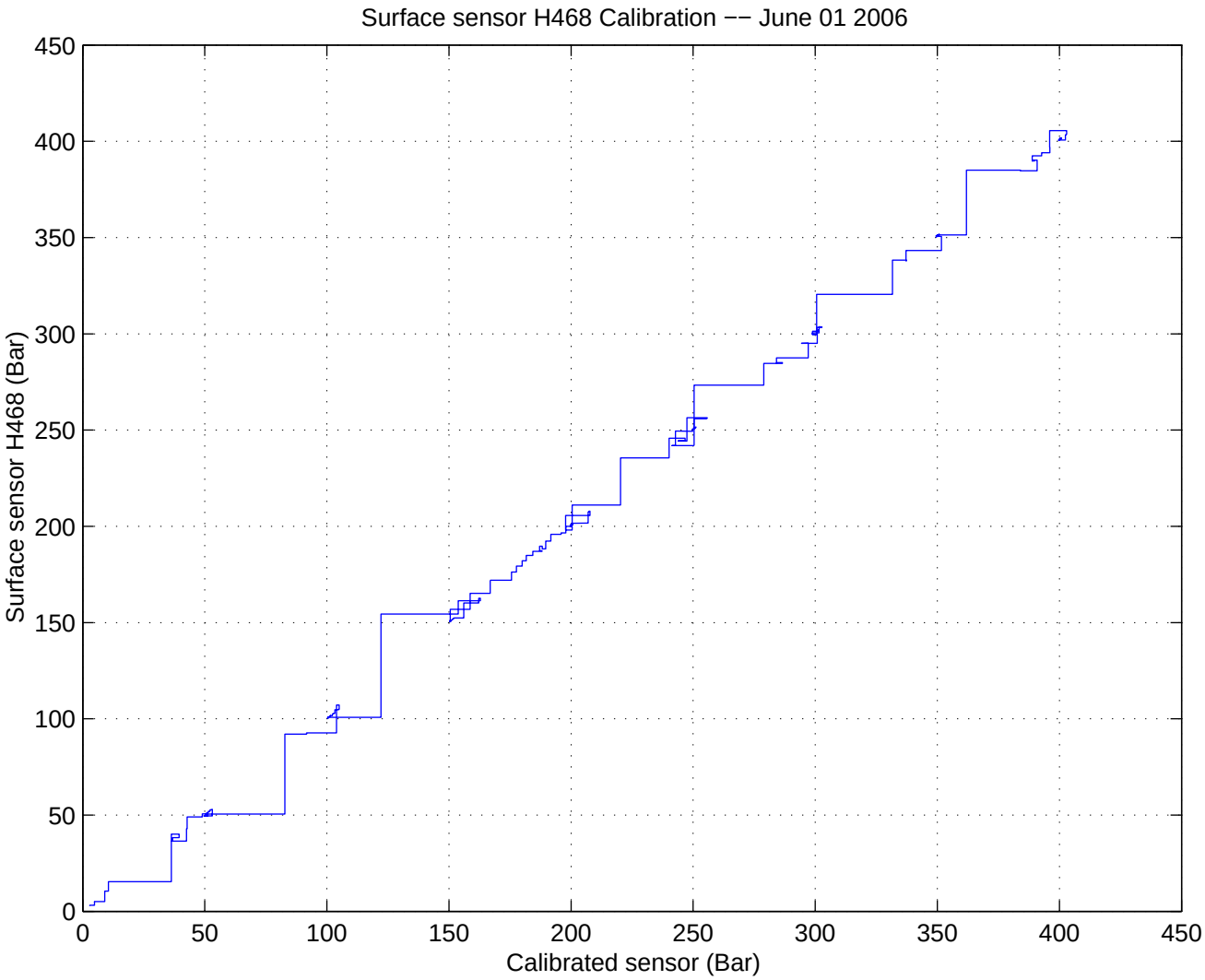
Surface sensor H468 Calibration −− June 01 2006
Surface sensor H468 (Bar)
Calibrated sensor (Bar)
0
50
100
150
200
250
300
350
400
450

Report of Calibration

Flow rate sensor

The flow rate sensor used to the measurement of flow rate are calibrated and tested with BetaGauge 311 Calibrator (Martel Electronics). This calibrator is calibrated and tested on December 20, 2005 by Martel electronics (Calibration Report Number 08444812202005 9043035). Others instruments used for calibration : precision scale and stopwash.

Instruments calibrated

Sensor

Manufacturer :	Micro Motion Rosemout	Calibration date :	June 17, 2006
Model :	DH012S (D12), 5kg/min, 393bars	Report date :	June 27, 2006
Serial number :	M206446-2	Temperature :	30°C
Flow accuracy :	±2% of rate ±0.001 (kg/min) zero stability 0.001 kg/min (20°C)		

Transmitter

Manufacturer :	Micro Motion Rosemout	Calibration date :	June 17, 2006
Model :	RFT 9729 (output 4-20mA)	Report date :	June 27, 2006
Serial number :	M20854-19	Temperature :	30°C
Flow accuracy :	±0.004g/cm^3 (included sensor) ±3.10^{-5} g/cm^3/°C (transmitter only)		

Instruments used for calibration

- Transmitter calibrator

Manufacturer :	Martel Corporation	Calibration date :	December 20, 2005
Model :	311 10K psi	Report date :	December 20, 2005
Serial number :	9043035	Temperature :	23.1°C
Current accuracy :	±0.015% of reading ±0.002mA Add ±0.002% FS/°C (outside of 15°C to 35°C)		

- Precision scale

Manufacturer :	Terraillon Electronic	Calibration : controlled by Terraillon
Model :	Quartz 3kg	
Serial number :	-	
Accuracy :	1g for 0 to 1.2kg 2g for 1.2kg to 3kg	

- Stopwash

Manufacturer :	Casio	Calibration : controlled by Casio
Model :	W-102	
Serial number :	2684	
Accuracy :	0.01s	

Calibrated by Christophe BRUNET, IPGP

INSTITUT DE PHYSIQUE DU GLOBE DE PARIS
Département de Sismologie
Laboratoire de Mécanique des Roches
Tour 24, 4 place Jussieu, 75252 Paris cedex05, France

Tél : (33) (0)1 44 27 48 87 Fax : (33) (0)1 44 27 38 94 brunet@ipgp.jussieu.fr

D a t a s

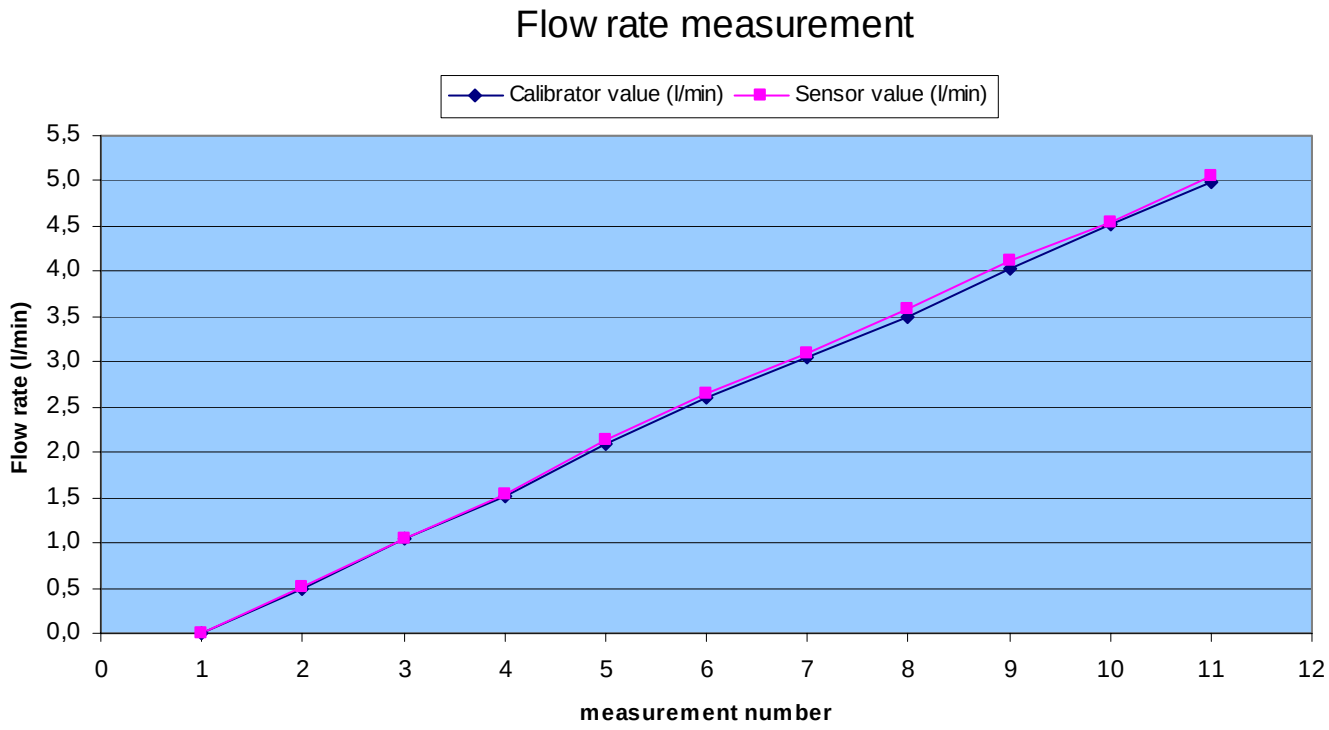

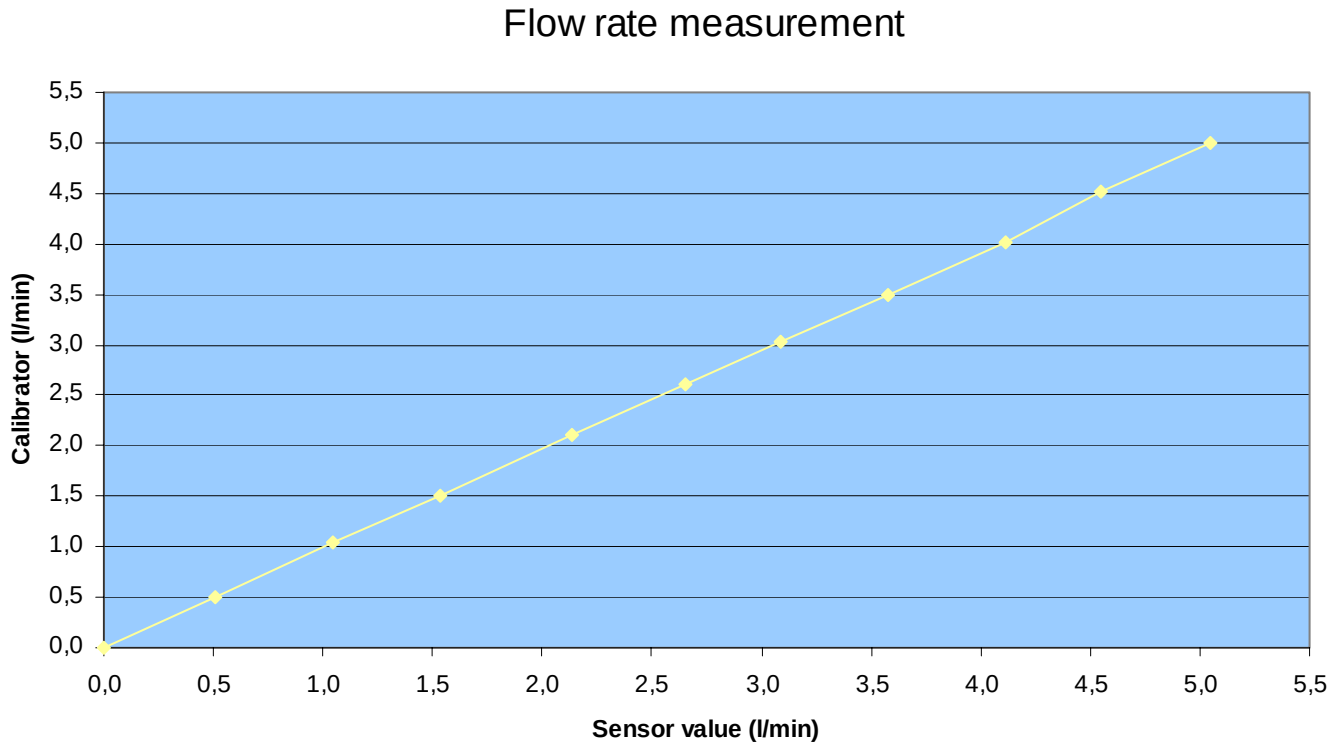

Calibration factor = 3.25 l/min/V (electric resistance used R= 500 ohm)

I N S T I T U T D E P H Y S I Q U E D U G L O B E D E P A R I S
D é p a r t e m e n t d e S i s m o l o g i e
L a b o r a t o i r e d e M é c a n i q u e d e s R o c h e s
T o u r 2 4 , 4 p l a c e J u s s i e u , 7 5 2 5 2 P a r i s c e d e x 0 5 , F r a n c e

T é l : (3 3) (0) 1 4 4 2 7 4 8 8 7 F a x : (3 3) (0) 1 4 4 2 7 3 8 9 4 b r u n e t @ i p g p . j u s s i e u . f r

Difference between sensor and calibrator values (l/min)

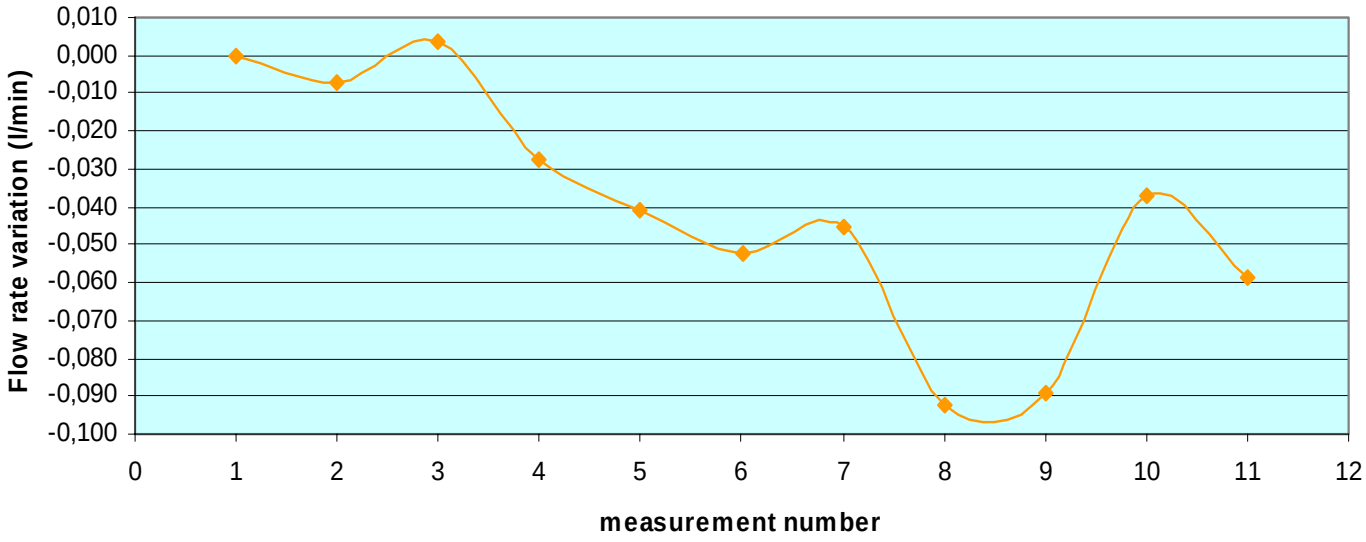

Difference between sensor and calibrator values (%)

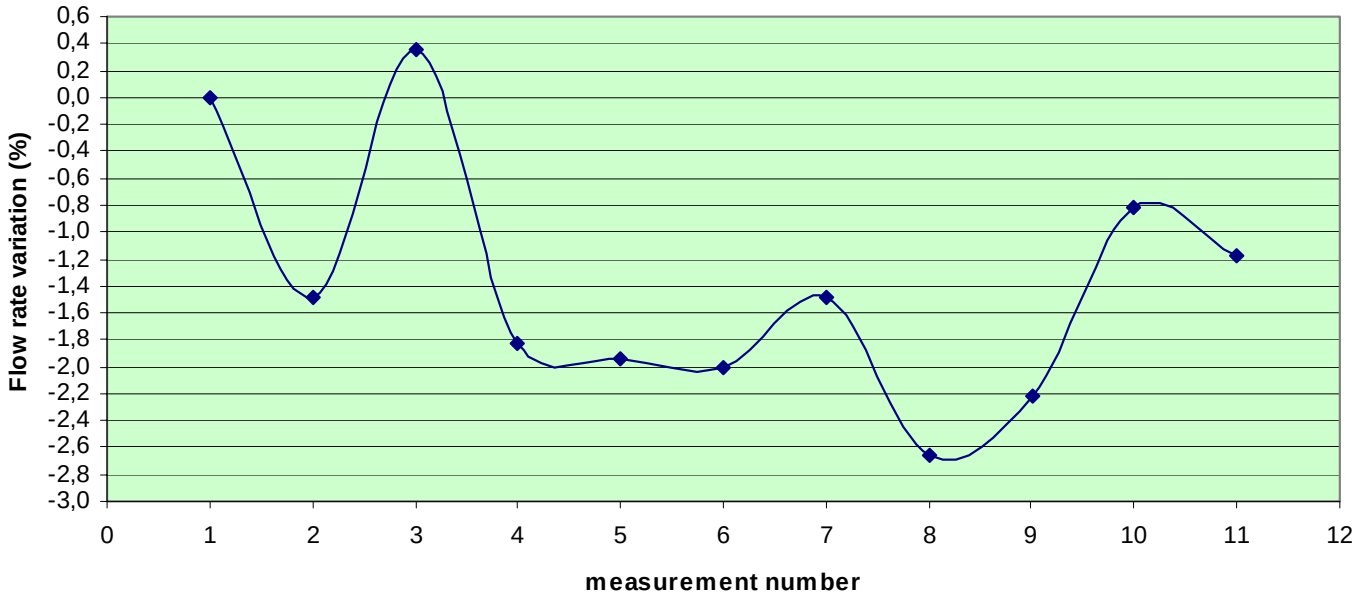

Value (%) = (difference between sensor and calibrator values)*100/ (calibrator value)

INSTITUT DE PHYSIQUE DU GLOBE DE PARIS
Département de Sismologie
Laboratoire de Mécanique des Roches
Tour 24, 4 place Jussieu, 75252 Paris cedex05, France

Tél : (33) (0)1 44 27 48 87 Fax : (33) (0)1 44 27 38 94 brunet@ipgp.jussieu.fr

APPENDIX 3

RECONNAISSANCE LOG FOR BOREHOLE KLX12A

KLX12A -- Reference Log # 1

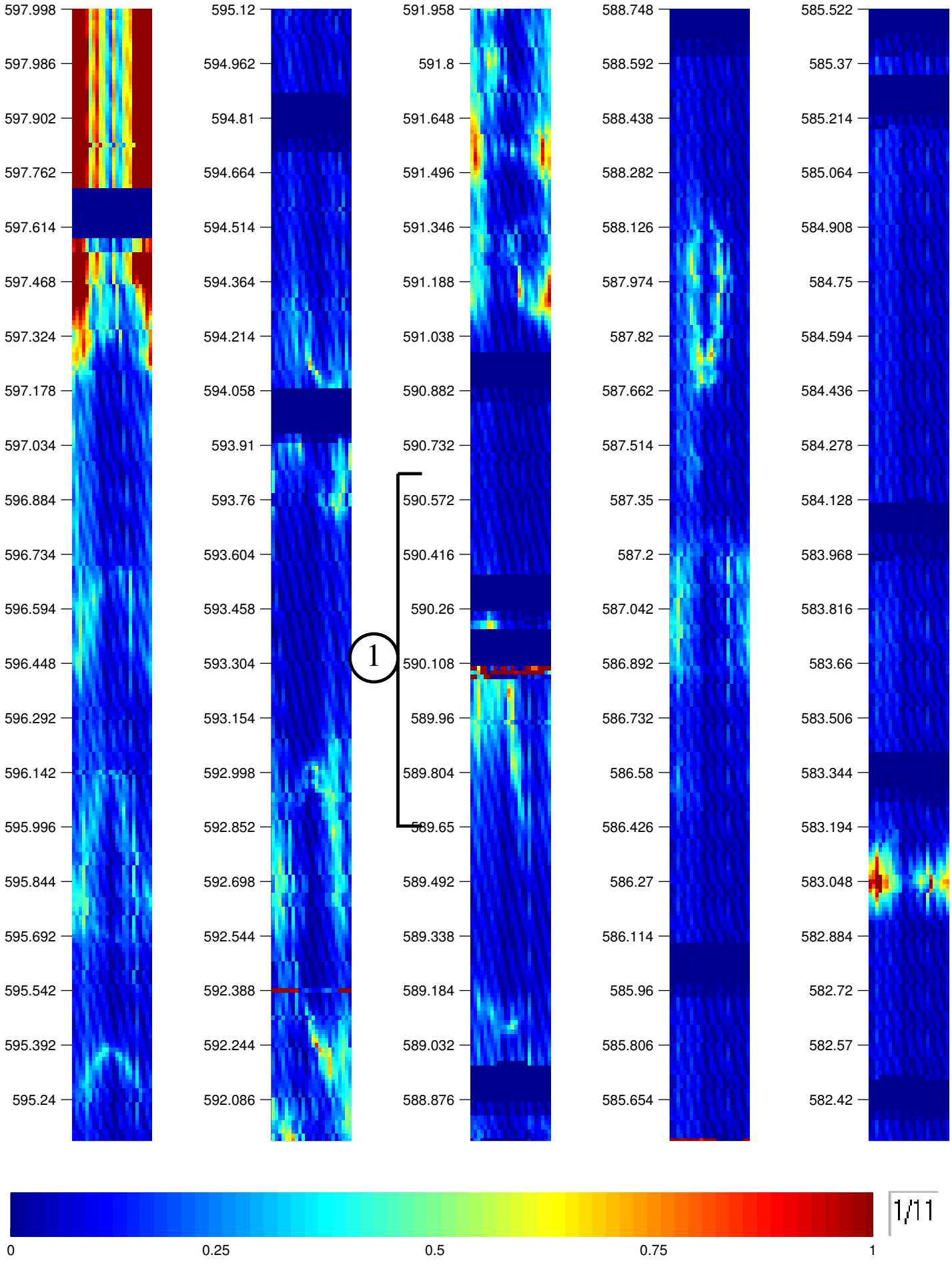

KLX12A -- Reference Log # 1

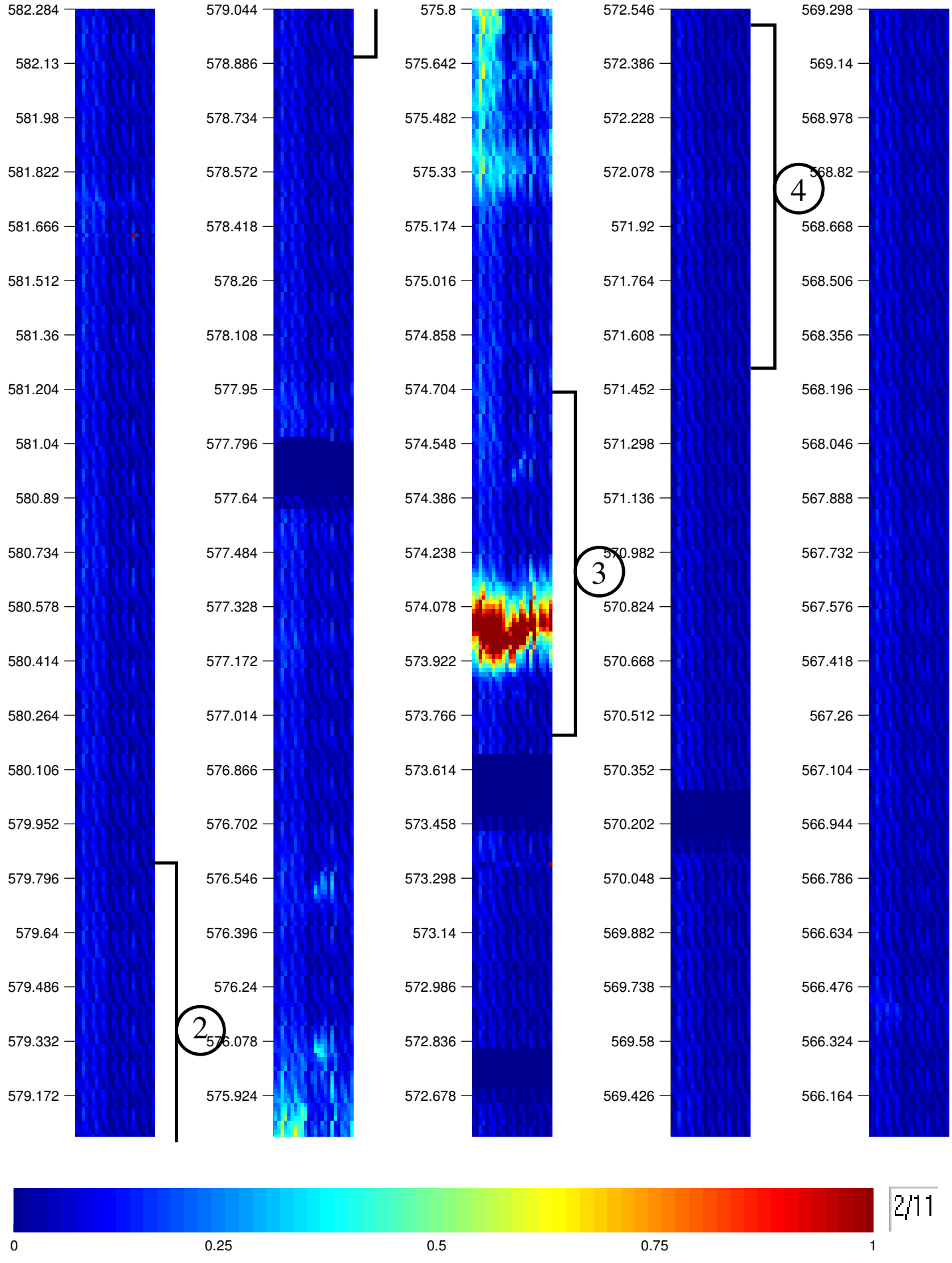

KLX12A -- Reference Log # 1

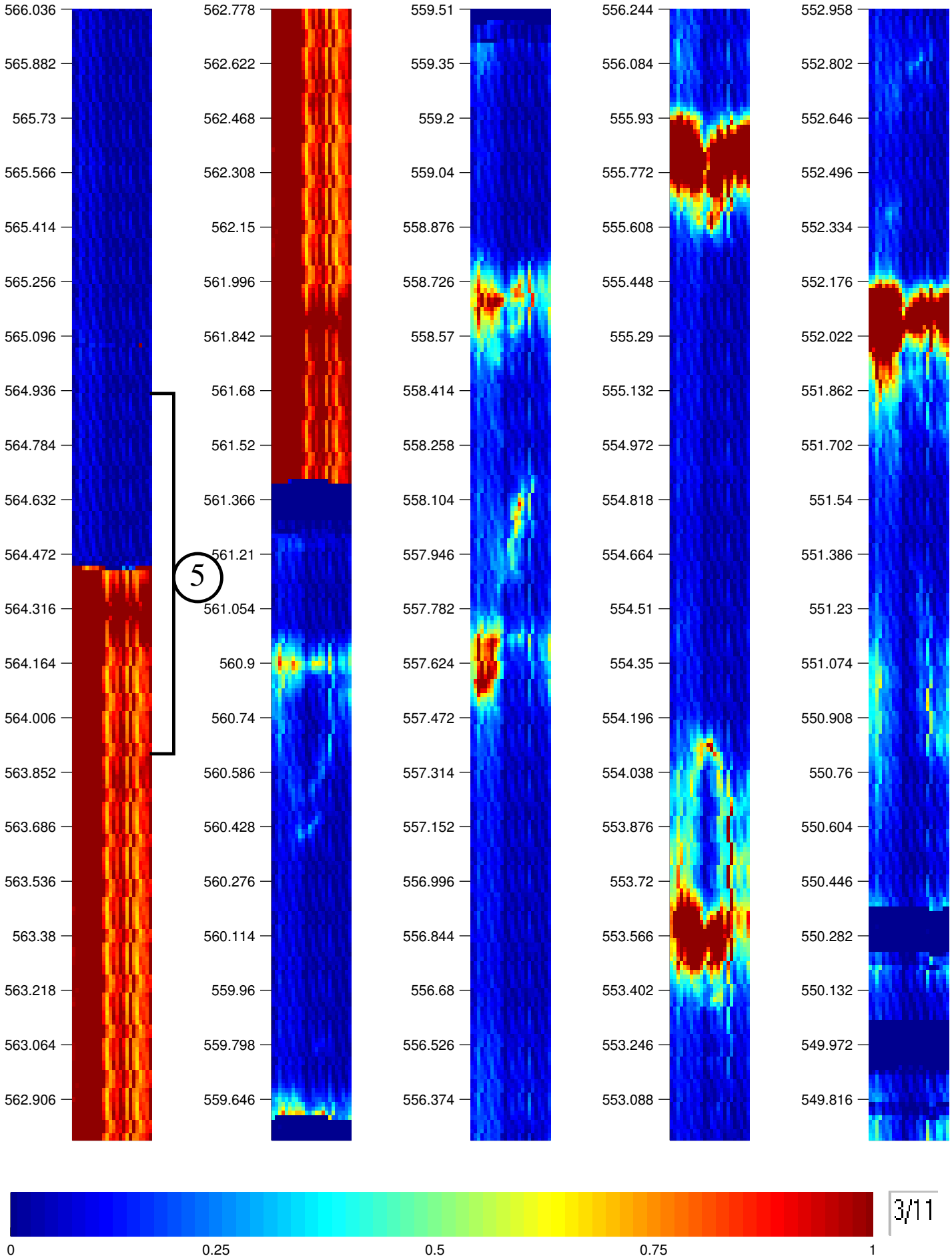

KLX12A -- Reference Log # 1

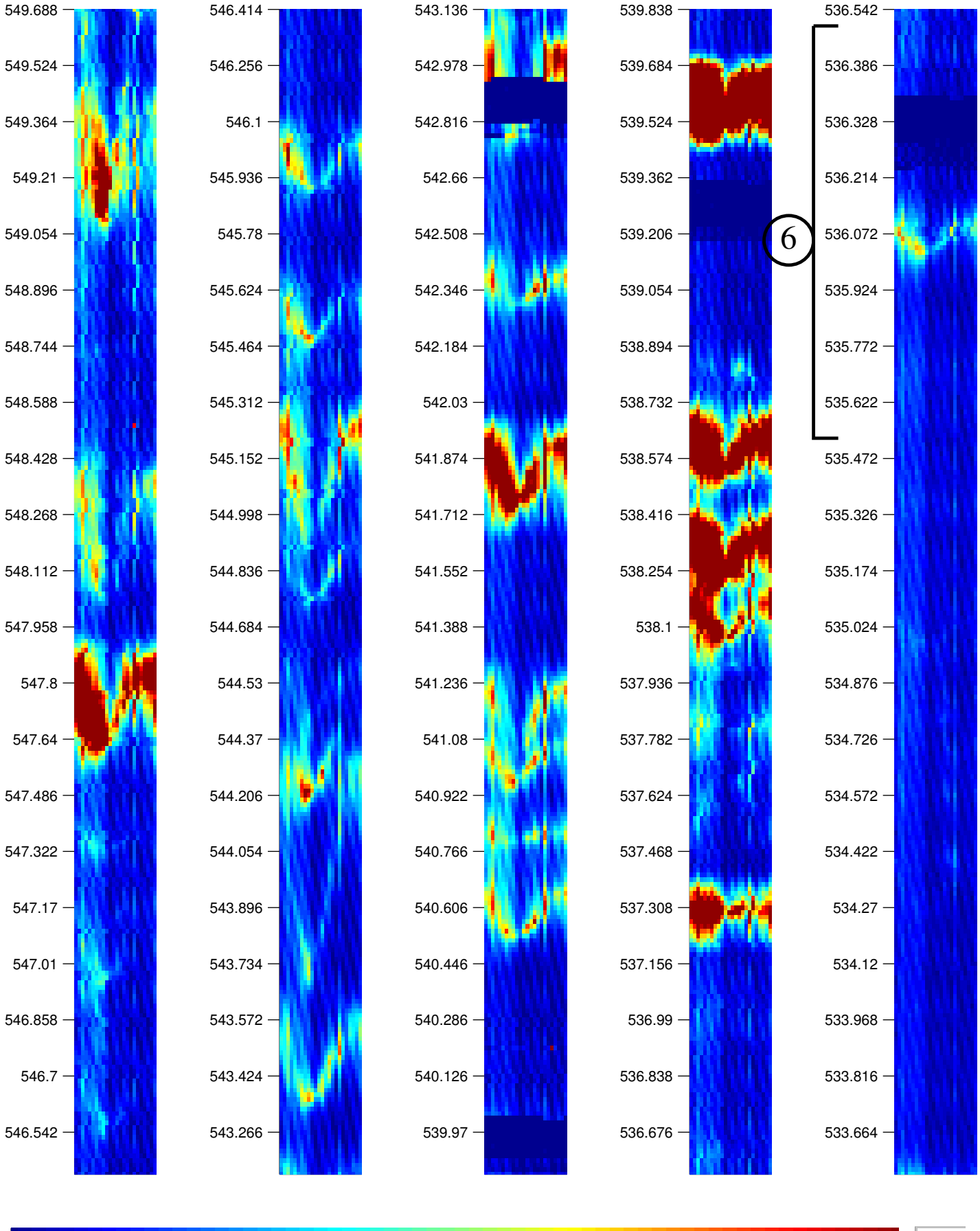

KLX12A -- Reference Log # 1

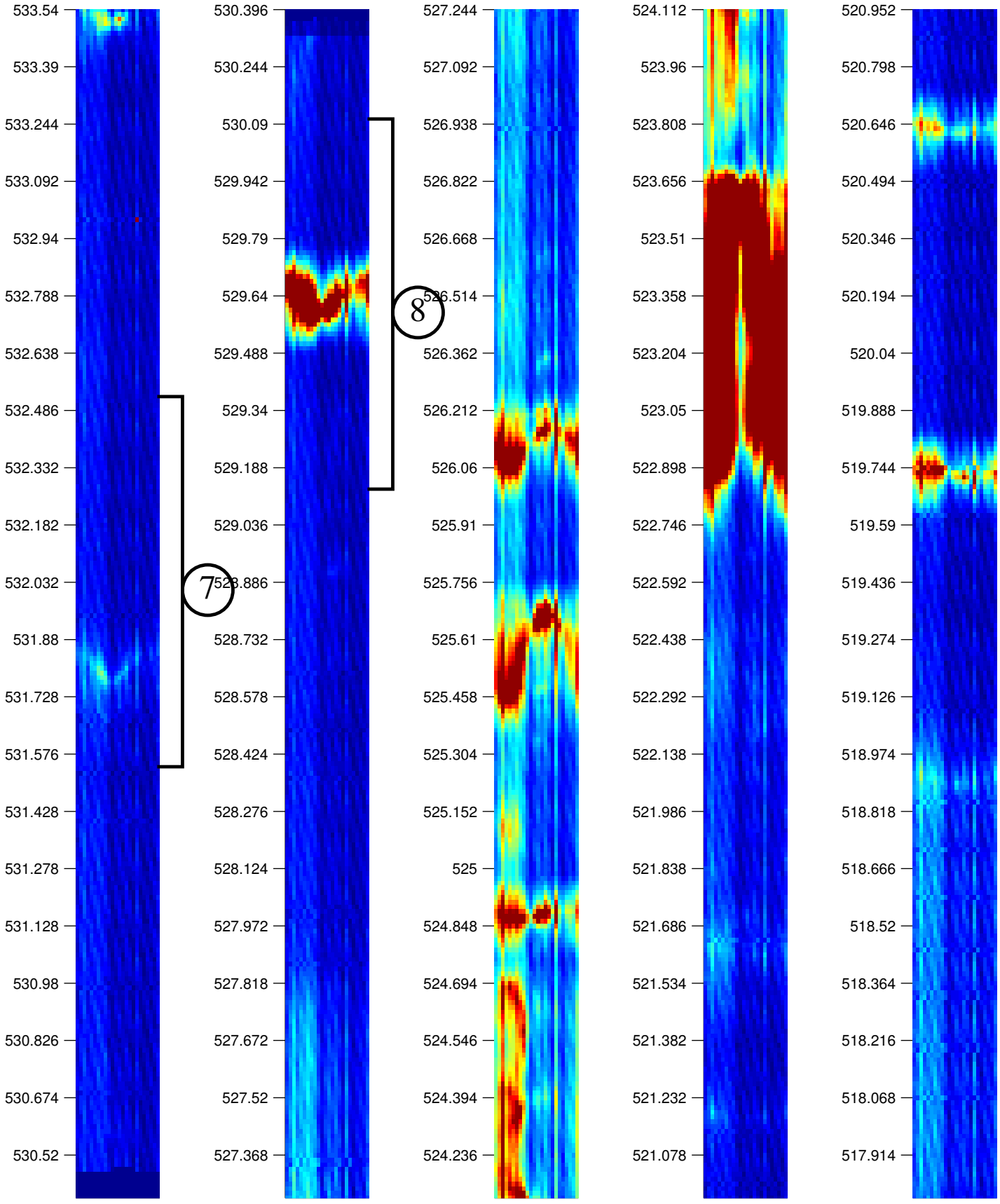

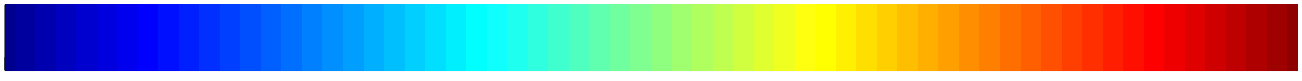

KLX12A -- Reference Log # 1

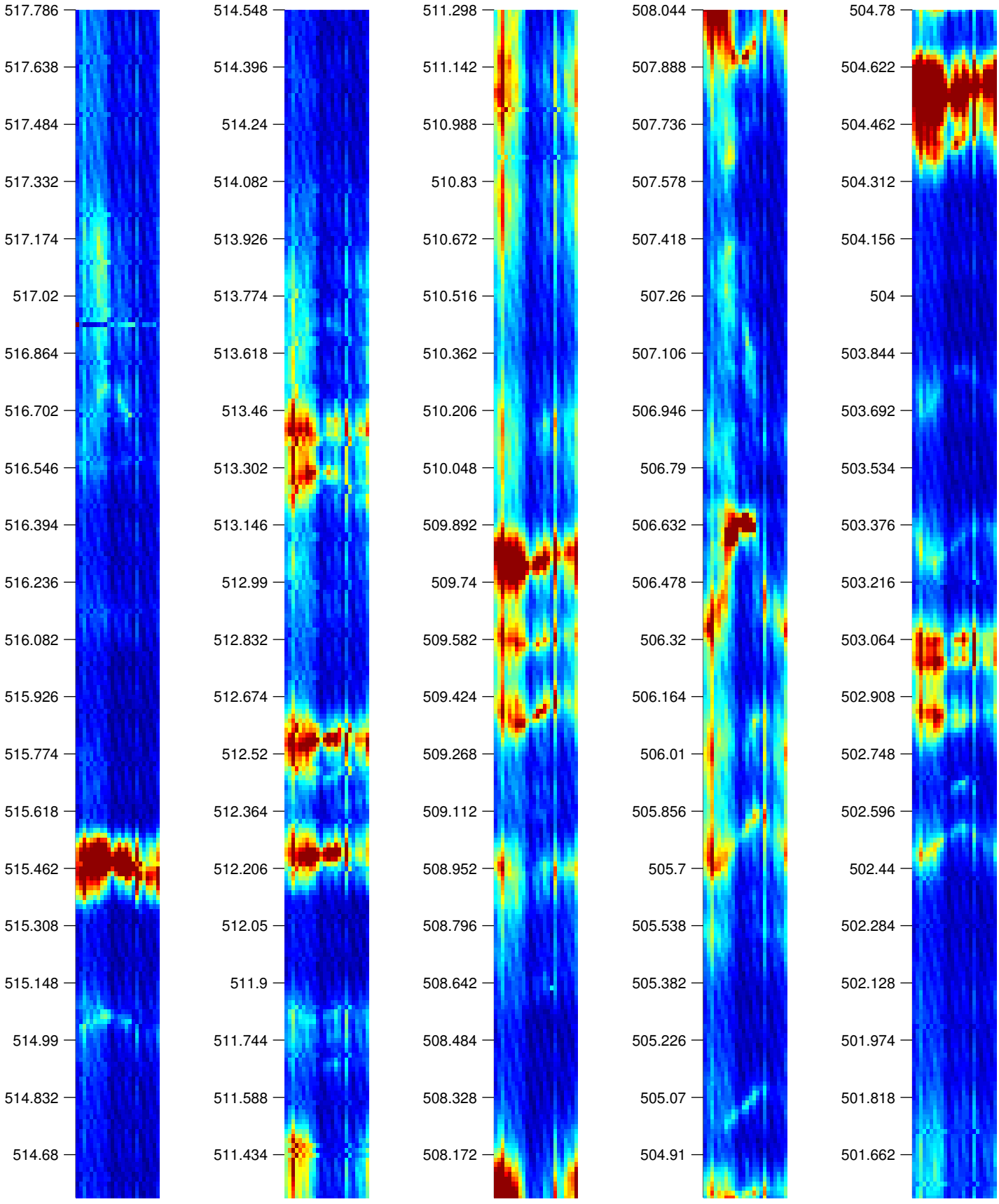

KLX12A -- Reference Log # 1

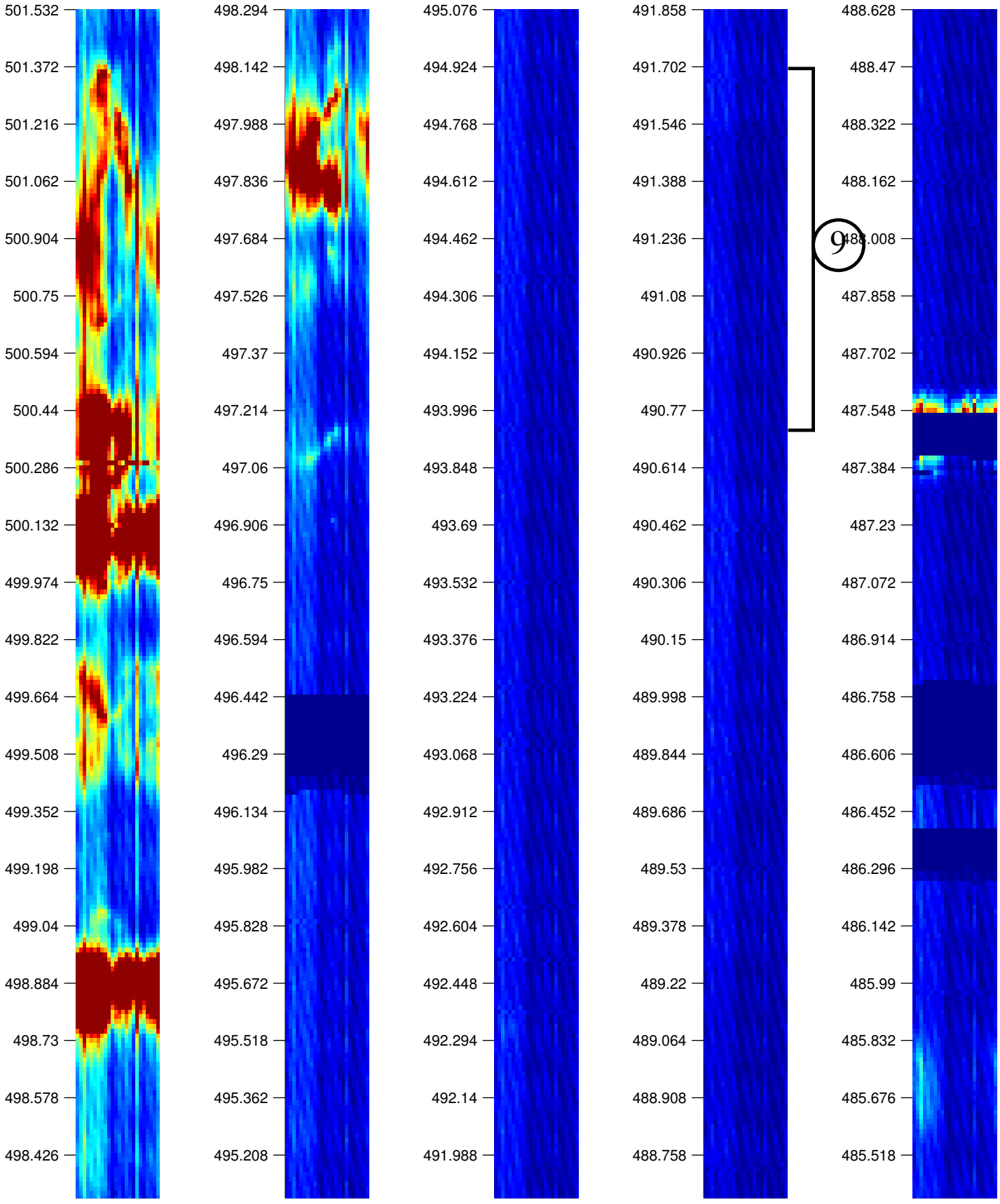

KLX12A -- Reference Log # 1

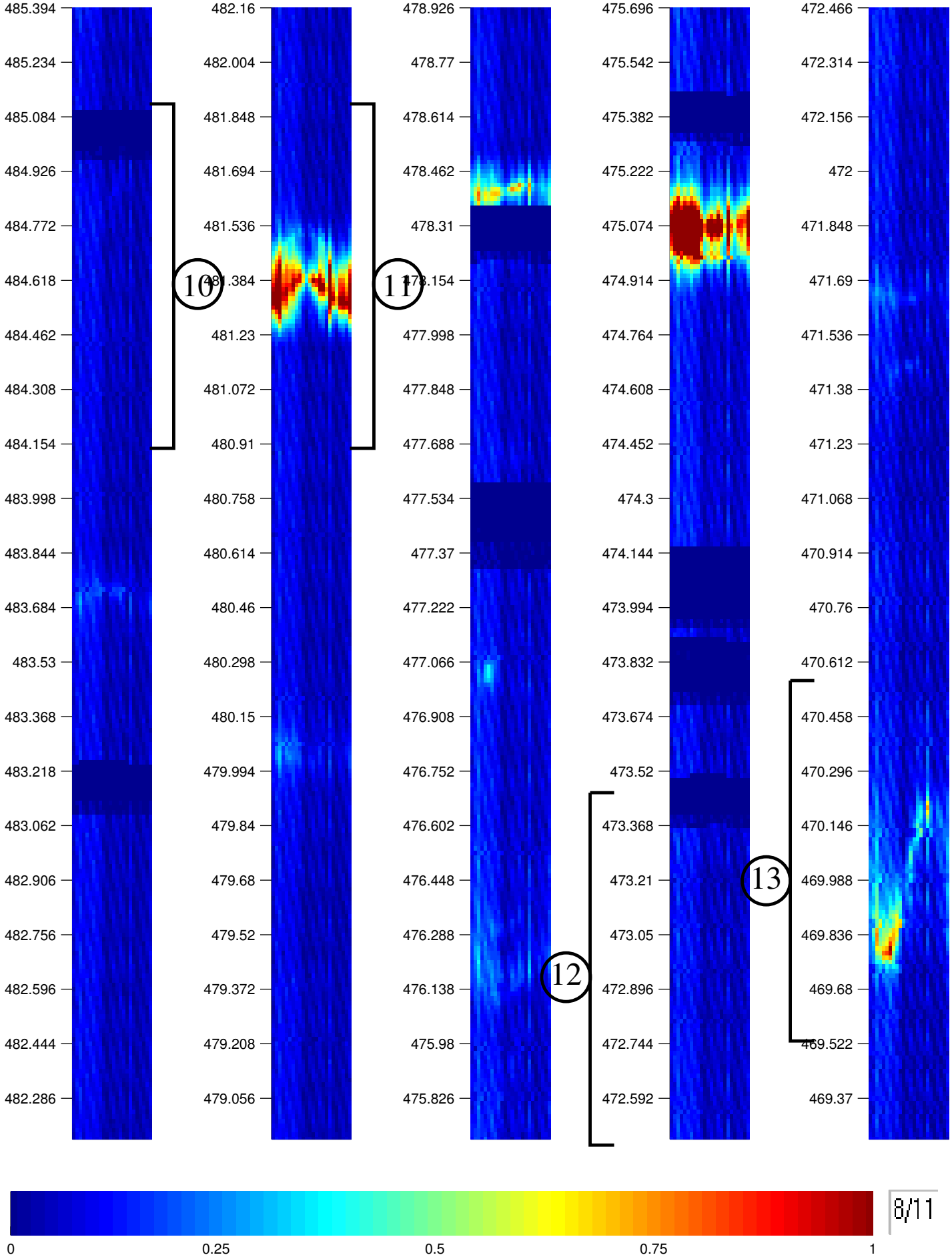

KLX12A -- Reference Log # 1

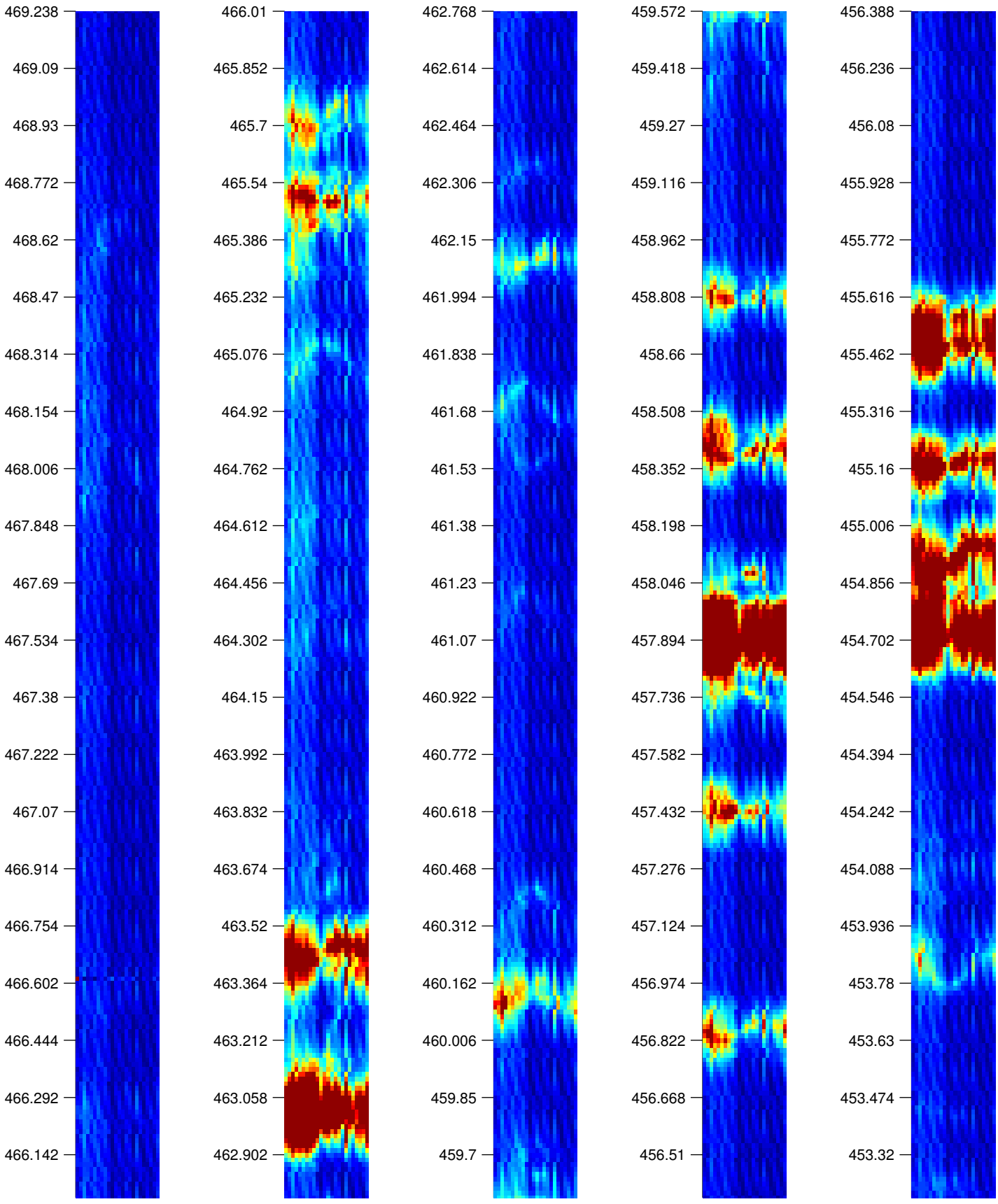

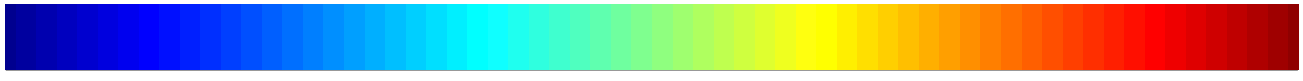

KLX12A -- Reference Log # 1

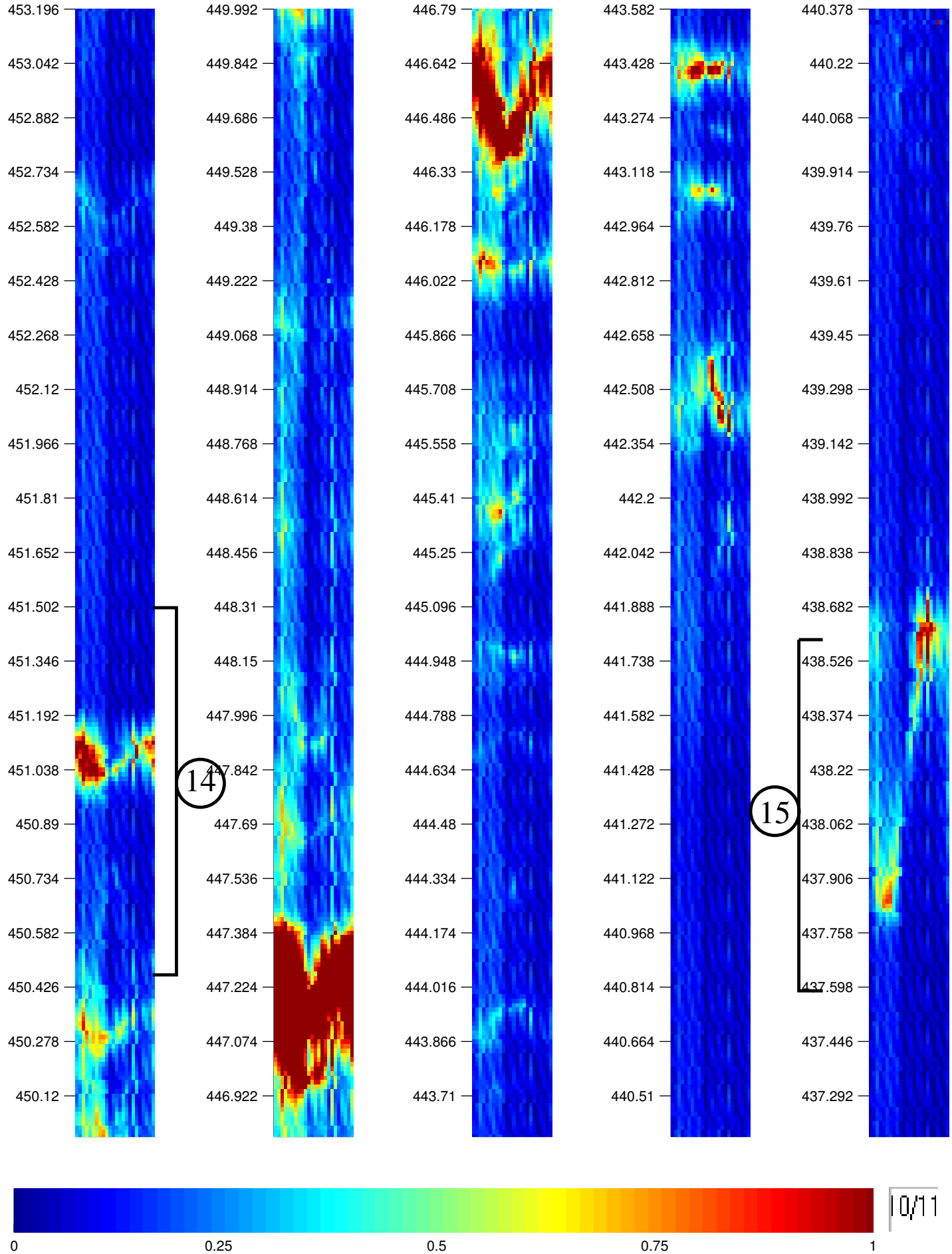

KLX12A -- Reference Log # 1

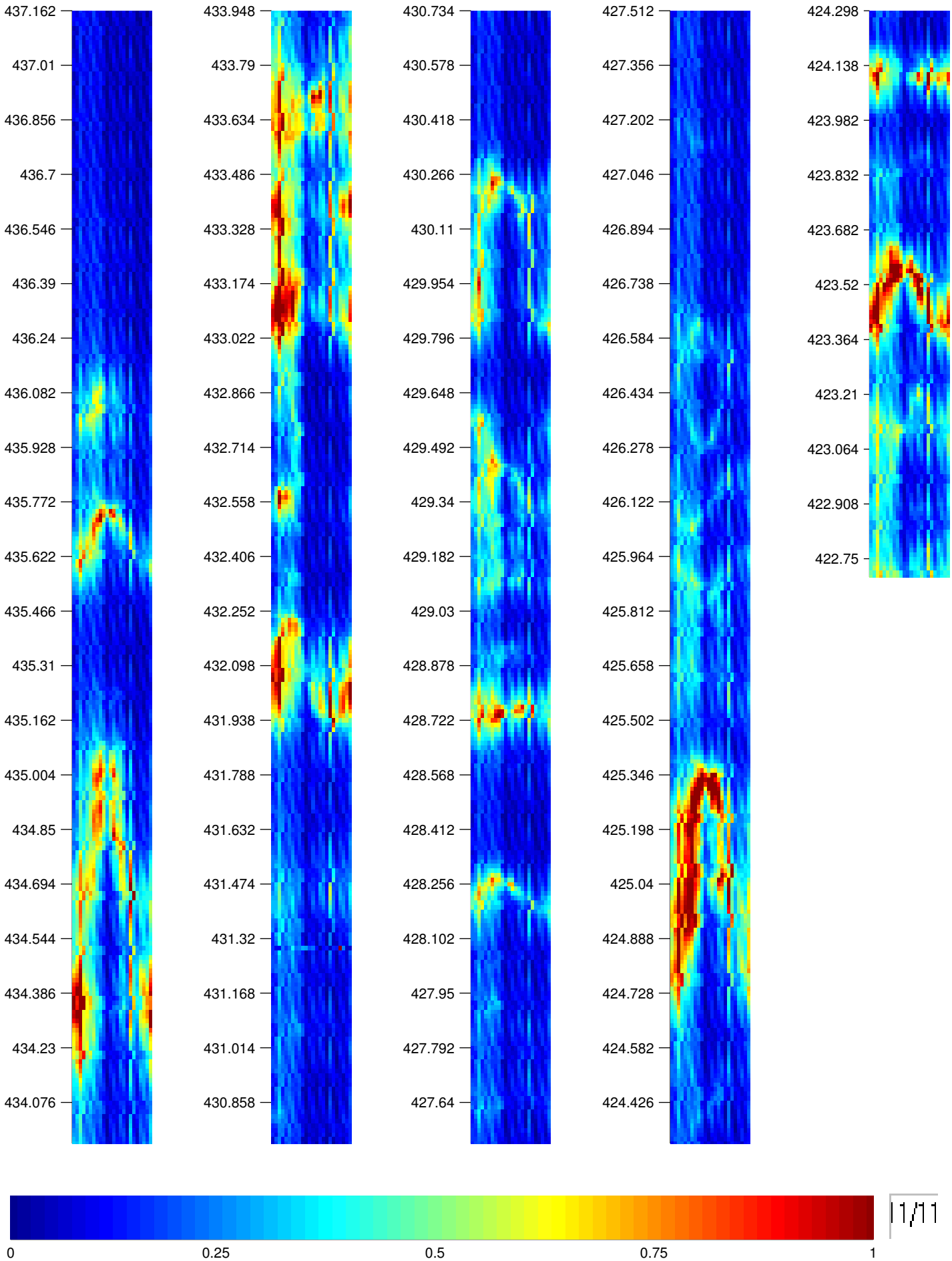

KLX12A -- Reference Log # 2

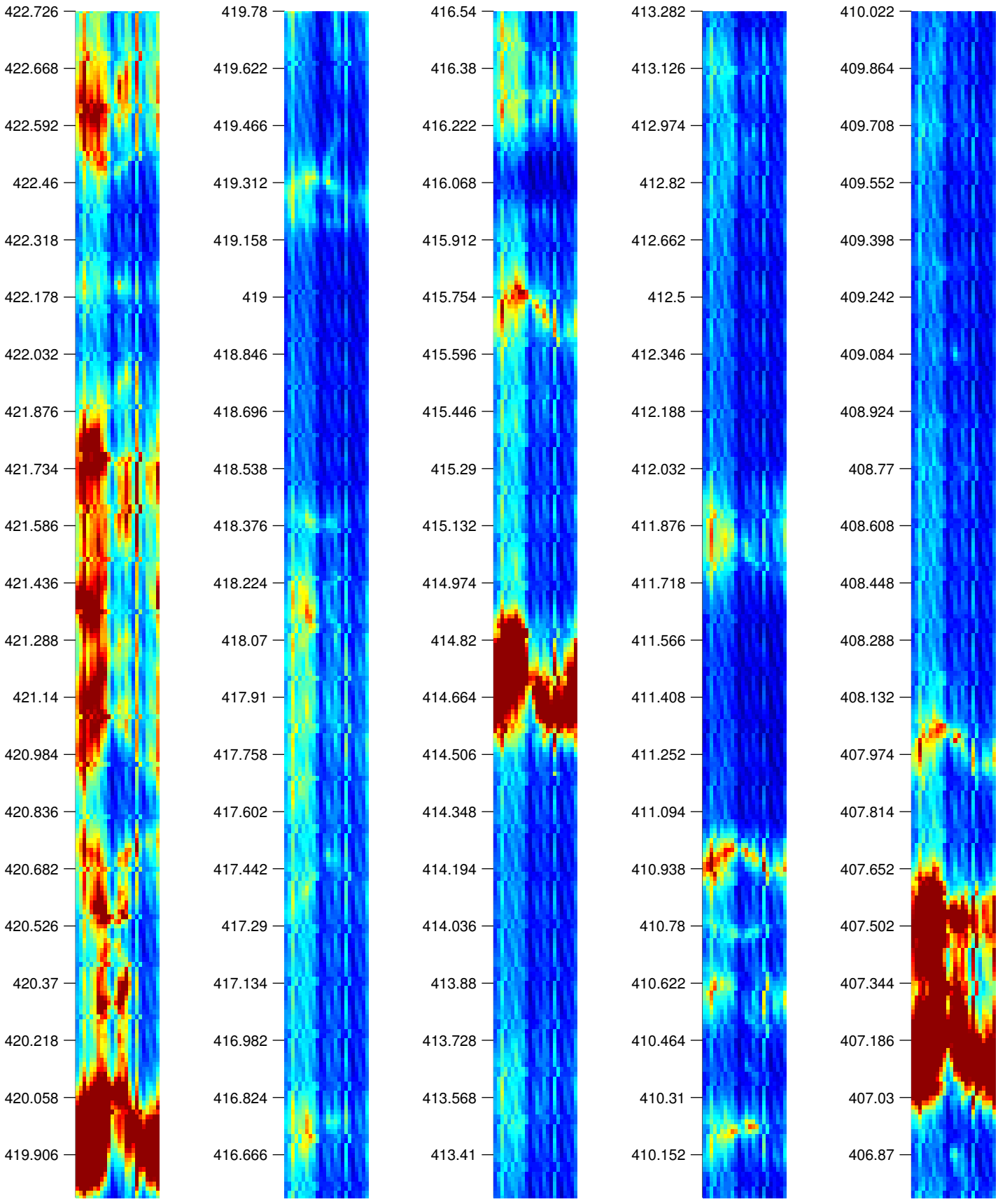

KLX12A -- Reference Log # 2

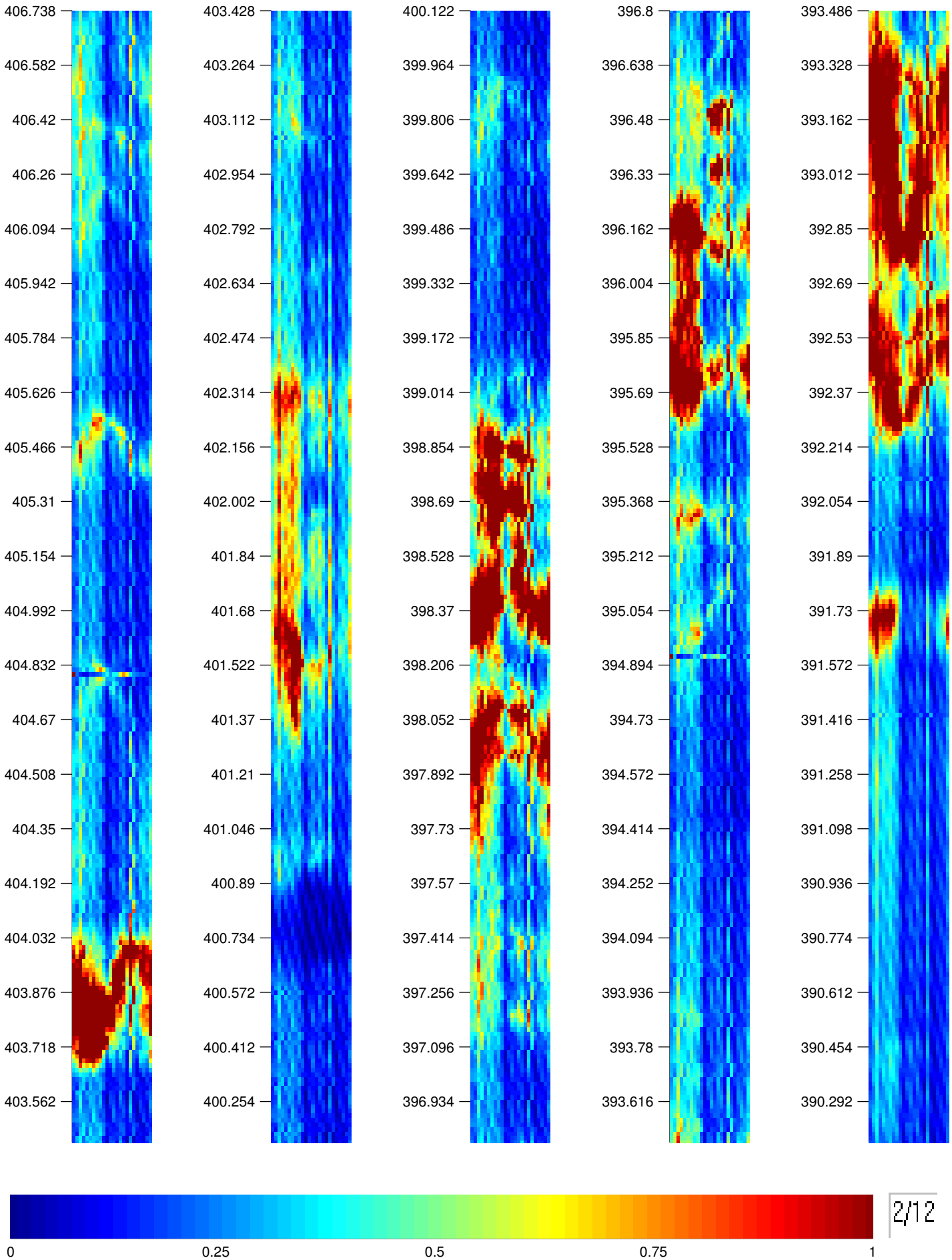

KLX12A -- Reference Log # 2

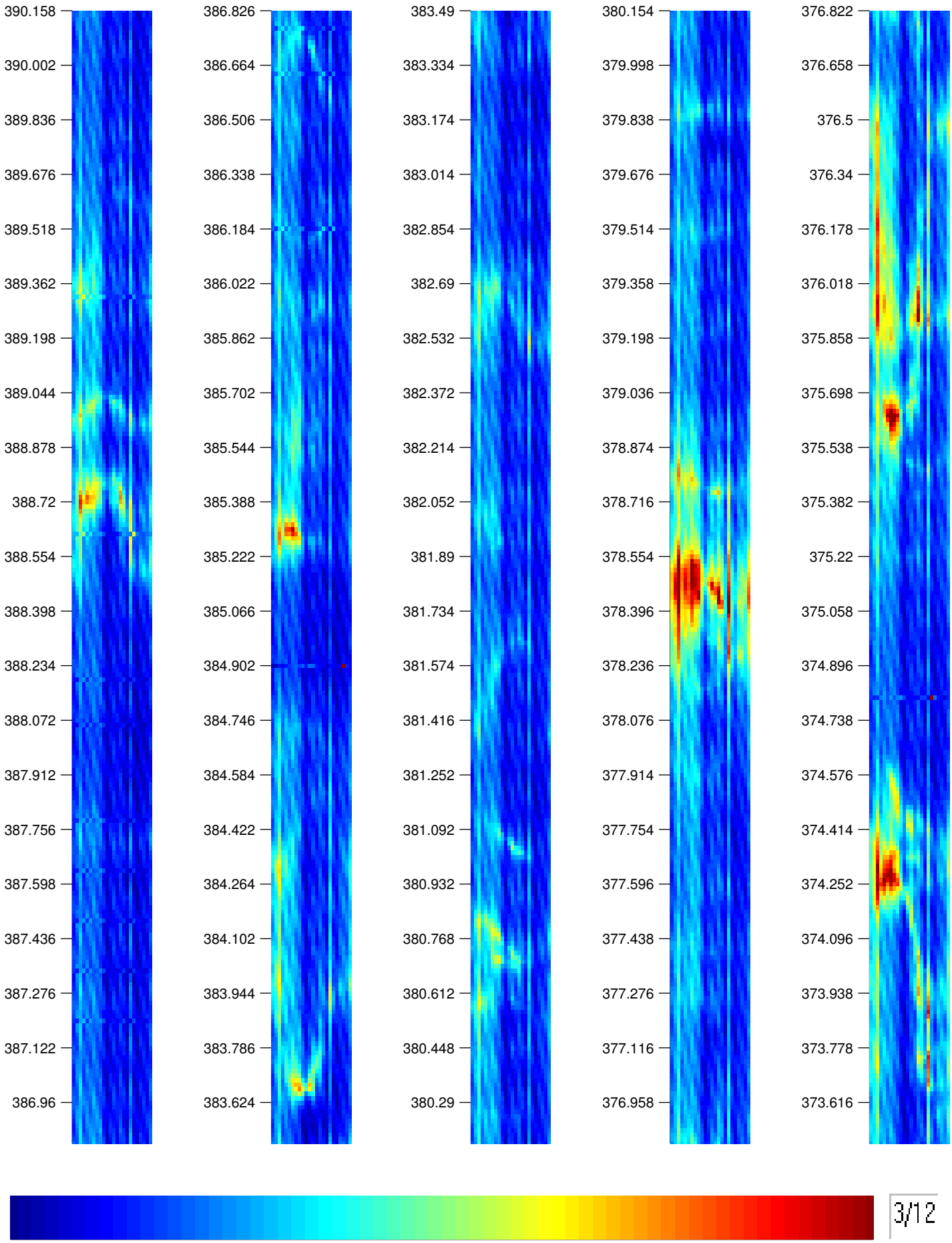

KLX12A -- Reference Log # 2

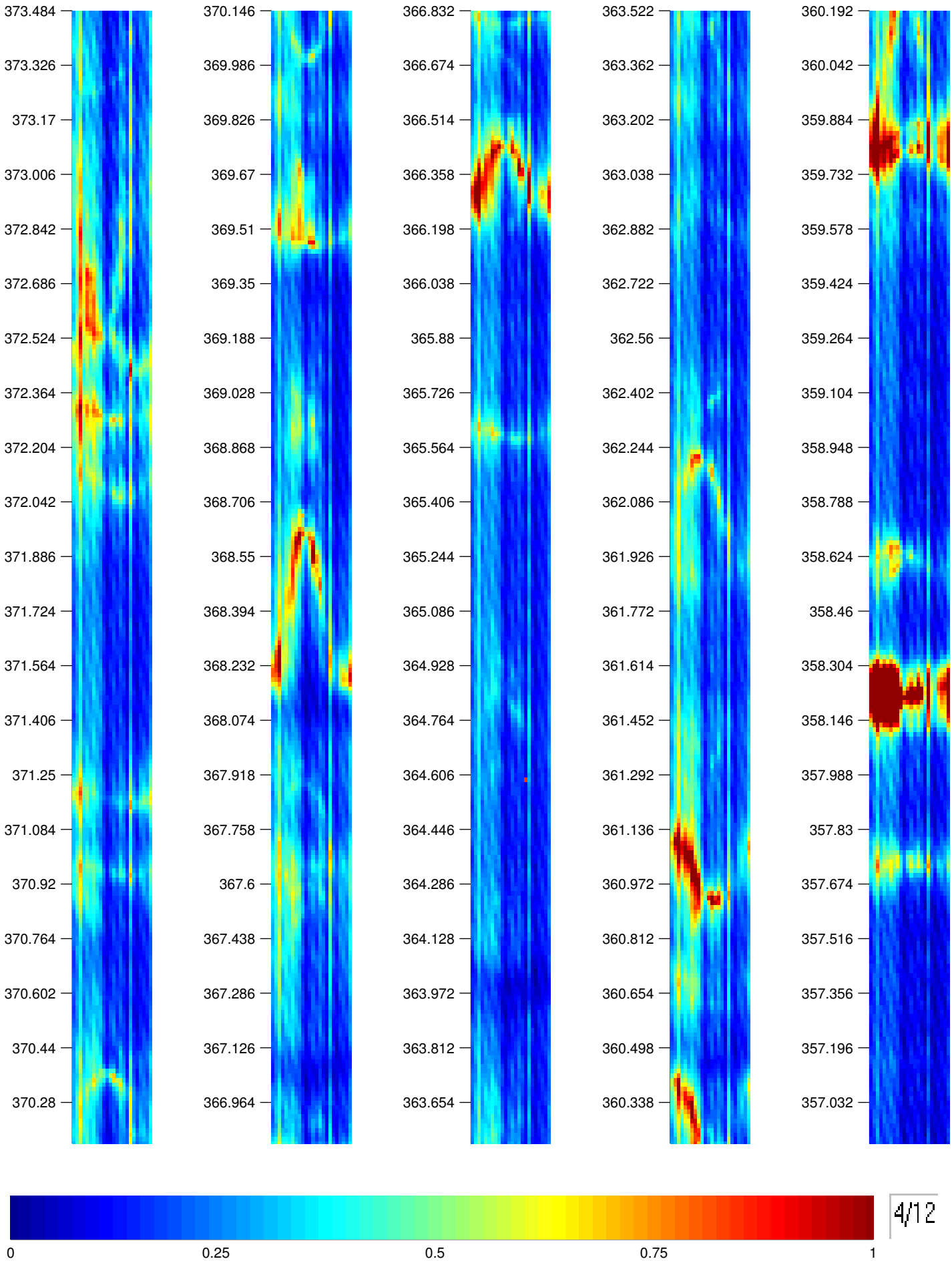

KLX12A -- Reference Log # 2

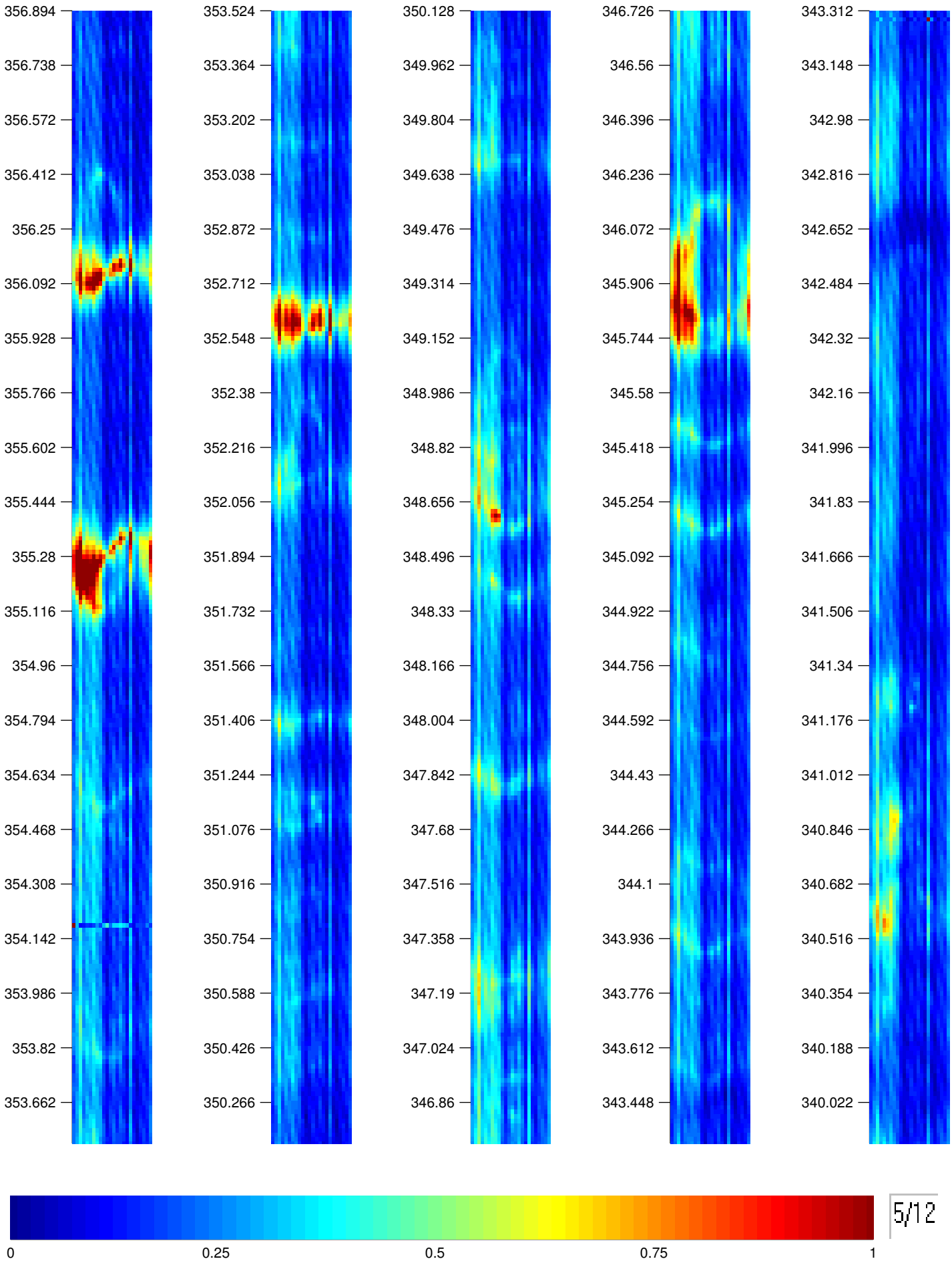

KLX12A -- Reference Log # 2

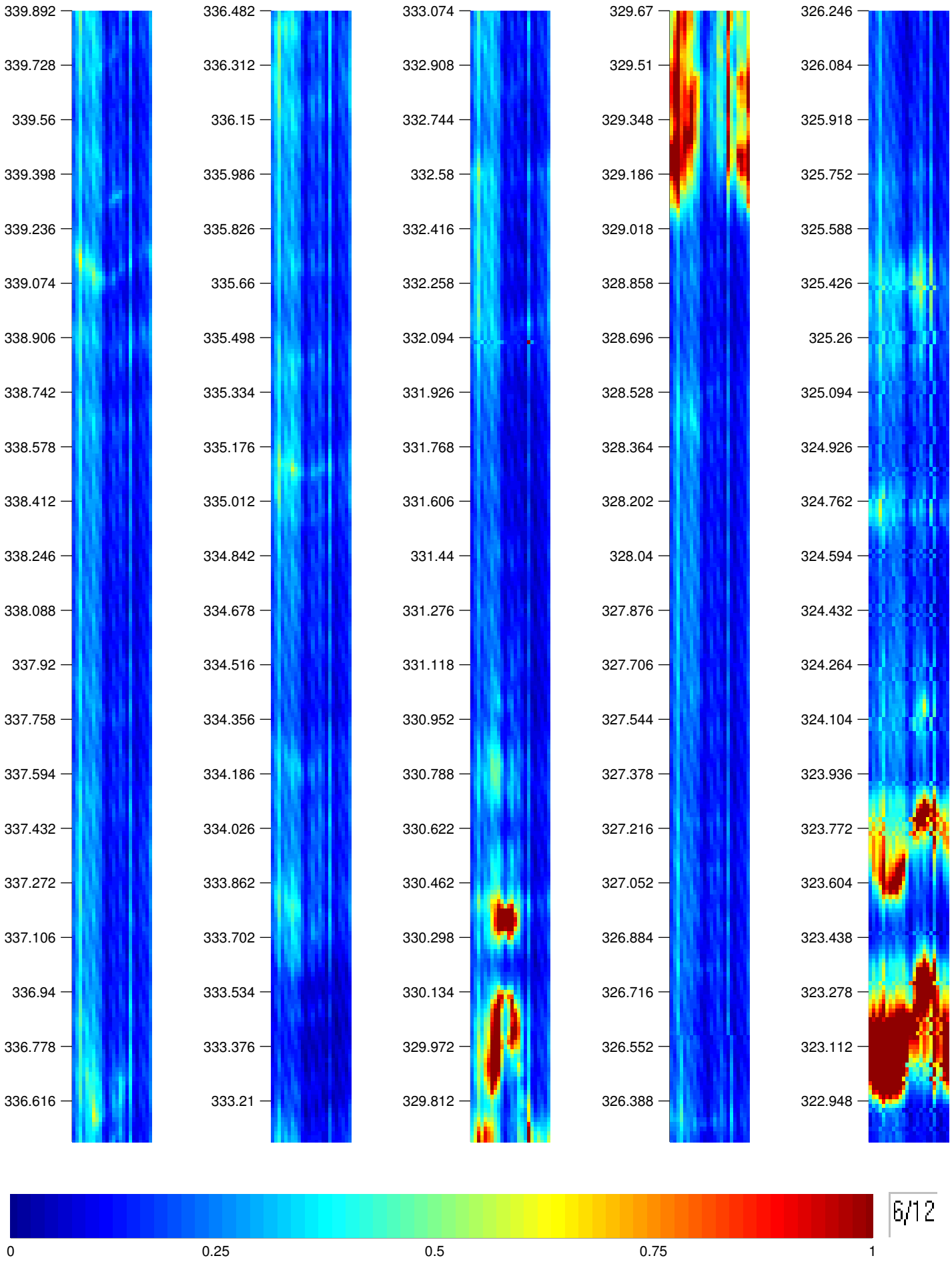

KLX12A -- Reference Log # 2

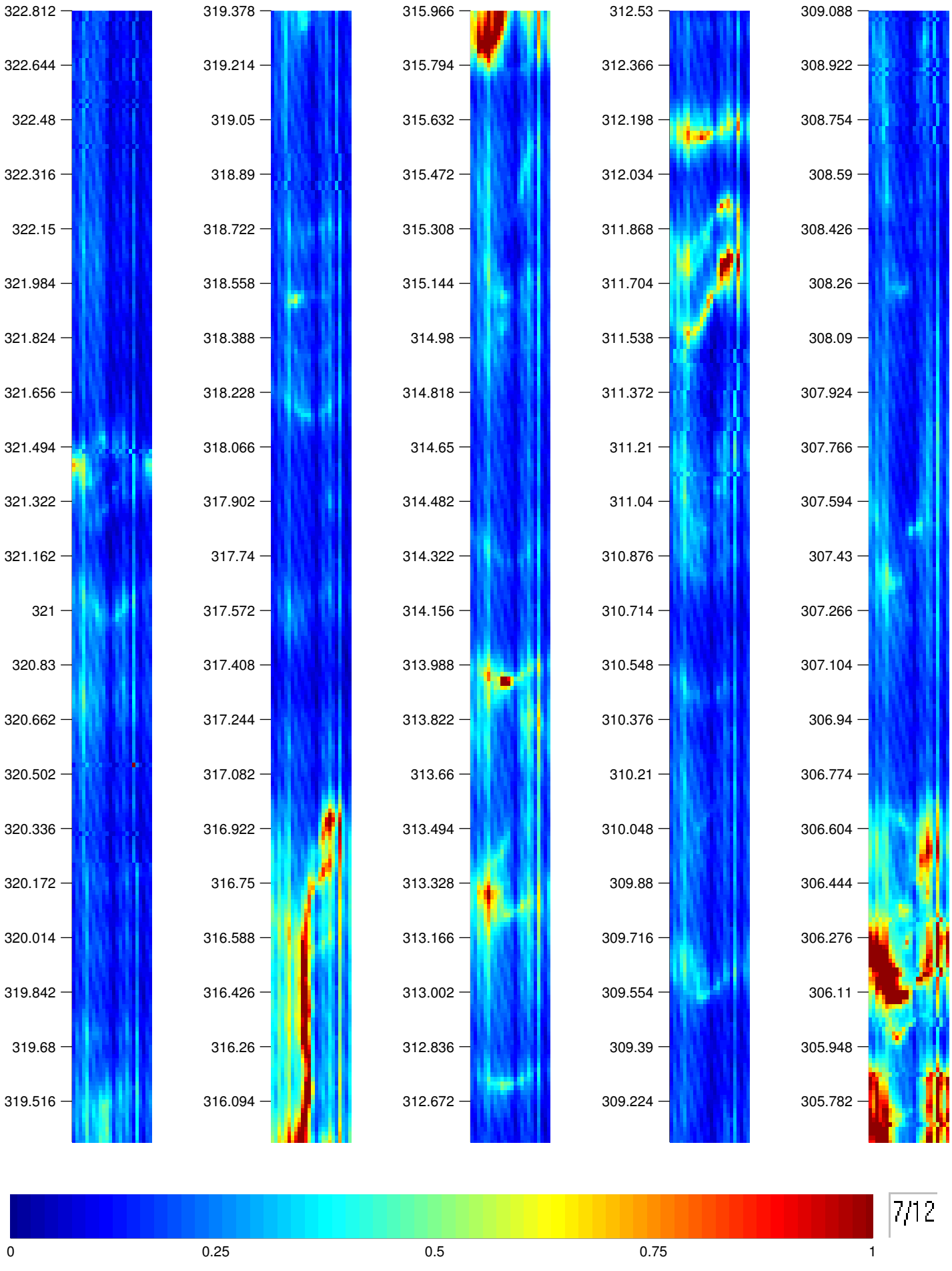

KLX12A -- Reference Log # 2

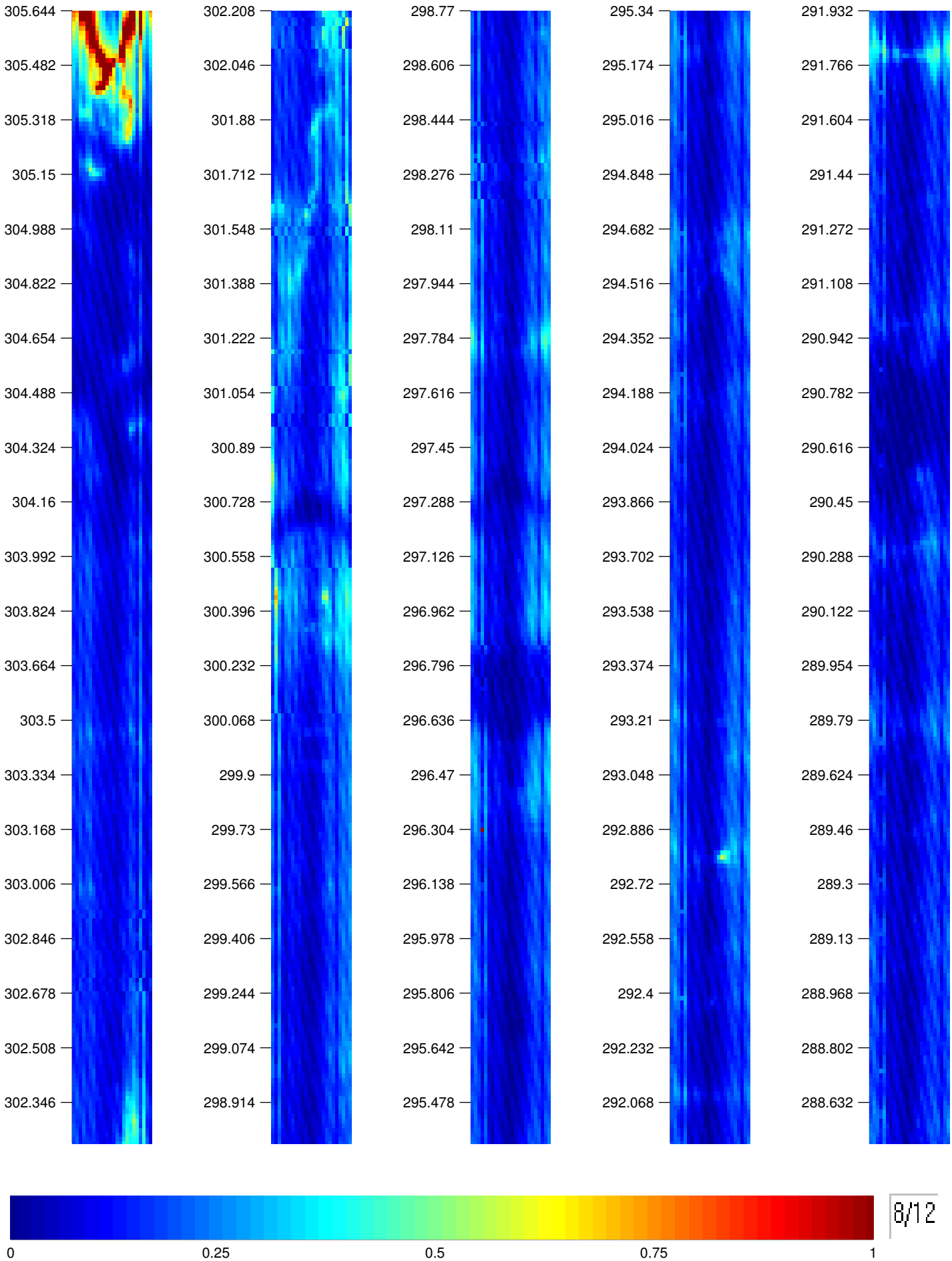

KLX12A -- Reference Log # 2

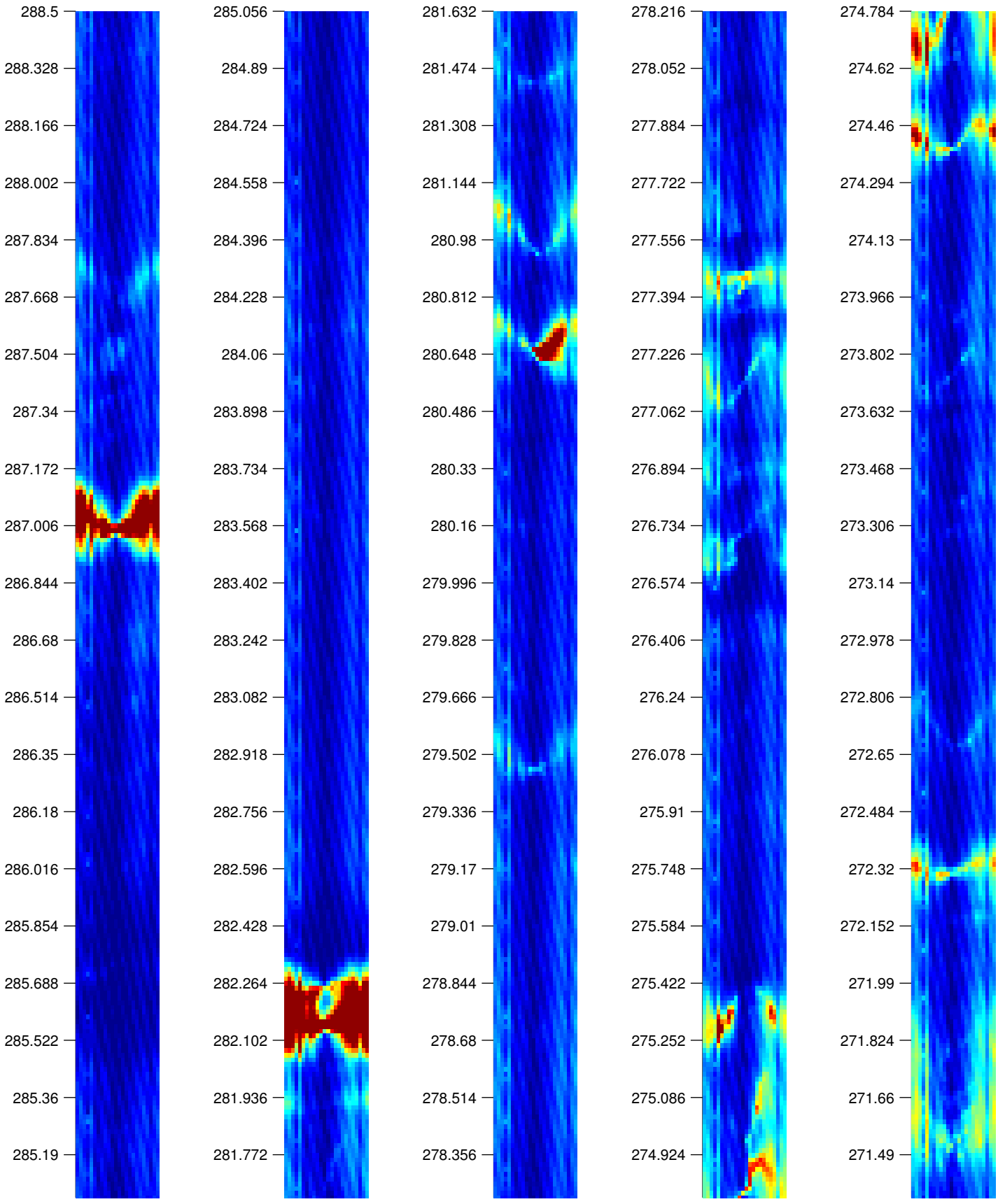

KLX12A -- Reference Log # 2

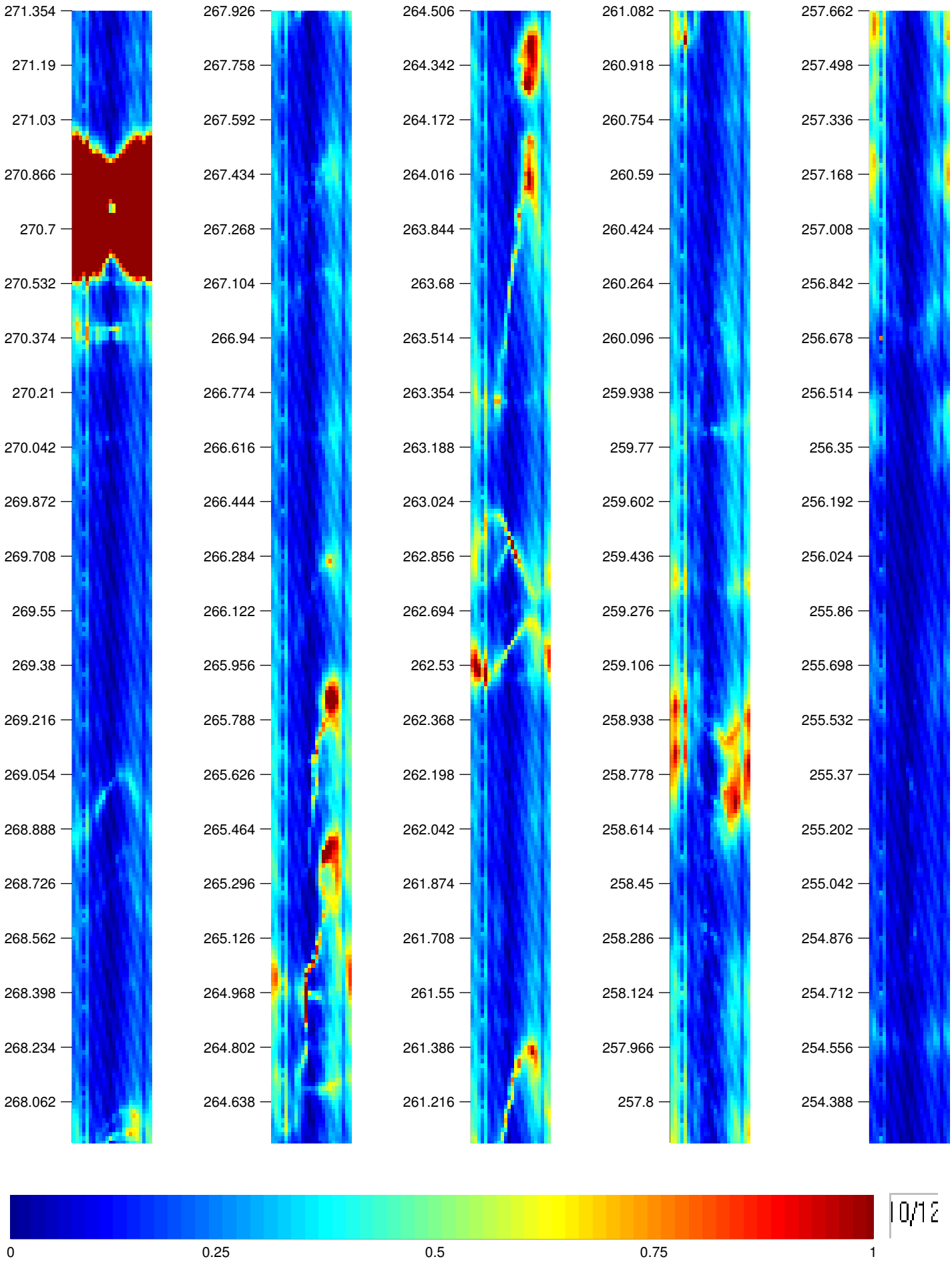

KLX12A -- Reference Log # 2

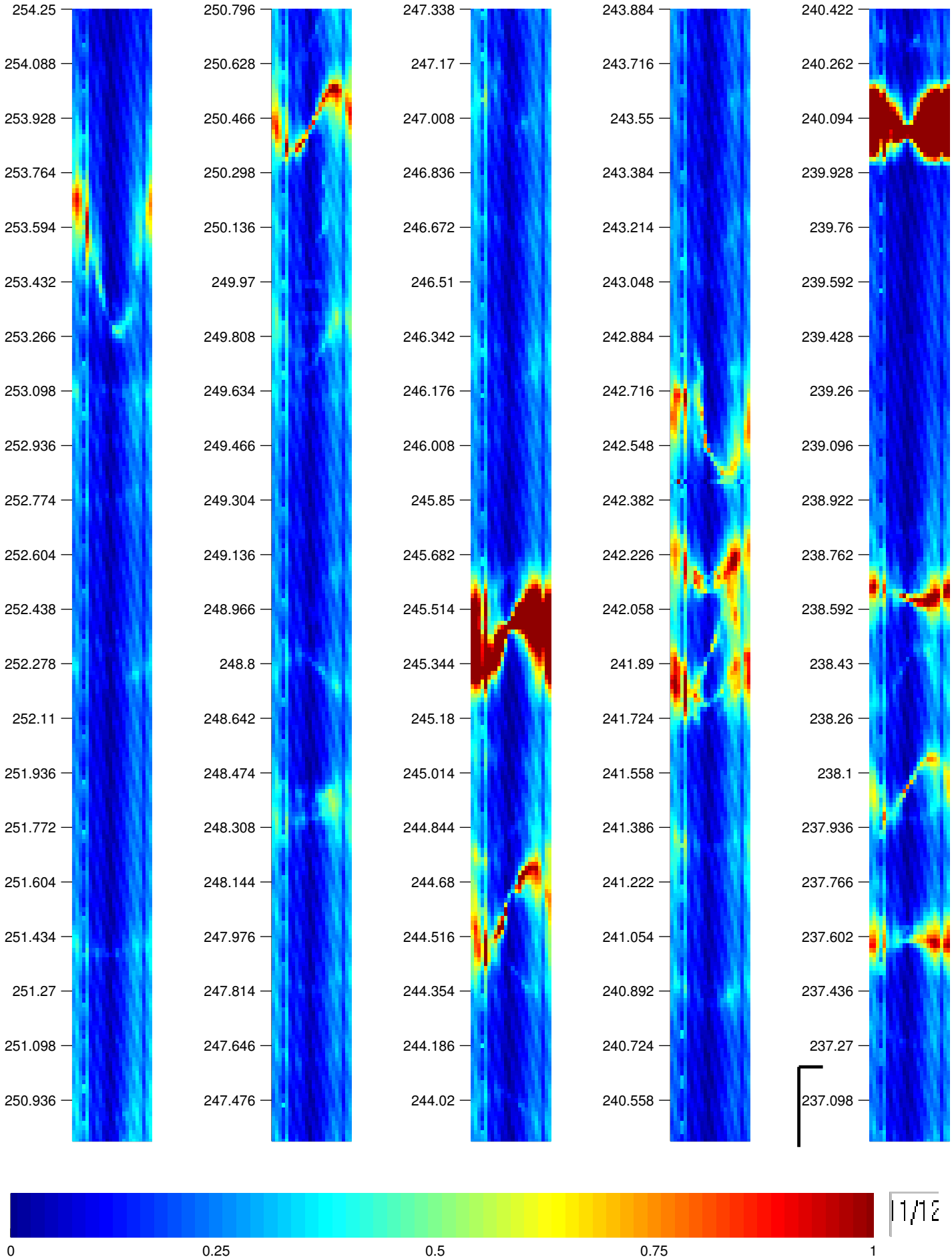

KLX12A -- Reference Log # 2

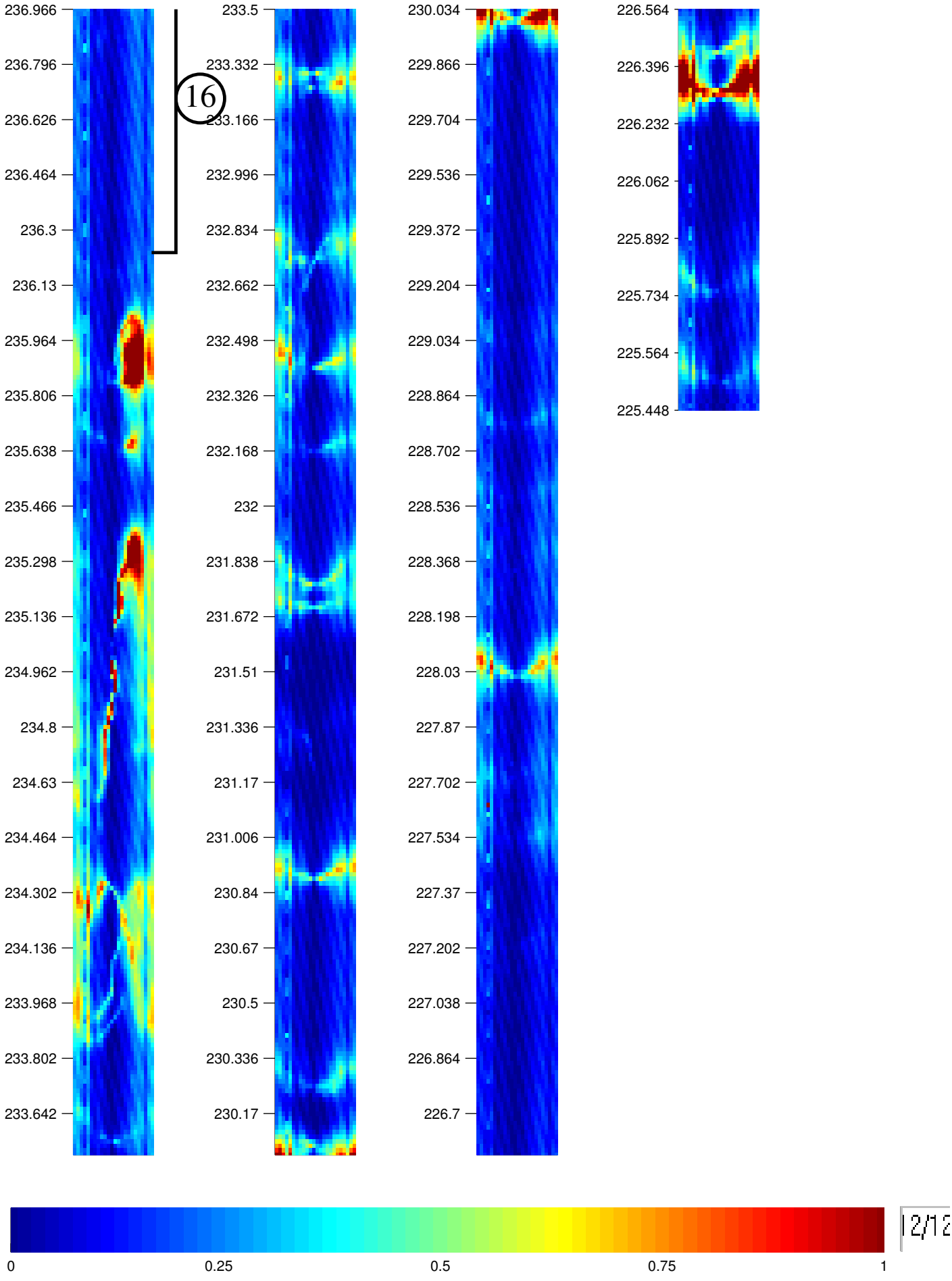

KLX12A -- Reference Log # 3

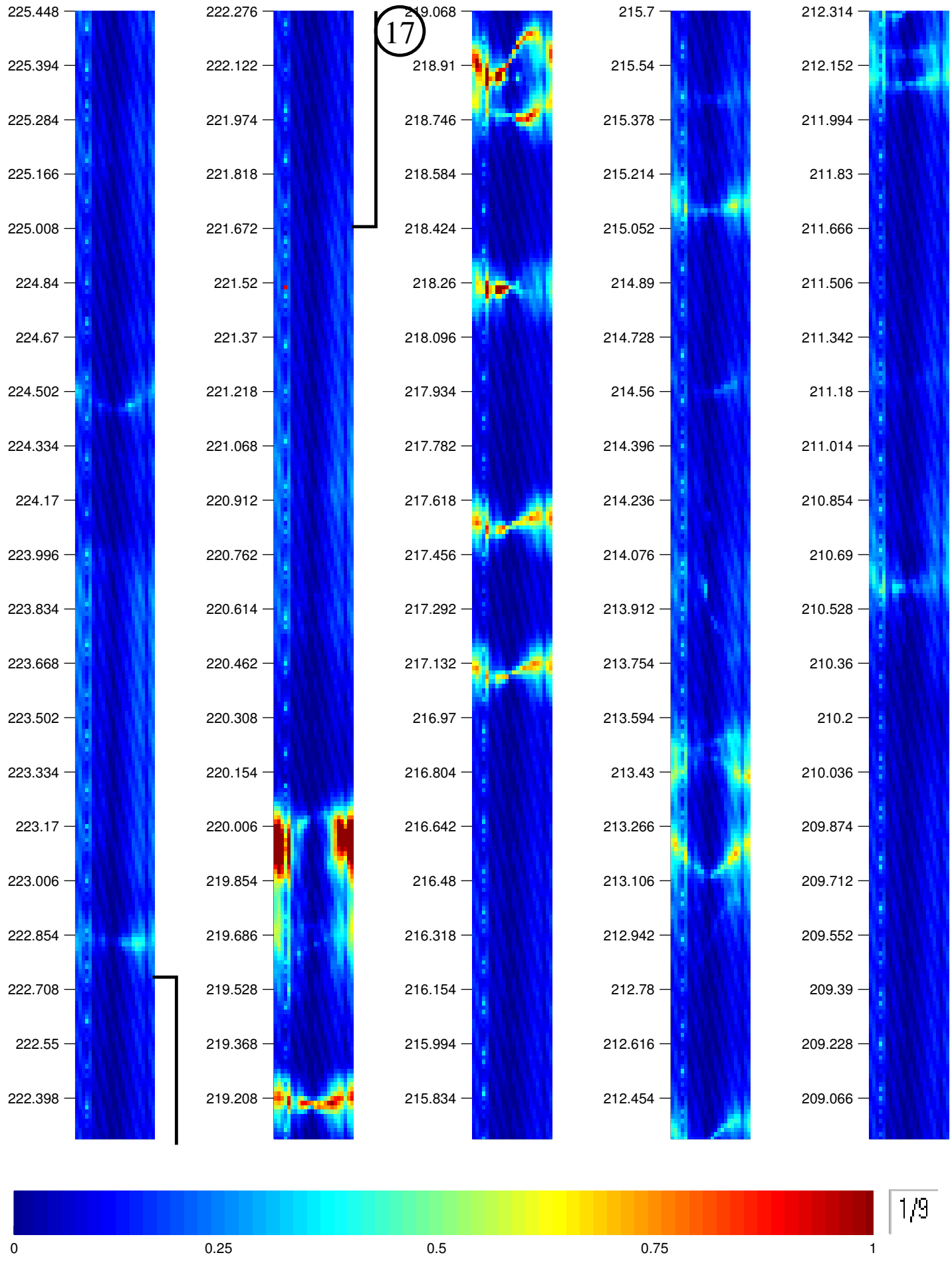

KLX12A -- Reference Log # 3

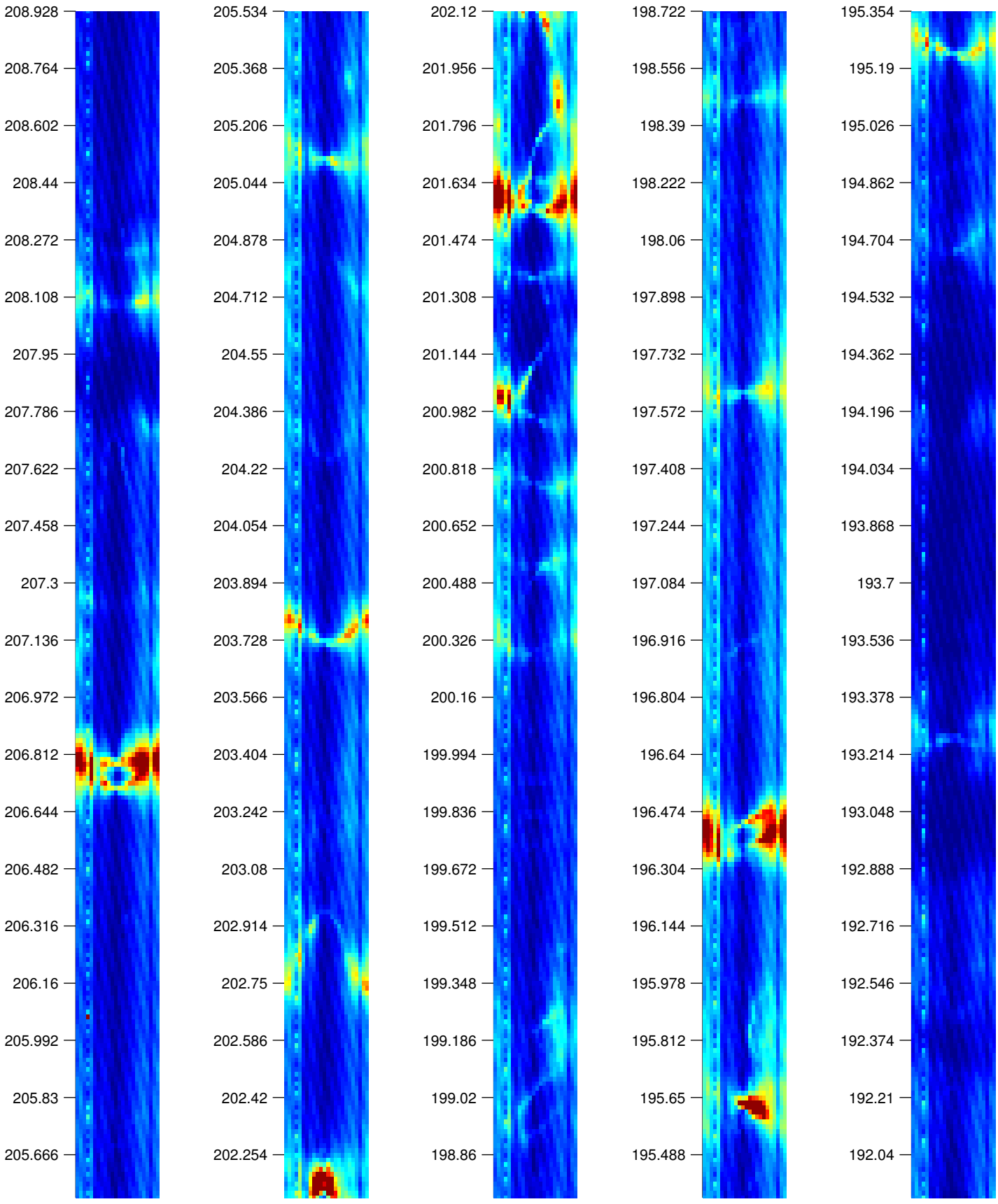

KLX12A -- Reference Log # 3

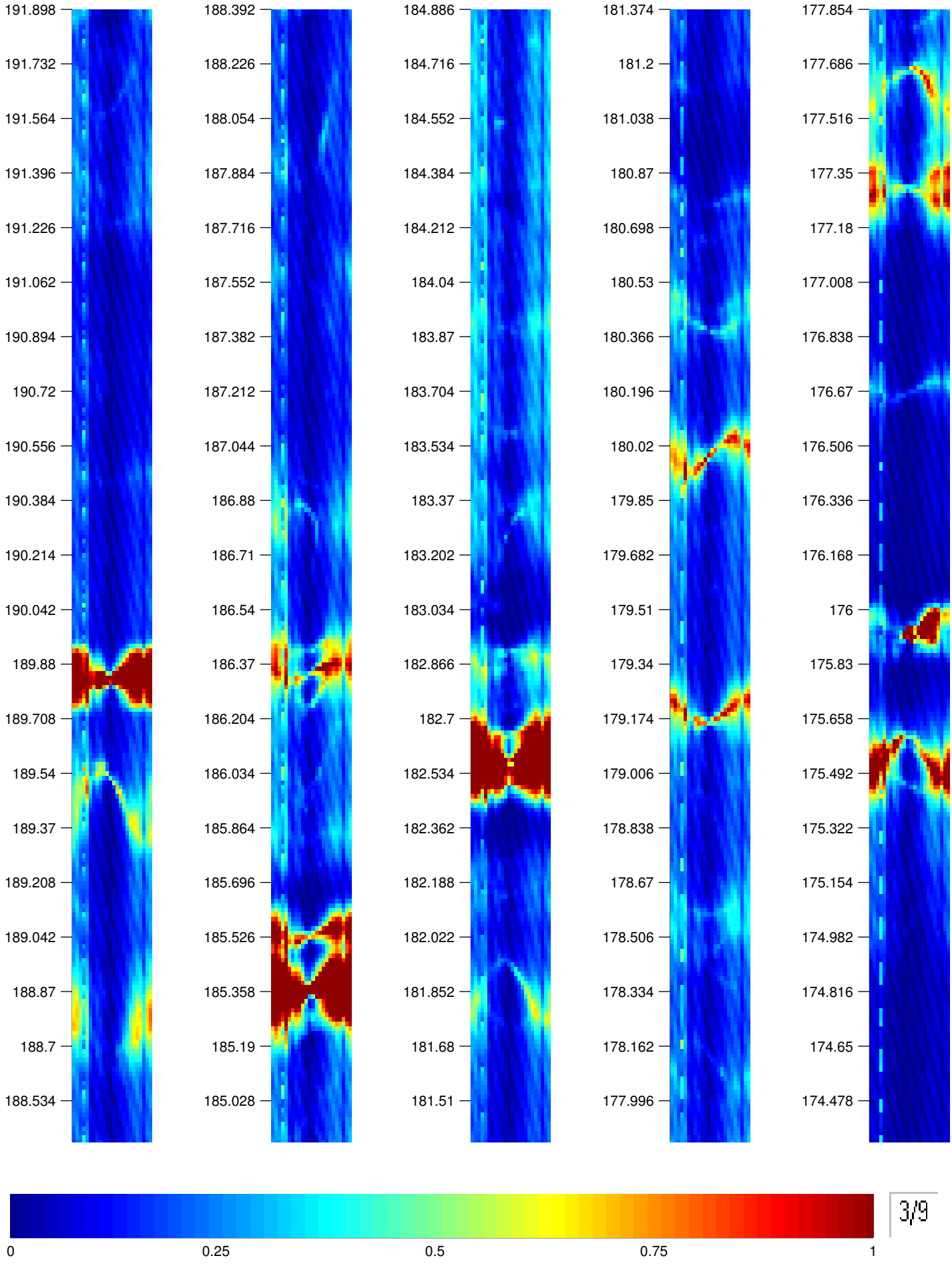

KLX12A -- Reference Log # 3

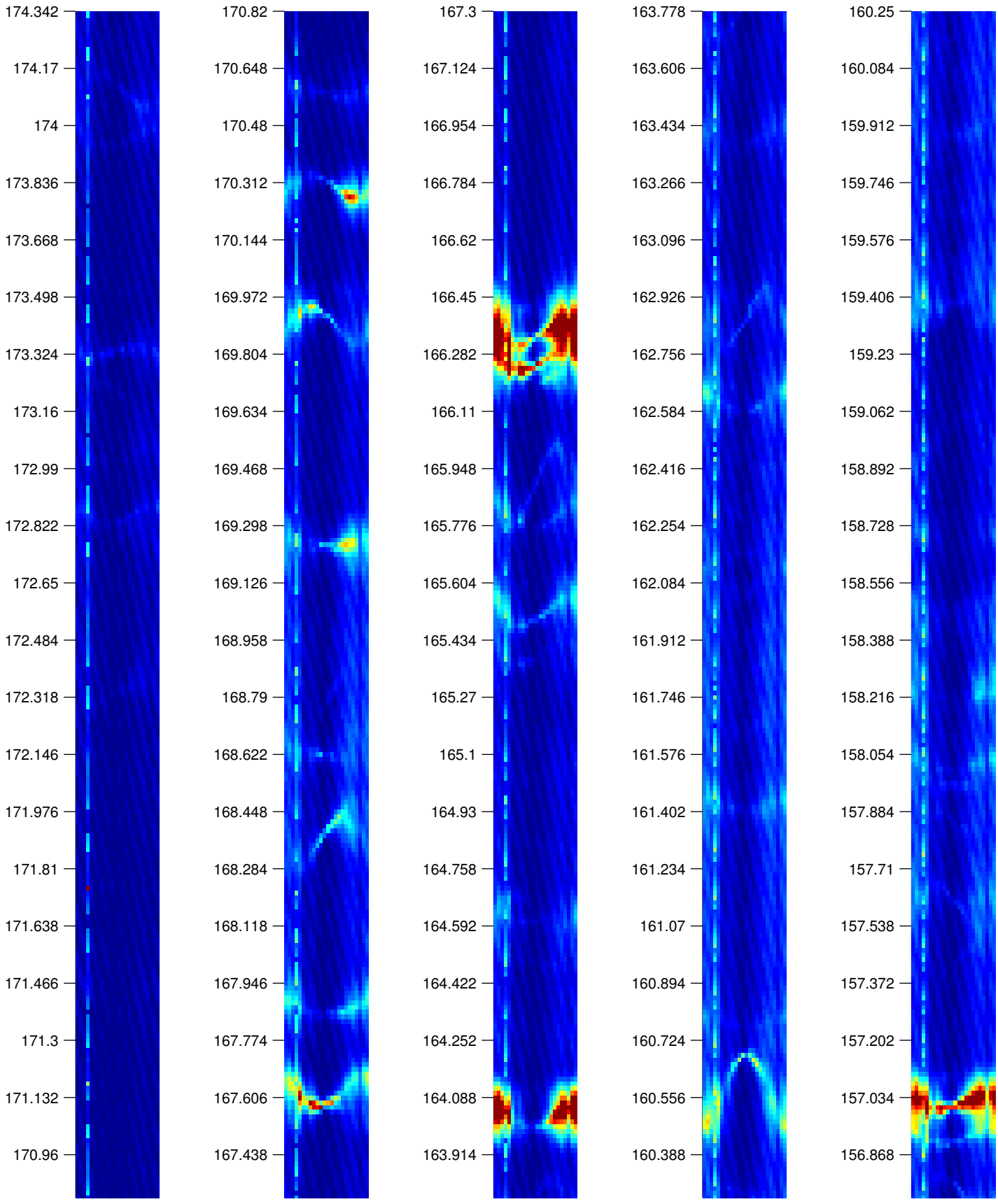

KLX12A -- Reference Log # 3

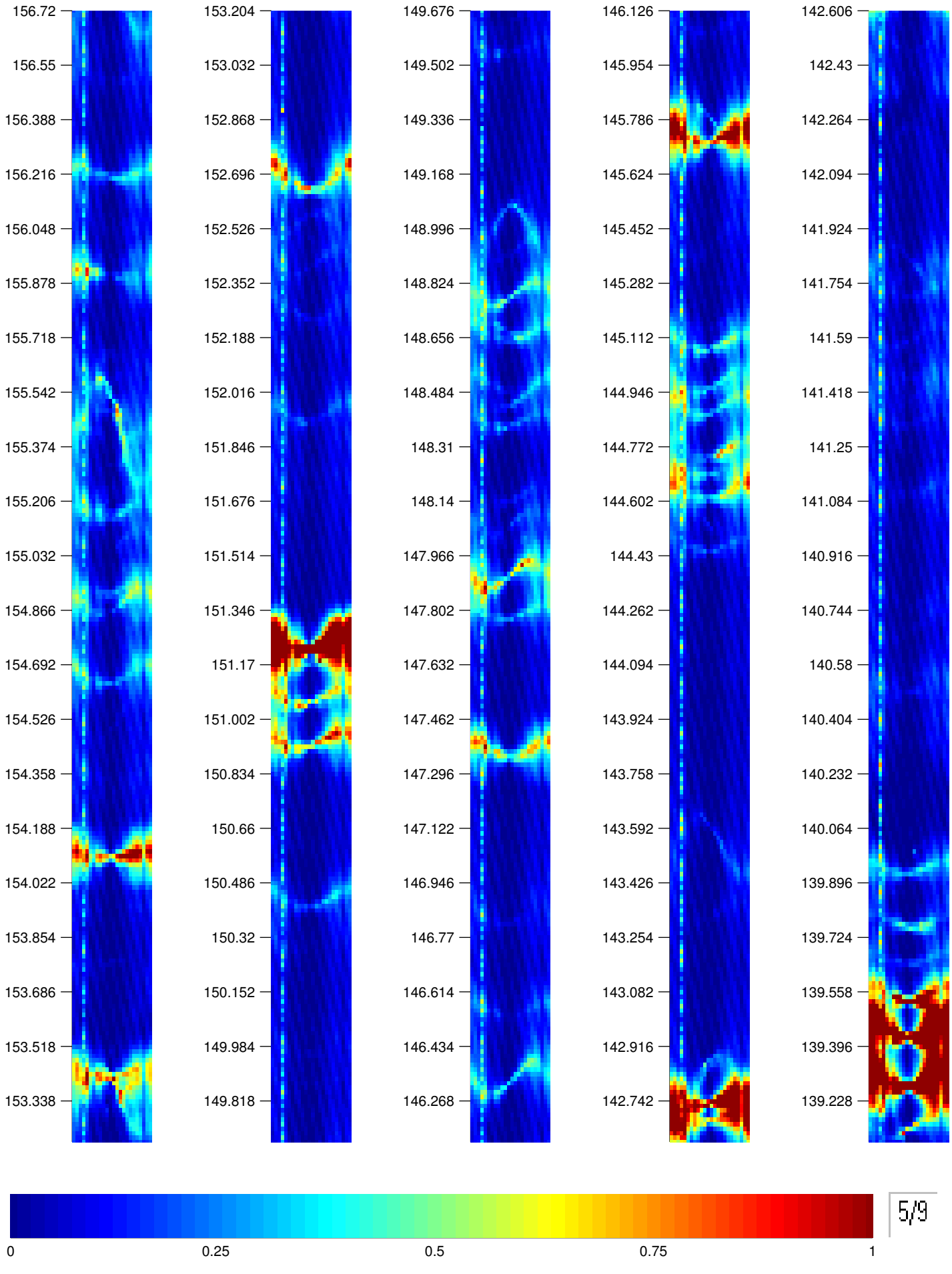

KLX12A -- Reference Log # 3

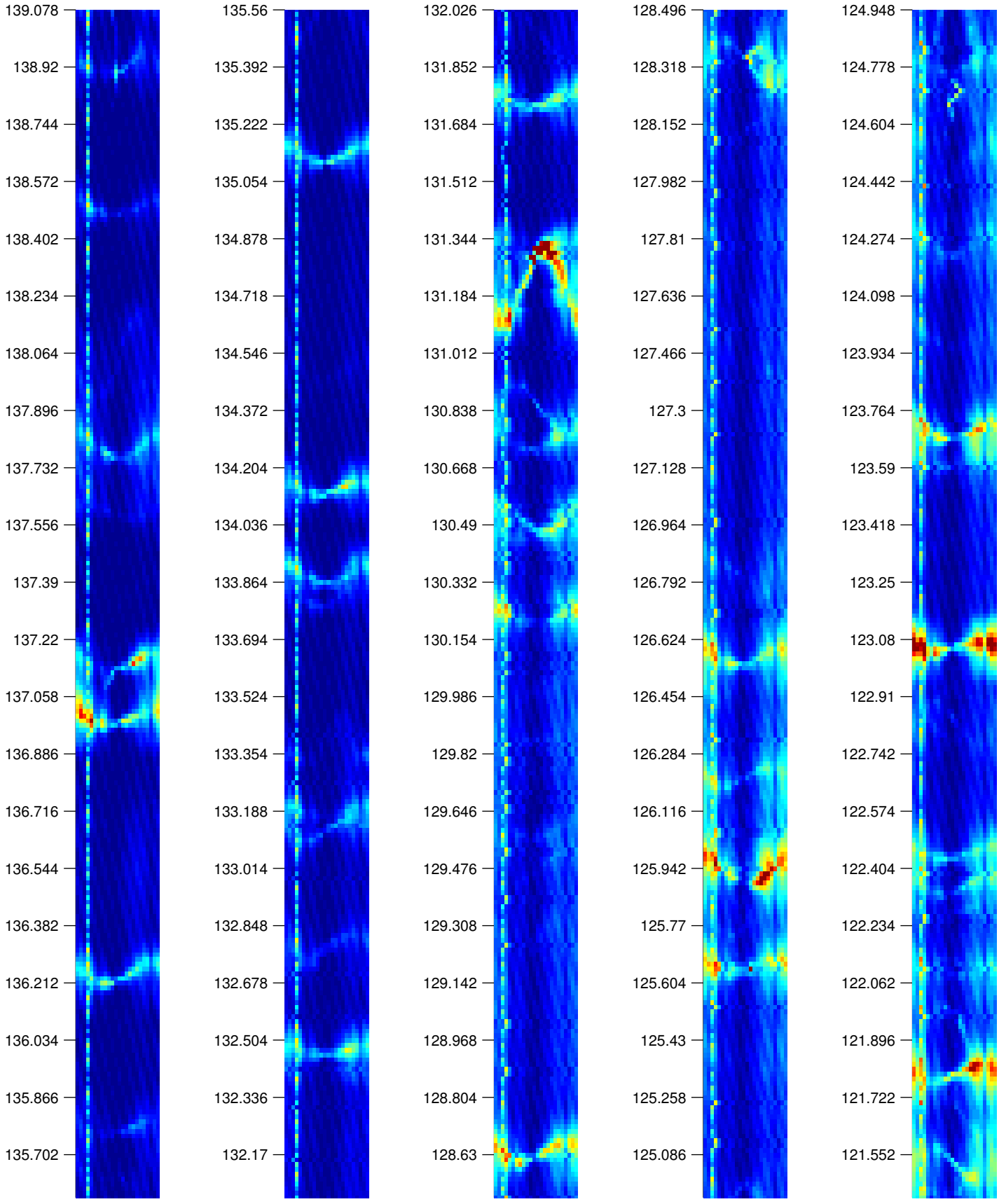

KLX12A -- Reference Log # 3

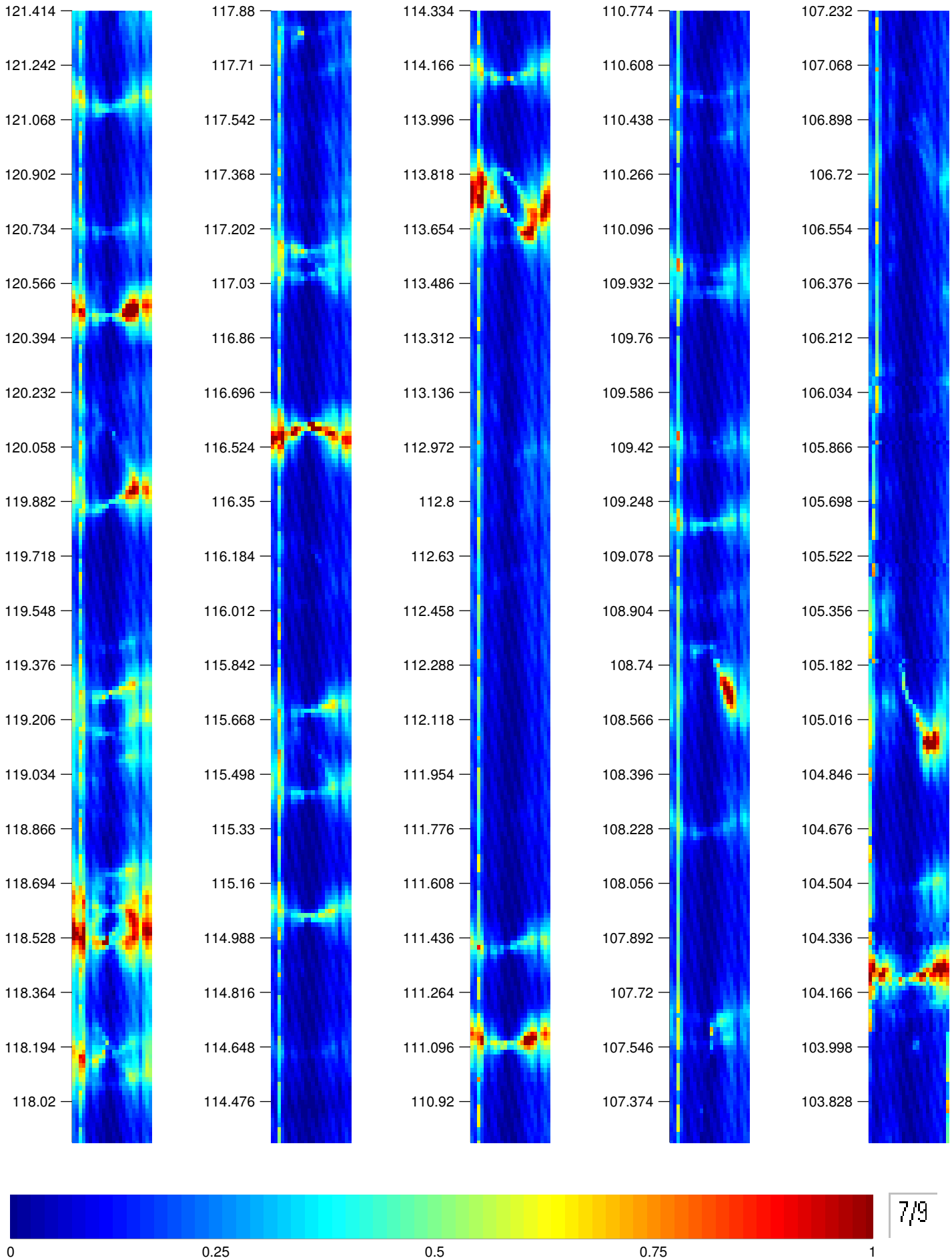

KLX12A -- Reference Log # 3

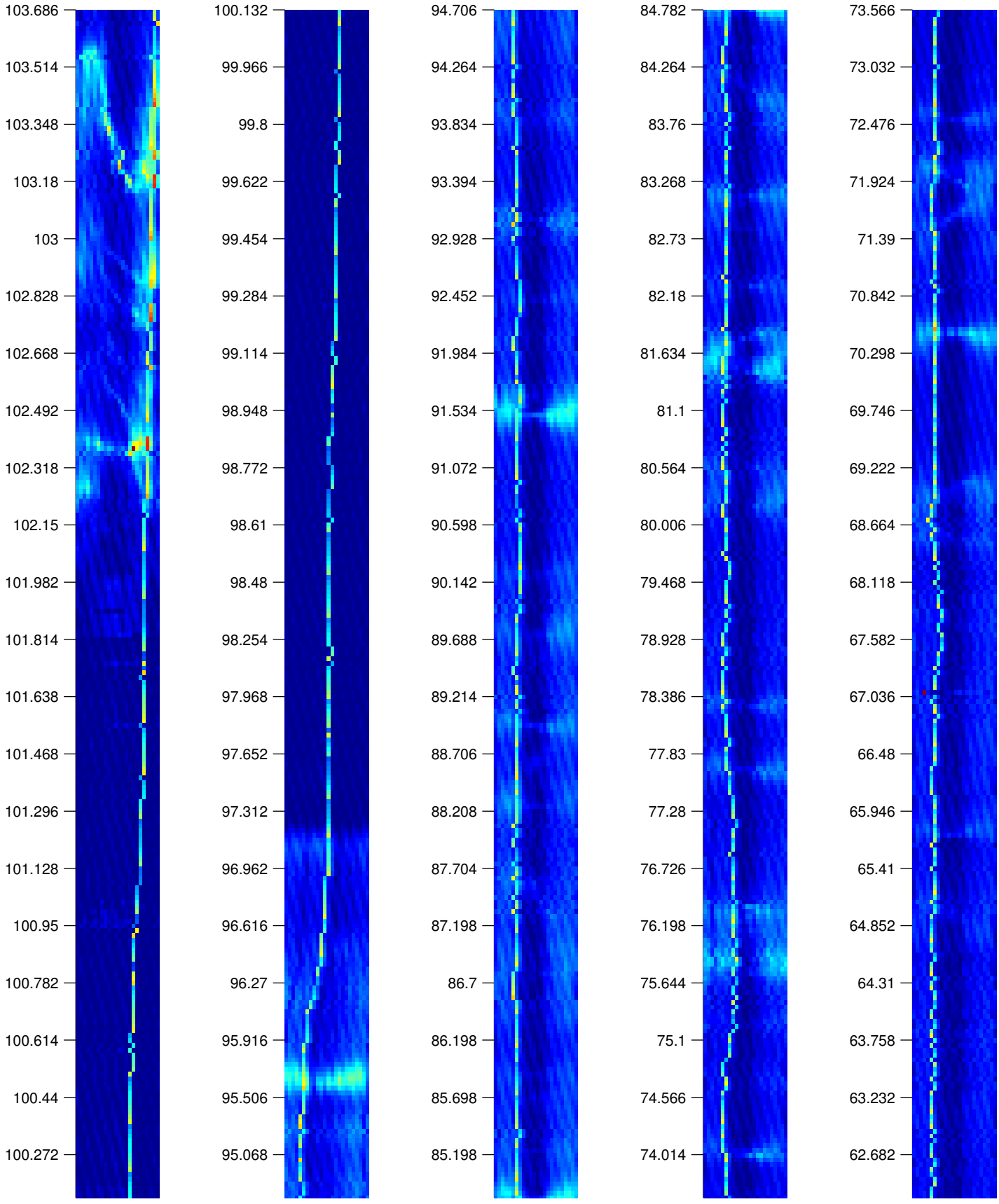

KLX12A -- Reference Log # 3

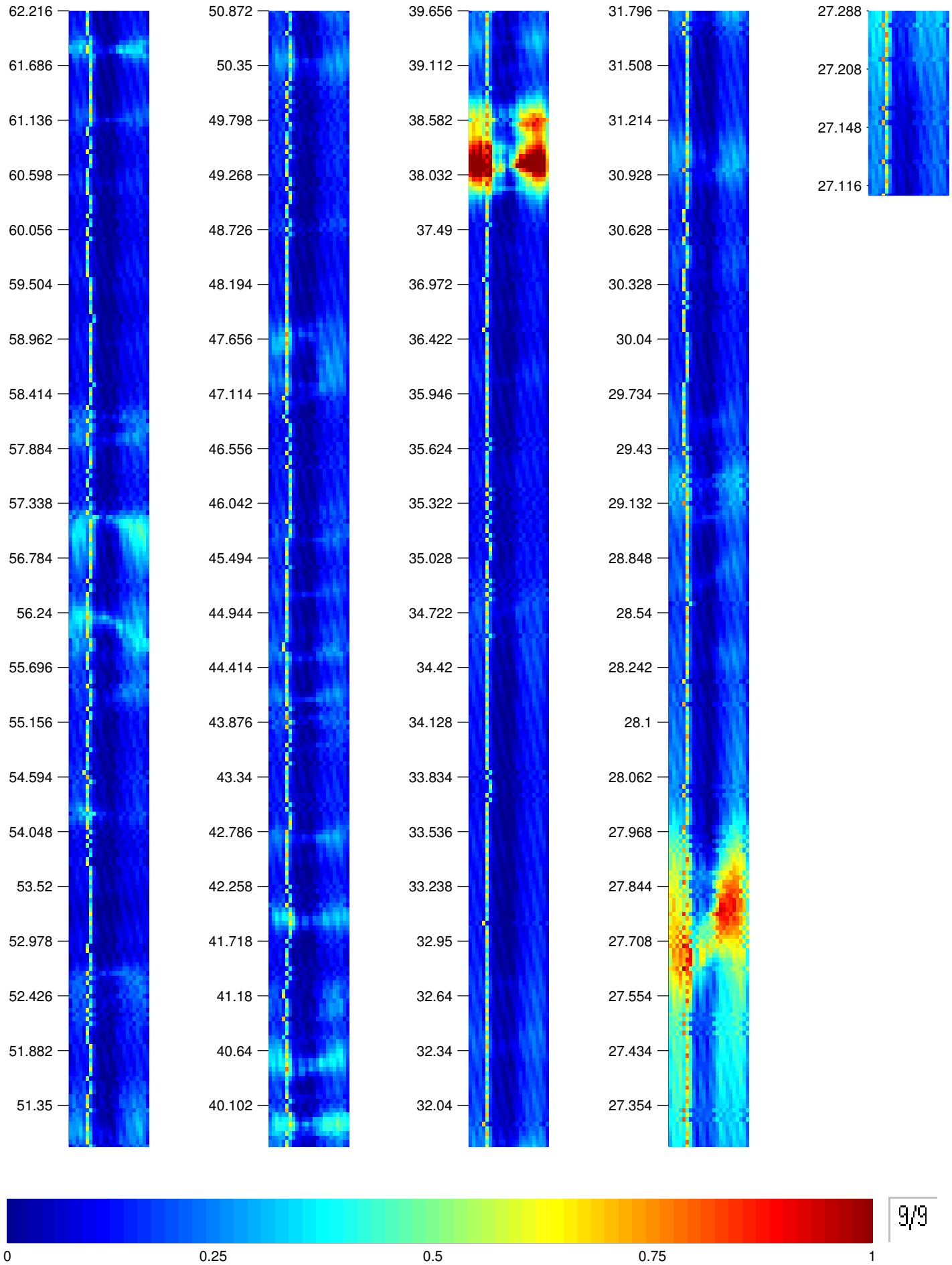

APPENDIX 4

TESTING CURVES, INTERPRETATION CURVES, AND POST-LOG FOR BOREHOLE KLX12A

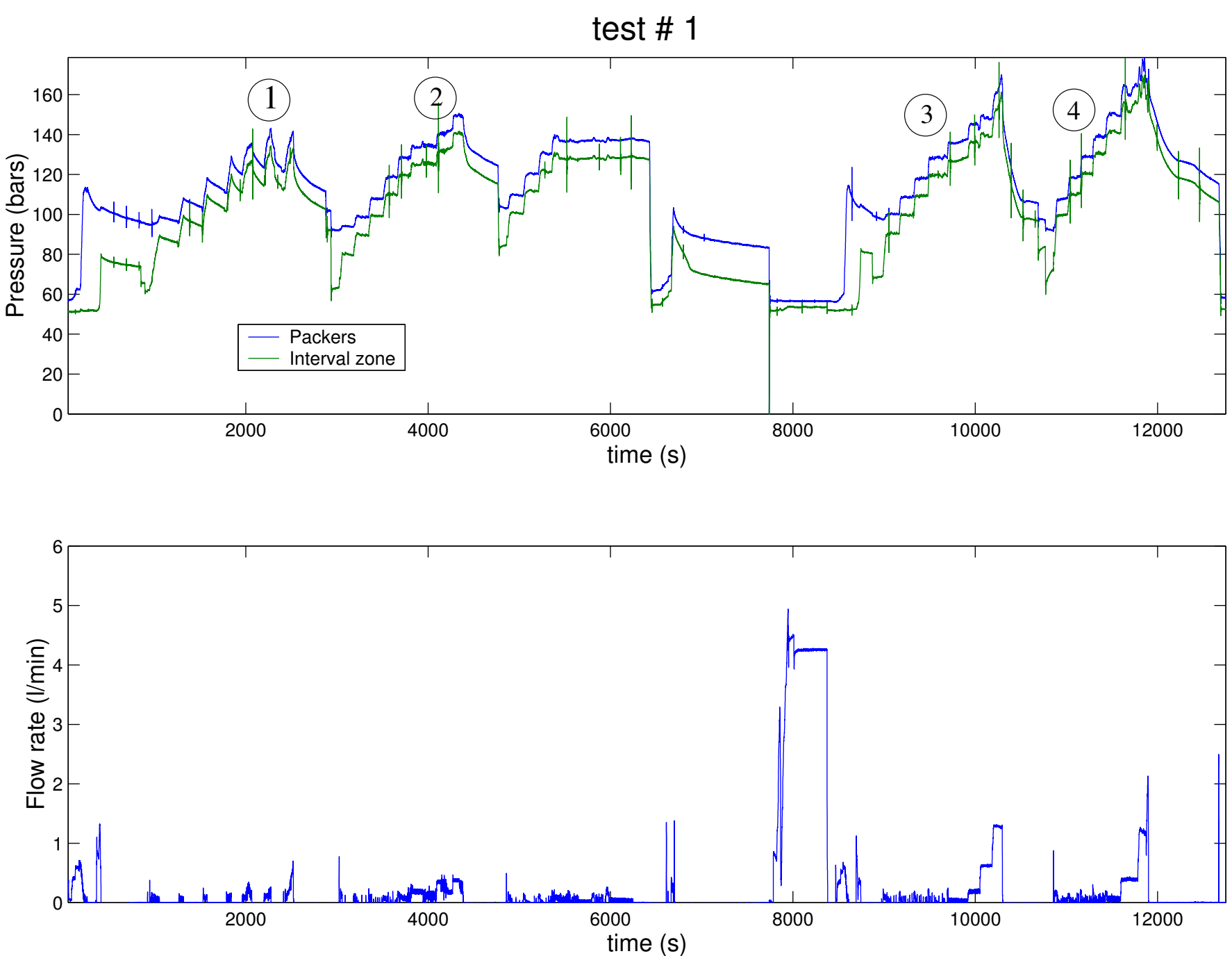
test # 1
Pressure (bars)
time (s)
Packers
Interval zone
1
2
3
4
Flow rate (l/min)
time (s)

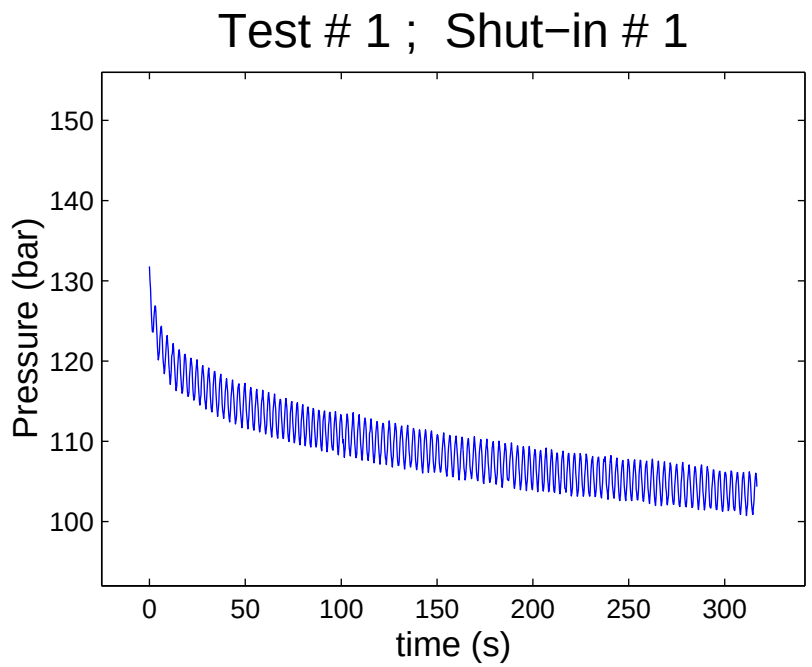
Test # 1 ; Shut−in # 1
Pressure (bar)
time (s)
150
140
130
120
110
100
0
50
100
150
200
250
300

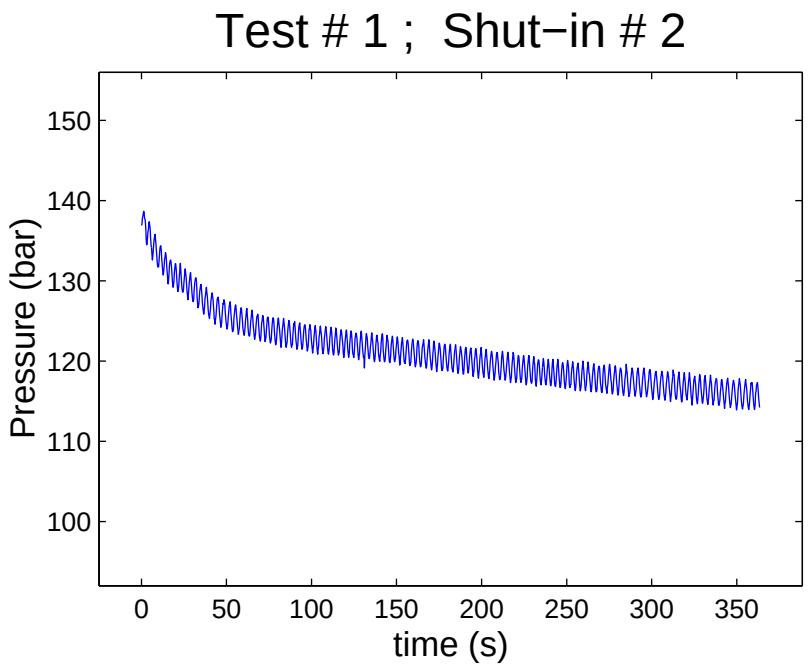
Test # 1 ; Shut−in # 2
Pressure (bar)
time (s)
150
140
130
120
110
100
0
50
100
150
200
250
300
350

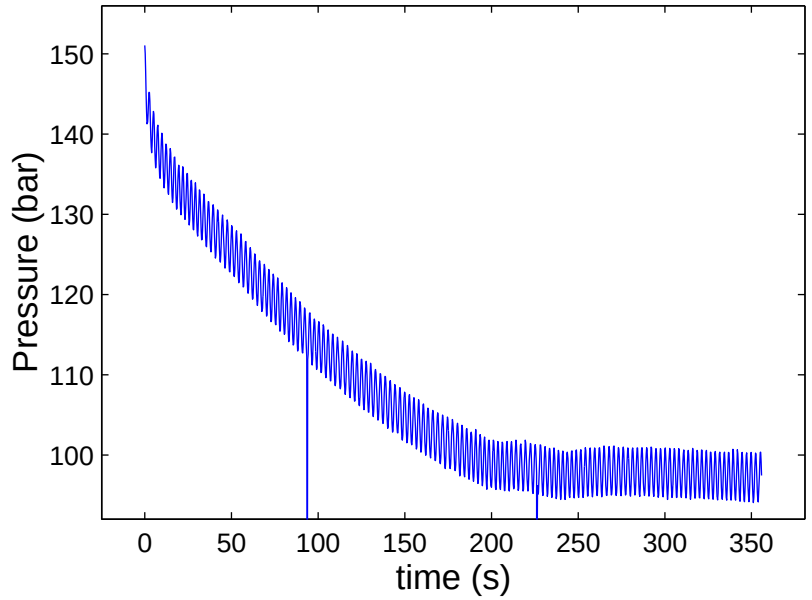
Test # 1 ; Shut−in # 3
Pressure (bar)
time (s)
150
140
130
120
110
100
0
50
100
150
200
250
300
350

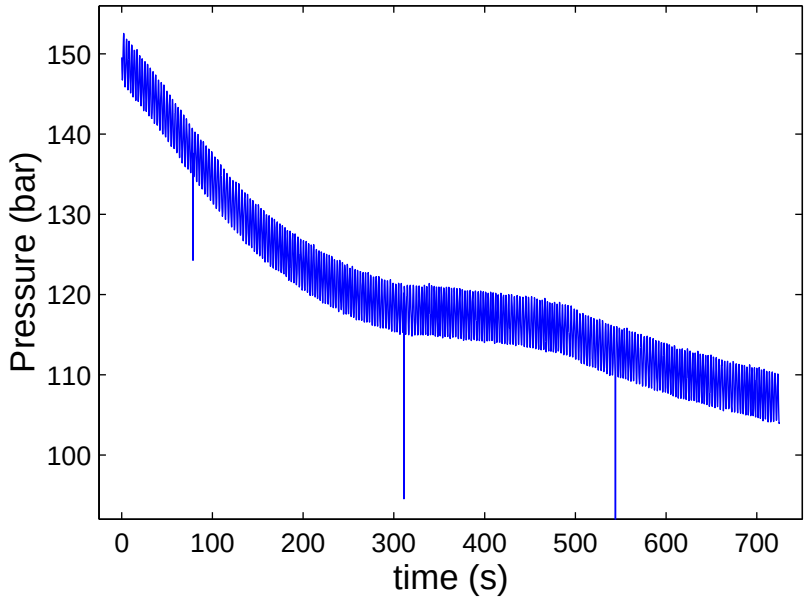
Test # 1 ; Shut−in # 4
Pressure (bar)
time (s)
150
140
130
120
110
100
0
100
200
300
400
500
600
700

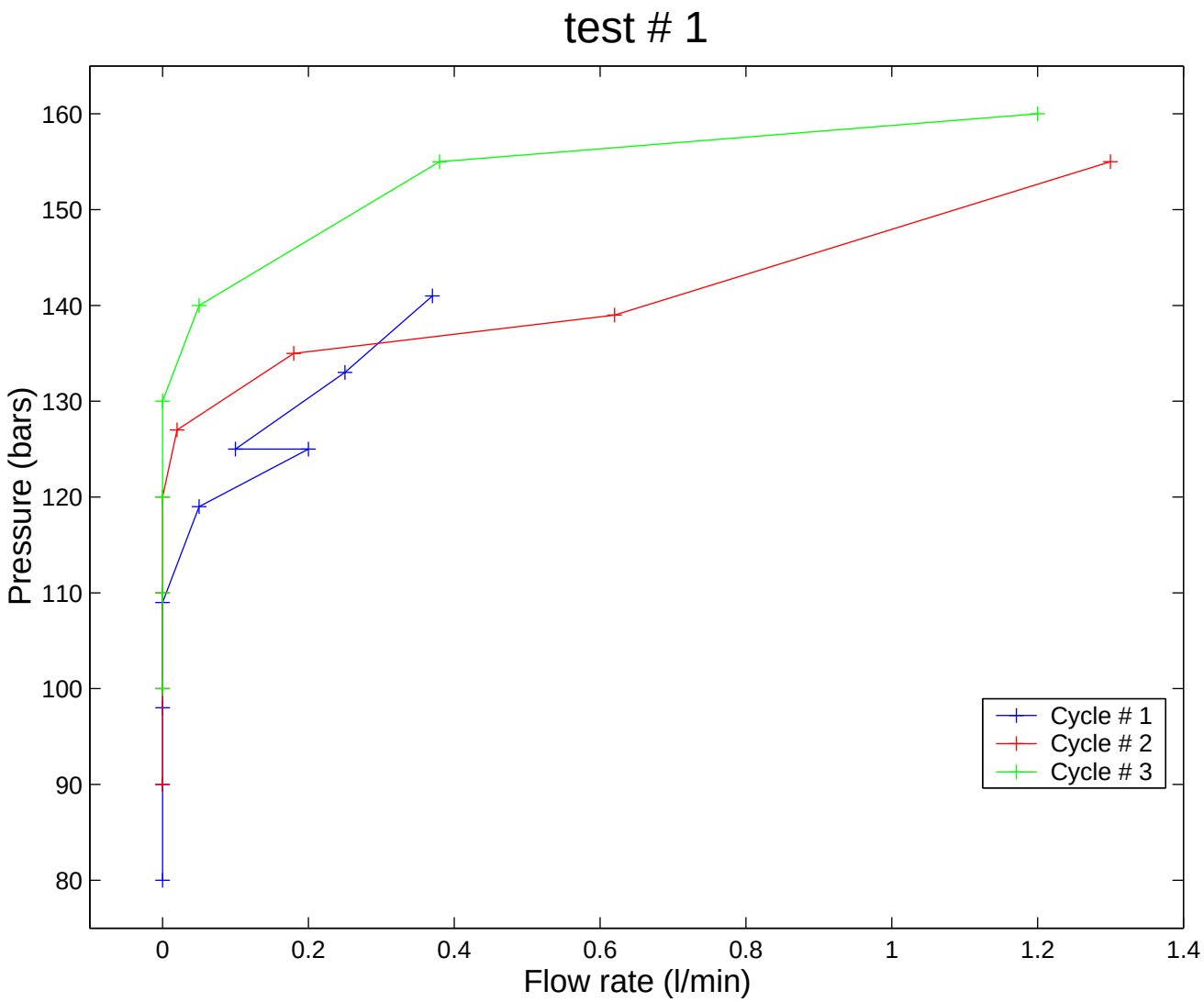
test # 1
Pressure (bars)
160
150
140
130
120
110
100
90
80
0
0.2
0.4
0.6
0.8
1
1.2
1.4
Flow rate (l/min)
Cycle # 1
Cycle # 2
Cycle # 3

KLX12A -- Post-frac Log # 1

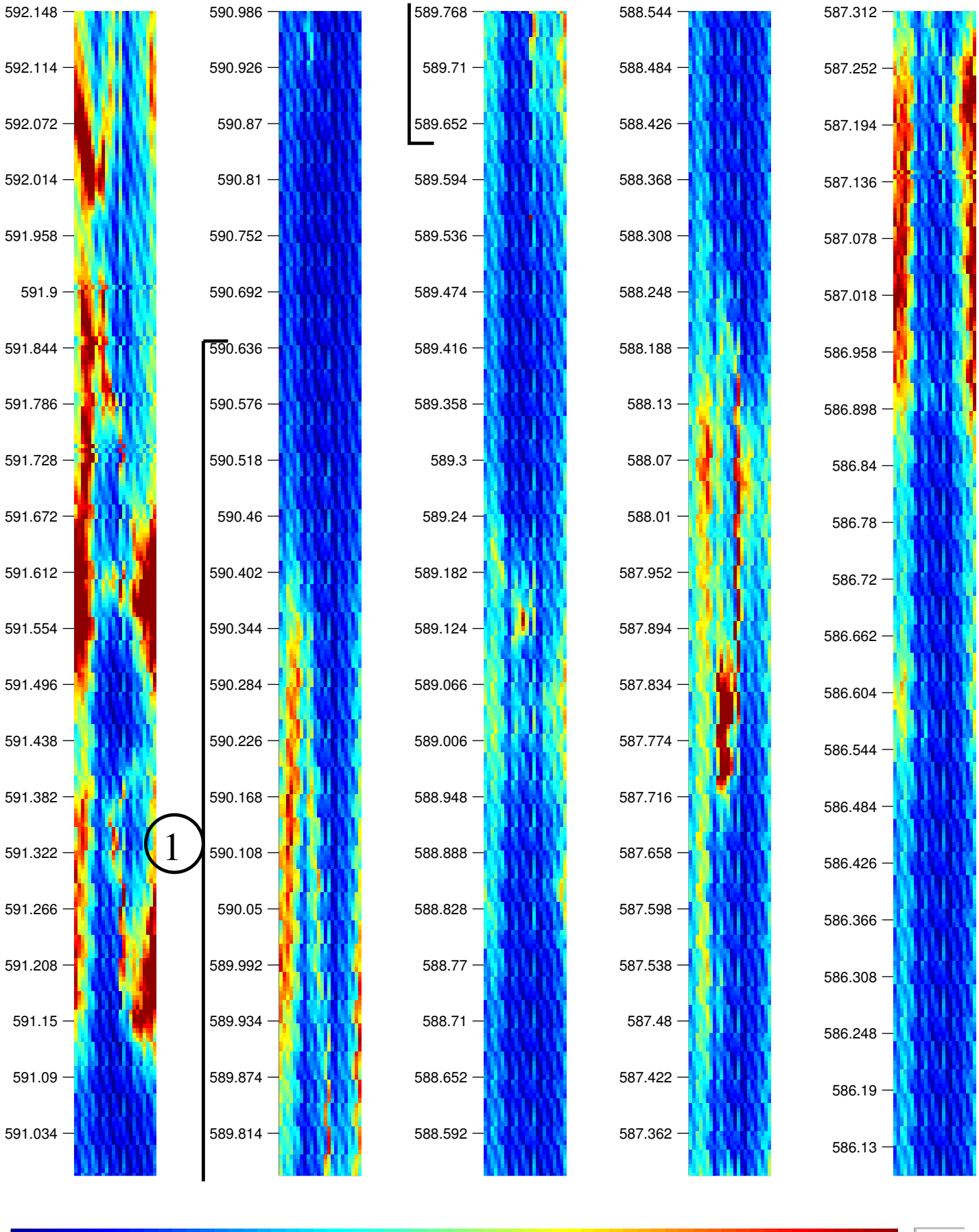

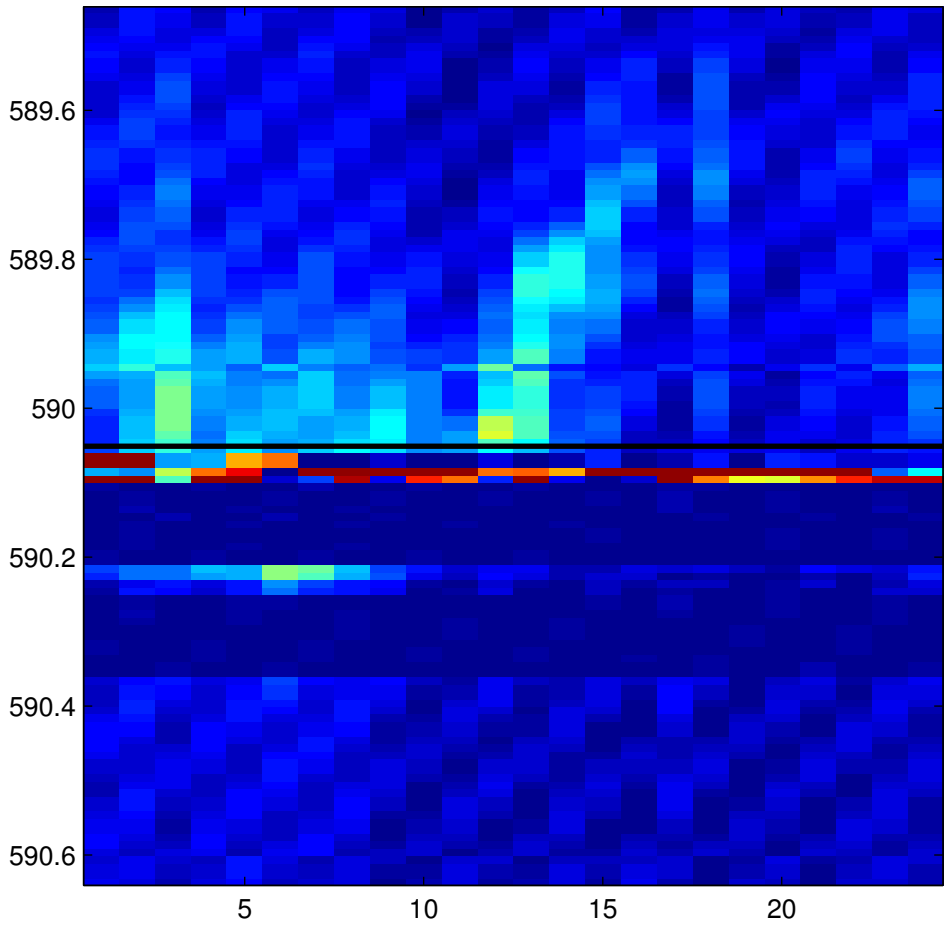

Repère du forage

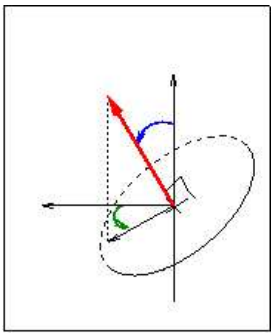

Repère absolu

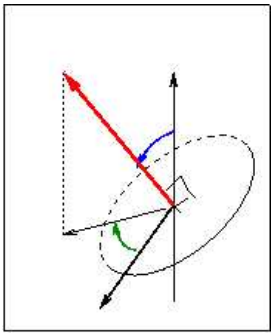

sinusoide visible

Diamètre 7.6 cm

Incidence ° Azimut °

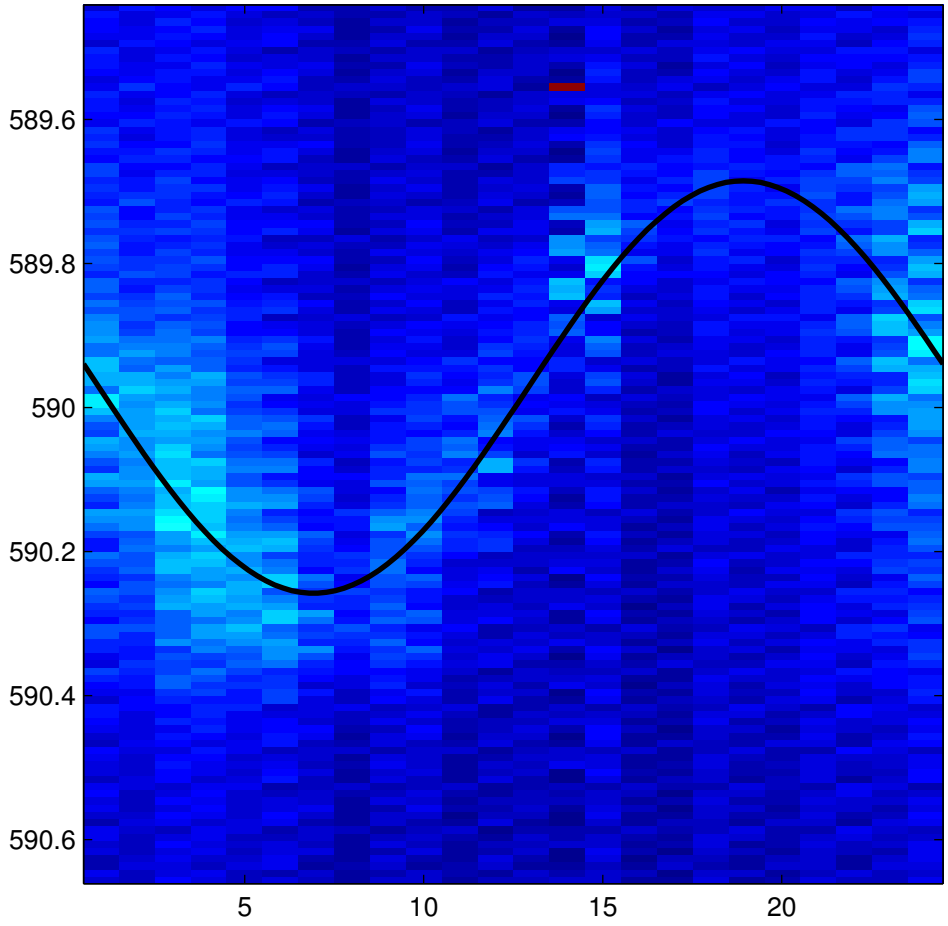

Repère du forage

277.2

82.4384

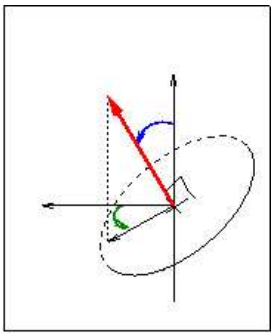

Repère absolu

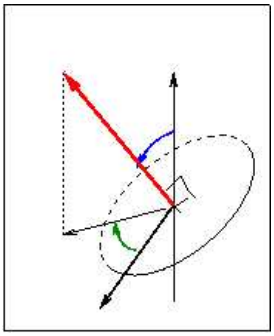

sinusoide visible

Diamètre 7.6 cm

Incidence ° Azimut °

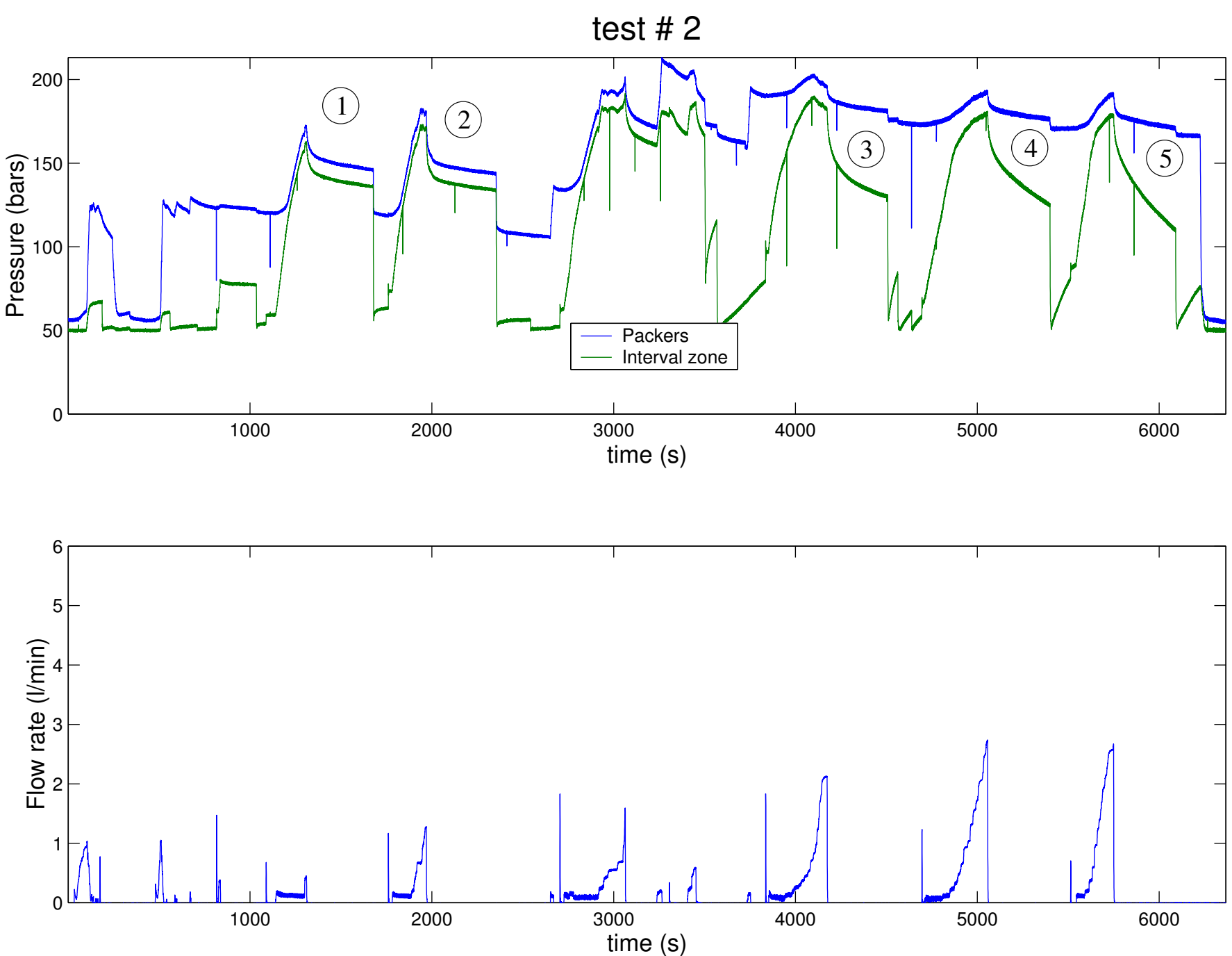
test # 2
Pressure (bars)
200
150
100
50
0
1
2
3
4
5
Packers
Interval zone
1000
2000
3000
4000
5000
6000
time (s)
Flow rate (l/min)
6
5
4
3
2
1
0
1000
2000
3000
4000
5000
6000
time (s)

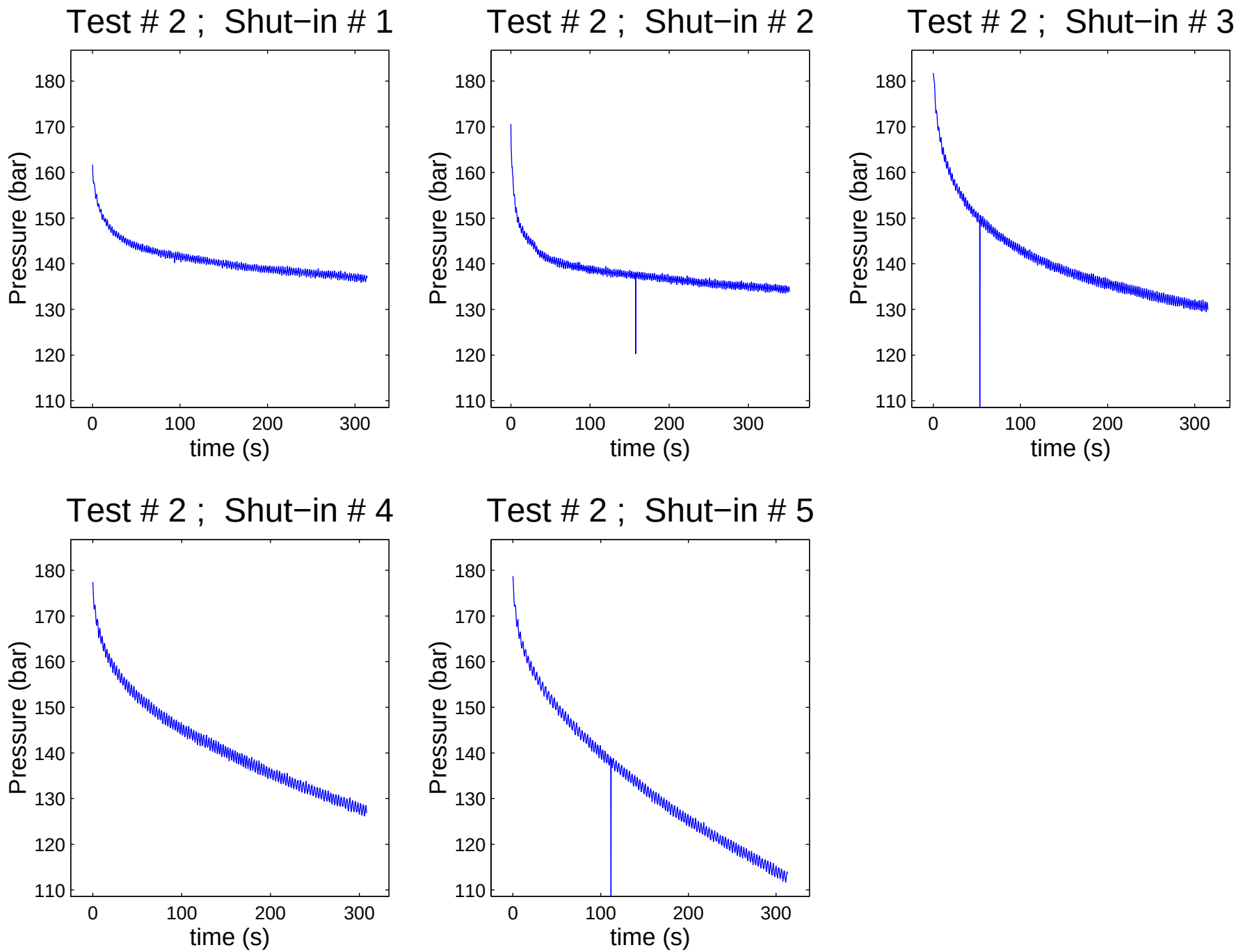
Test # 2 ; Shut−in # 1
Test # 2 ; Shut−in # 2
Test # 2 ; Shut−in # 3
Test # 2 ; Shut−in # 4
Test # 2 ; Shut−in # 5
Pressure (bar)
time (s)
180
170
160
150
140
130
120
110
0
100
200
300

KLX12A -- Post-frac Log # 2

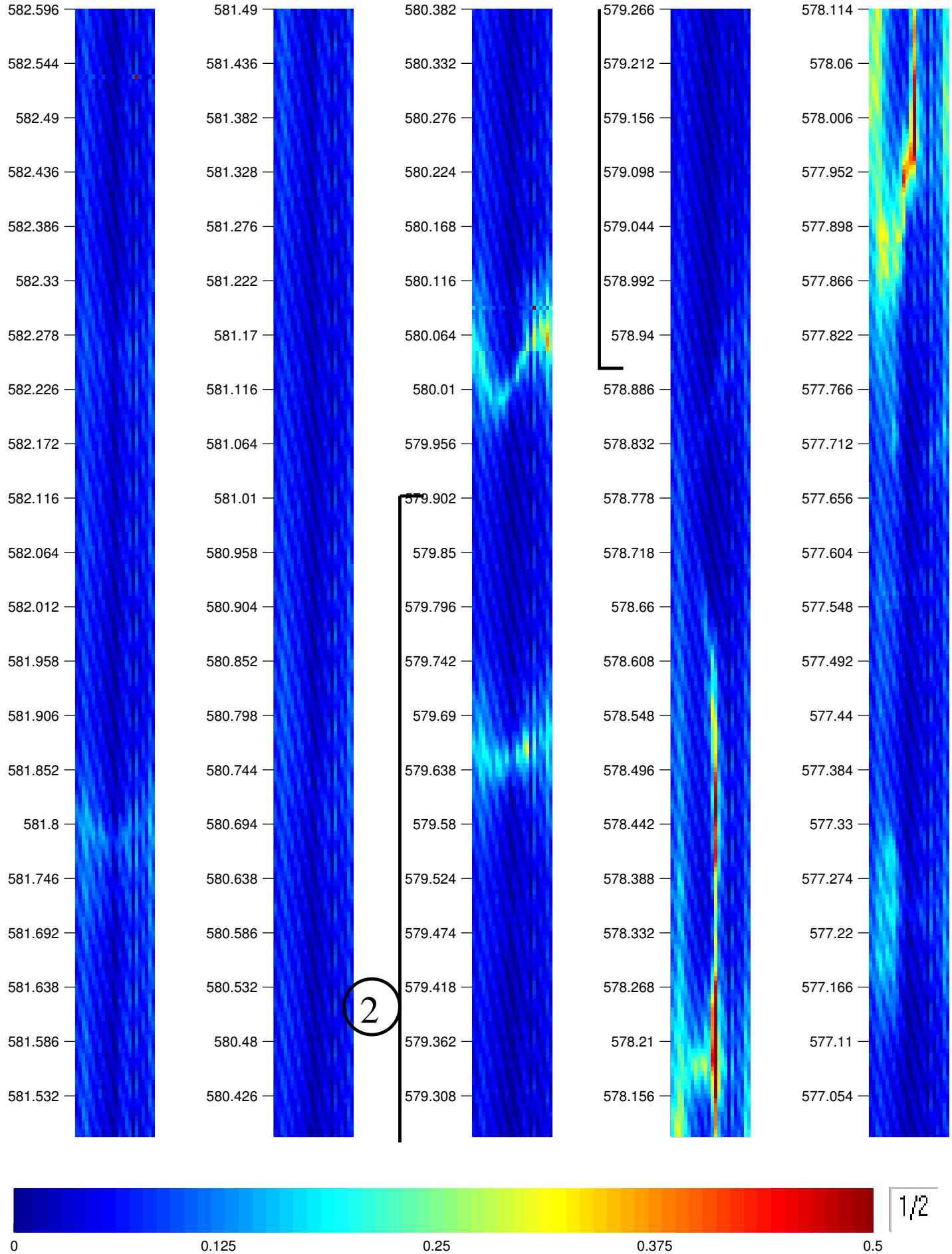

KLX12A -- Post-frac Log # 2

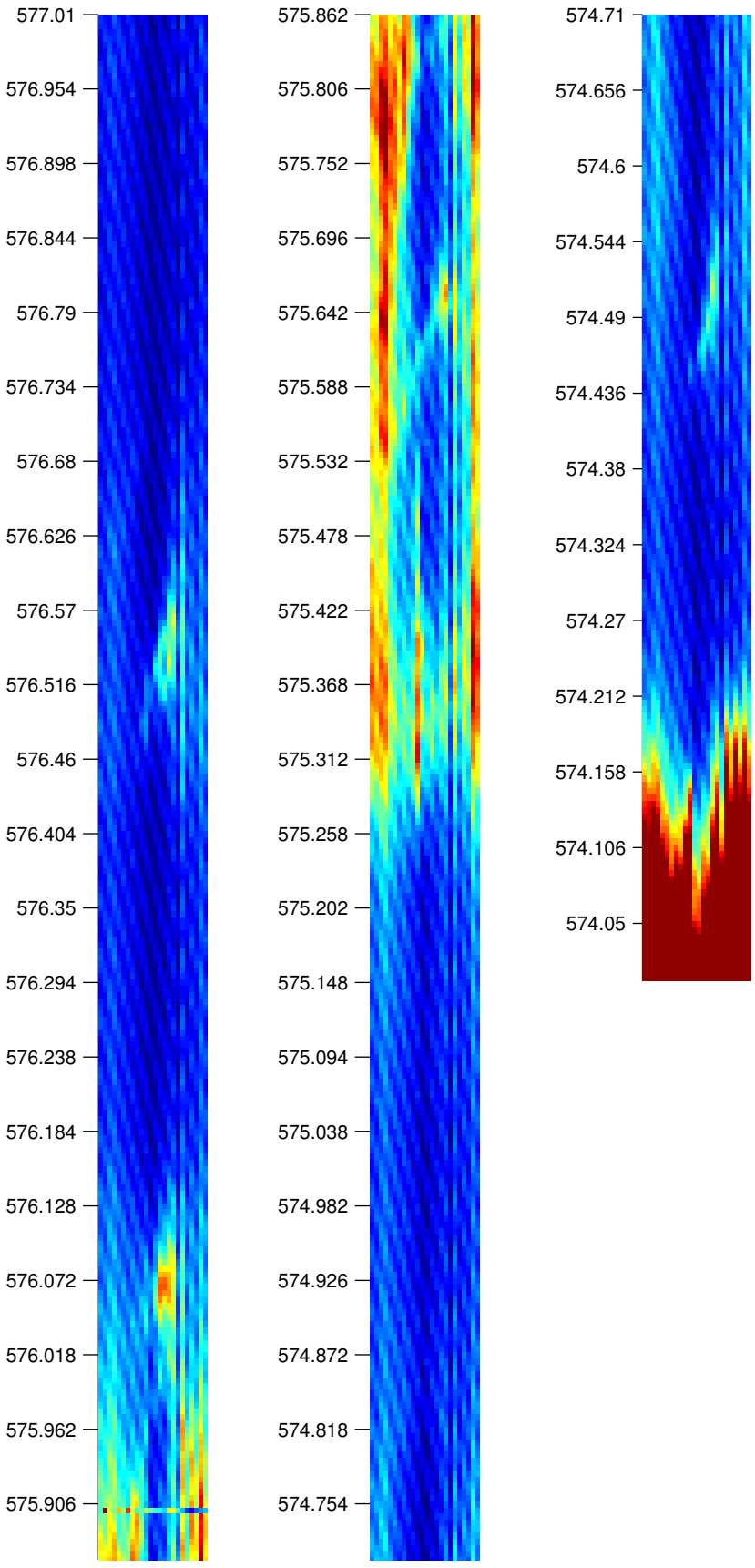

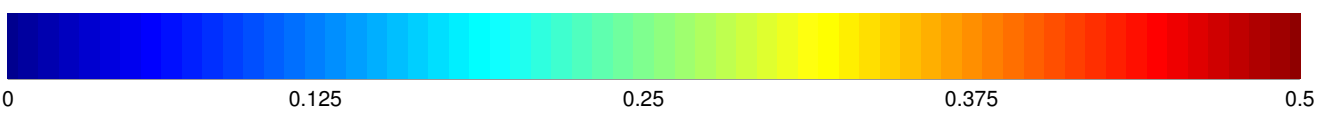

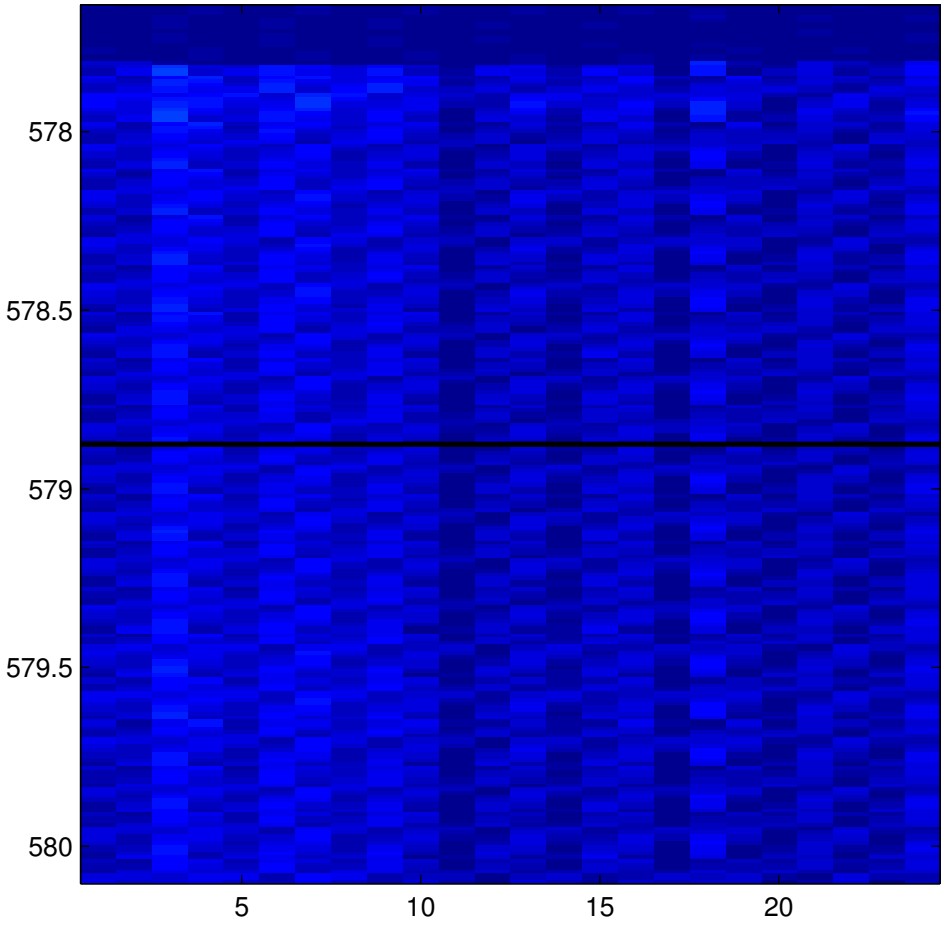

Repère du forage

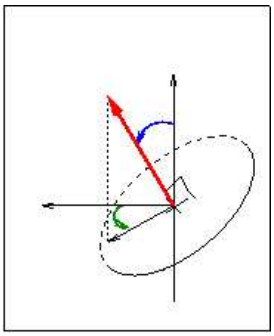

Repère absolu

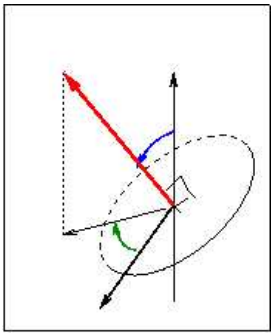

sinusoide visible

Diamètre 7.6 cm

Incidence ° Azimut °

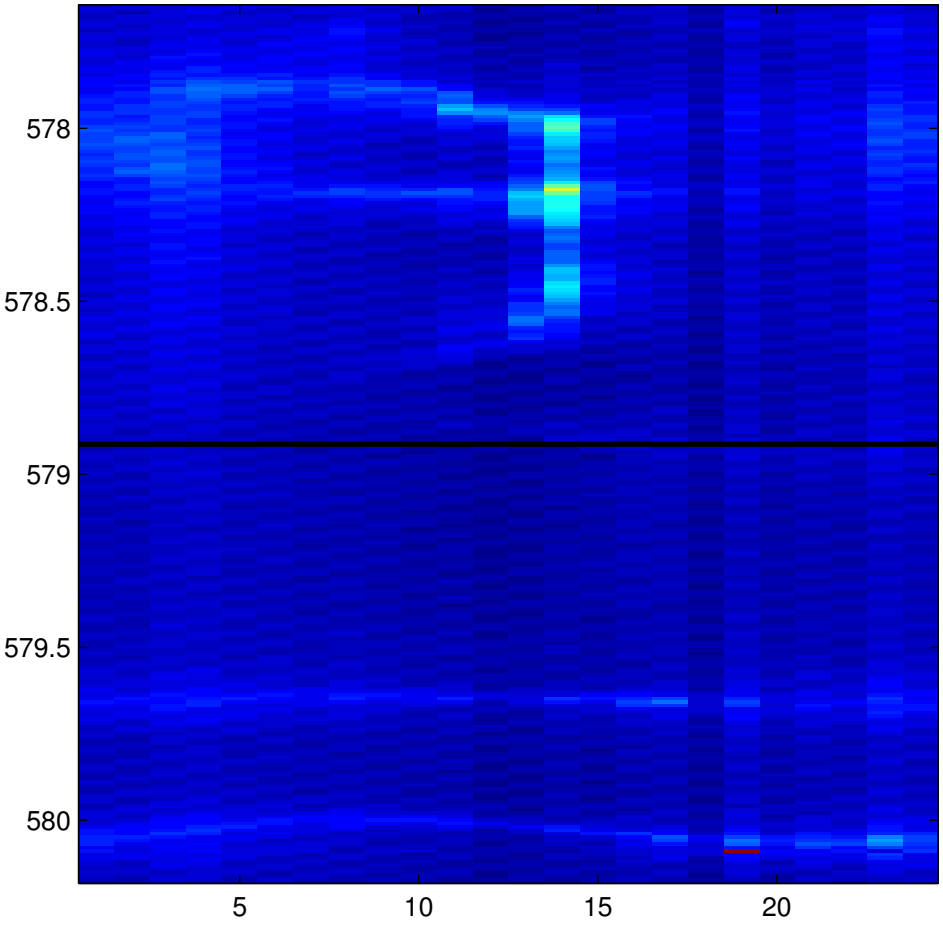

Repère du forage

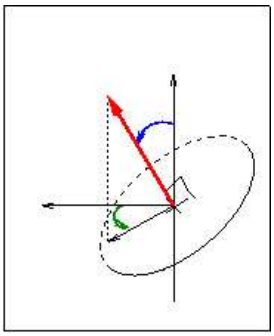

Repère absolu

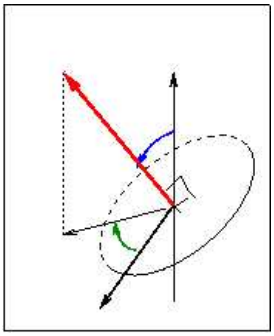

sinusoide visible

Diamètre 7.6 cm

Incidence ° Azimut °

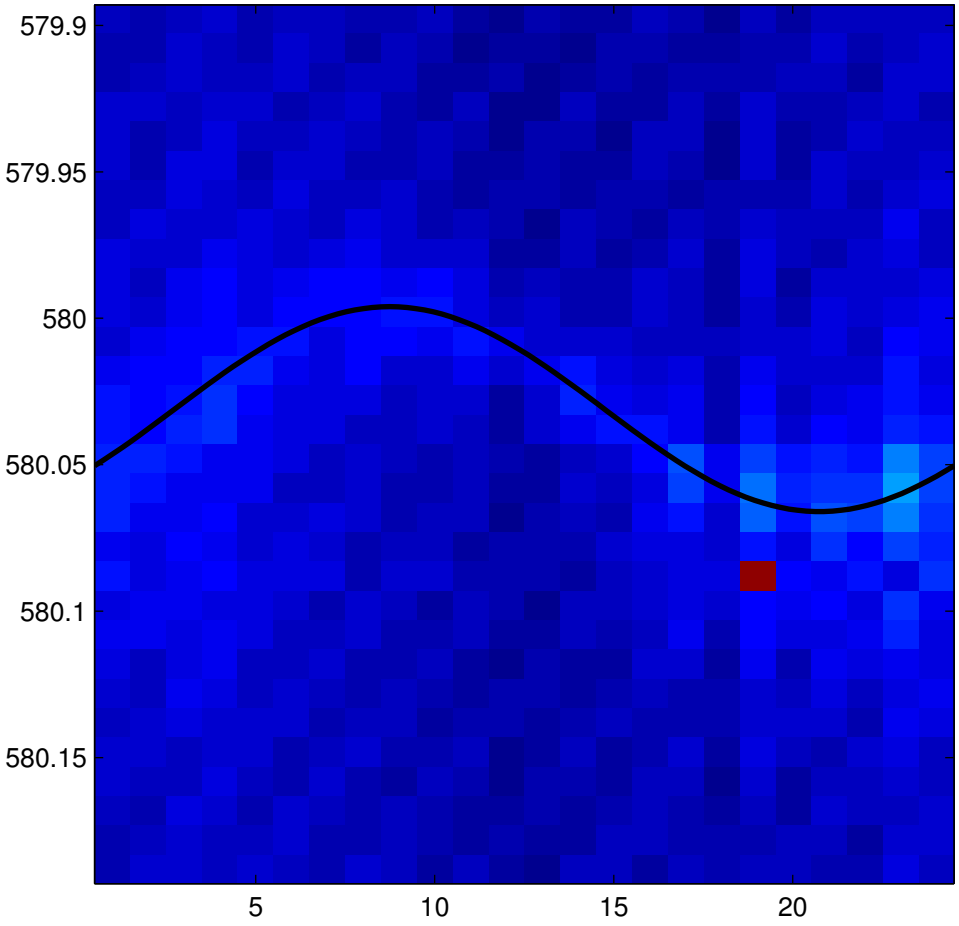

Repère du forage

126

42.6163

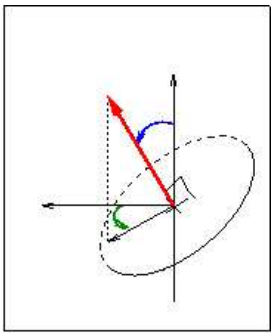

Repère absolu

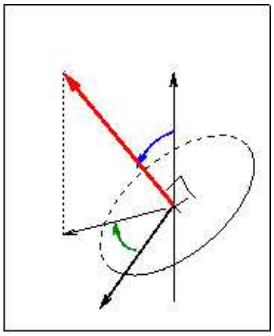

sinusoide visible

Diamètre 7.6 cm

Incidence ° Azimut °

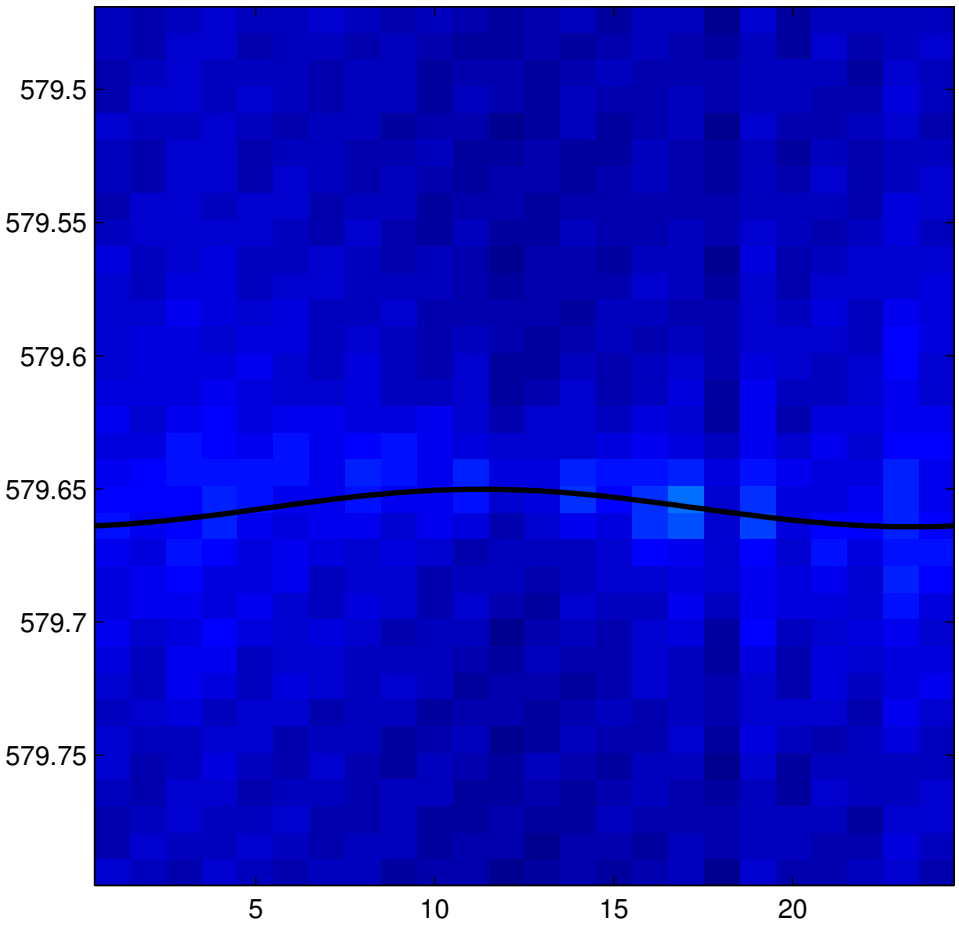

Repère du forage

165.6

10.4918

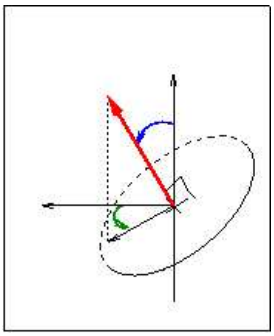

Repère absolu

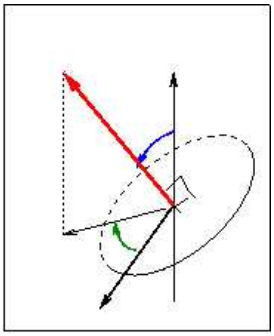

sinusoide visible

Diamètre 7.6 cm

Incidence ° Azimut °

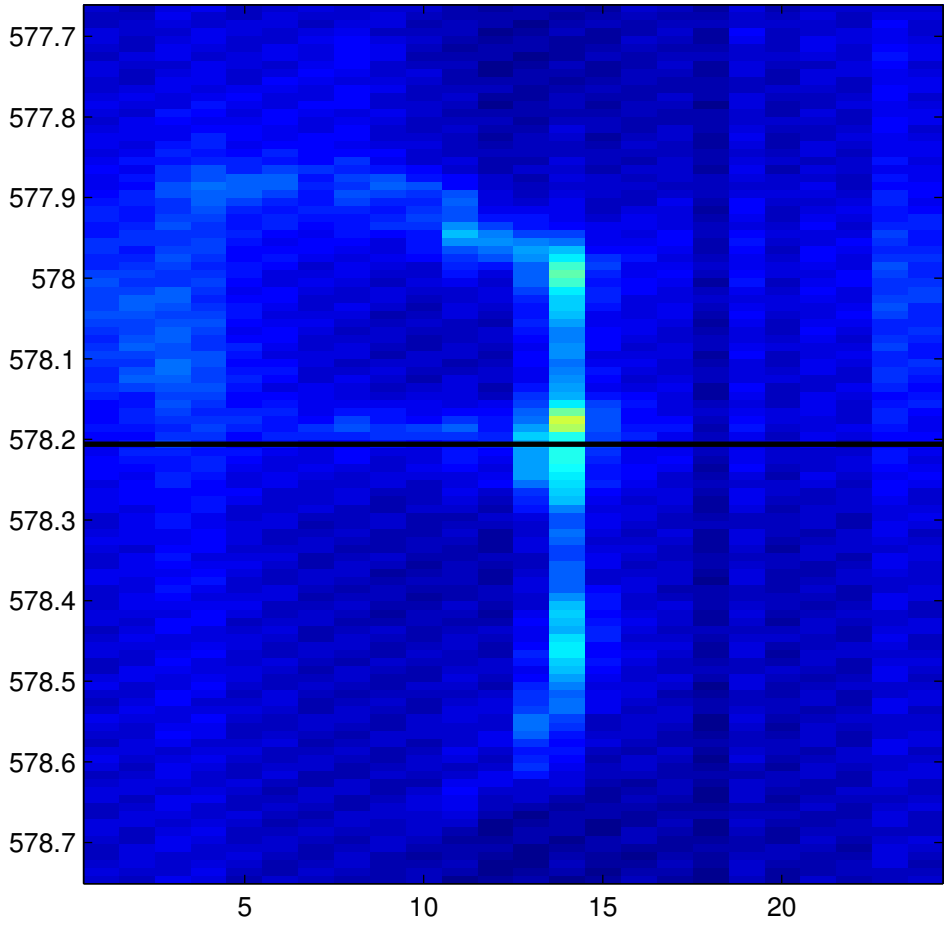

Repère du forage

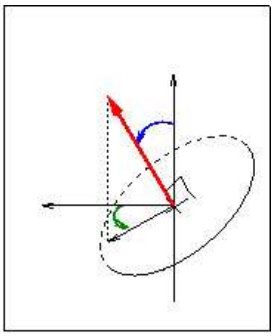

Repère absolu

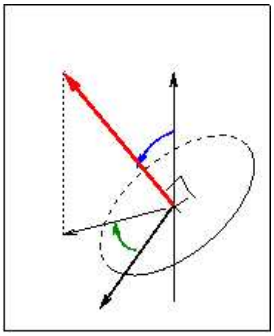

sinusoide visible

Diamètre 7.6 cm

Incidence ° Azimut °

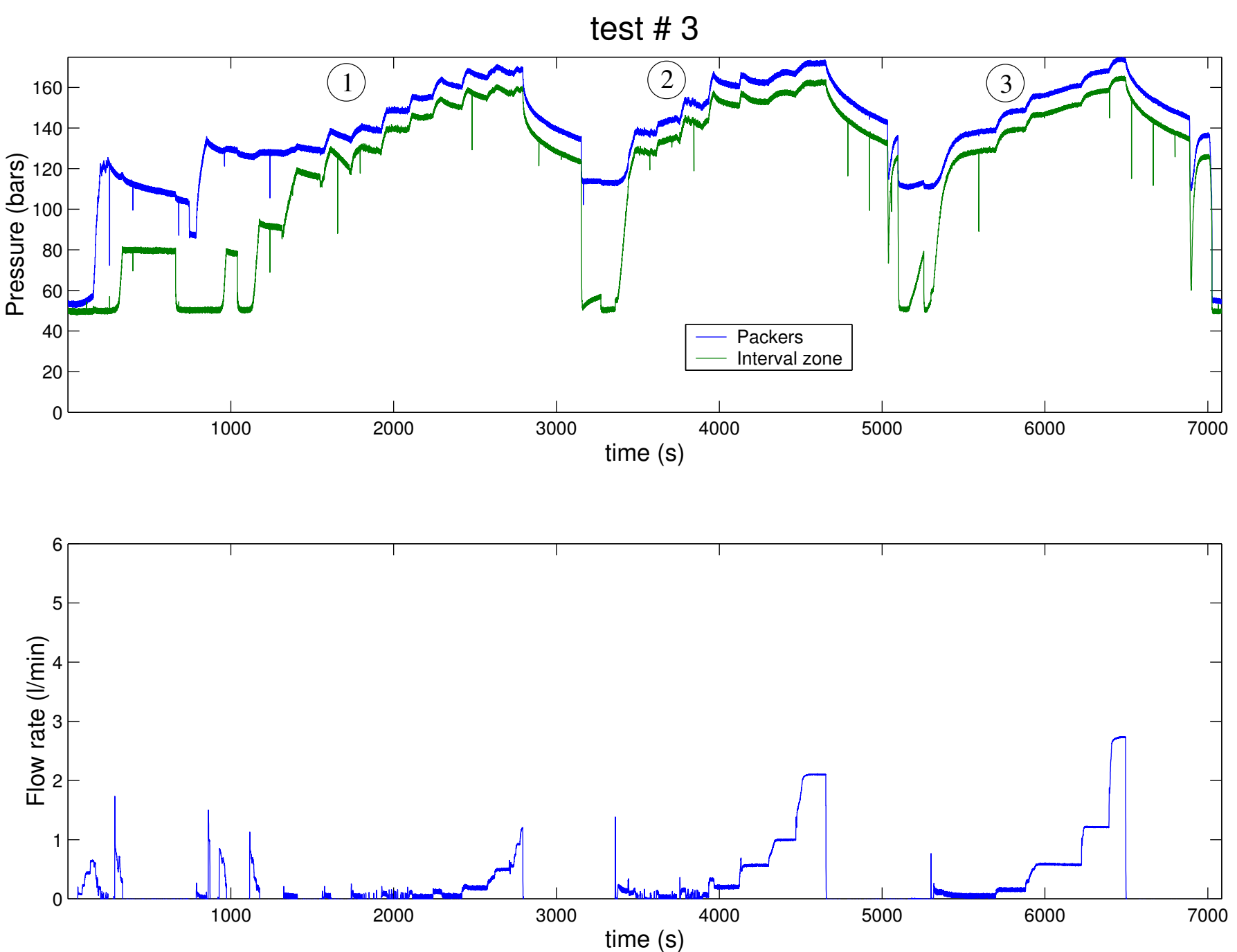
test # 3
1
2
3
Pressure (bars)
0
20
40
60
80
100
120
140
160
Packers
Interval zone
1000
2000
3000
4000
5000
6000
7000
time (s)
Flow rate (l/min)
0
1
2
3
4
5
6
1000
2000
3000
4000
5000
6000
7000
time (s)

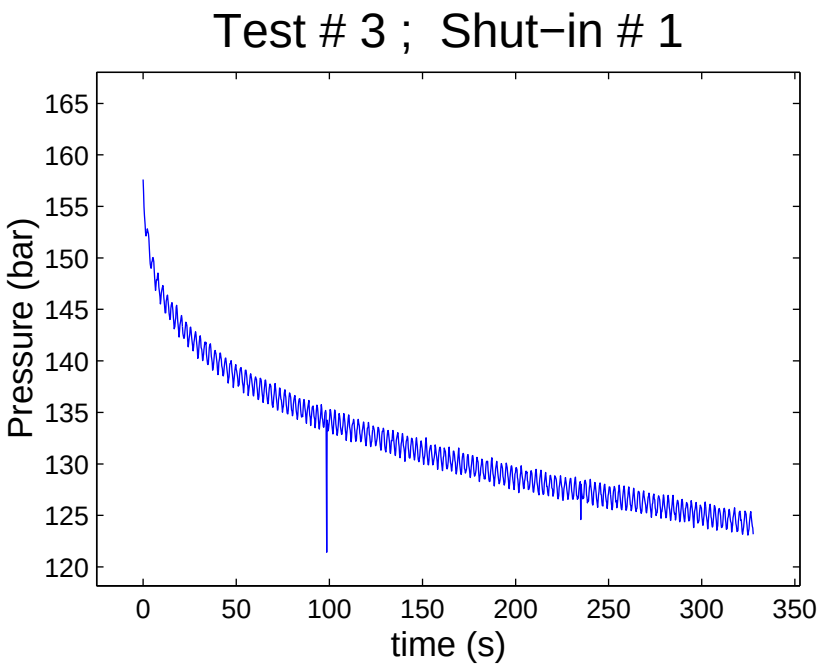
Test # 3 ; Shut−in # 1
Pressure (bar)
time (s)
165
160
155
150
145
140
135
130
125
120
0
50
100
150
200
250
300
350

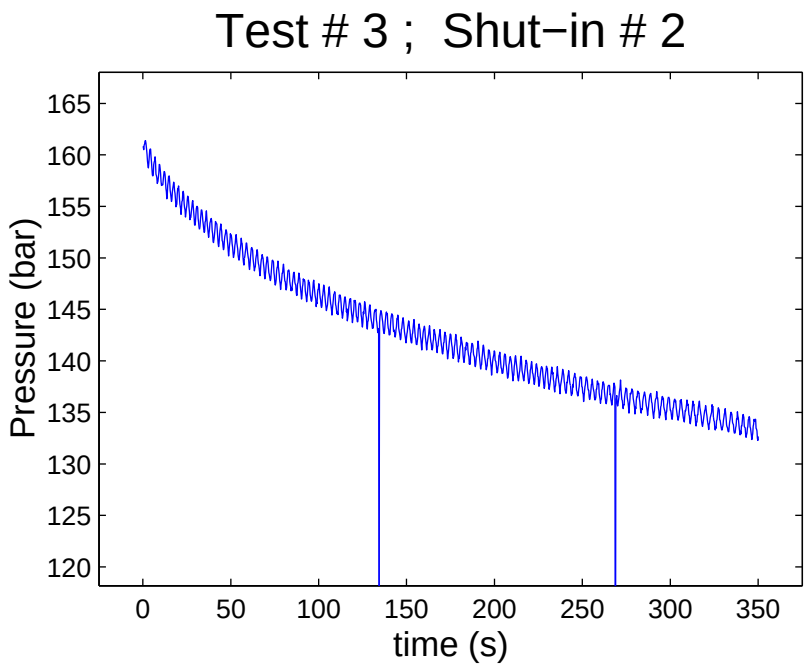
Test # 3 ; Shut−in # 2
Pressure (bar)
time (s)
165
160
155
150
145
140
135
130
125
120
0
50
100
150
200
250
300
350

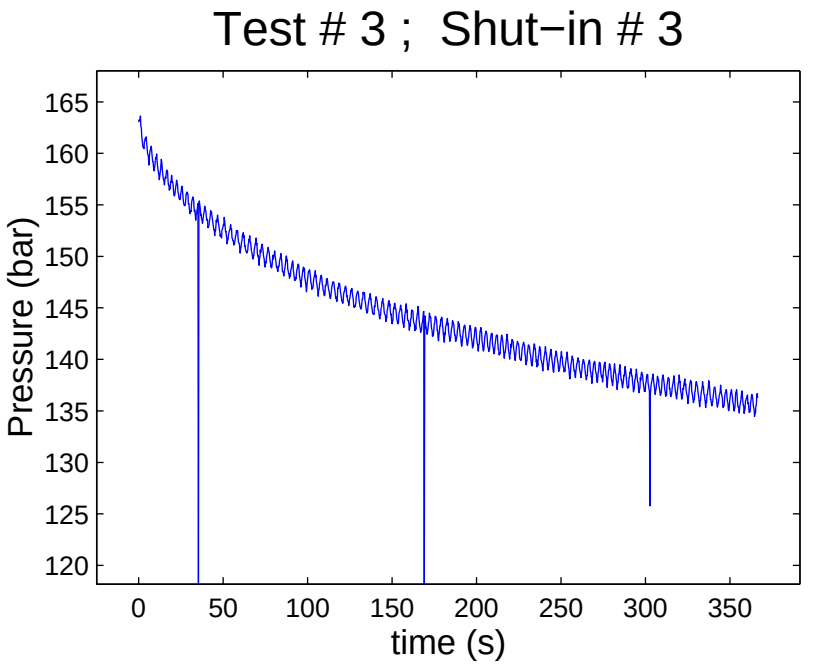
Test # 3 ; Shut−in # 3
Pressure (bar)
time (s)
165
160
155
150
145
140
135
130
125
120
0
50
100
150
200
250
300
350

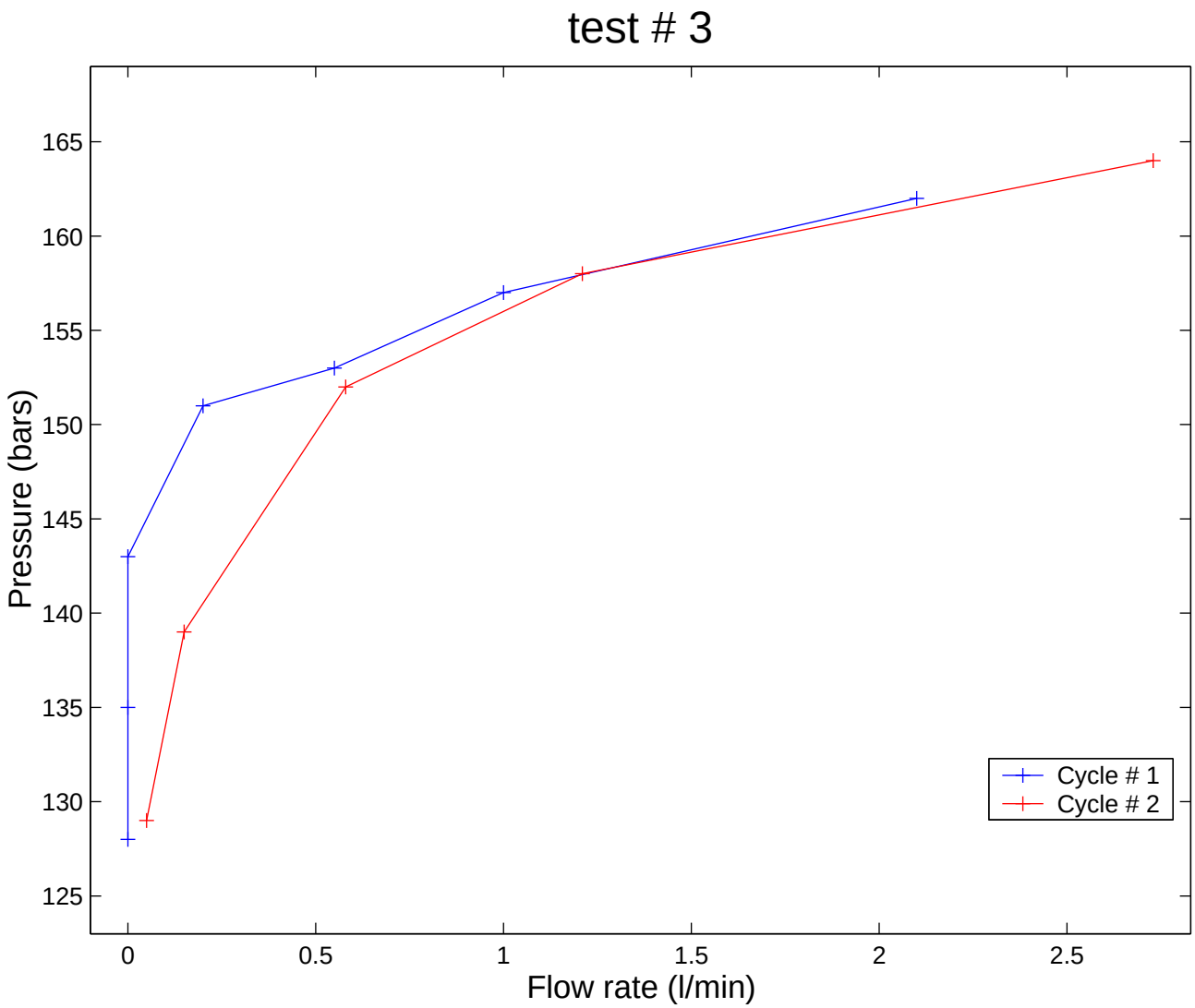
test # 3
Pressure (bars)
165
160
155
150
145
140
135
130
125
0
0.5
1
1.5
2
2.5
Flow rate (l/min)
Cycle # 1
Cycle # 2

KLX12A -- Post-frac Log # 3

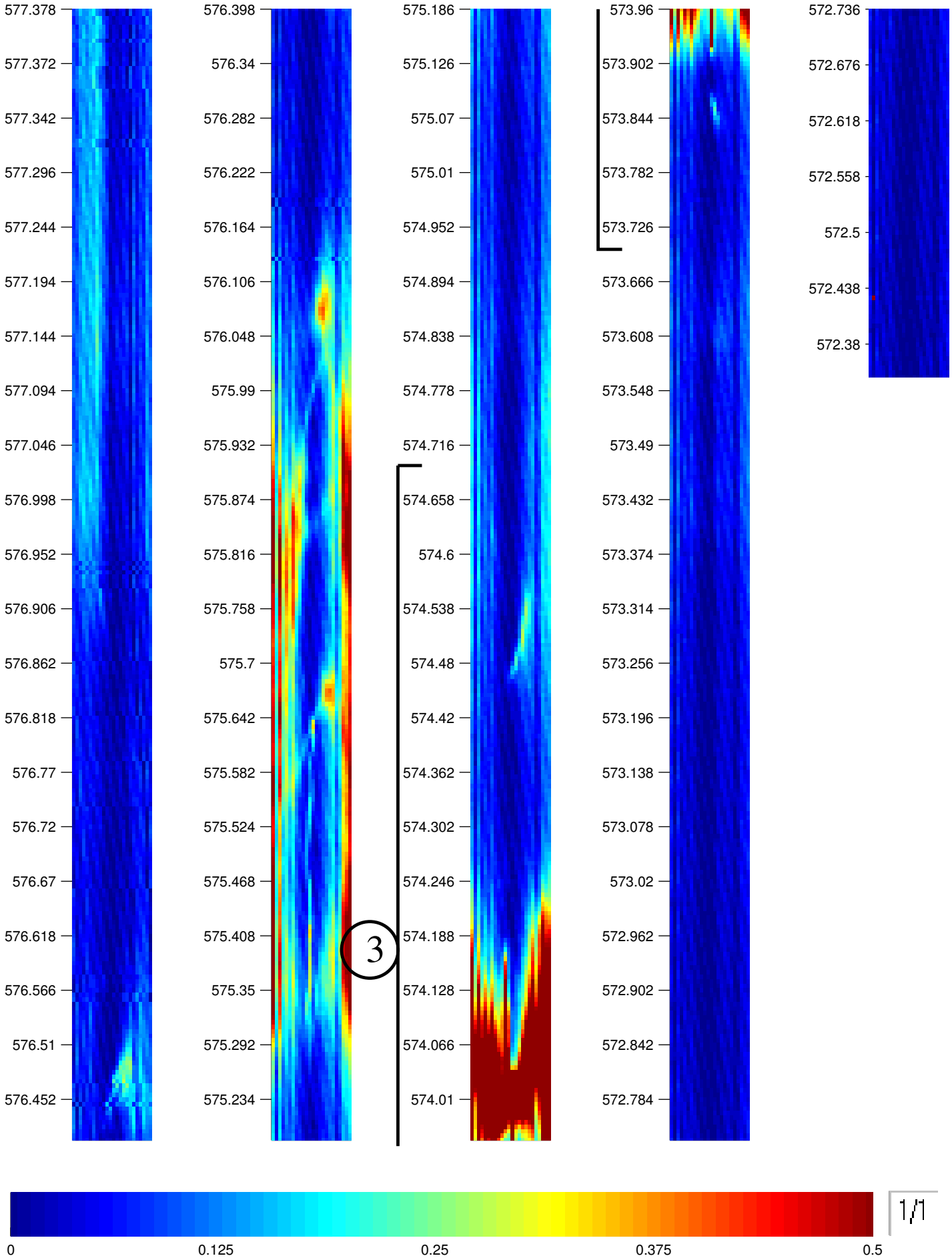

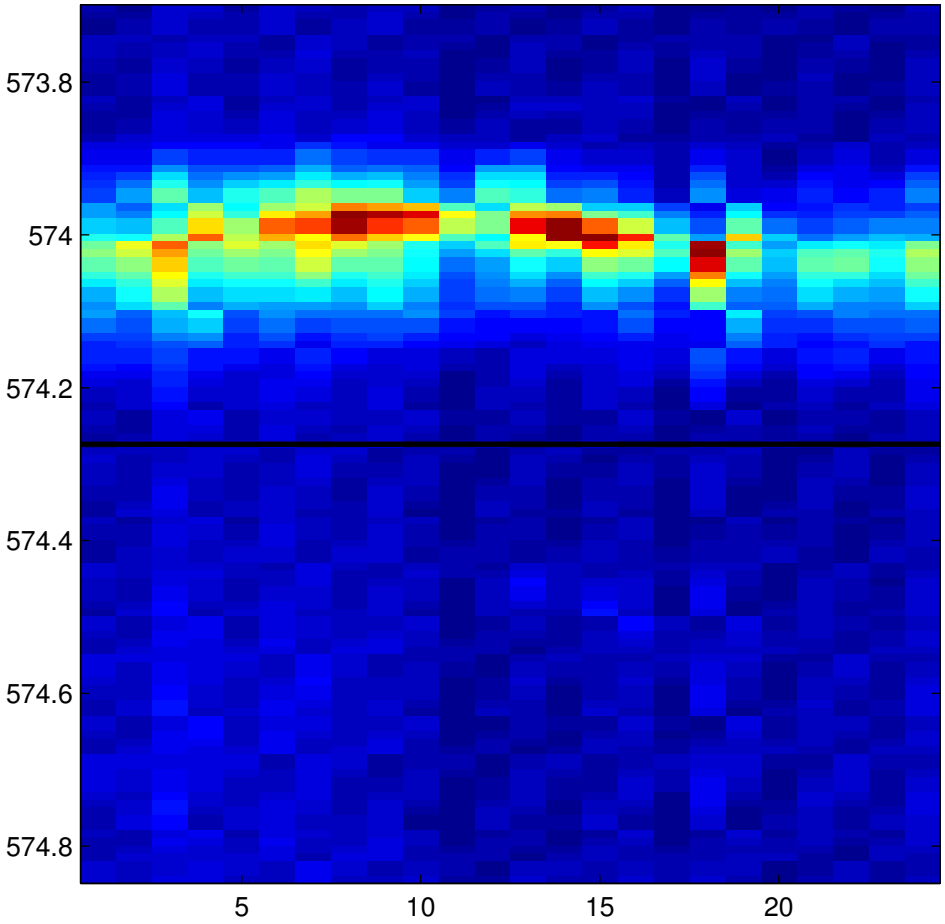

Repère du forage

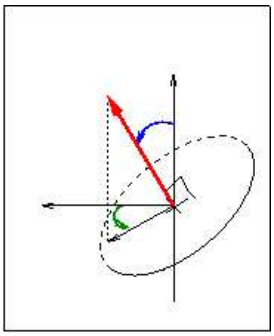

Repère absolu

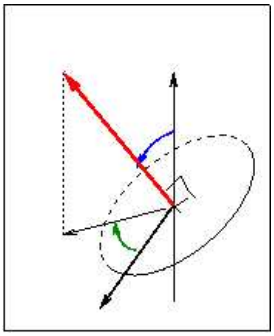

sinusoide visible

Diamètre 7.6 cm

Incidence ° Azimut °

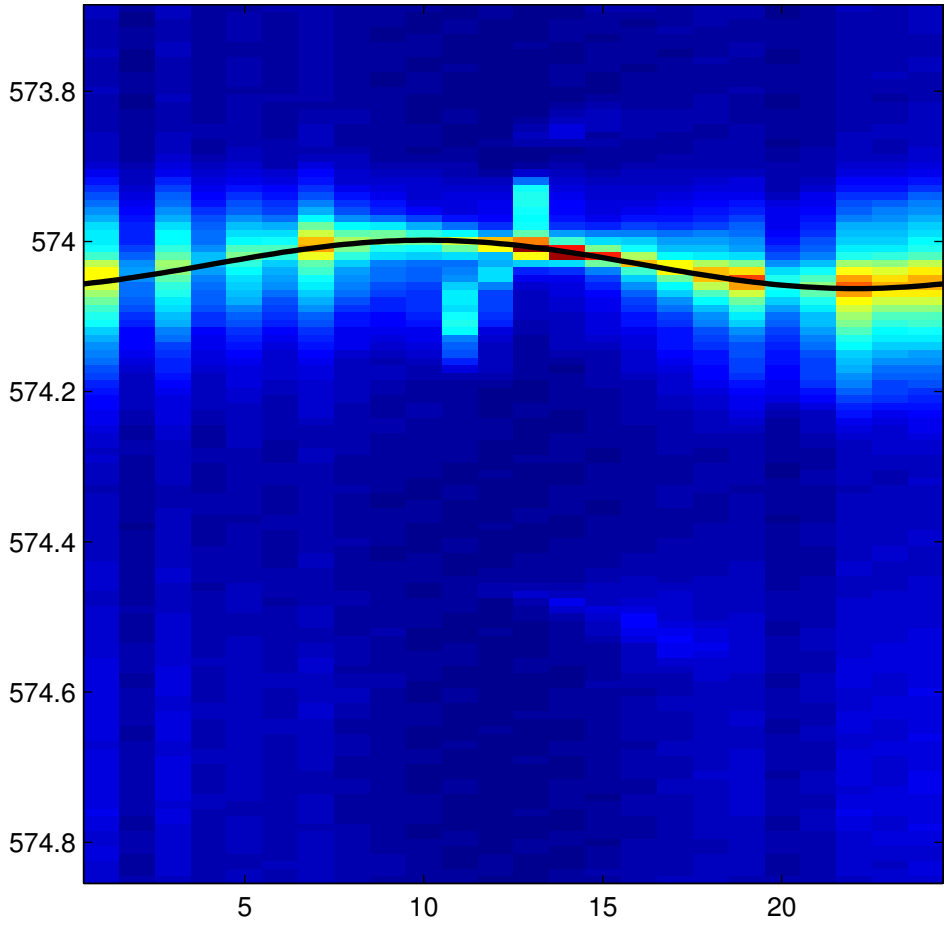

Repère du forage

144

40.2851

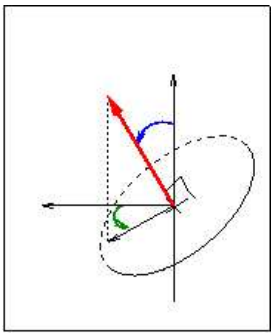

Repère absolu

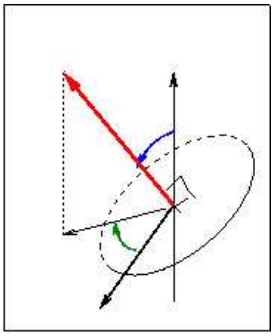

sinusoide visible

Diamètre 7.6 cm

Incidence ° Azimut °

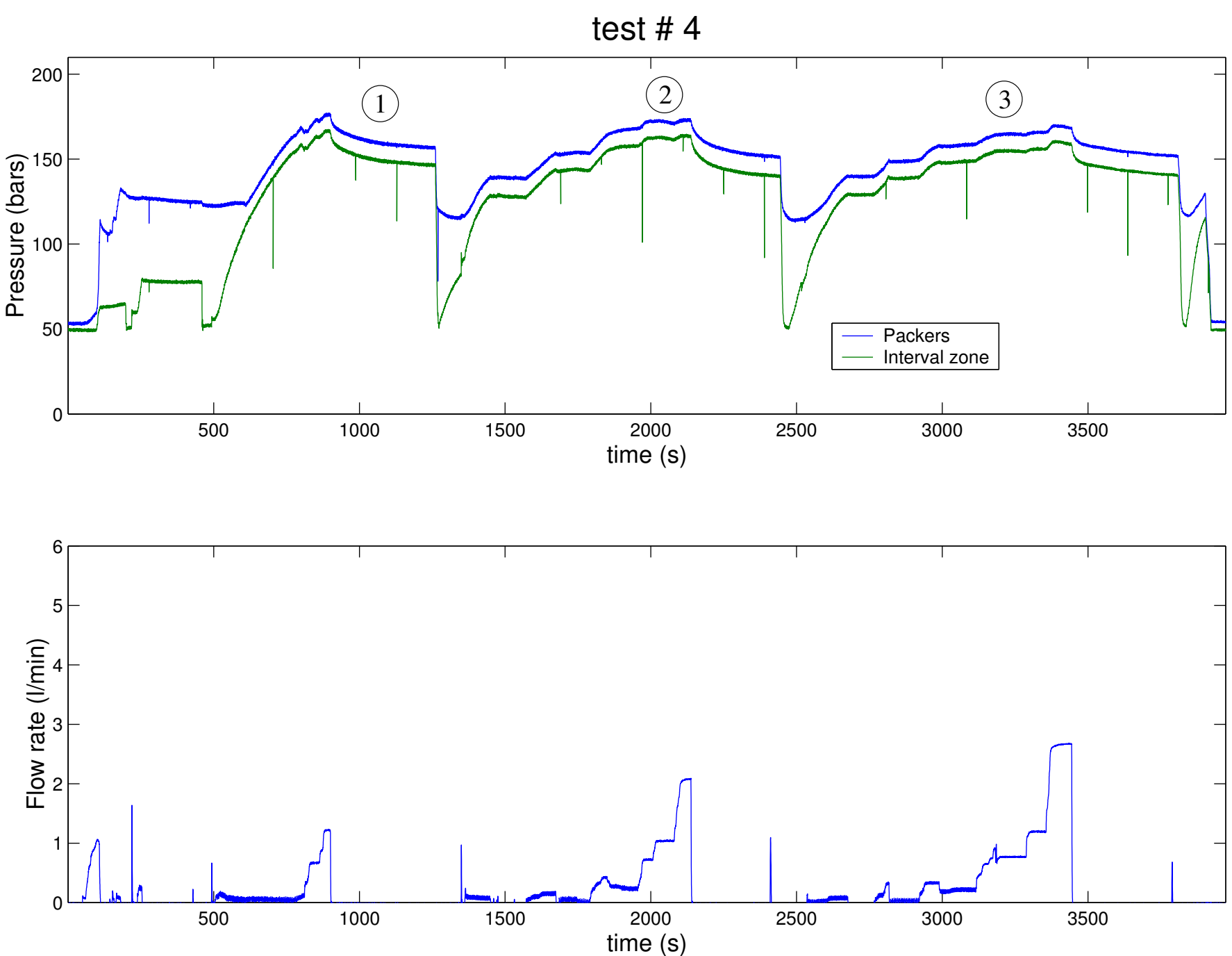
test # 4
Pressure (bars)
200
150
100
50
0
1
2
3
Packers
Interval zone
500
1000
1500
2000
2500
3000
3500
time (s)
Flow rate (l/min)
6
5
4
3
2
1
0
500
1000
1500
2000
2500
3000
3500
time (s)

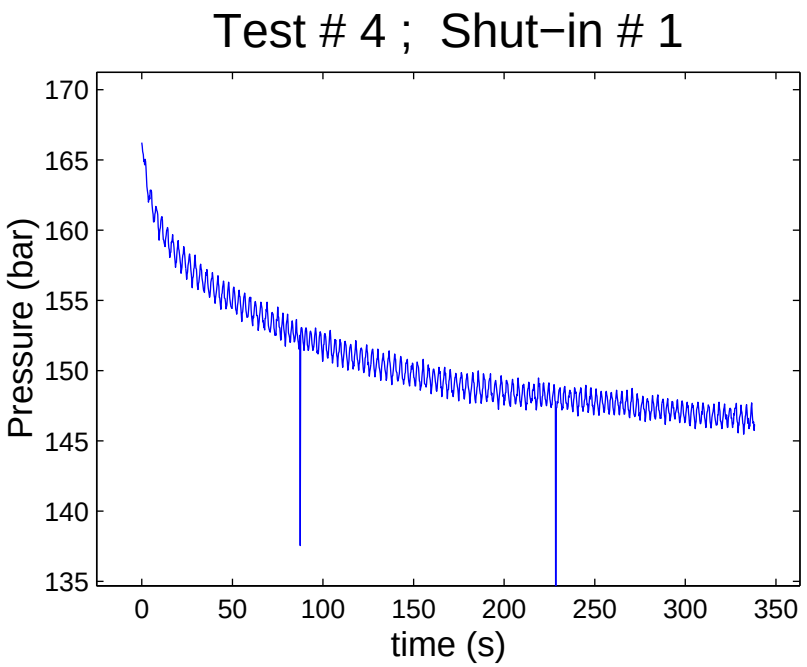
Test # 4 ; Shut−in # 1
Pressure (bar)
time (s)
170
165
160
155
150
145
140
135
0
50
100
150
200
250
300
350

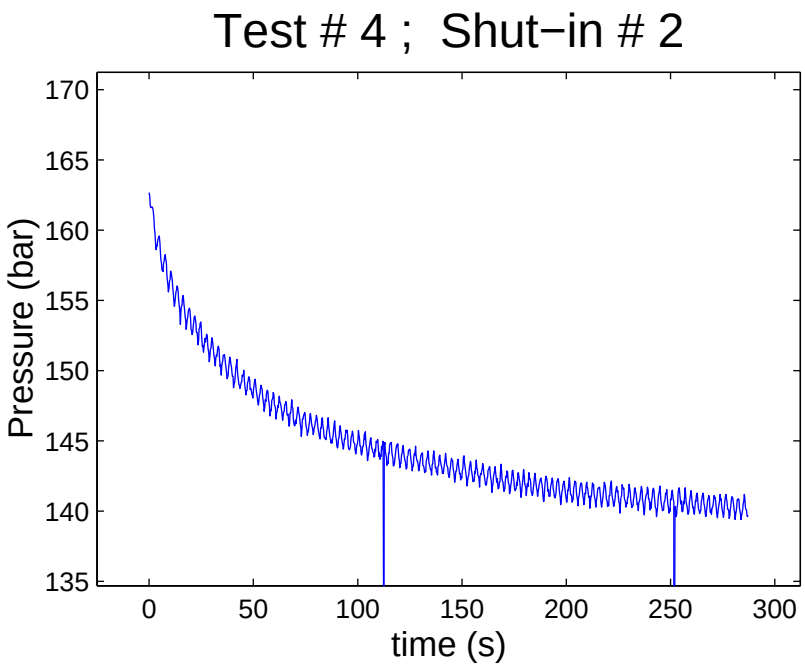
Test # 4 ; Shut−in # 2
Pressure (bar)
time (s)
170
165
160
155
150
145
140
135
0
50
100
150
200
250
300

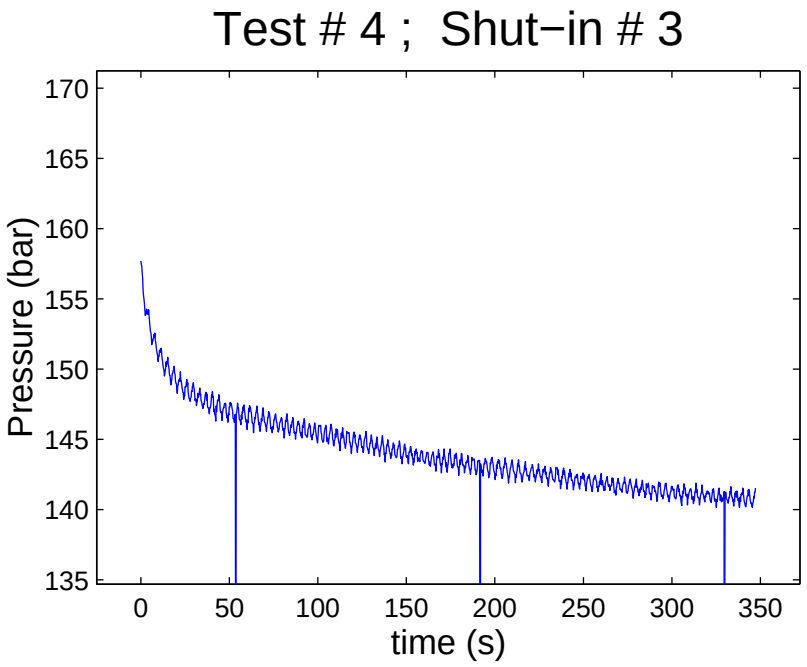
Test # 4 ; Shut−in # 3
Pressure (bar)
time (s)
170
165
160
155
150
145
140
135
0
50
100
150
200
250
300
350

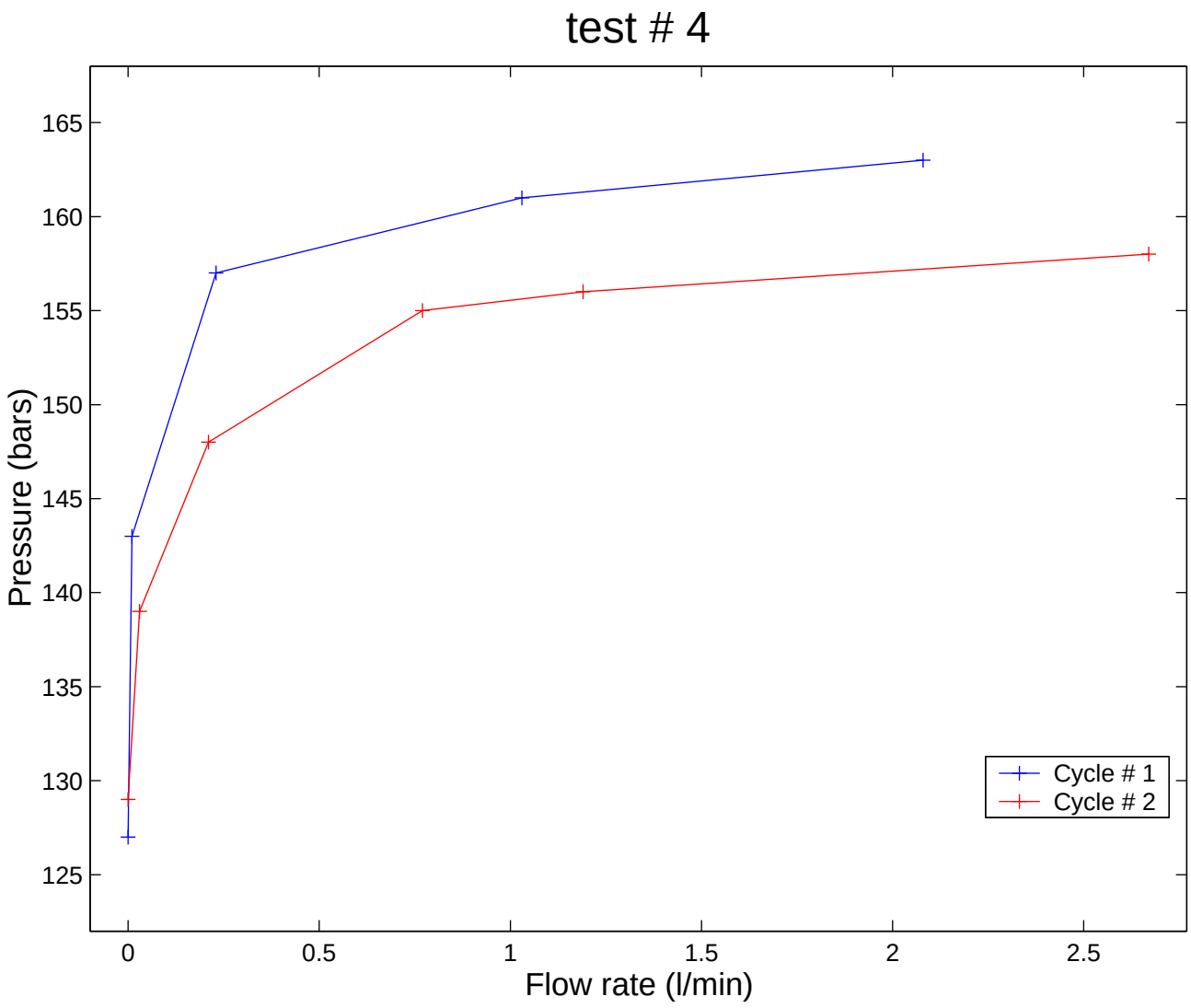
test # 4
Pressure (bars)
165
160
155
150
145
140
135
130
125
0
0.5
1
1.5
2
2.5
Flow rate (l/min)
Cycle # 1
Cycle # 2

KLX12A -- Post-frac Log # 4

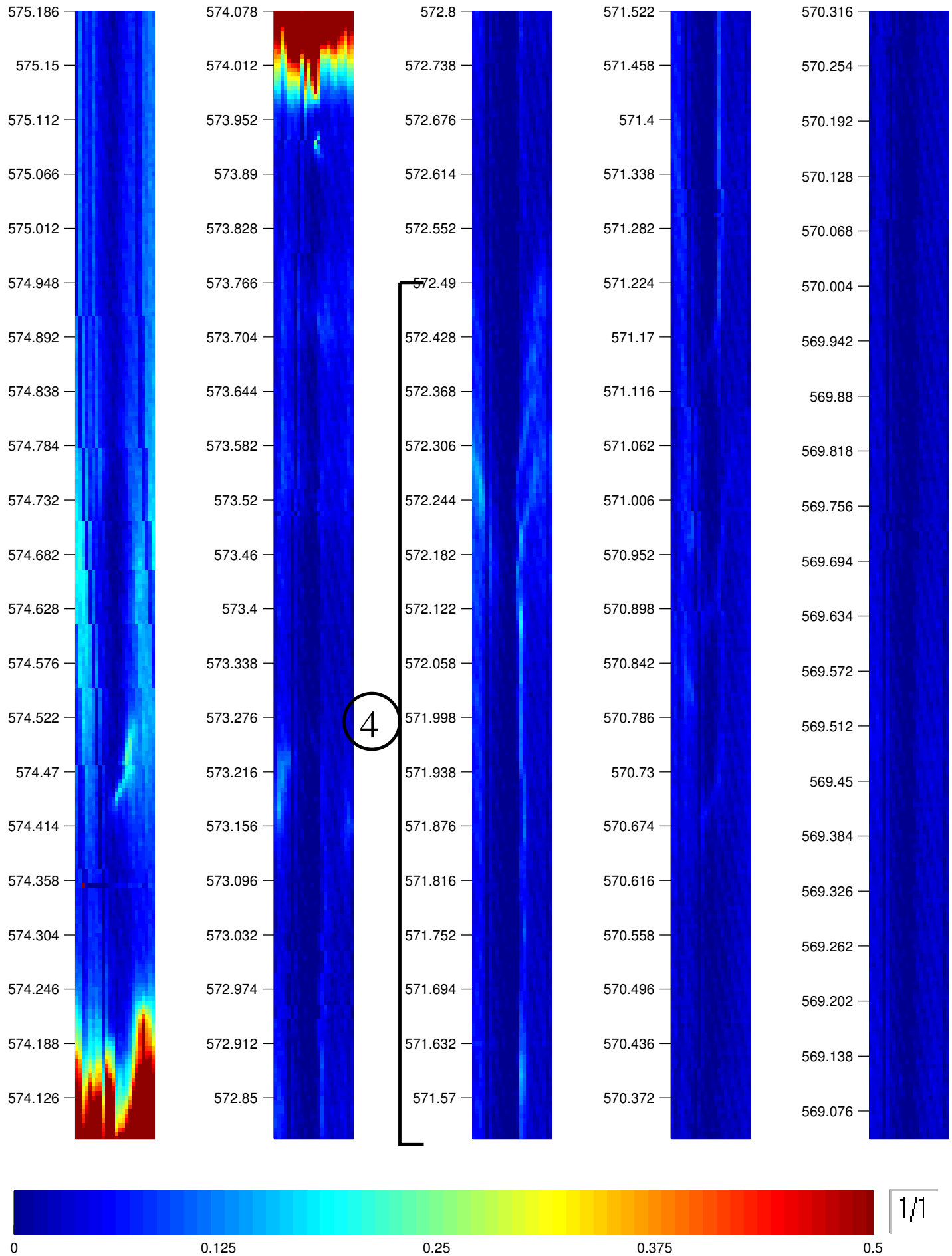

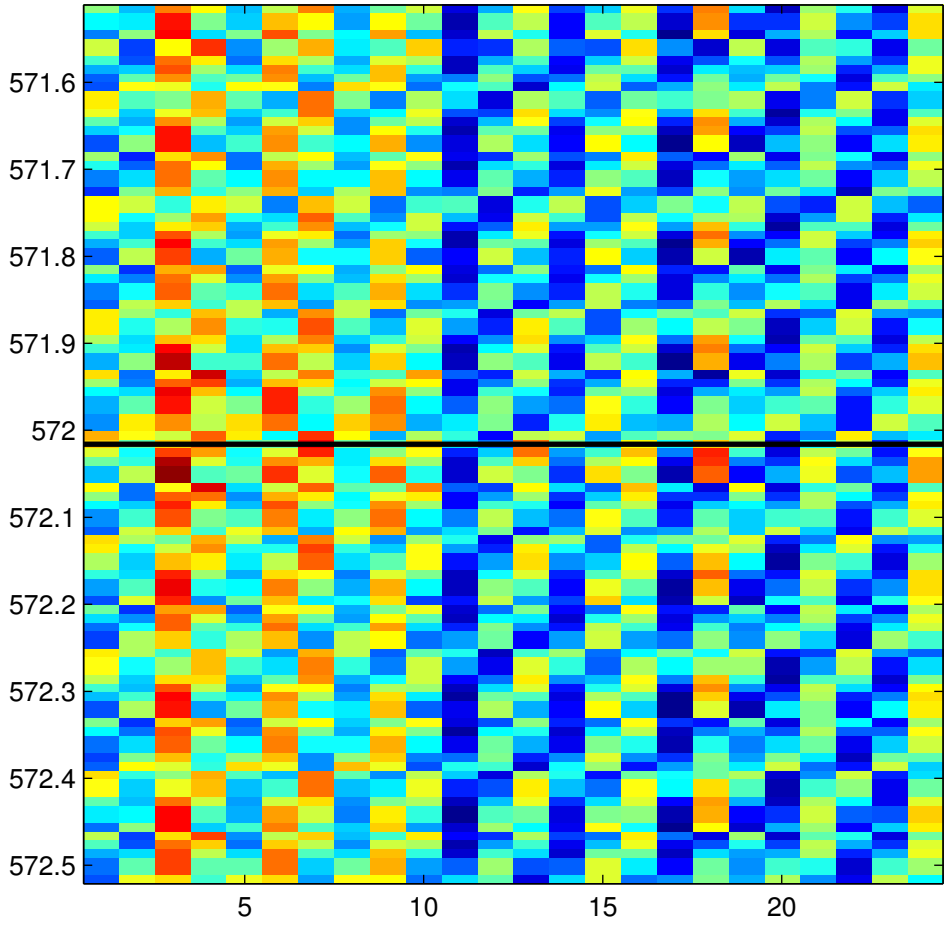

Repère du forage

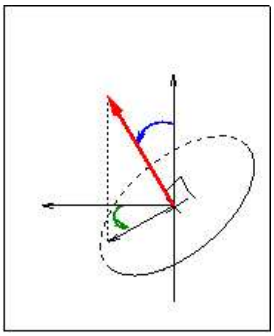

Repère absolu

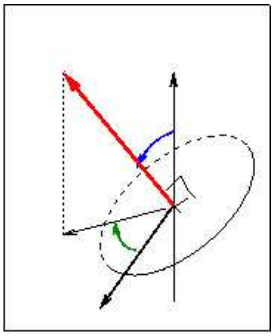

sinusoide visible

Diamètre 7.6 cm

Incidence ° Azimut °

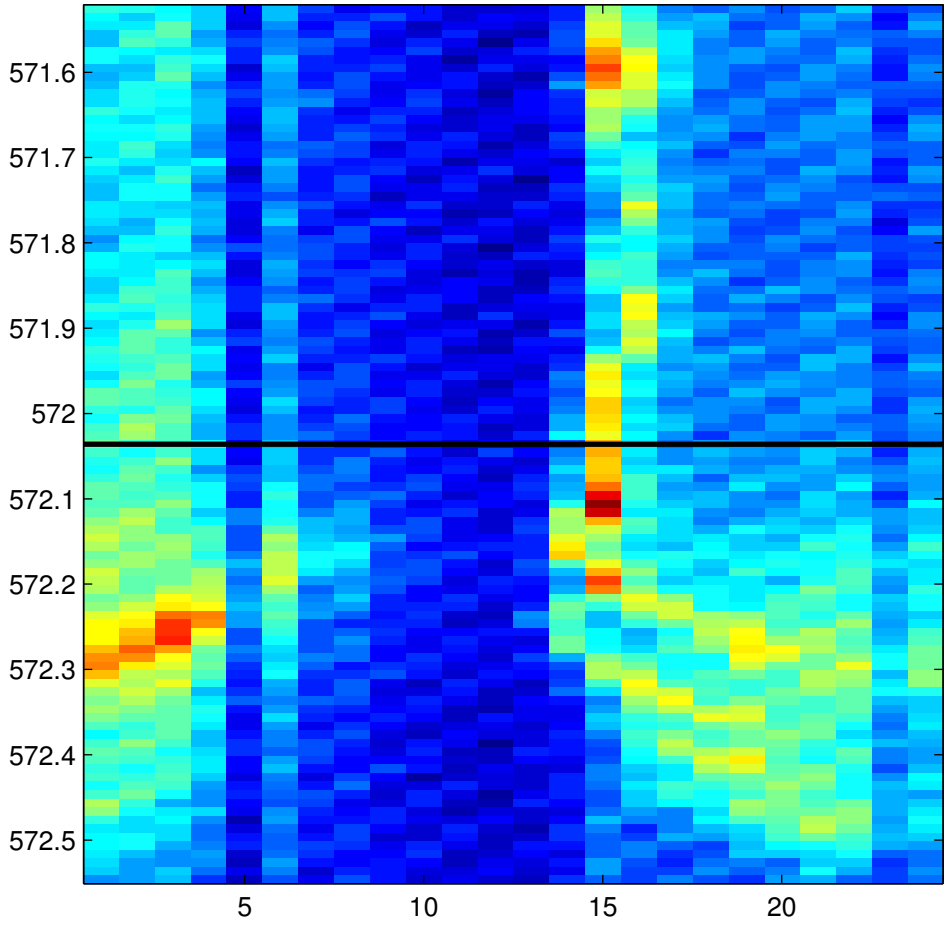

Repère du forage

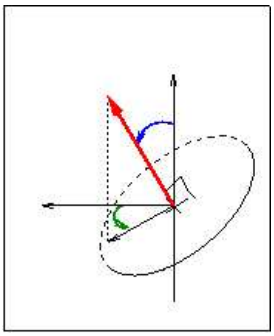

Repère absolu

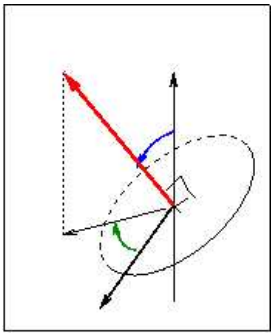

sinusoide visible

Diamètre 7.6 cm

Incidence ° Azimut °

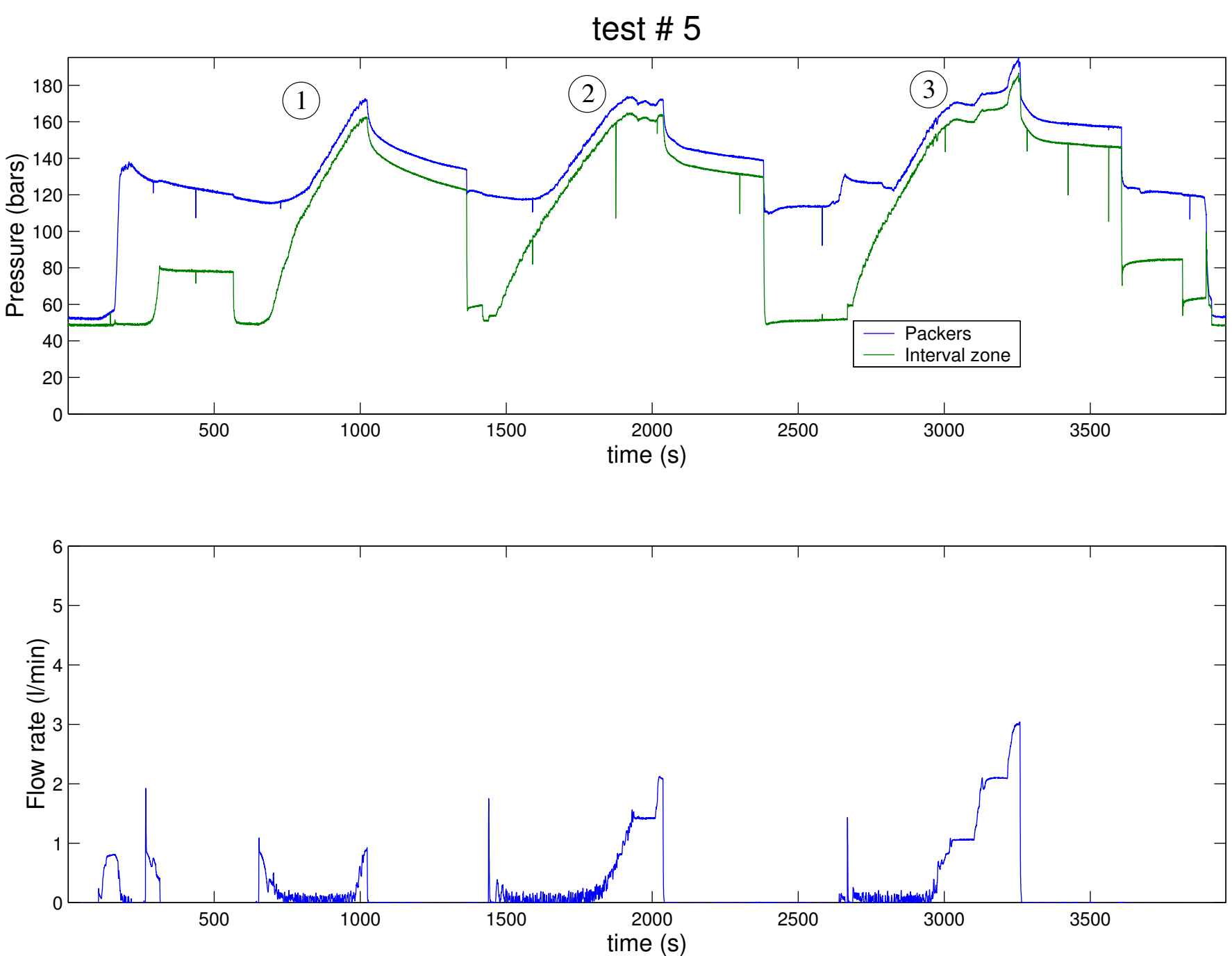
test # 5
Pressure (bars)
time (s)
1
2
3
Packers
Interval zone
Flow rate (l/min)
time (s)

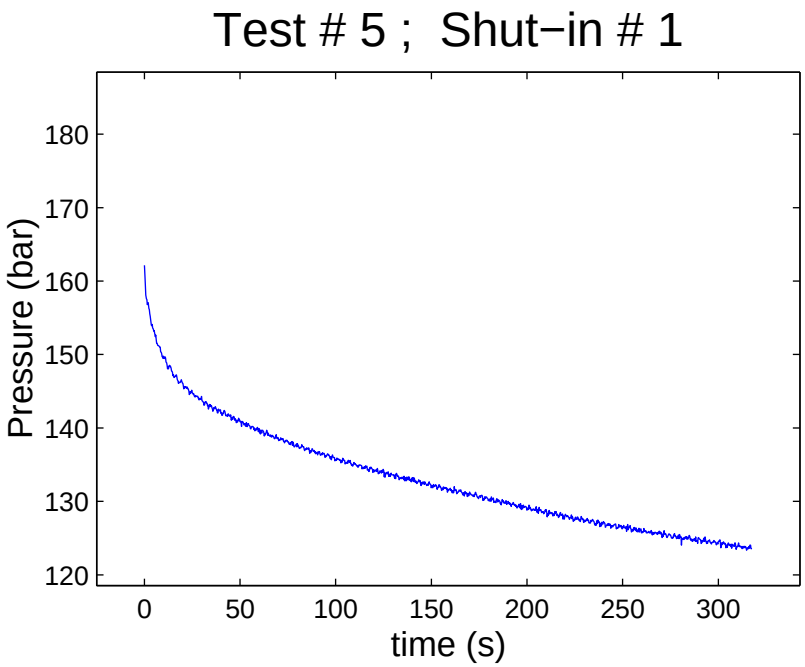
Test # 5 ; Shut−in # 1
Pressure (bar)
time (s)
120
130
140
150
160
170
180
0
50
100
150
200
250
300

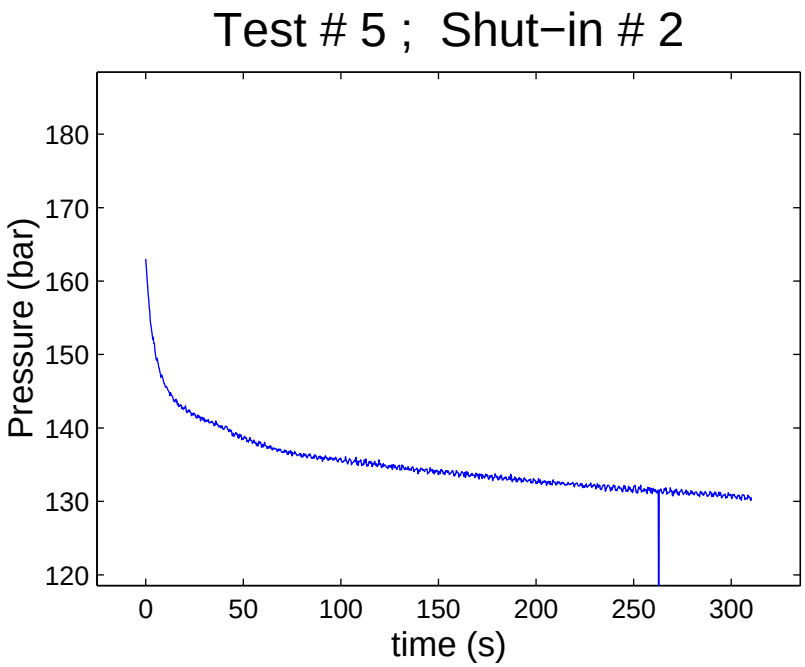
Test # 5 ; Shut−in # 2
Pressure (bar)
time (s)
120
130
140
150
160
170
180
0
50
100
150
200
250
300

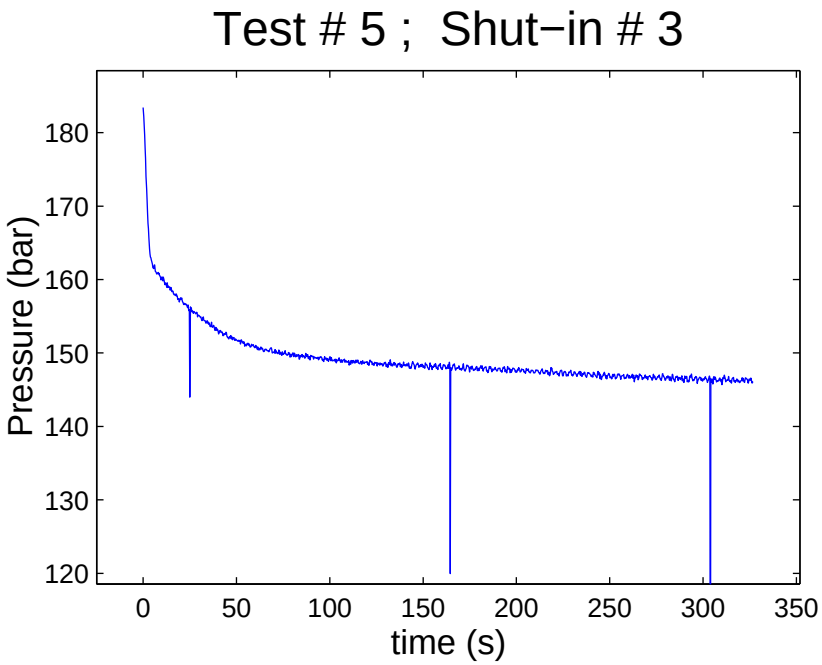
Test # 5 ; Shut−in # 3
Pressure (bar)
time (s)
120
130
140
150
160
170
180
0
50
100
150
200
250
300
350

KLX12A -- Post-frac Log # 5

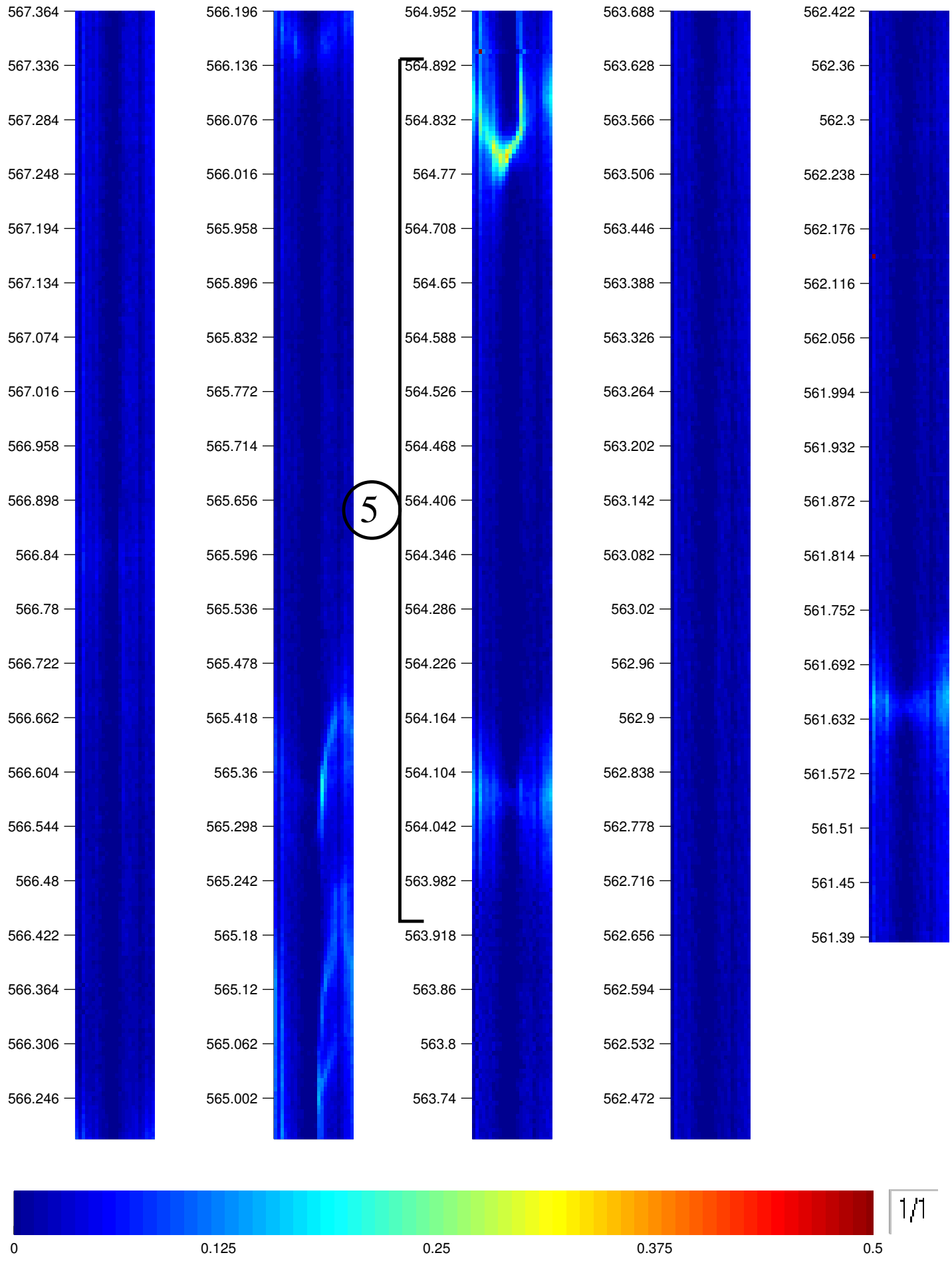

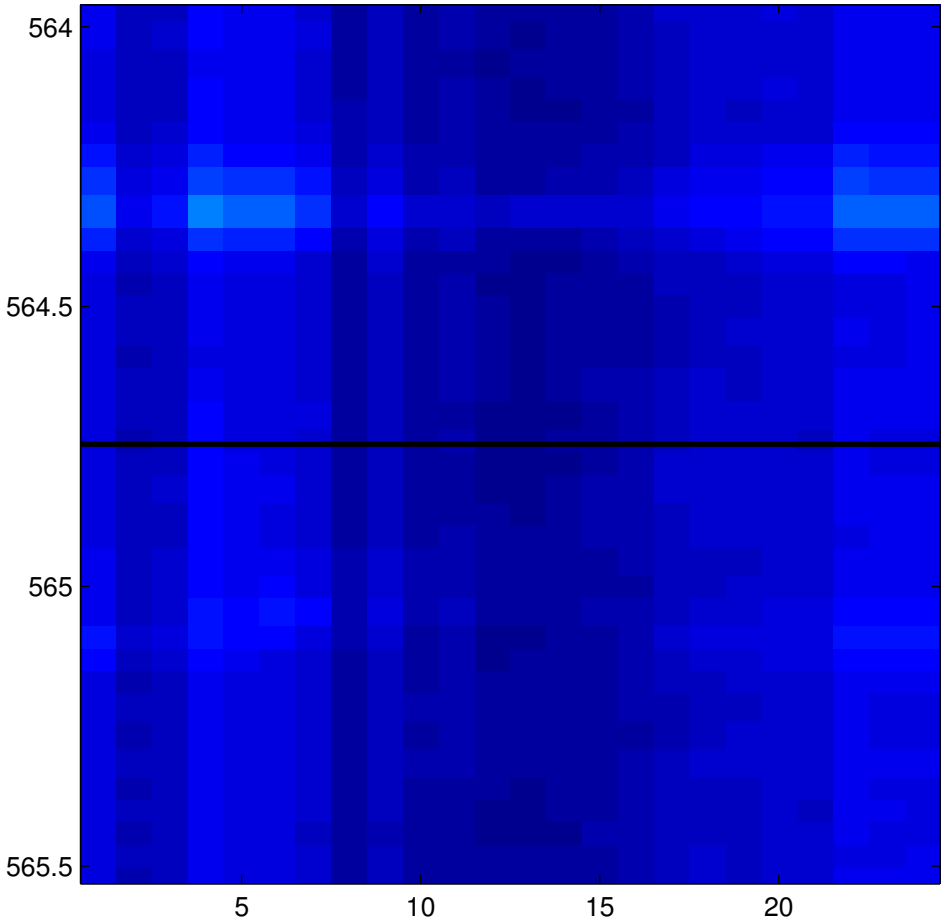

Repère du forage

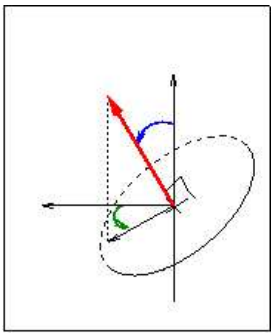

Repère absolu

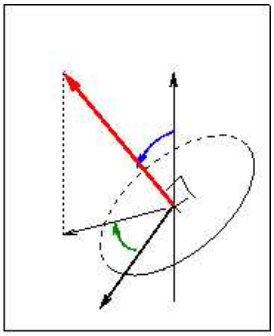

sinusoide visible

Diamètre 7.6 cm

Incidence ° Azimut °

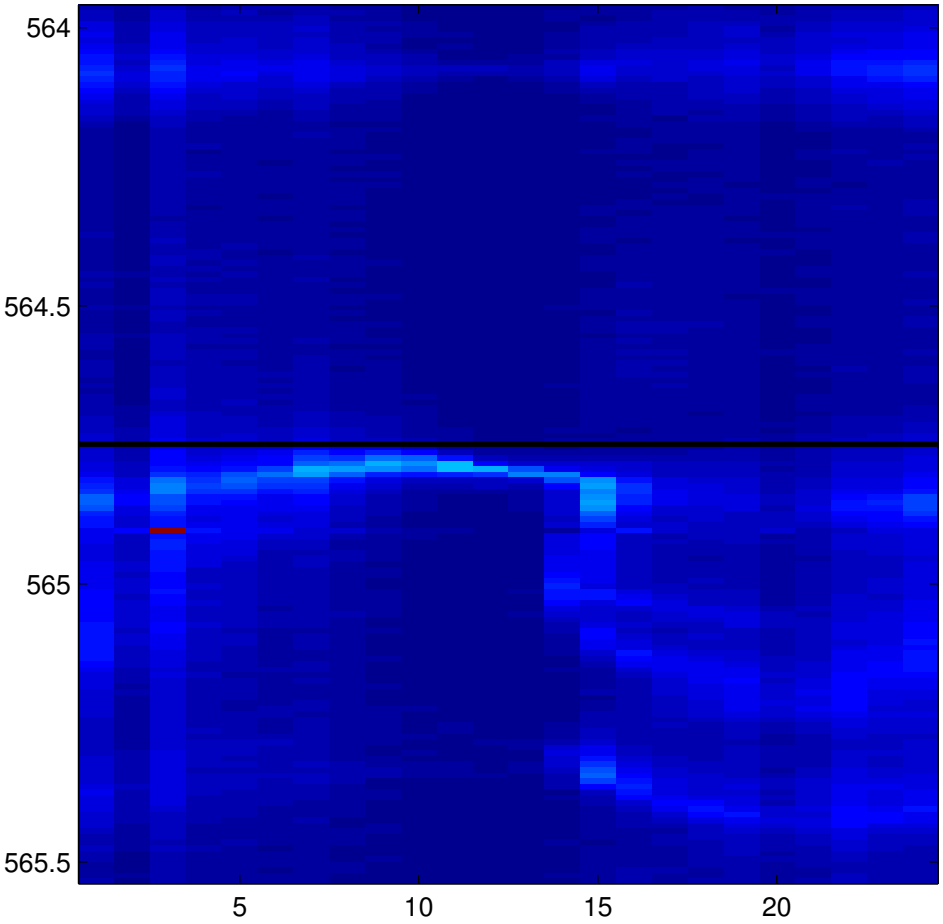

Repère du forage

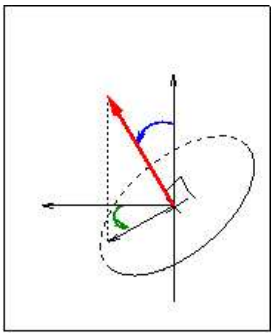

Repère absolu

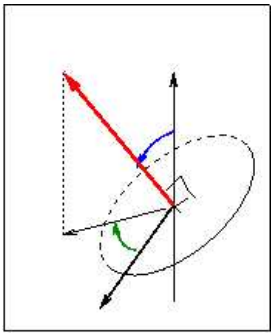

sinusoide visible

Diamètre 7.6 cm

Incidence ° Azimut °

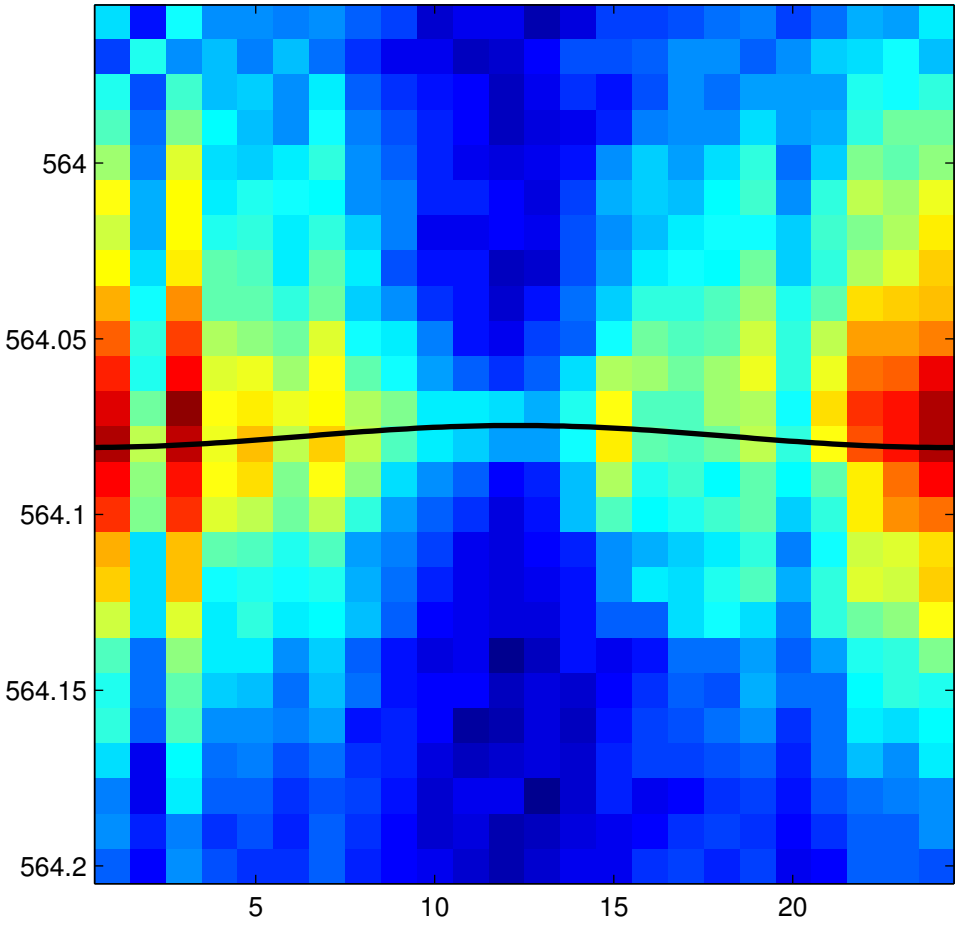

Repère du forage

180

4.7214

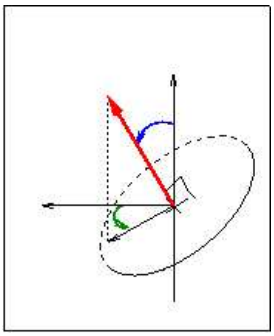

Repère absolu

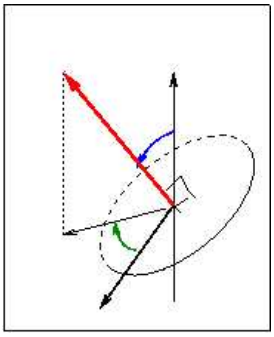

sinusoide visible

Diamètre 7.6 cm

Incidence ° Azimut °

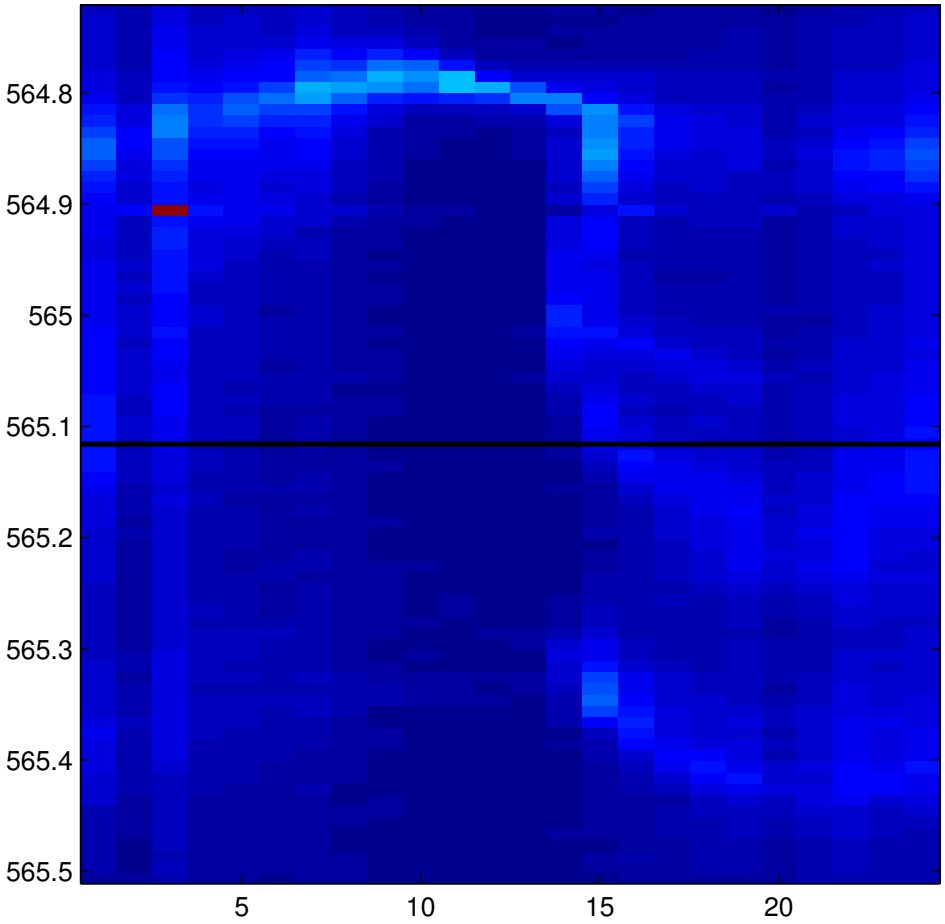

Repère du forage

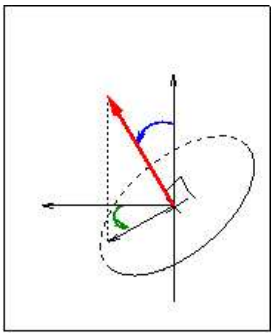

Repère absolu

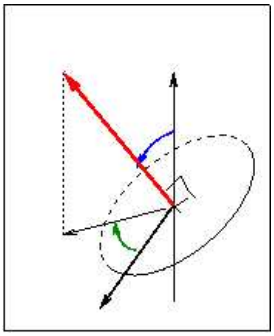

sinusoide visible

Diamètre 7.6 cm

Incidence ° Azimut °

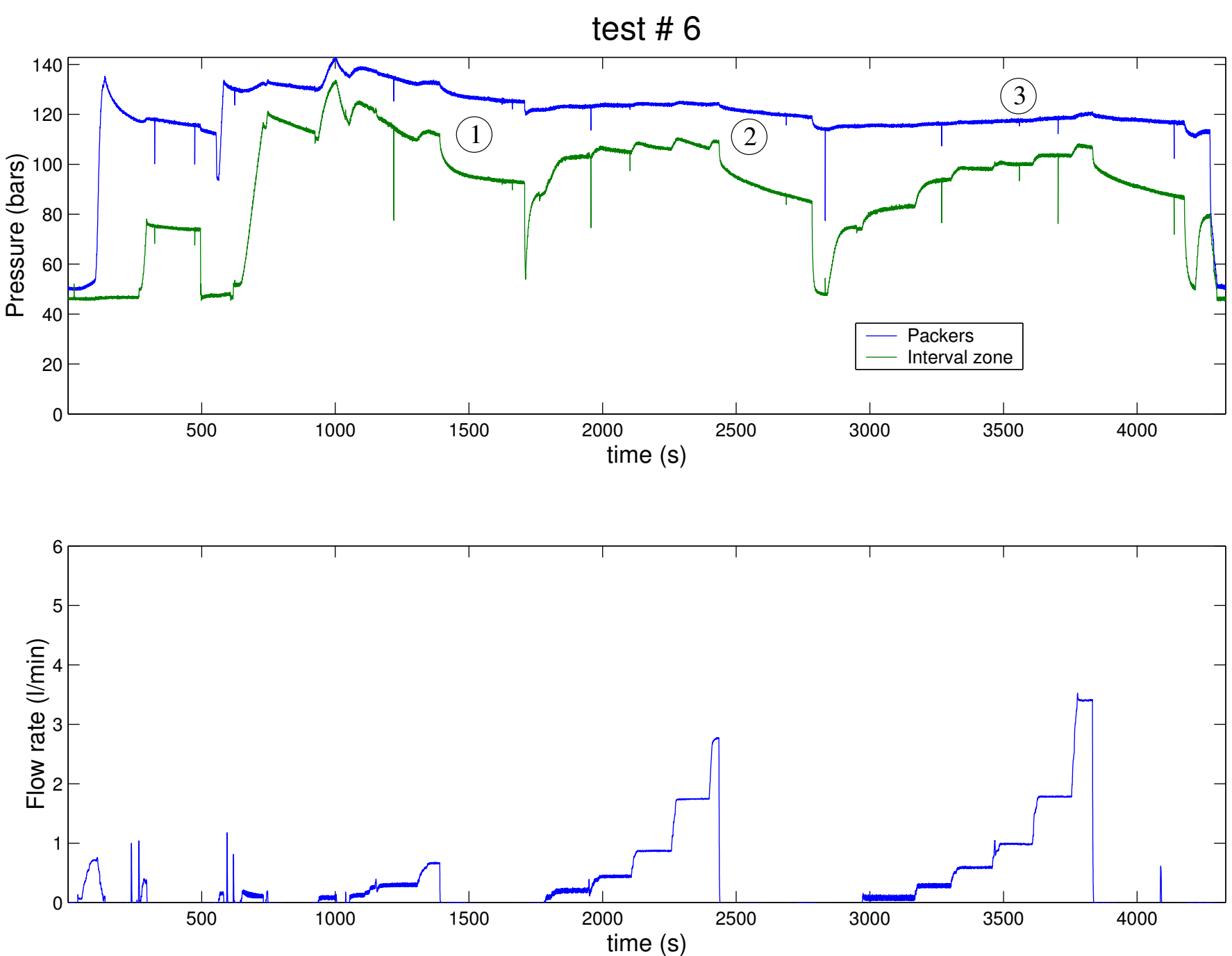
test # 6
Pressure (bars)
time (s)
Packers
Interval zone
1
2
3
Flow rate (l/min)
time (s)

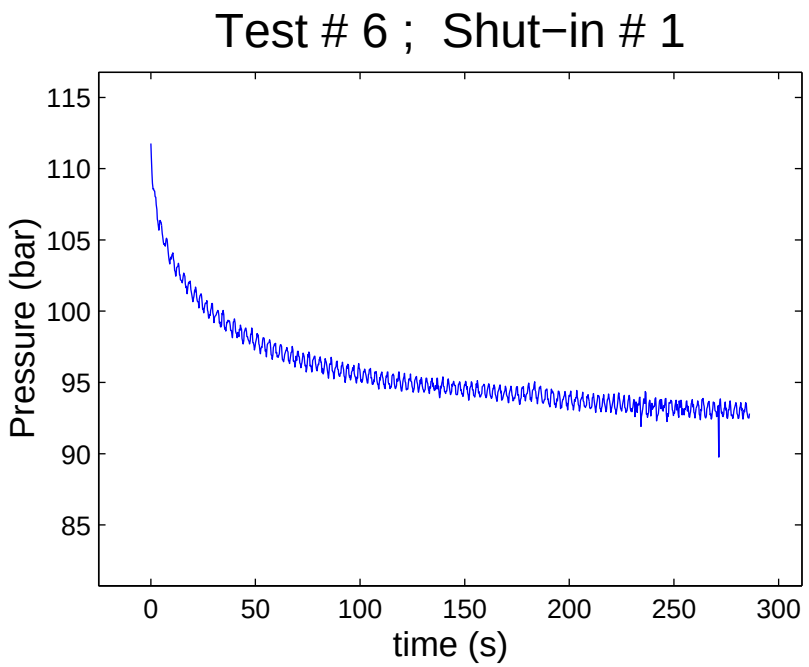
Test # 6 ; Shut−in # 1
Pressure (bar)
time (s)
115
110
105
100
95
90
85
0
50
100
150
200
250
300

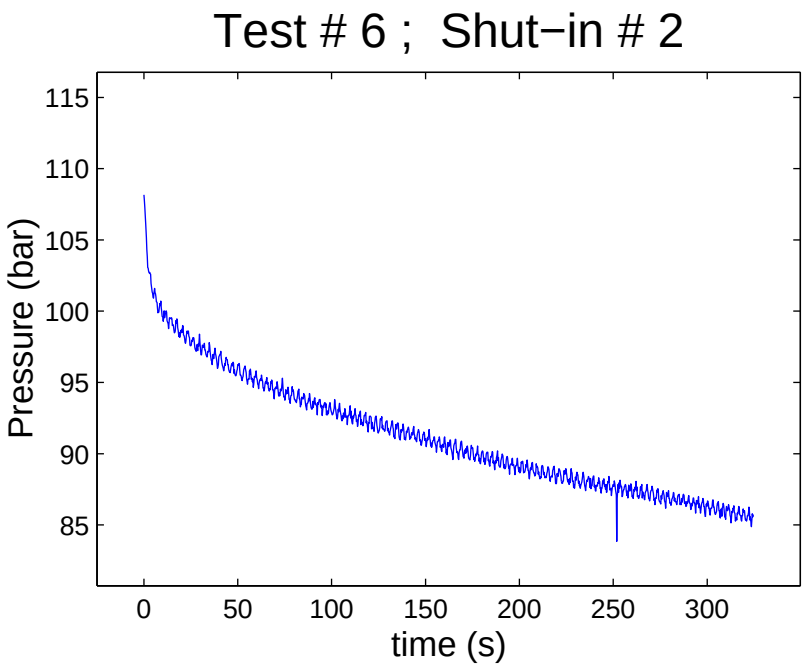
Test # 6 ; Shut−in # 2
Pressure (bar)
time (s)
115
110
105
100
95
90
85
0
50
100
150
200
250
300

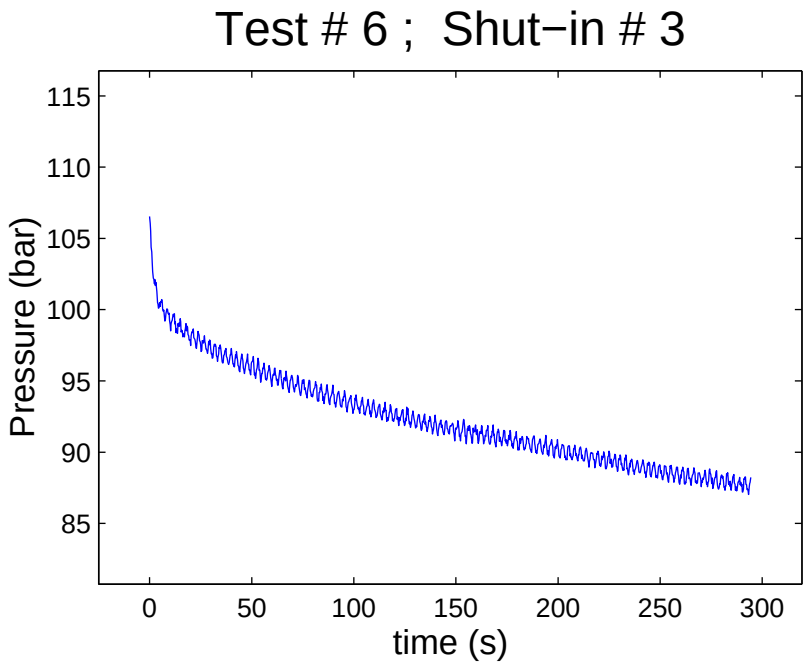
Test # 6 ; Shut−in # 3
Pressure (bar)
time (s)
115
110
105
100
95
90
85
0
50
100
150
200
250
300

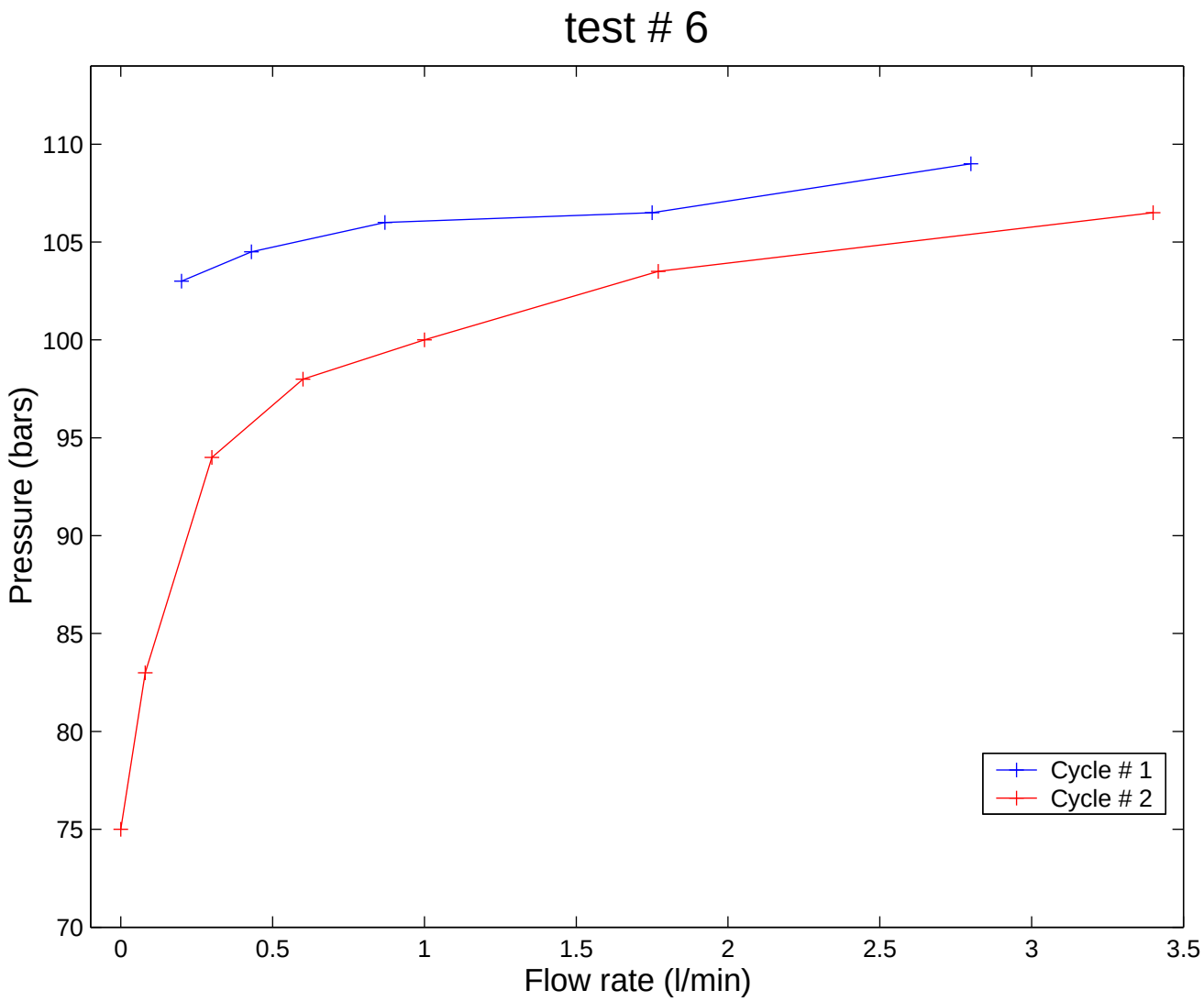
test # 6
Pressure (bars)
110
105
100
95
90
85
80
75
70
0
0.5
1
1.5
2
2.5
3
3.5
Flow rate (l/min)
Cycle # 1
Cycle # 2

KLX12A -- Post-frac Log # 6

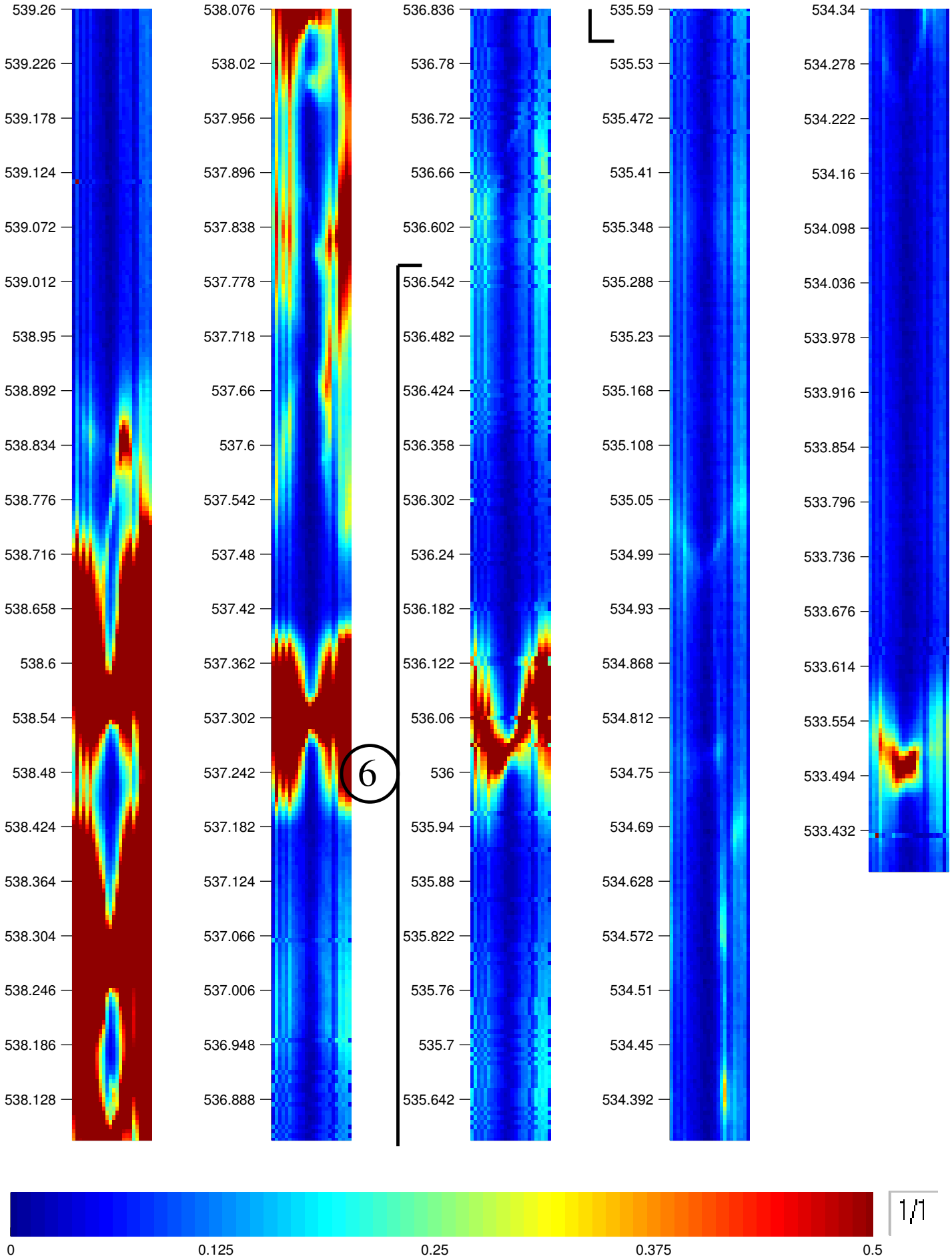

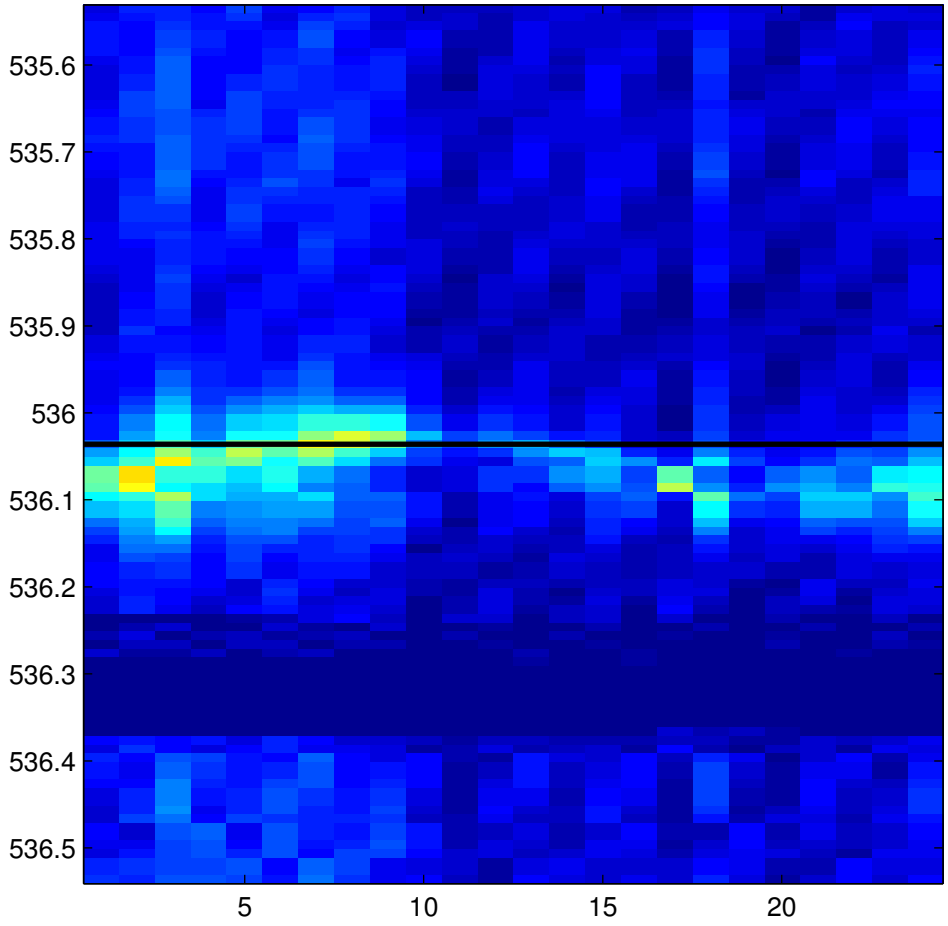

Repère du forage

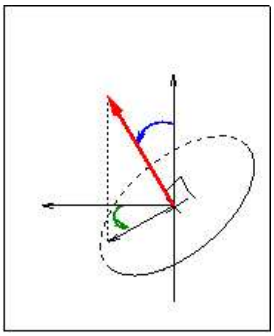

Repère absolu

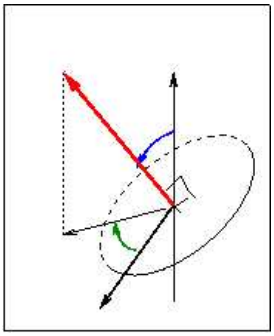

sinusoide visible

Diamètre 7.6 cm

Incidence ° Azimut °

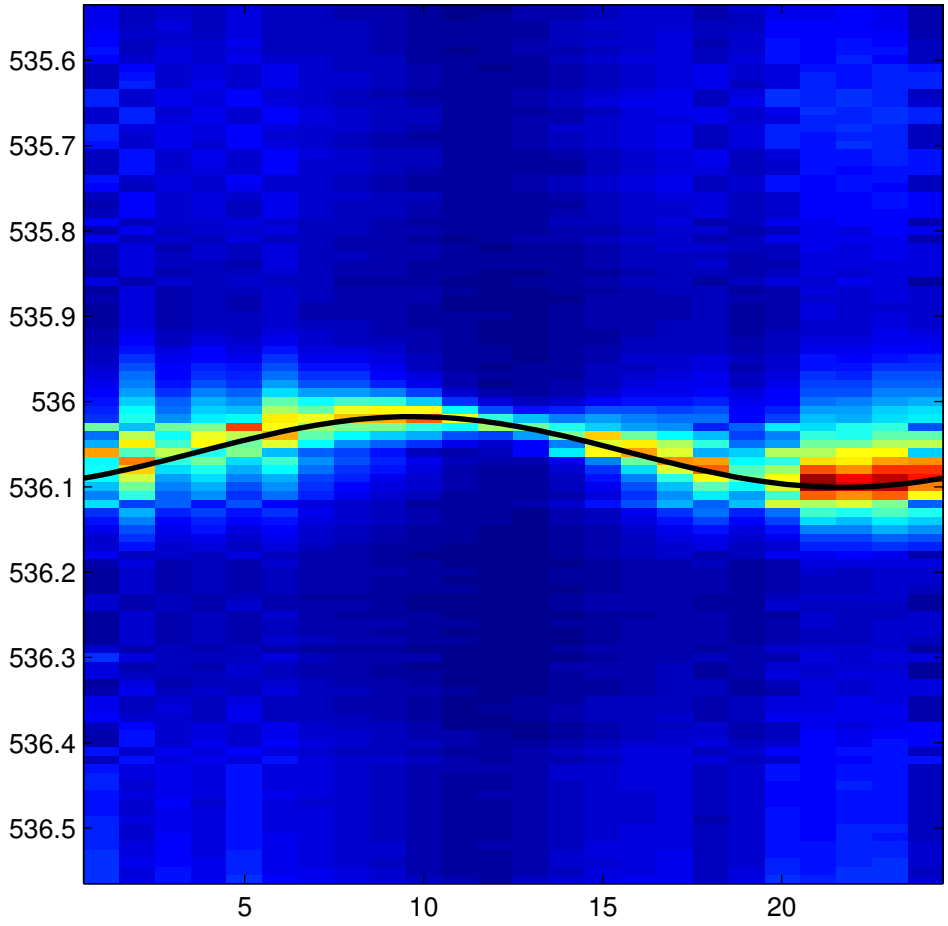

Repère du forage

140.4

47.4184

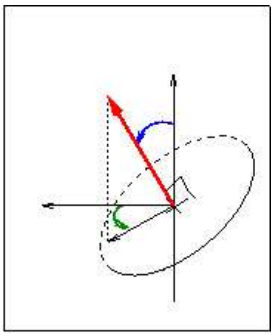

Repère absolu

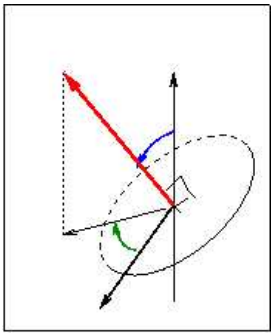

sinusoide visible

Diamètre 7.6 cm

Incidence ° Azimut °

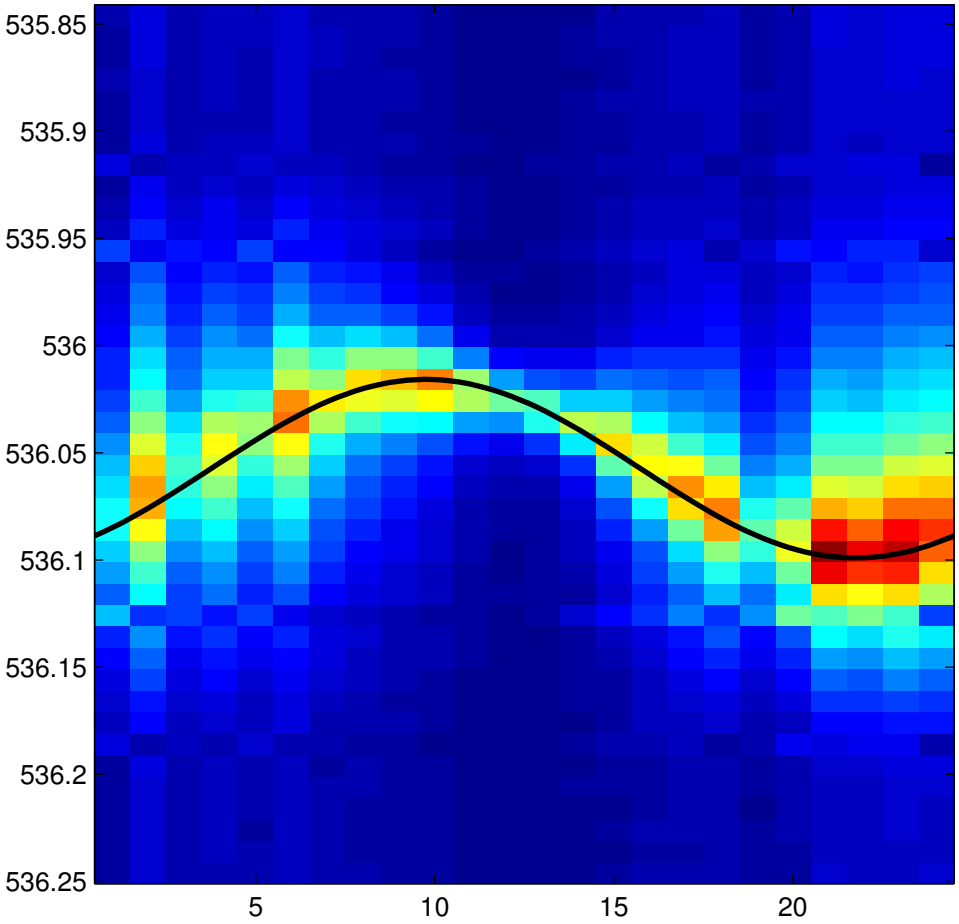

Repère du forage

140.4

47.6184

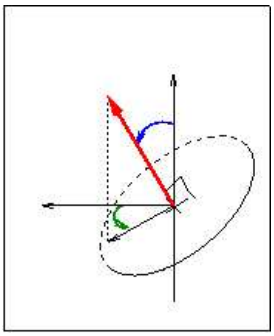

Repère absolu

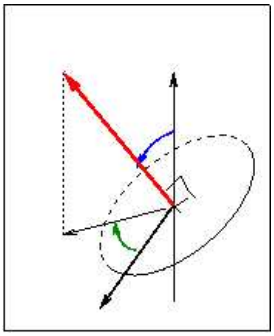

sinusoide visible

Diamètre 7.6 cm

Incidence ° Azimut °

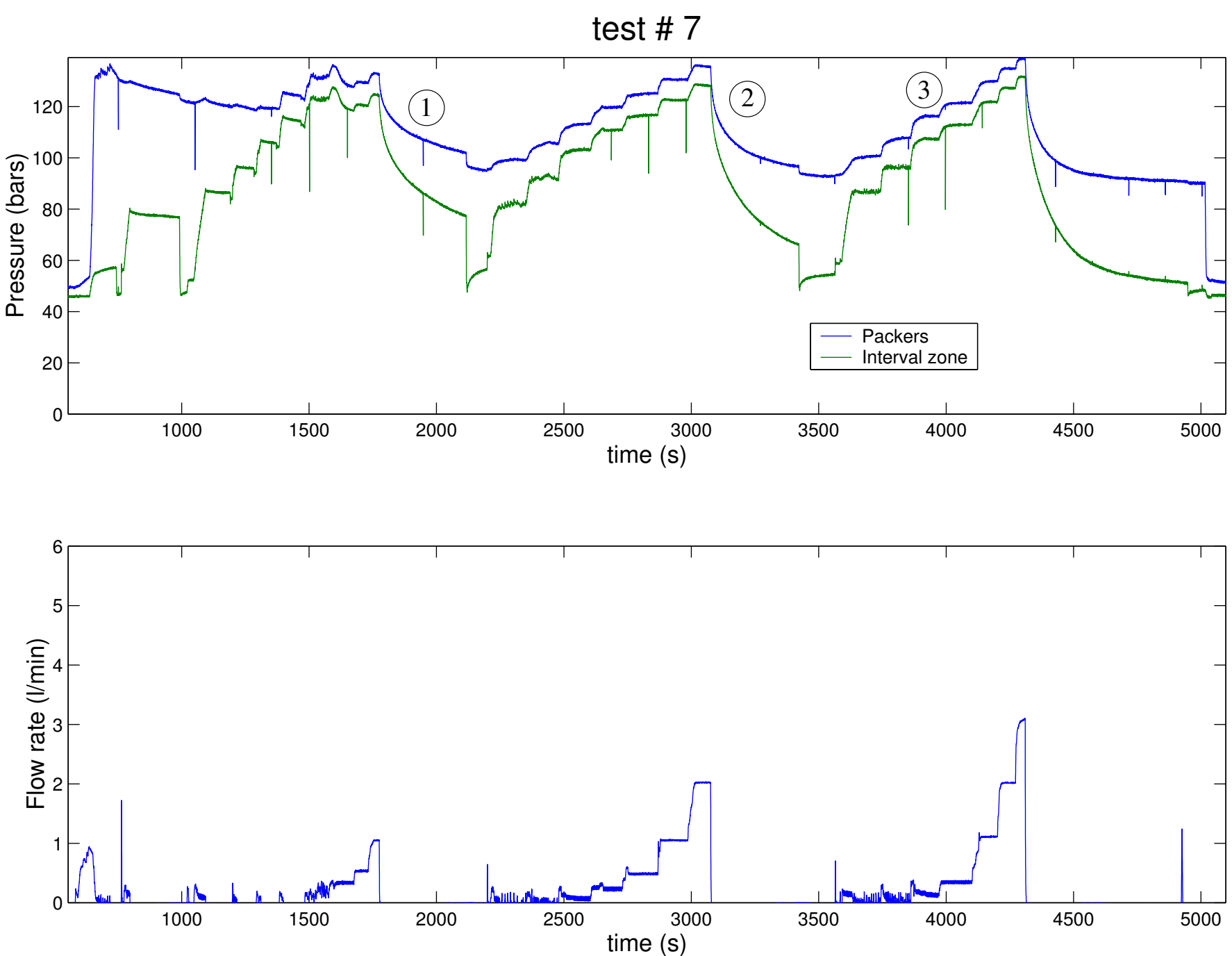
test # 7
Pressure (bars)
0
20
40
60
80
100
120
1
2
3
Packers
Interval zone
1000
1500
2000
2500
3000
3500
4000
4500
5000
time (s)
Flow rate (l/min)
0
1
2
3
4
5
6
1000
1500
2000
2500
3000
3500
4000
4500
5000
time (s)

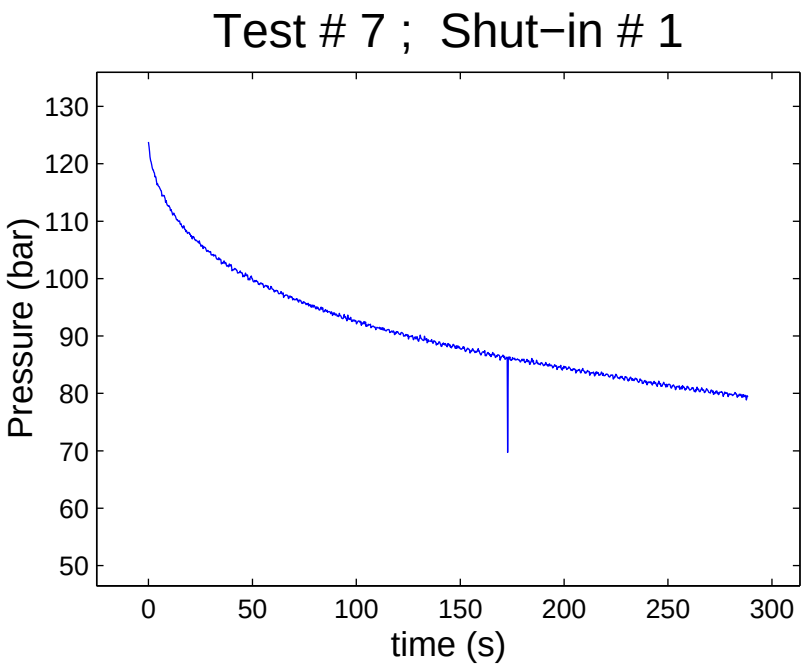
Test # 7 ; Shut−in # 1
Pressure (bar)
time (s)
130
120
110
100
90
80
70
60
50
0
50
100
150
200
250
300

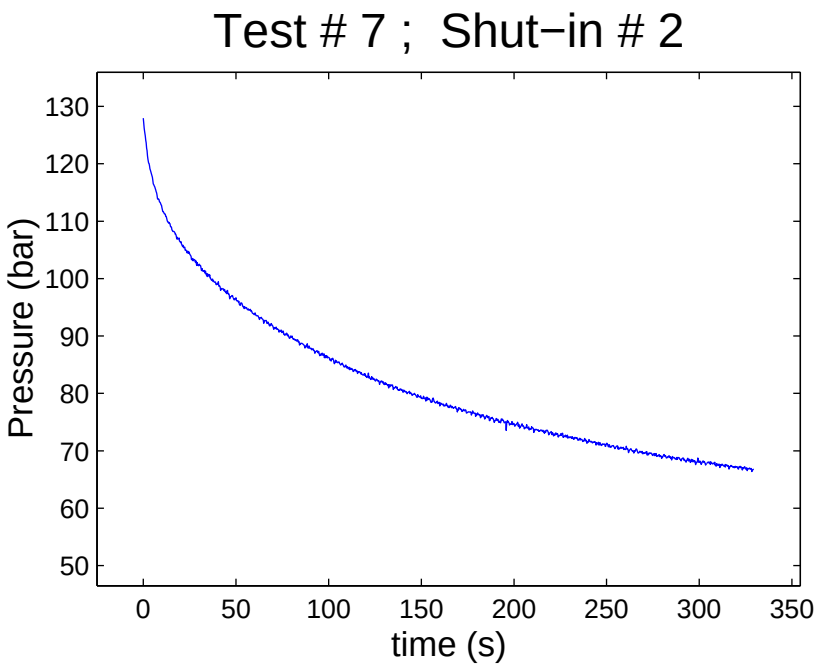
Test # 7 ; Shut−in # 2
Pressure (bar)
time (s)
130
120
110
100
90
80
70
60
50
0
50
100
150
200
250
300
350

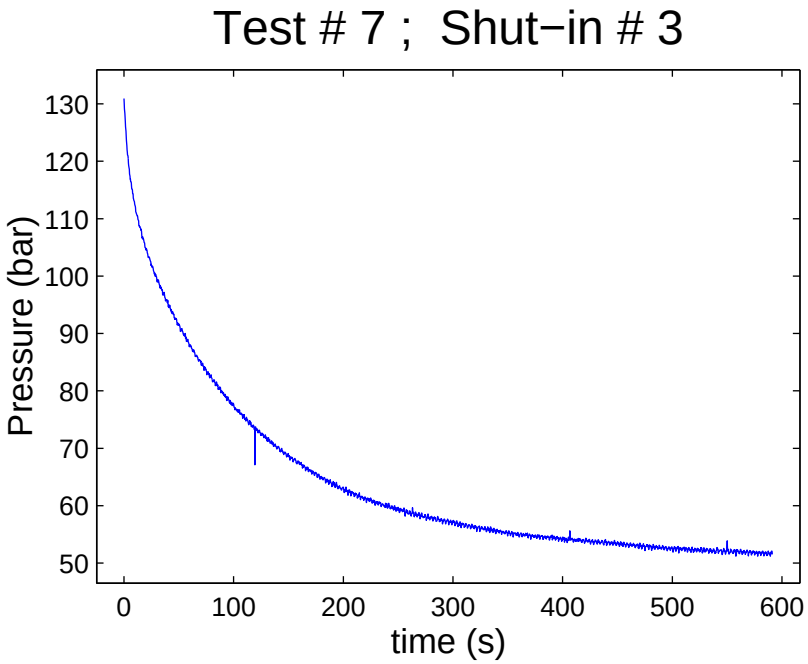
Test # 7 ; Shut−in # 3
Pressure (bar)
time (s)
130
120
110
100
90
80
70
60
50
0
100
200
300
400
500
600

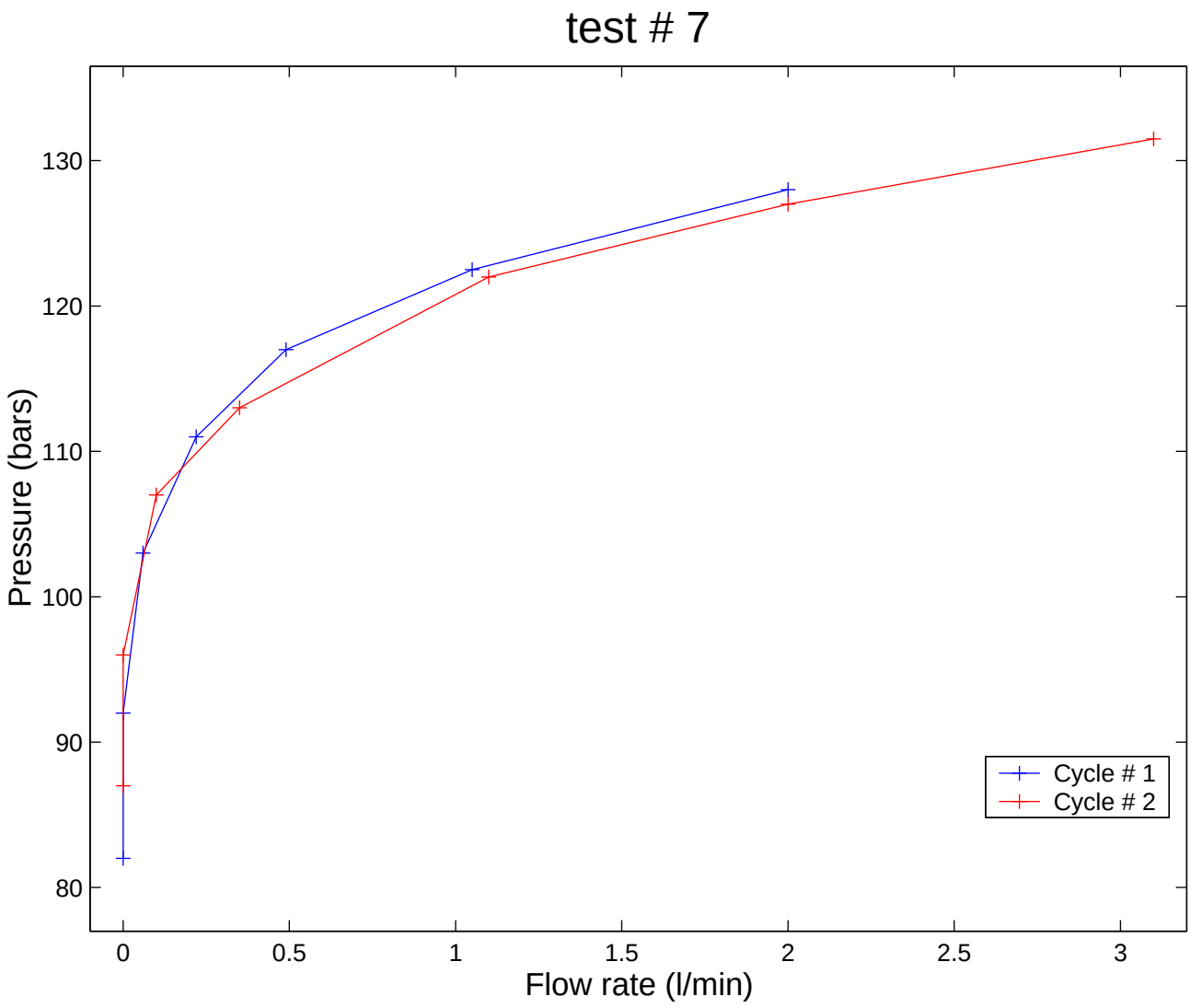
test # 7
Pressure (bars)
130
120
110
100
90
80
0
0.5
1
1.5
2
2.5
3
Flow rate (l/min)
Cycle # 1
Cycle # 2

KLX12A -- Post-frac Log # 7

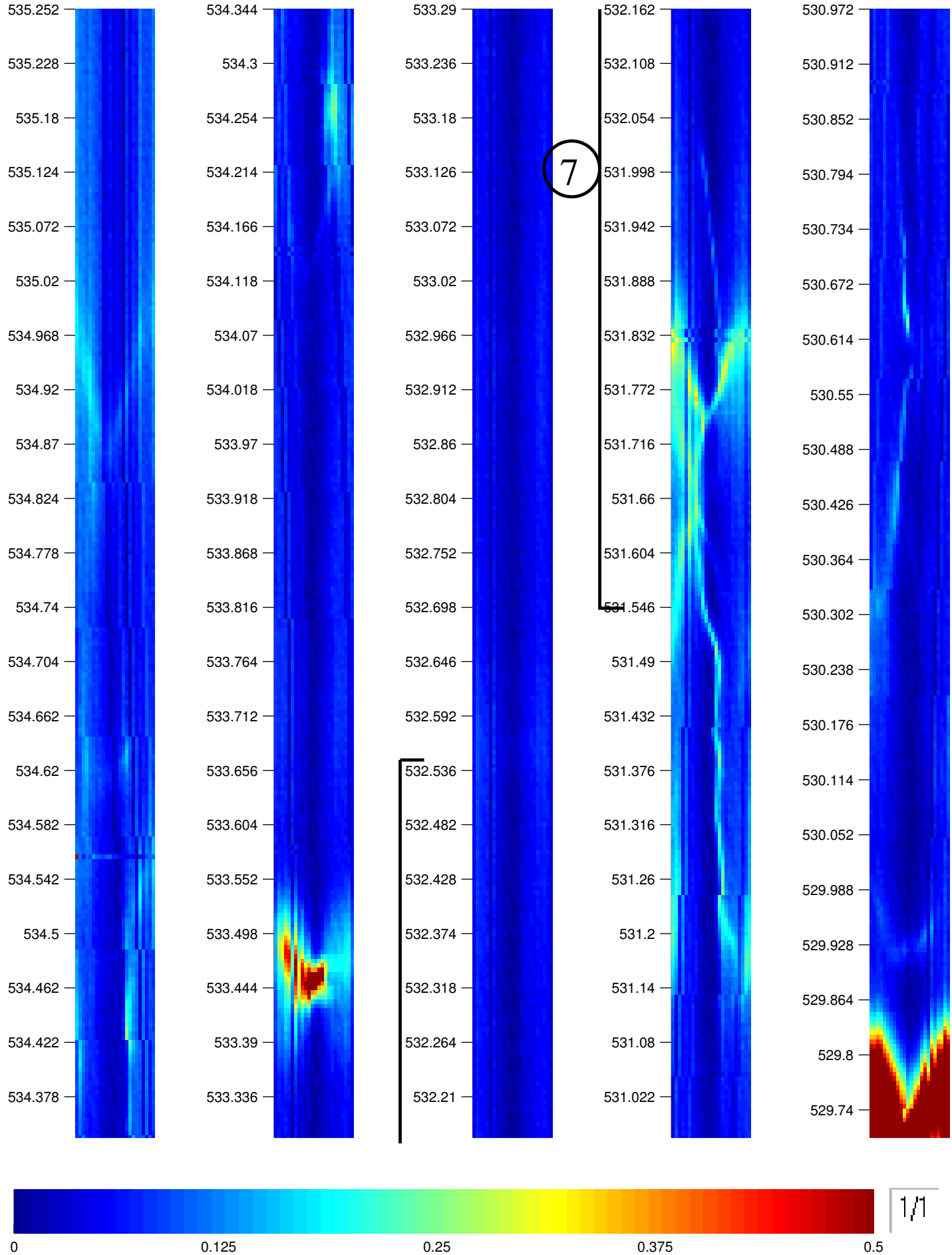

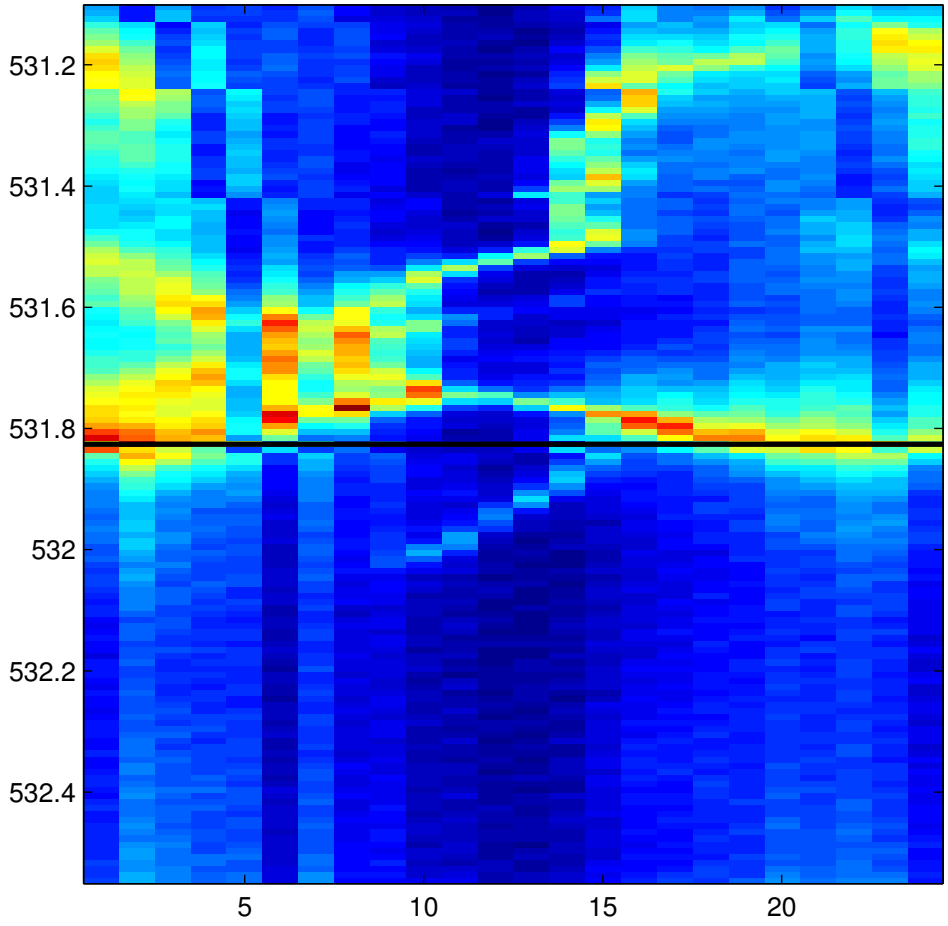

Repère du forage

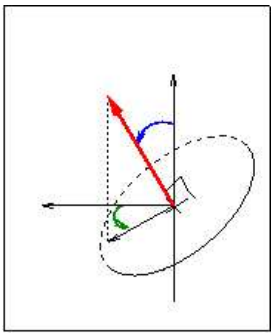

Repère absolu

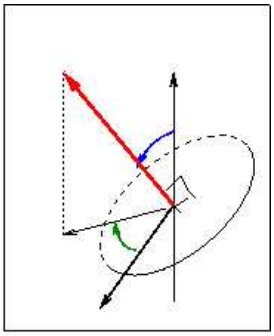

sinusoide visible

Diamètre 7.6 cm

Incidence ° Azimut °

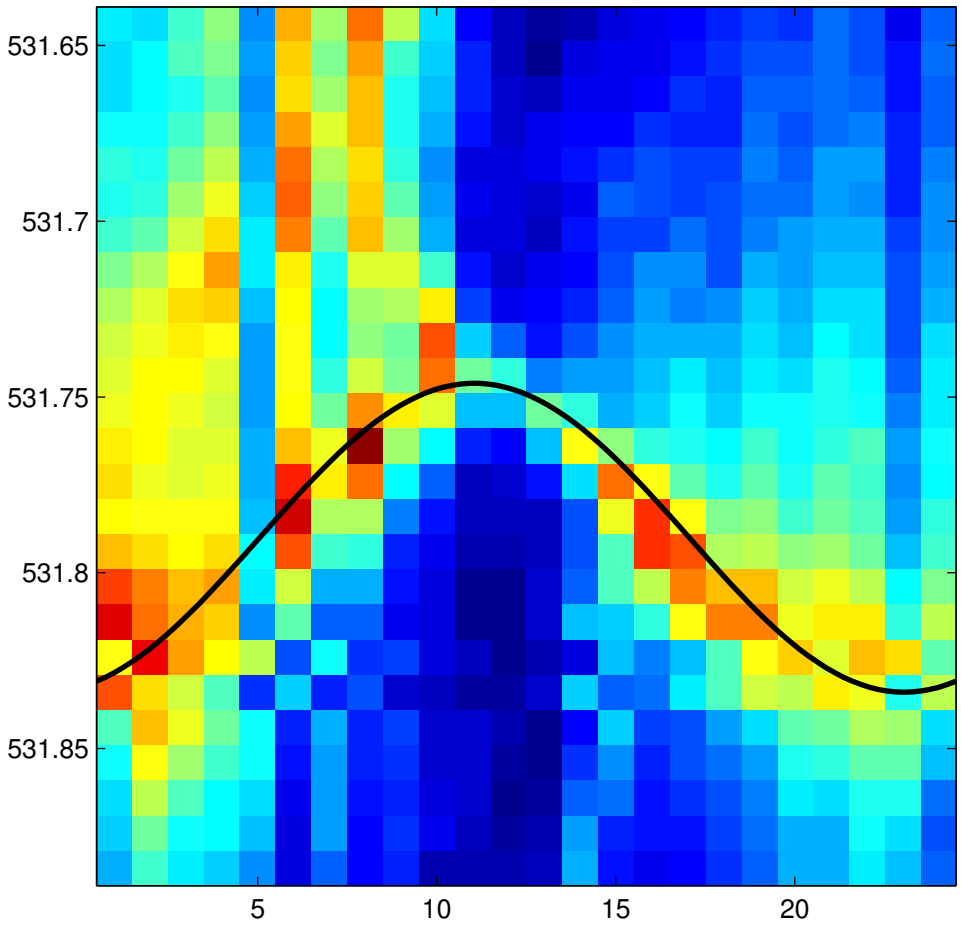

Repère du forage

162

49.1428

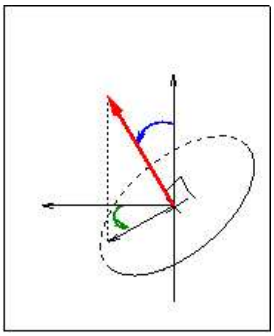

Repère absolu

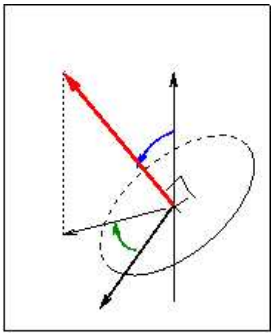

sinusoide visible

Diamètre 7.6 cm

Incidence ° Azimut °

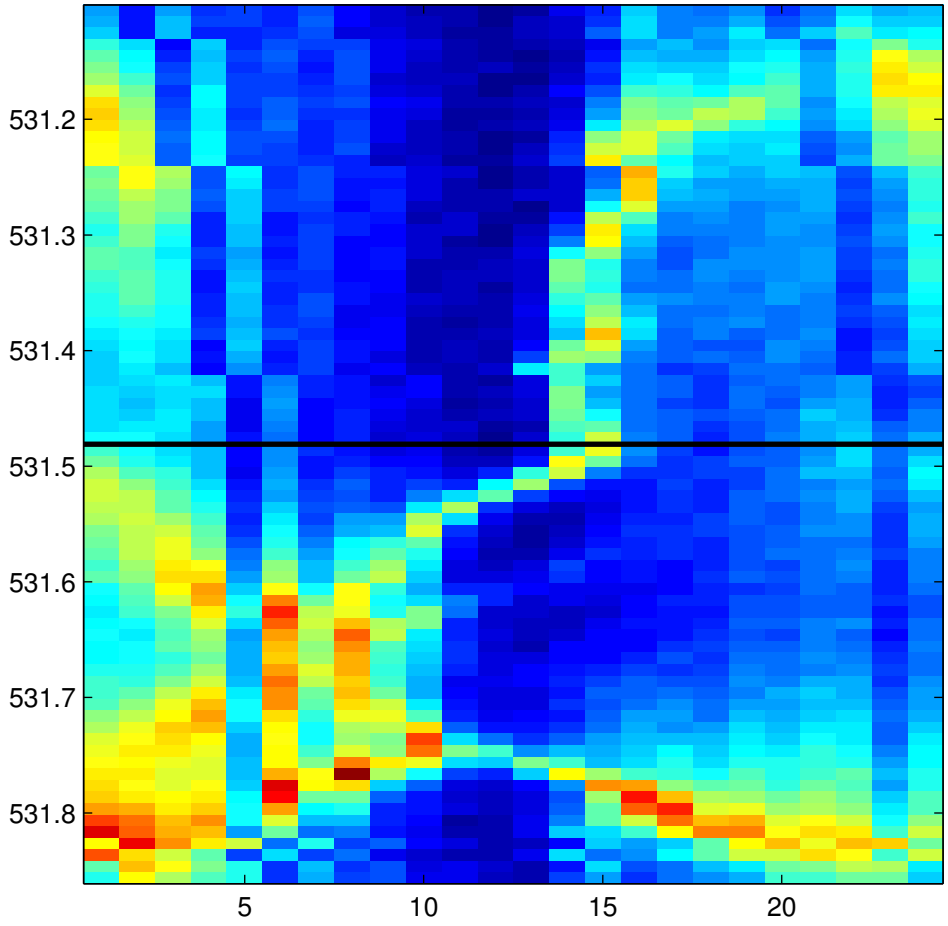

Repère du forage

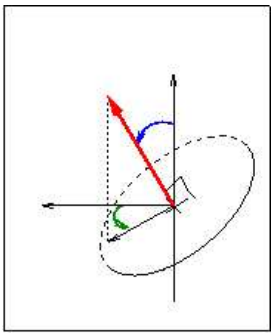

Repère absolu

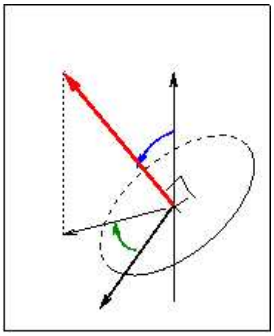

sinusoide visible

Diamètre 7.6 cm

Incidence ° Azimut °

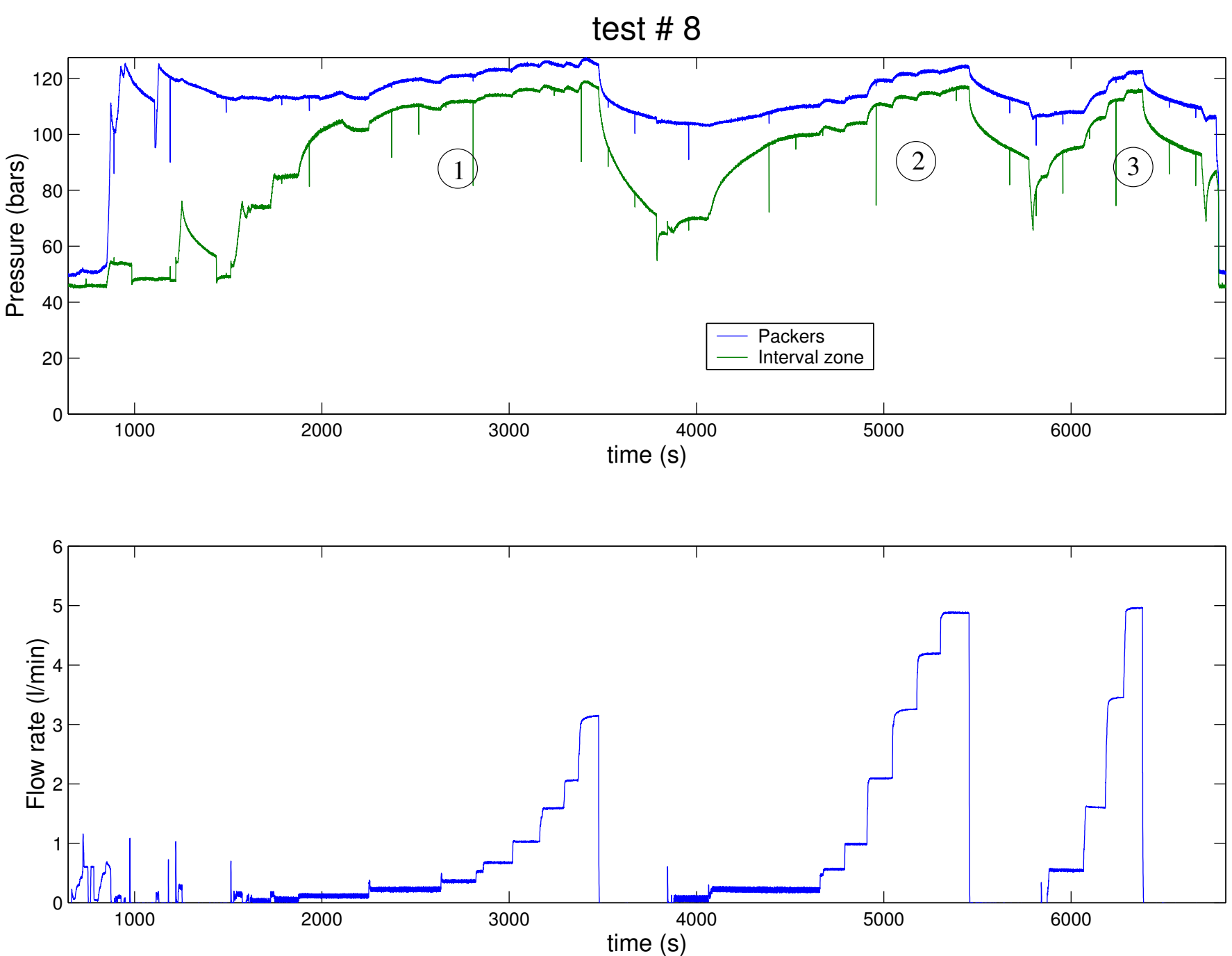
test # 8
Pressure (bars)
time (s)
Packers
Interval zone
1
2
3
Flow rate (l/min)
time (s)

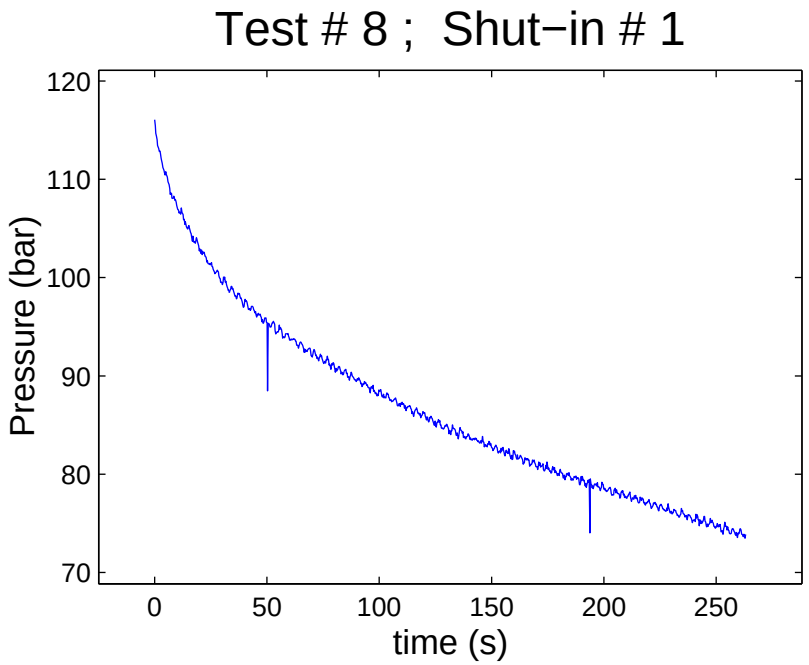
Test # 8 ; Shut−in # 1
Pressure (bar)
time (s)
120
110
100
90
80
70
0
50
100
150
200
250

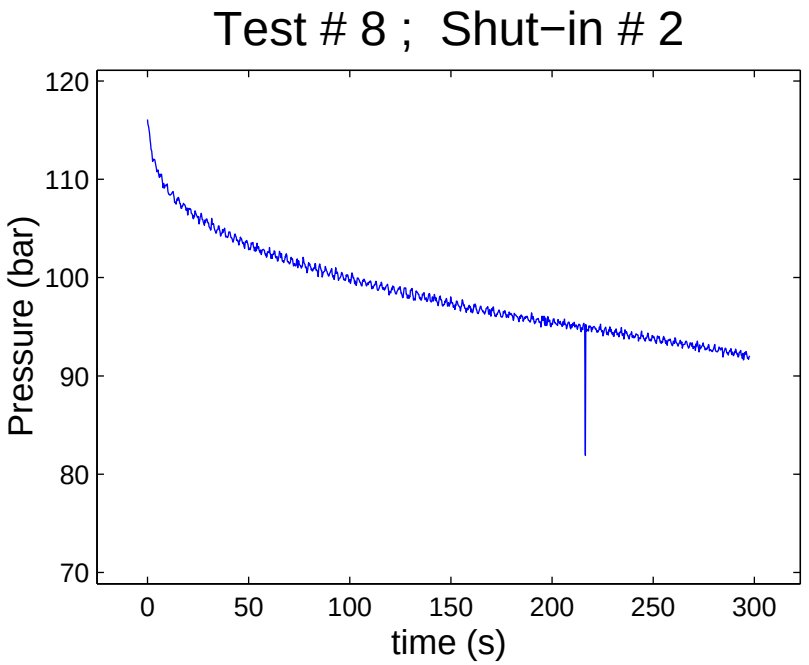
Test # 8 ; Shut−in # 2
Pressure (bar)
time (s)
120
110
100
90
80
70
0
50
100
150
200
250
300

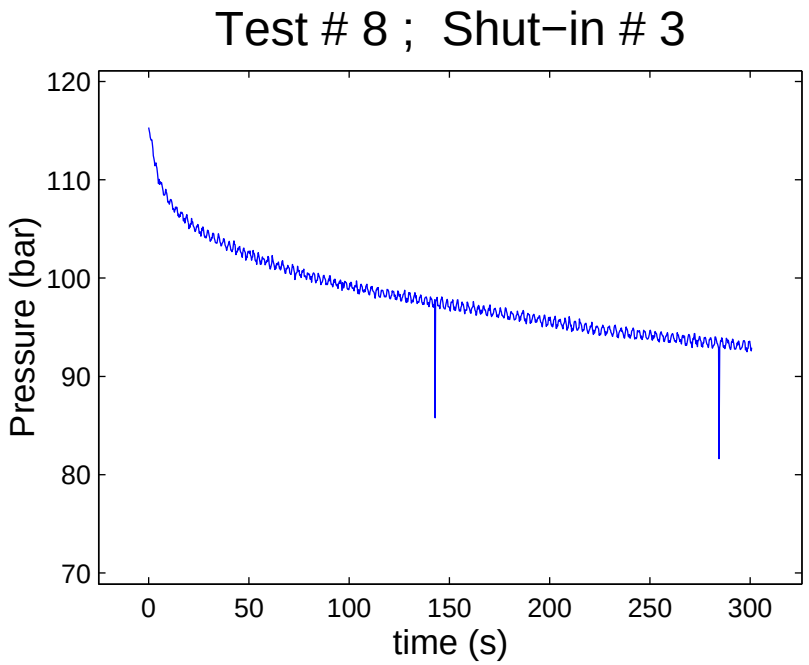
Test # 8 ; Shut−in # 3
Pressure (bar)
time (s)
120
110
100
90
80
70
0
50
100
150
200
250
300

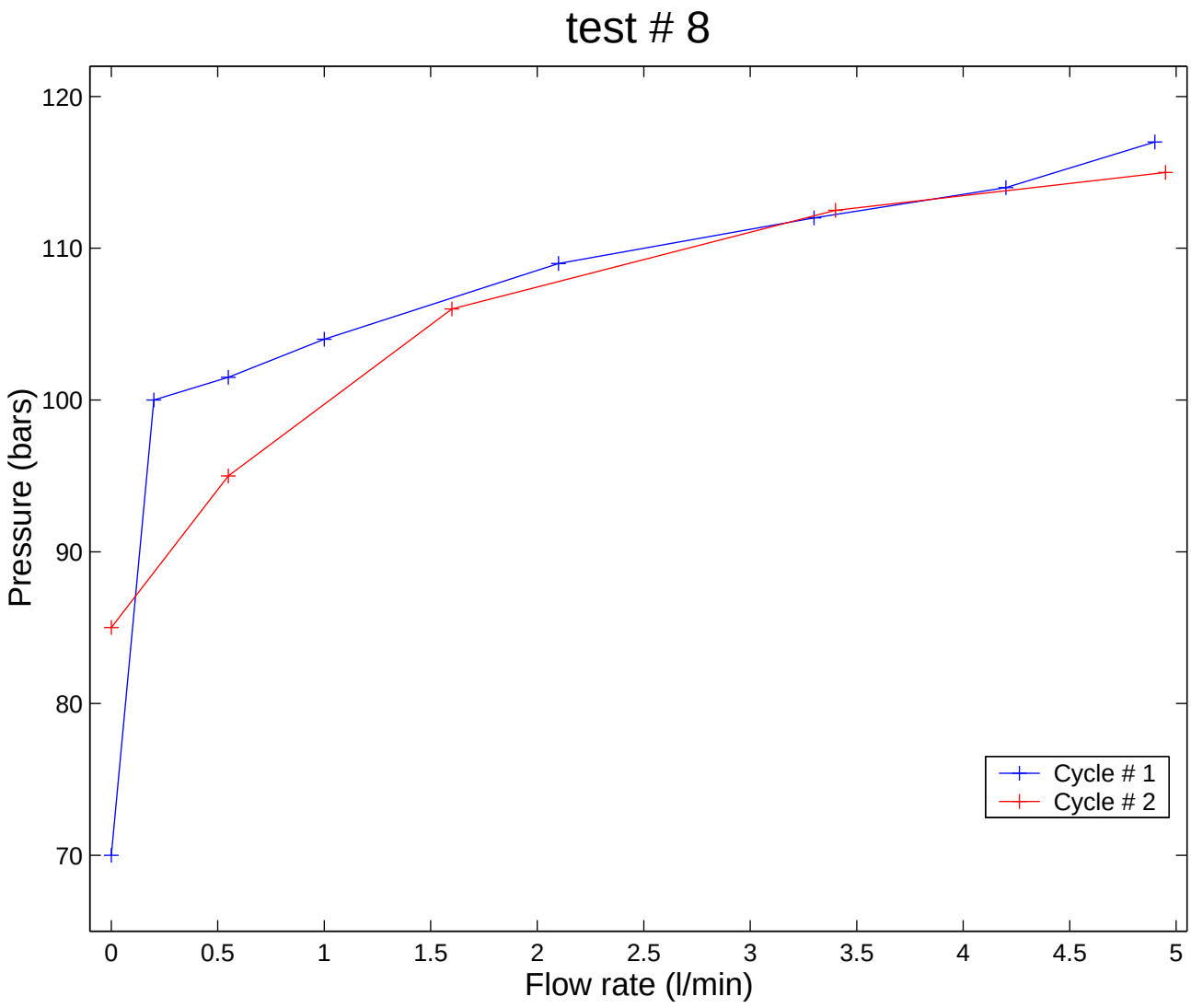
test # 8
Pressure (bars)
120
110
100
90
80
70
0
0.5
1
1.5
2
2.5
3
3.5
4
4.5
5
Flow rate (l/min)
Cycle # 1
Cycle # 2

KLX12A -- Post-frac Log # 8

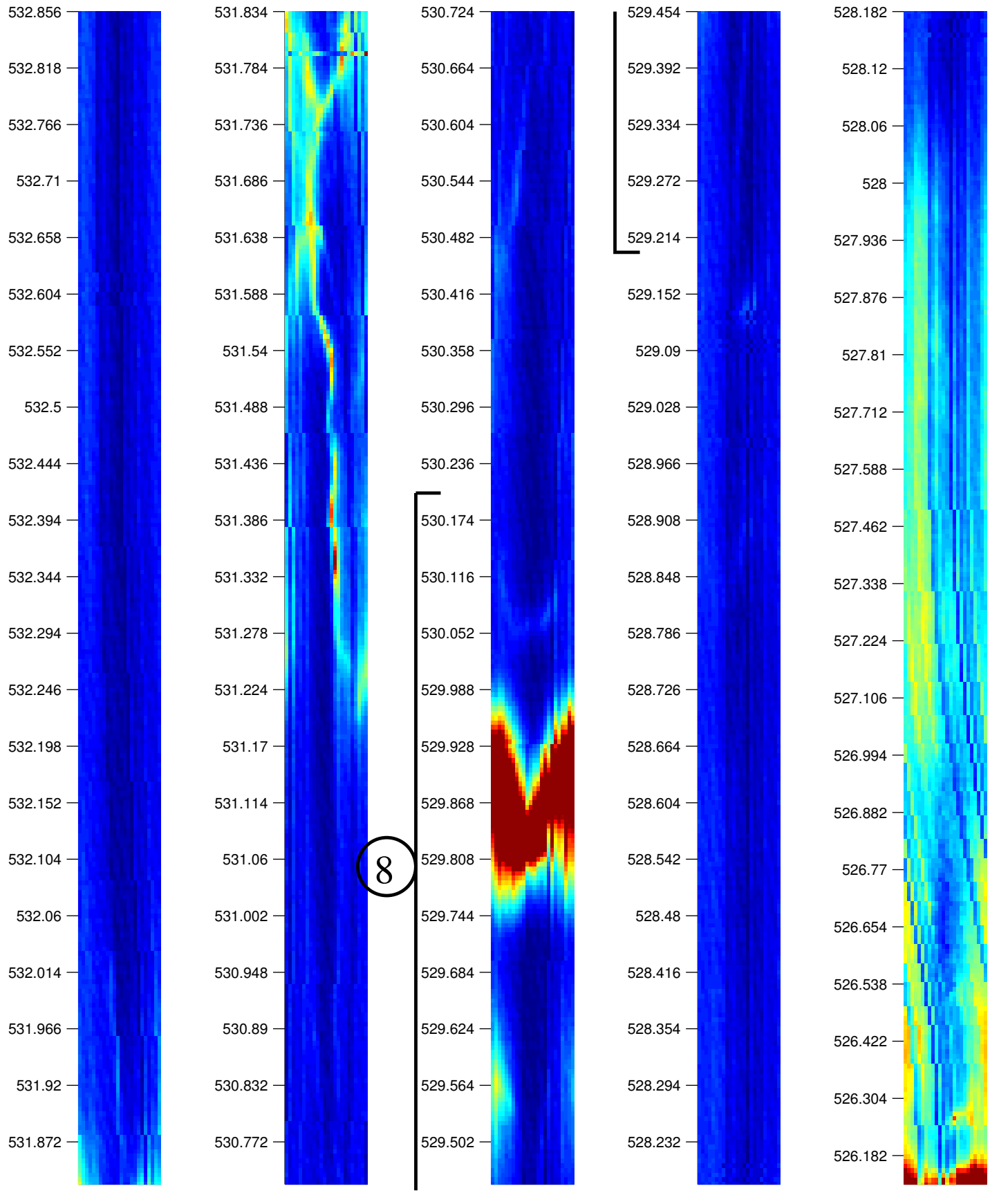

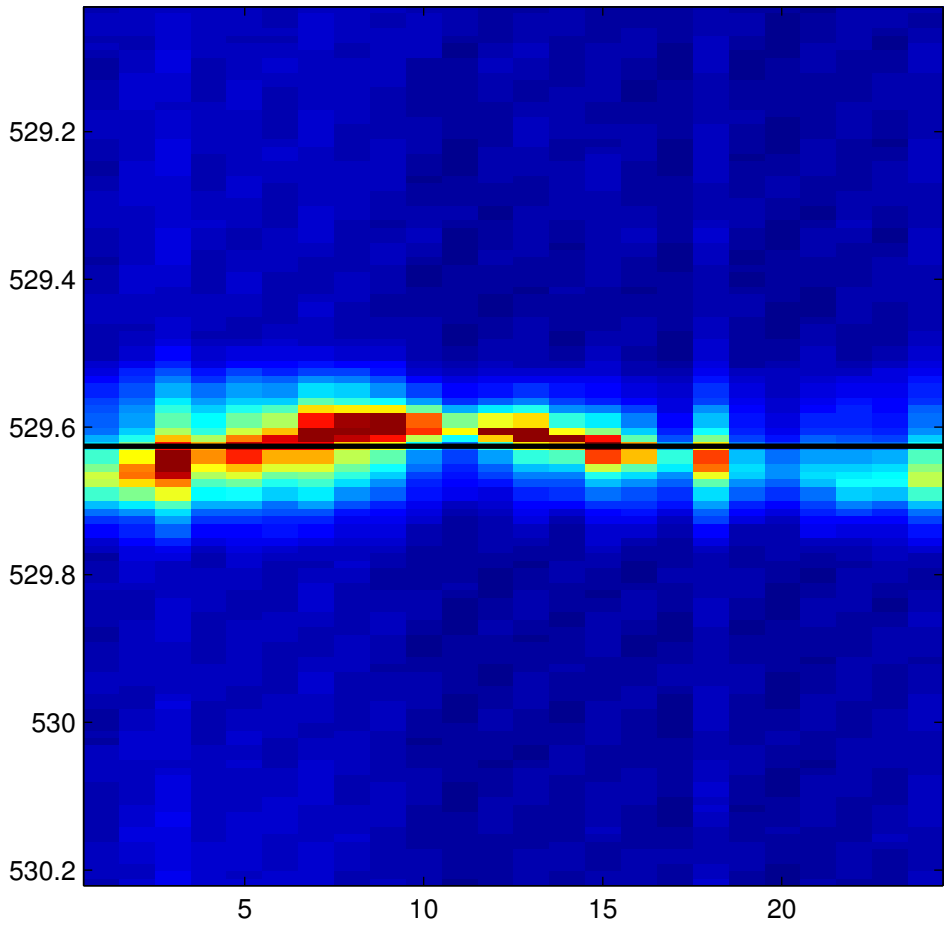

Repère du forage

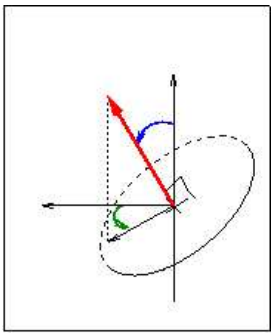

Repère absolu

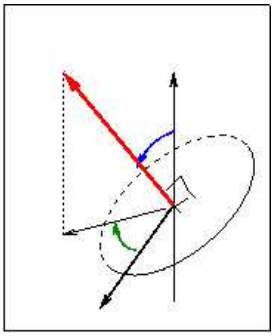

sinusoide visible

Diamètre 7.6 cm

Incidence ° Azimut °

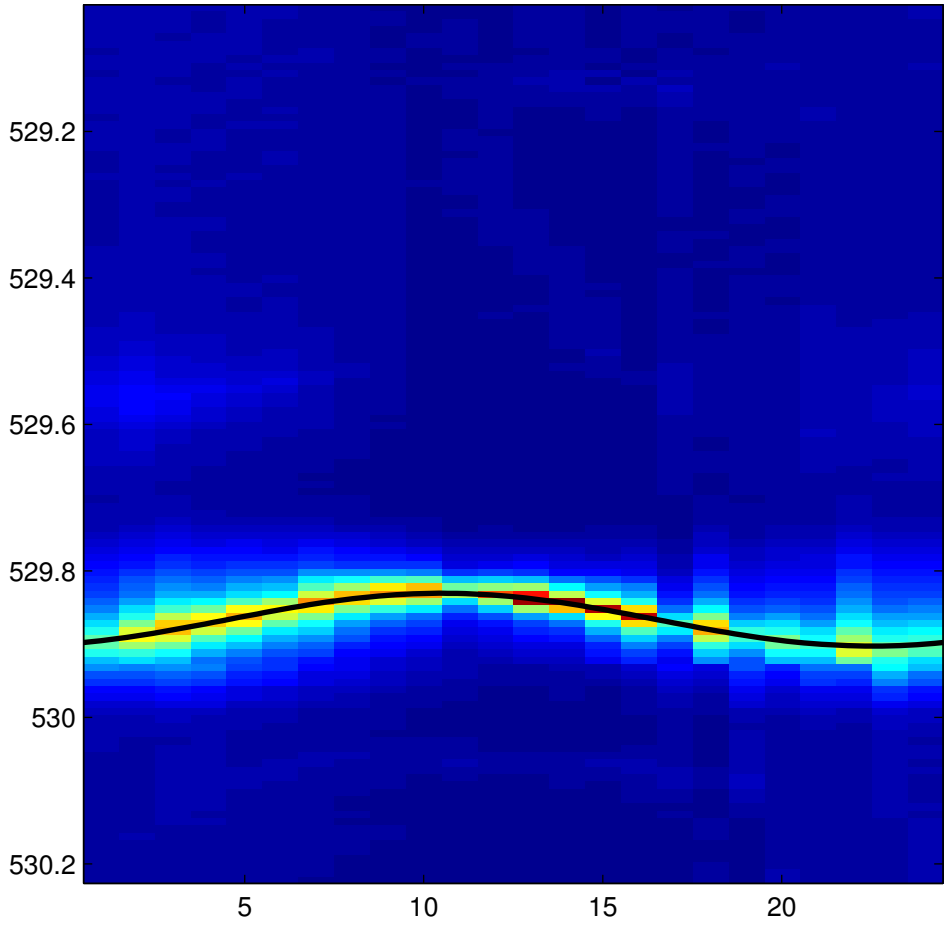

Repère du forage

151.2

43.4834

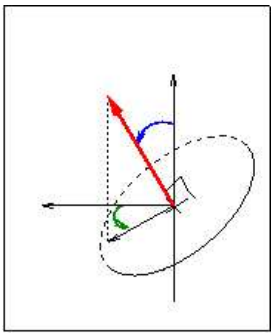

Repère absolu

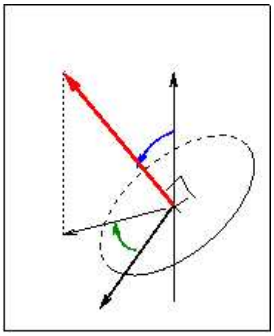

sinusoide visible

Diamètre 7.6 cm

Incidence °

Azimut °

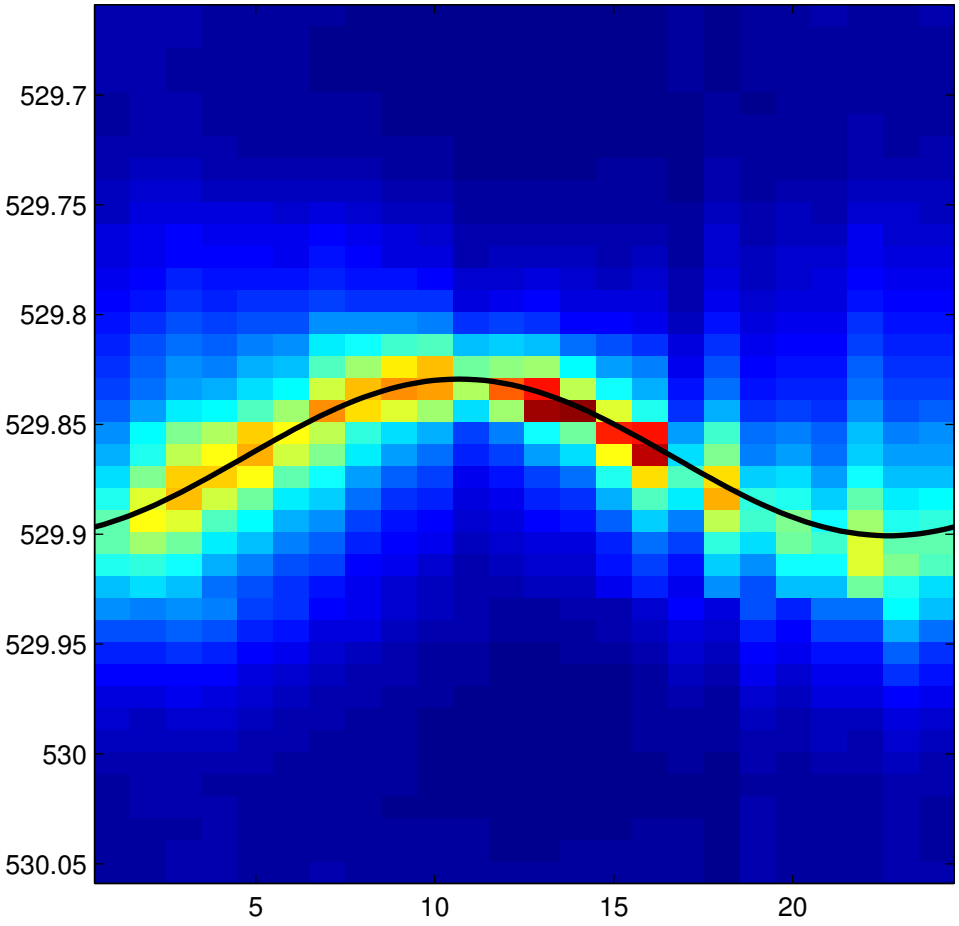

Repère du forage

154.8

43.169

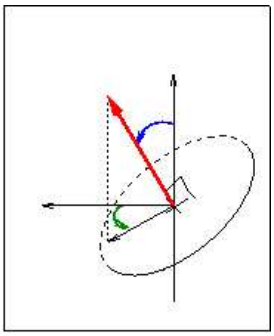

Repère absolu

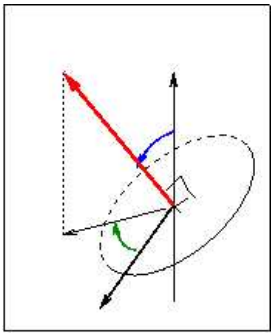

sinusoide visible

Diamètre 7.6 cm

Incidence ° Azimut °

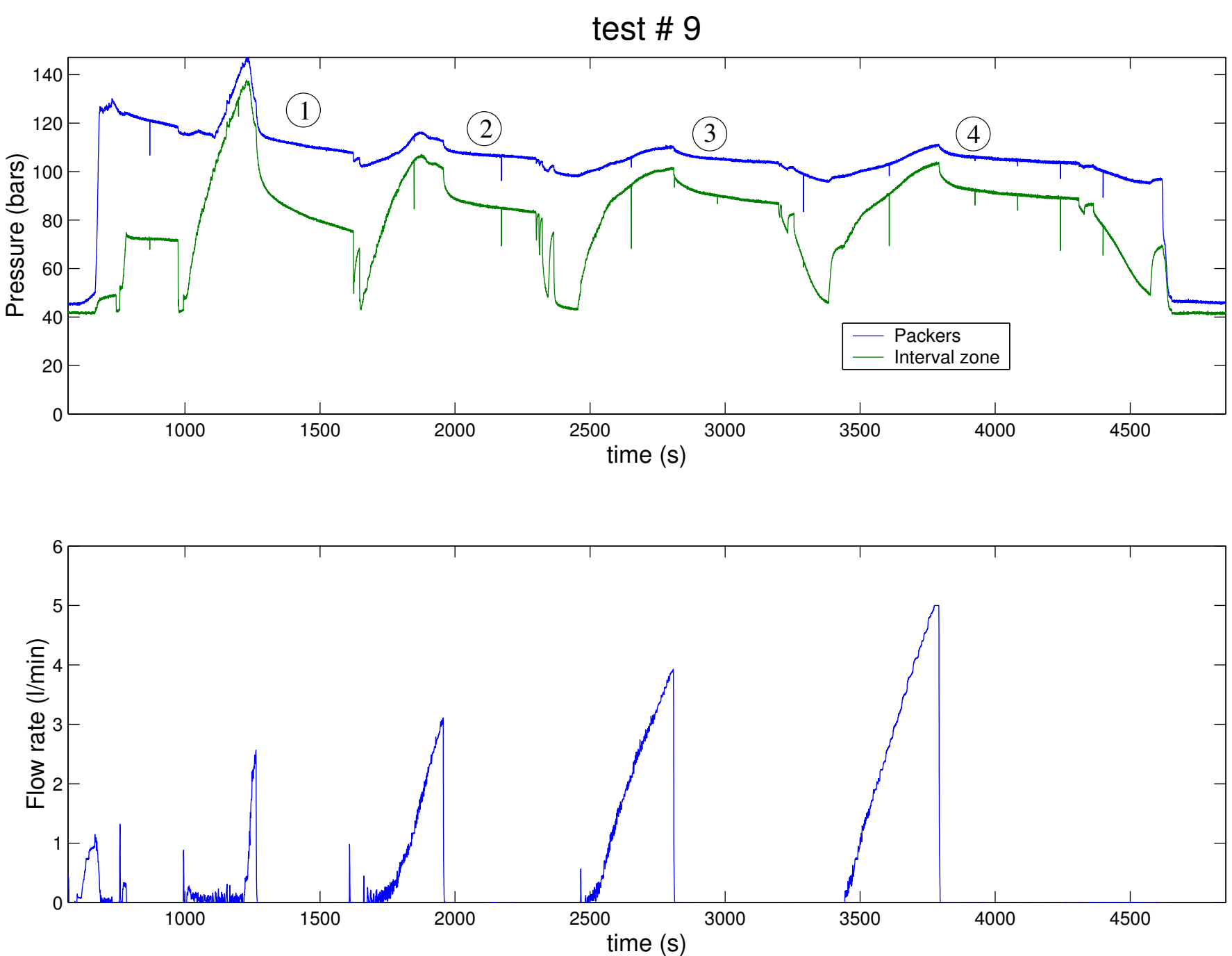
test # 9
Pressure (bars)
time (s)
Packers
Interval zone
1
2
3
4
Flow rate (l/min)
time (s)

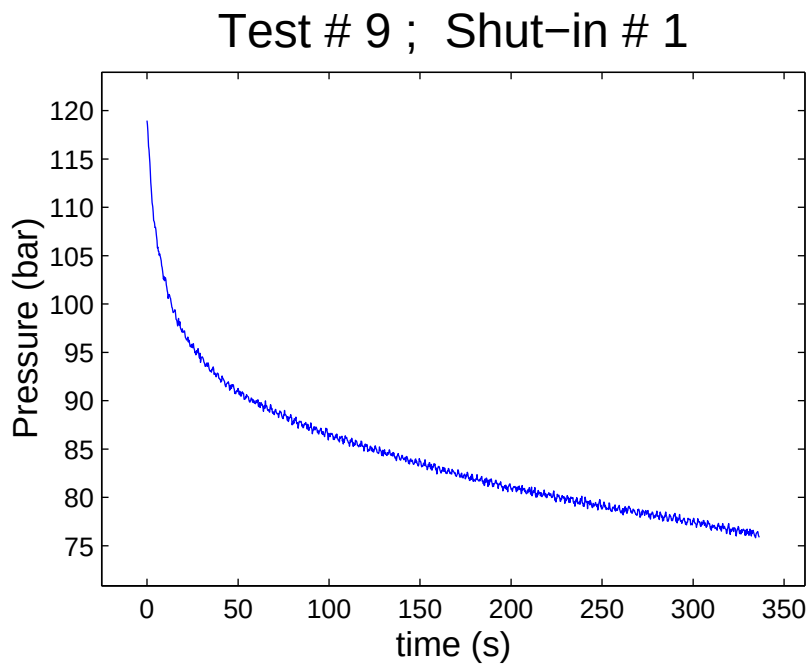
Test # 9 ; Shut−in # 1
Pressure (bar)
time (s)
120
115
110
105
100
95
90
85
80
75
0
50
100
150
200
250
300
350

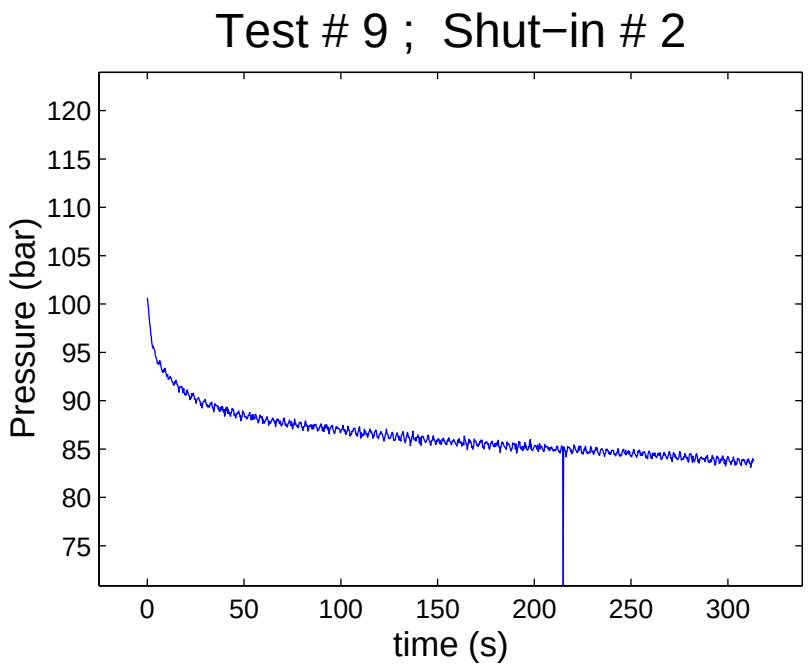
Test # 9 ; Shut−in # 2
Pressure (bar)
time (s)
120
115
110
105
100
95
90
85
80
75
0
50
100
150
200
250
300

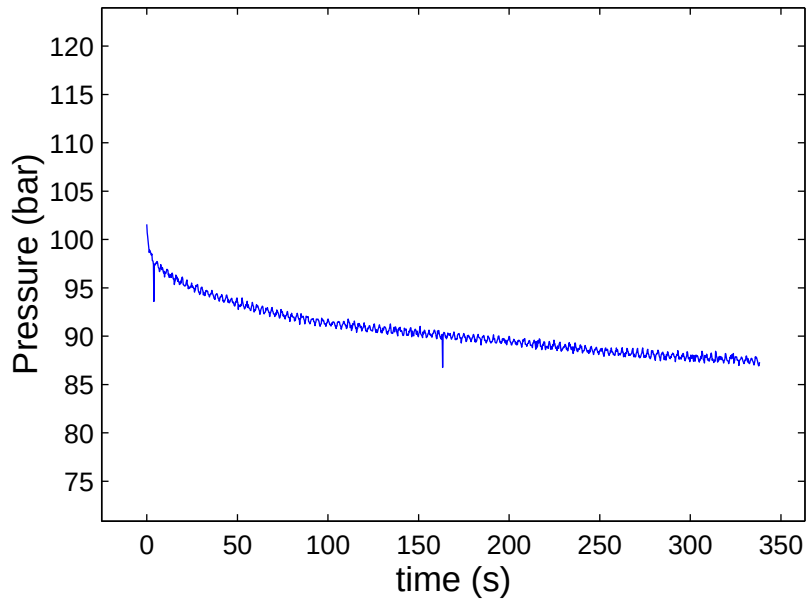
Test # 9 ; Shut−in # 3
Pressure (bar)
time (s)
120
115
110
105
100
95
90
85
80
75
0
50
100
150
200
250
300
350

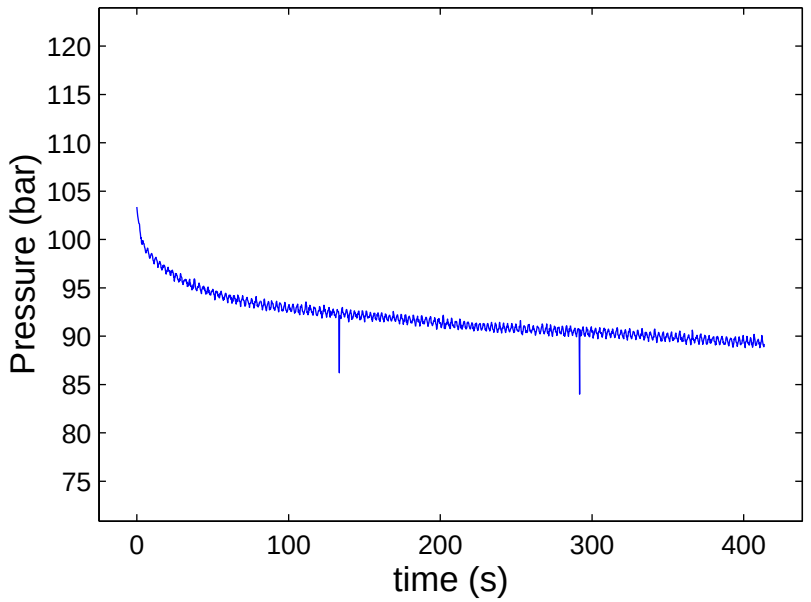
Test # 9 ; Shut−in # 4
Pressure (bar)
time (s)
120
115
110
105
100
95
90
85
80
75
0
100
200
300
400

KLX12A -- Post-frac Log # 9

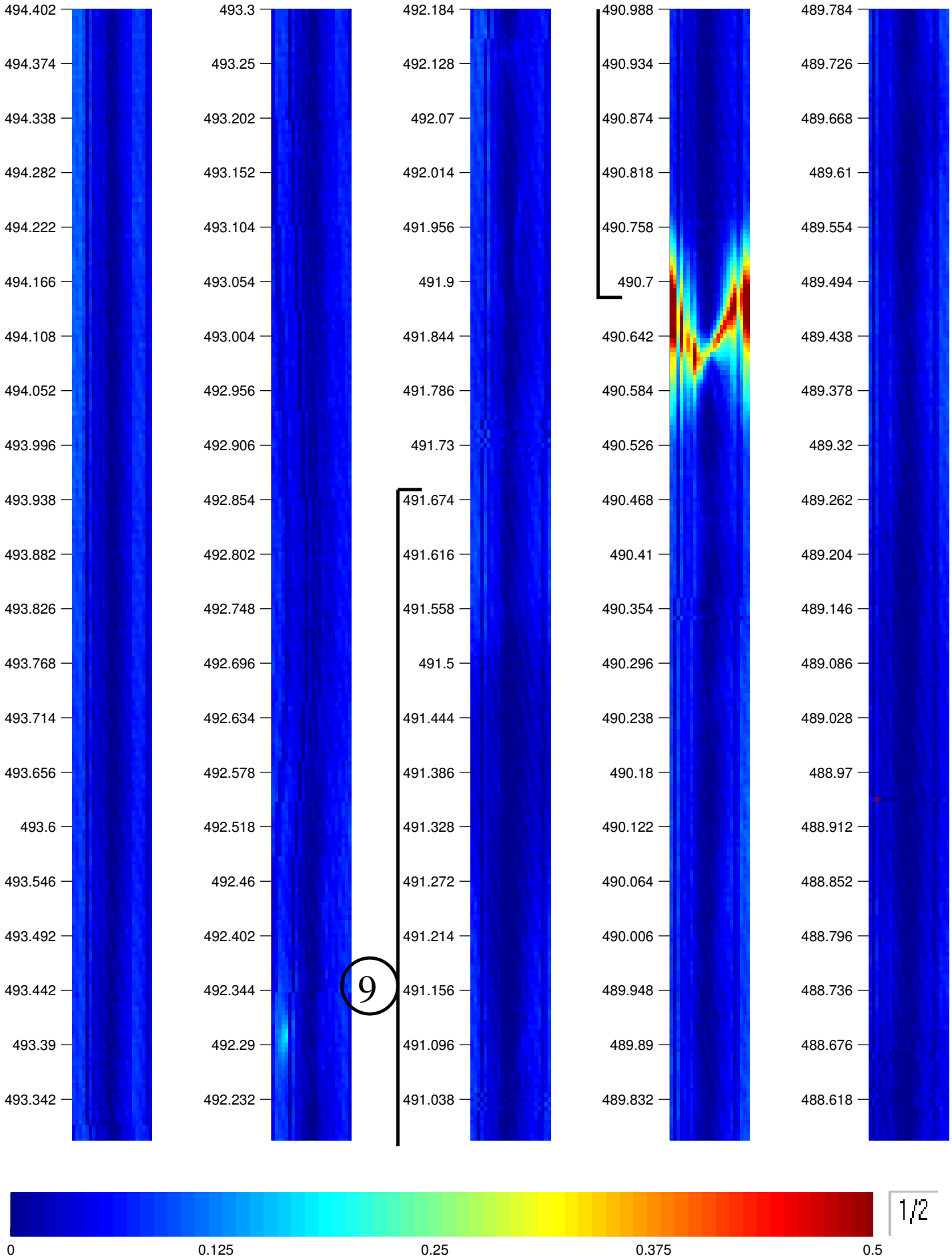

KLX12A -- Post-frac Log # 9

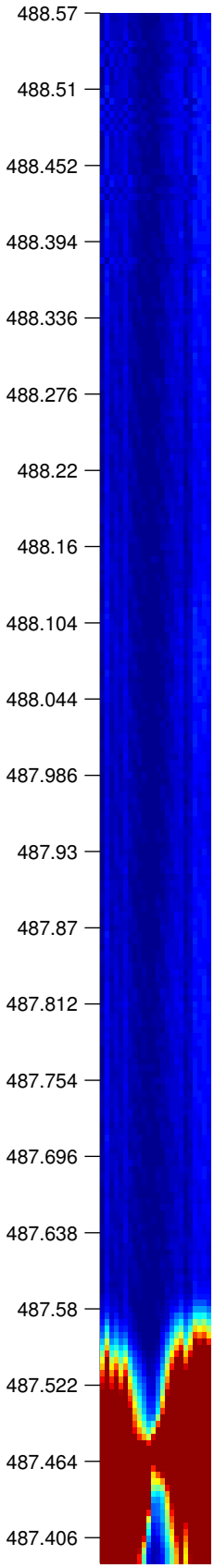

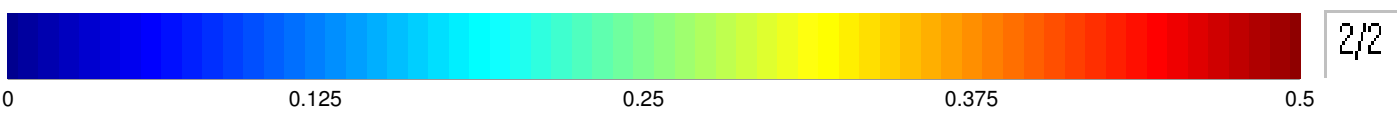

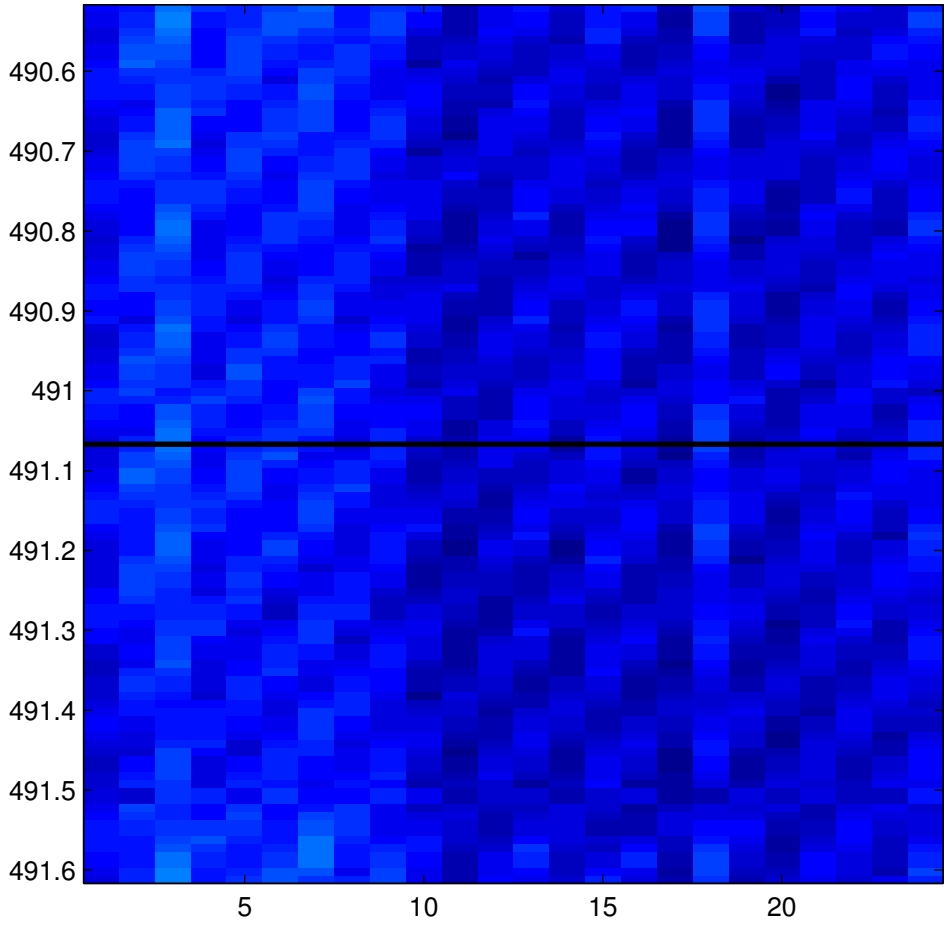

Repère du forage

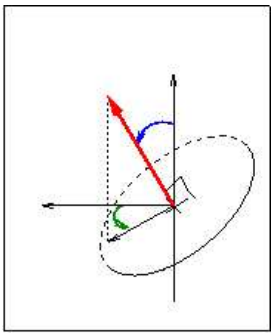

Repère absolu

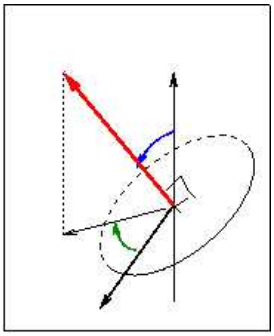

sinusoide visible

Diamètre 7.6 cm

Incidence ° Azimut °

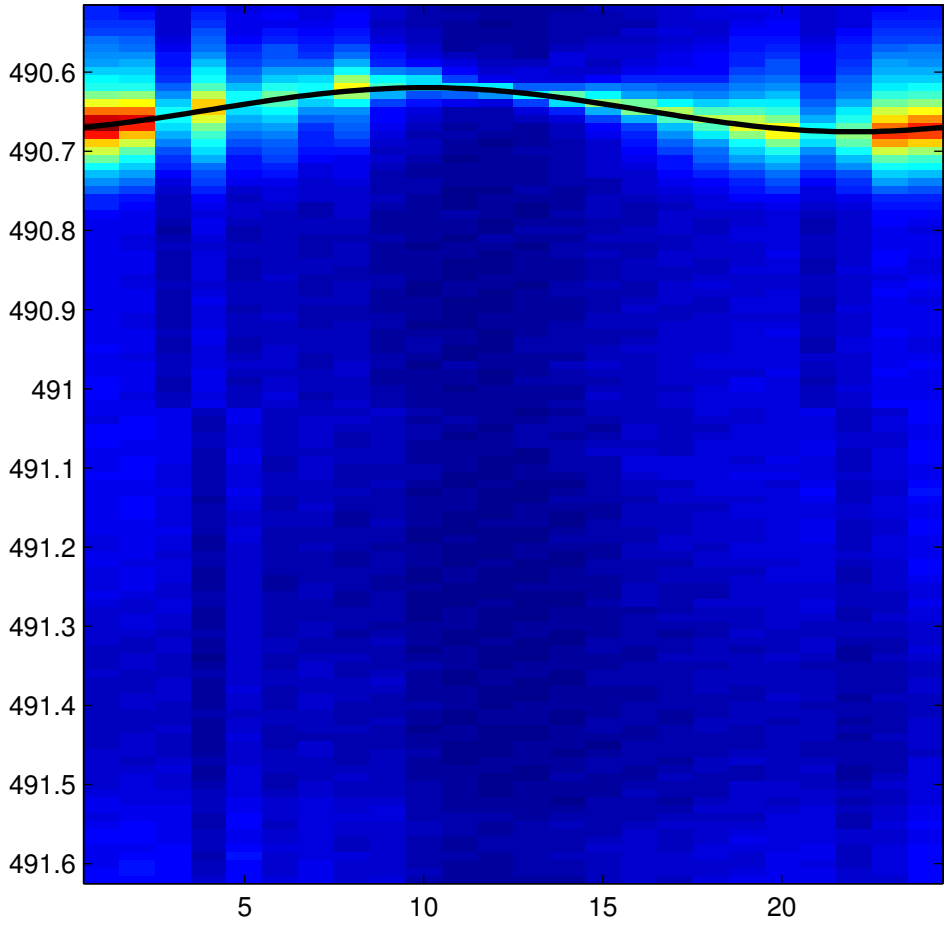

Repère du forage

144

36.2494

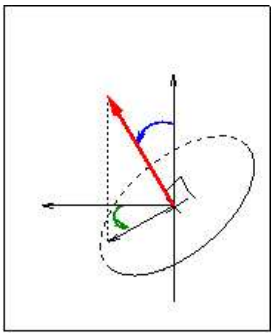

Repère absolu

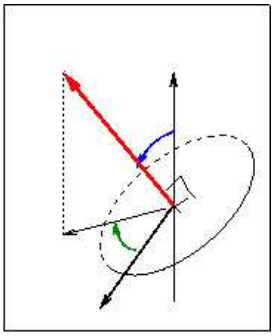

sinusoide visible

Diamètre 7.6 cm

Incidence °

Azimut °

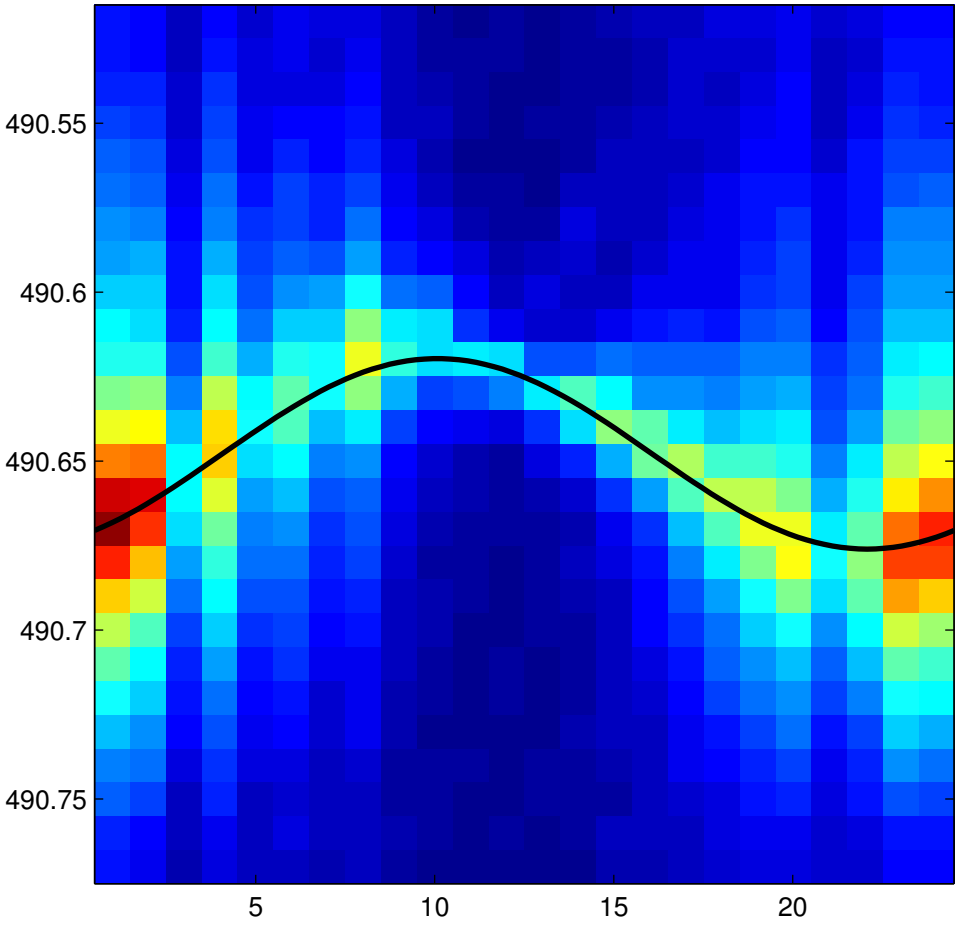

Repère du forage

144

36.5586

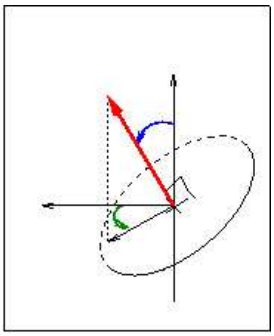

Repère absolu

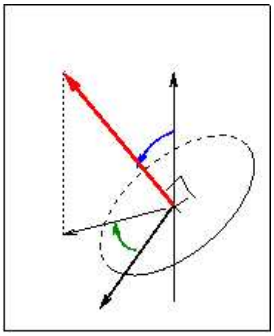

sinusoide visible

Diamètre 7.6 cm

Incidence ° Azimut °

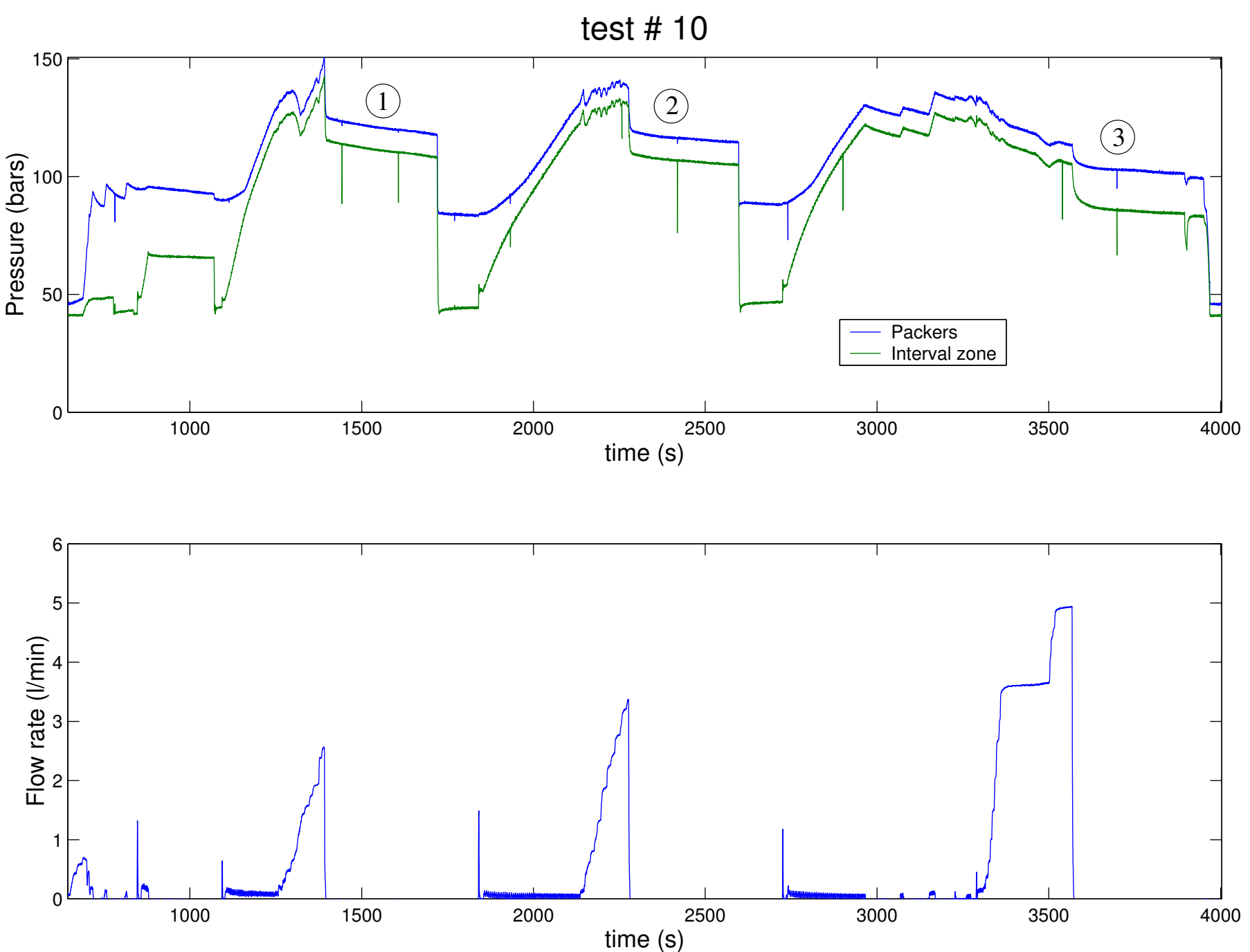
test # 10
Pressure (bars)
150
100
50
0
1
2
3
Packers
Interval zone
1000
1500
2000
2500
3000
3500
4000
time (s)
Flow rate (l/min)
6
5
4
3
2
1
0
1000
1500
2000
2500
3000
3500
4000
time (s)

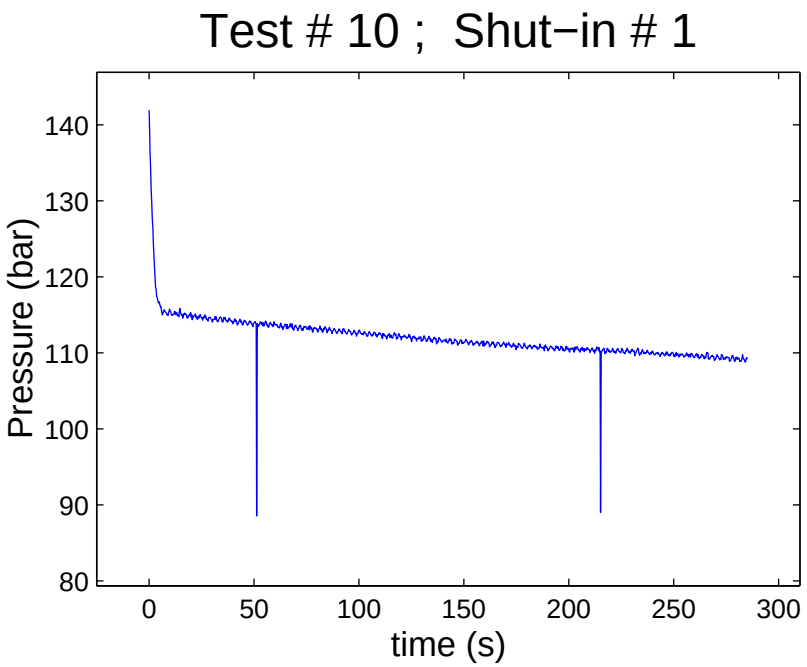
Test # 10 ; Shut−in # 1
Pressure (bar)
time (s)
140
130
120
110
100
90
80
0
50
100
150
200
250
300

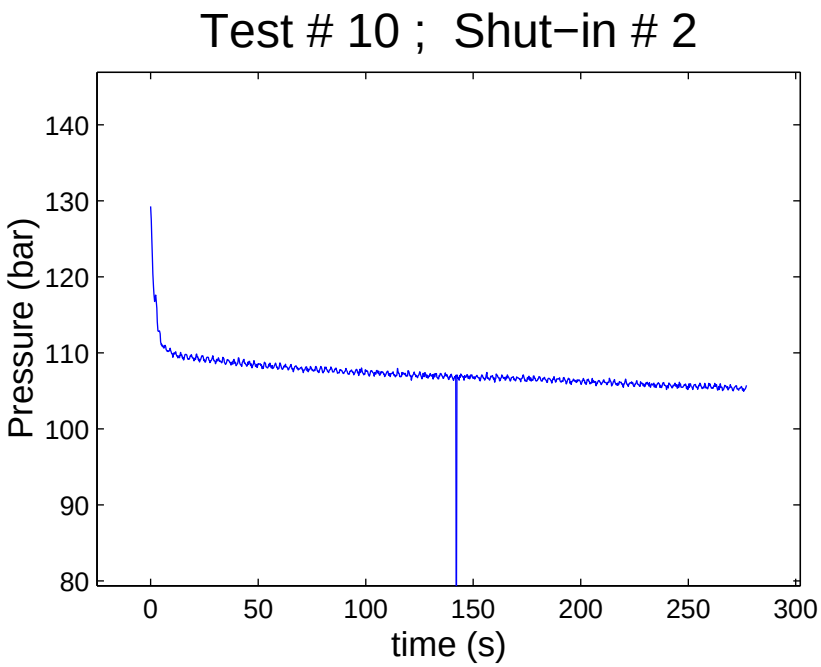
Test # 10 ; Shut−in # 2
Pressure (bar)
time (s)
140
130
120
110
100
90
80
0
50
100
150
200
250
300

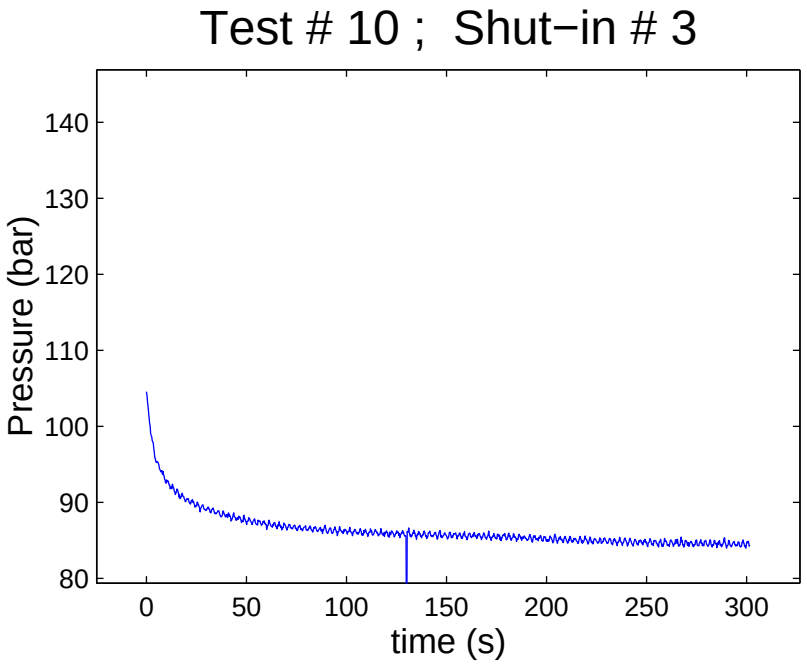
Test # 10 ; Shut−in # 3
Pressure (bar)
time (s)
140
130
120
110
100
90
80
0
50
100
150
200
250
300

KLX12A -- Post-frac Log # 10

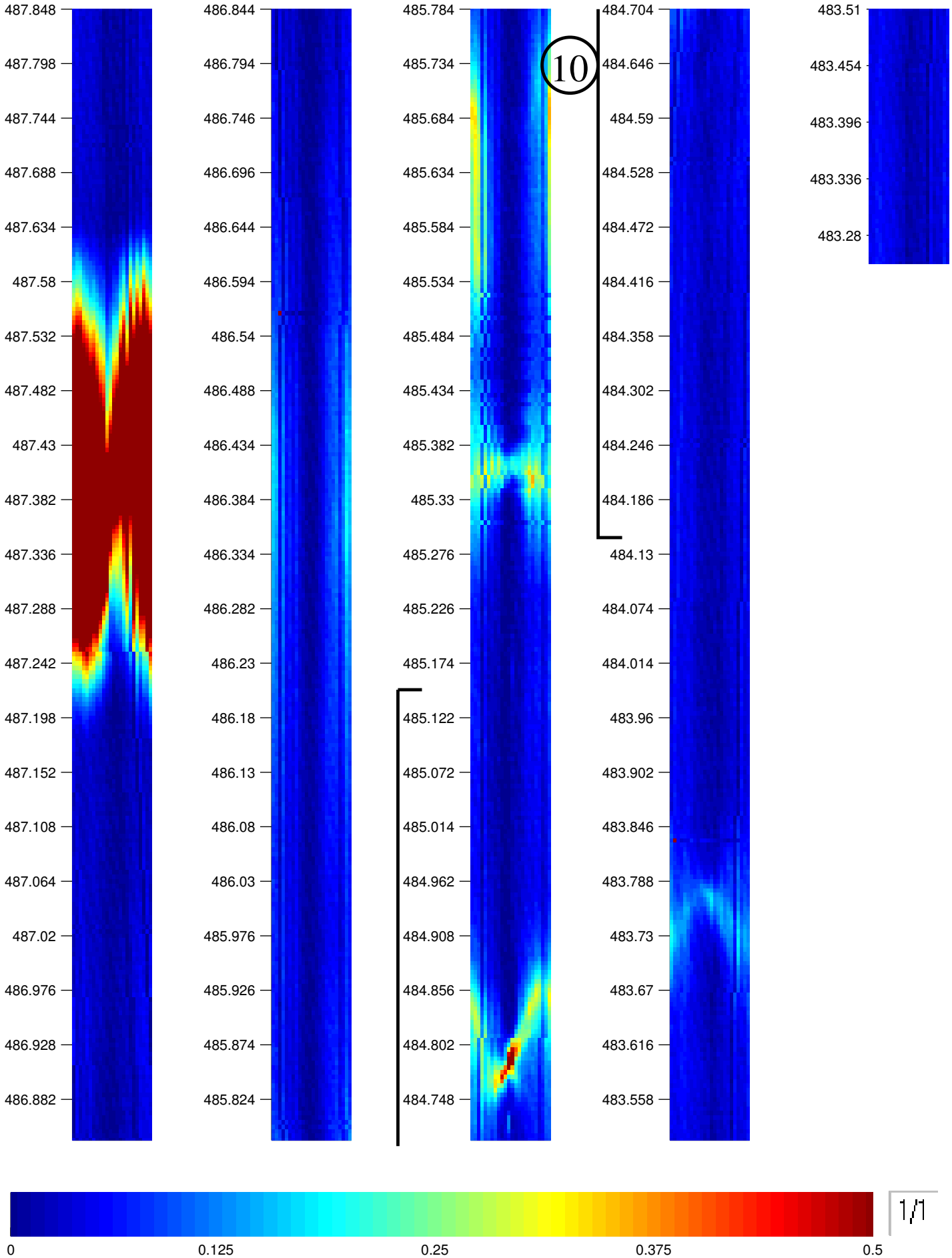

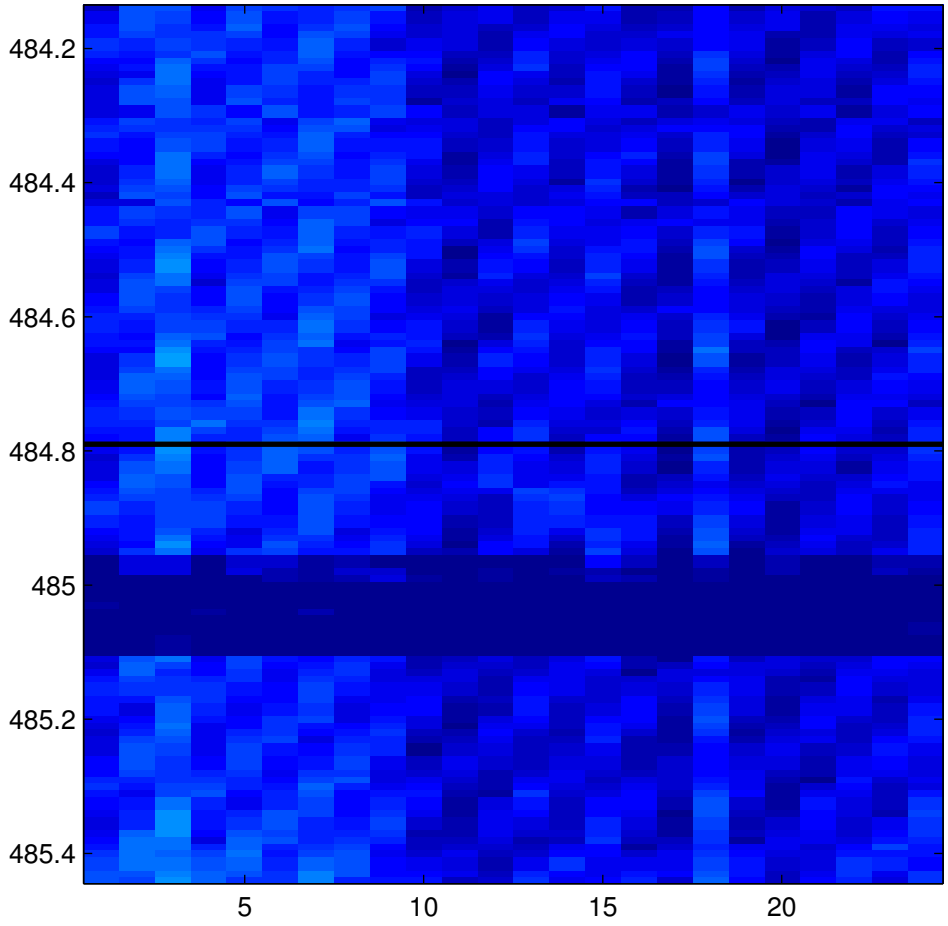

Repère du forage

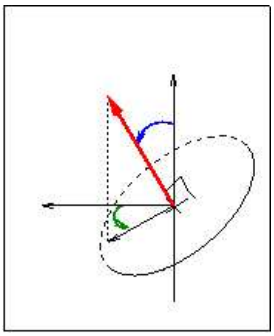

Repère absolu

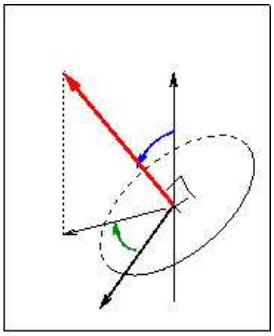

sinusoide visible

Diamètre 7.6 cm

Incidence ° Azimut °

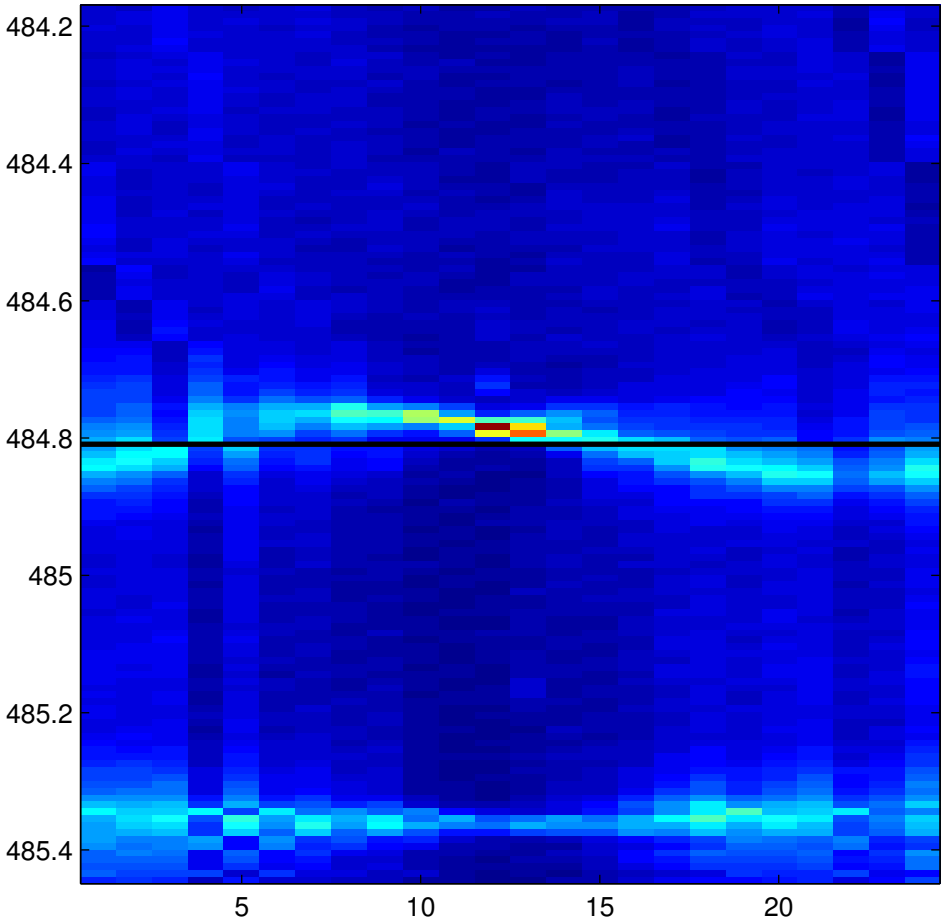

Repère du forage

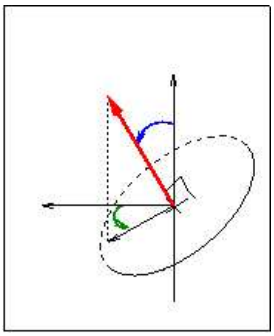

Repère absolu

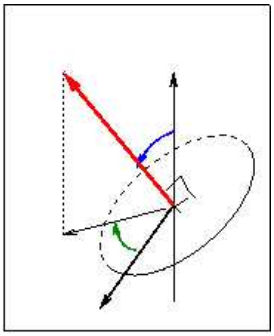

sinusoide visible

Diamètre 7.6 cm

Incidence ° Azimut °

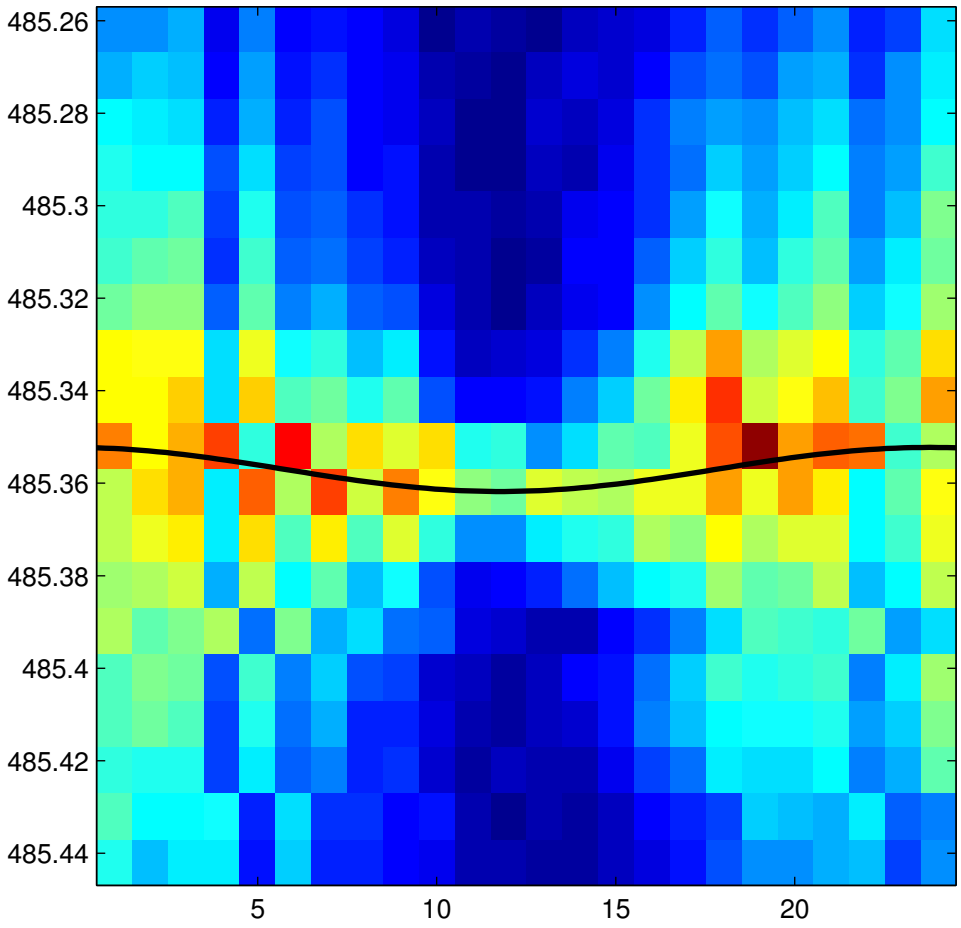

Repère du forage

349.2

7.1441

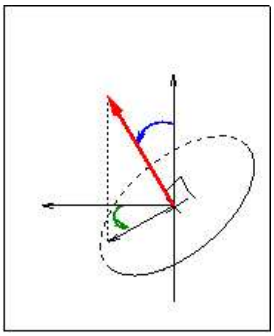

Repère absolu

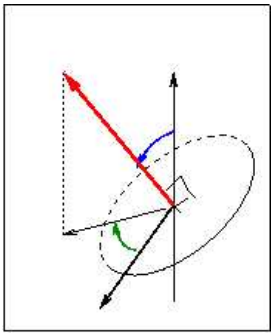

sinusoide visible

Diamètre 7.6 cm

Incidence ° Azimut °

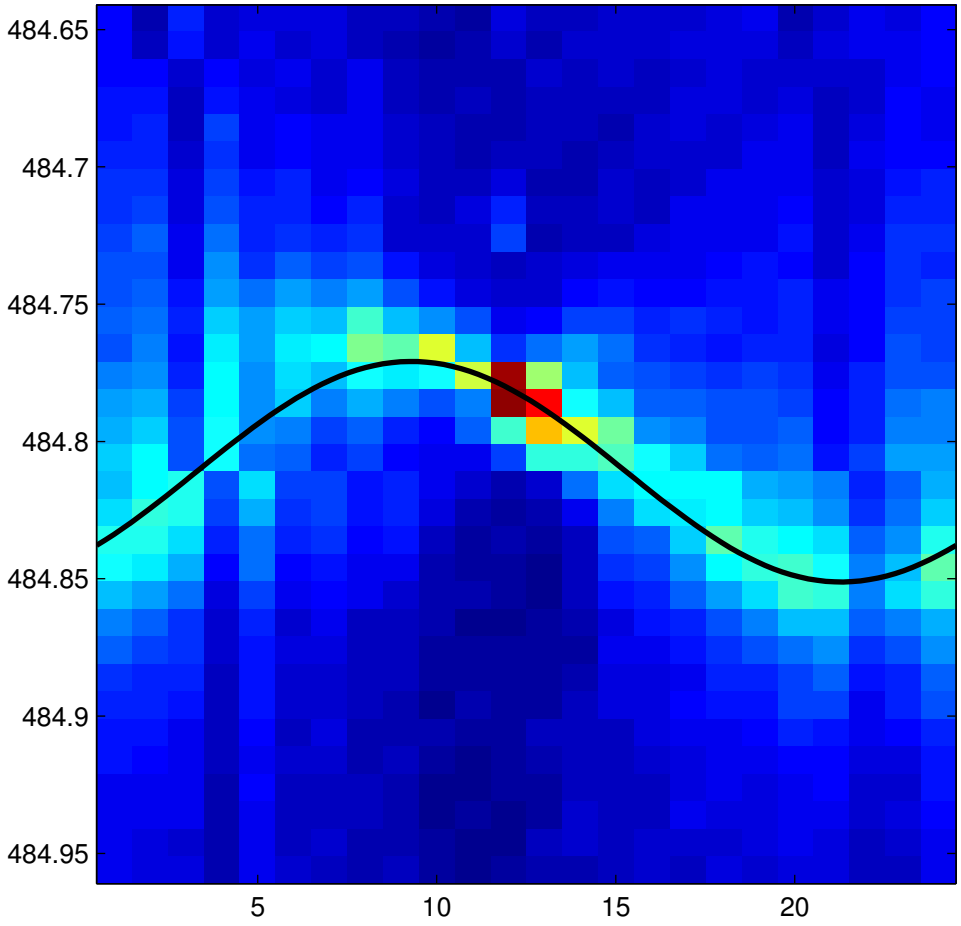

Repère du forage

133.2

46.5818

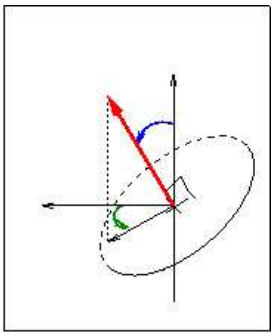

Repère absolu

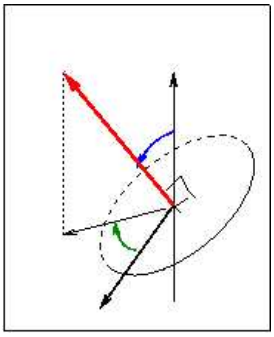

sinusoide visible

Diamètre 7.6 cm

Incidence ° Azimut °

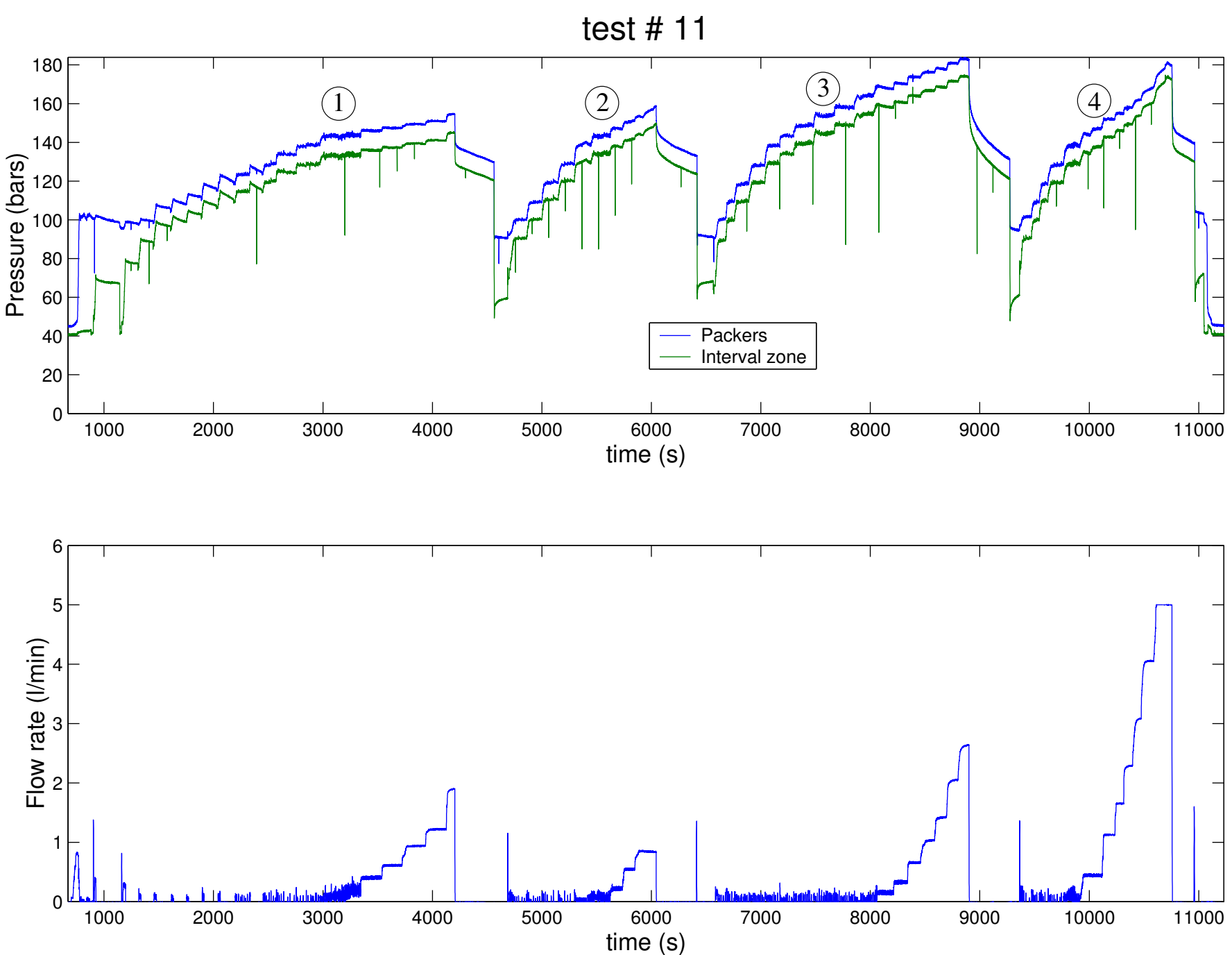
test # 11
Pressure (bars)
time (s)
Packers
Interval zone
1
2
3
4
Flow rate (l/min)
time (s)

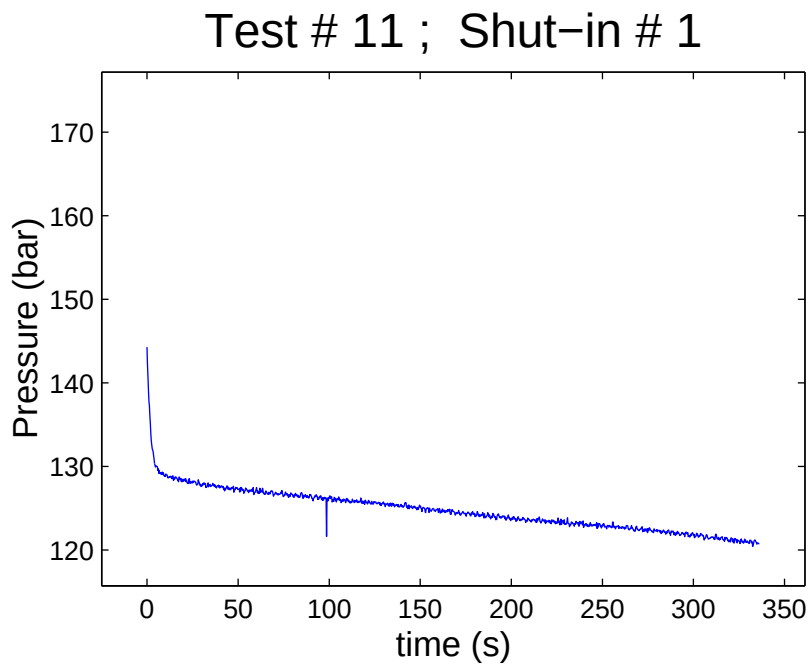
Test # 11 ; Shut−in # 1
Pressure (bar)
time (s)
120
130
140
150
160
170
0
50
100
150
200
250
300
350

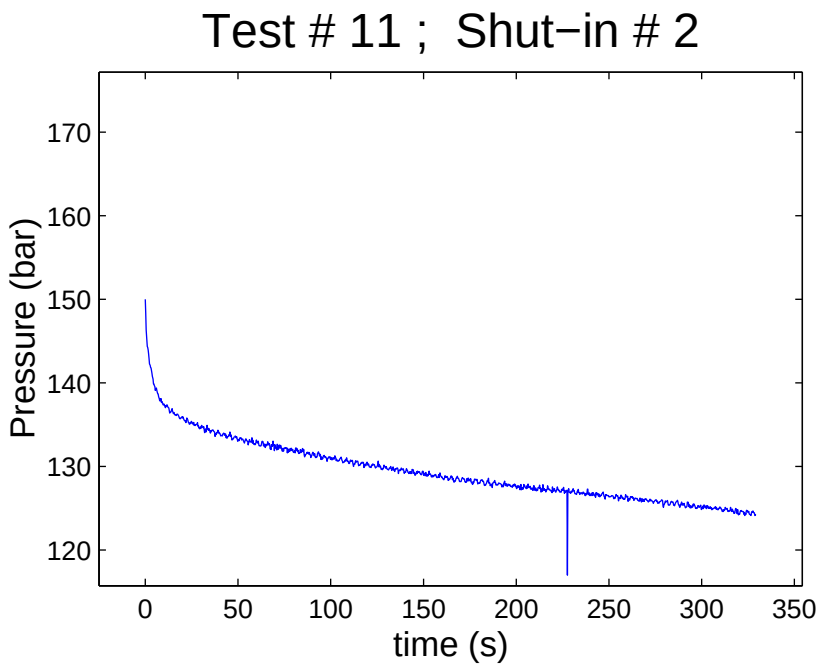
Test # 11 ; Shut−in # 2
Pressure (bar)
time (s)
120
130
140
150
160
170
0
50
100
150
200
250
300
350

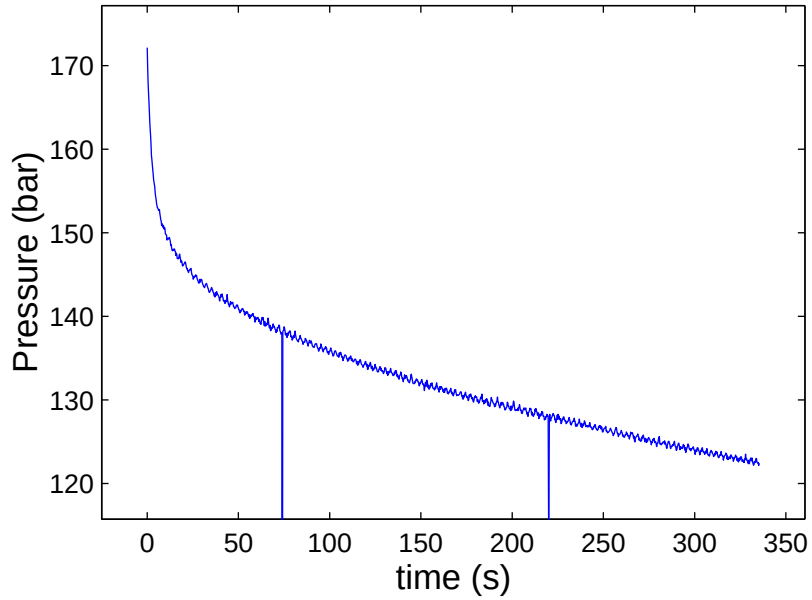
Test # 11 ; Shut−in # 3
Pressure (bar)
time (s)
120
130
140
150
160
170
0
50
100
150
200
250
300
350

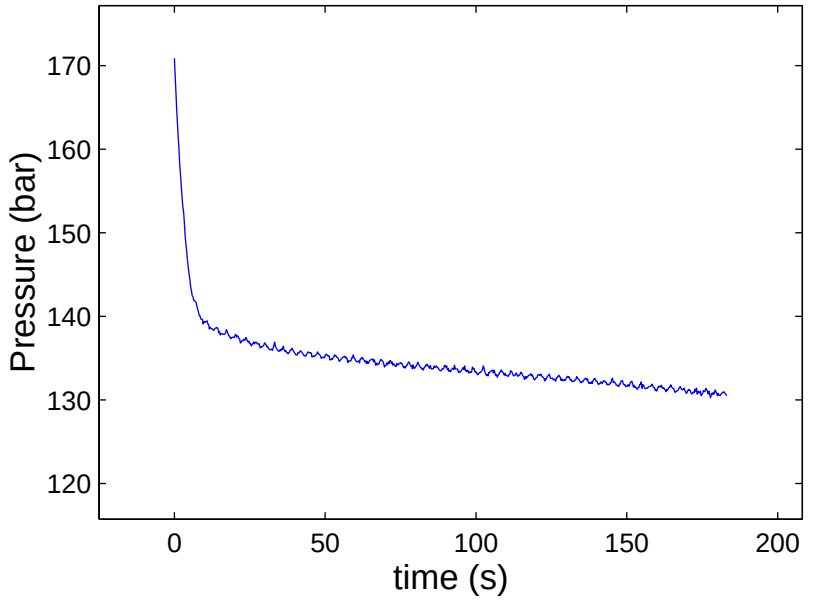
Test # 11 ; Shut−in # 4
Pressure (bar)
time (s)
120
130
140
150
160
170
0
50
100
150
200

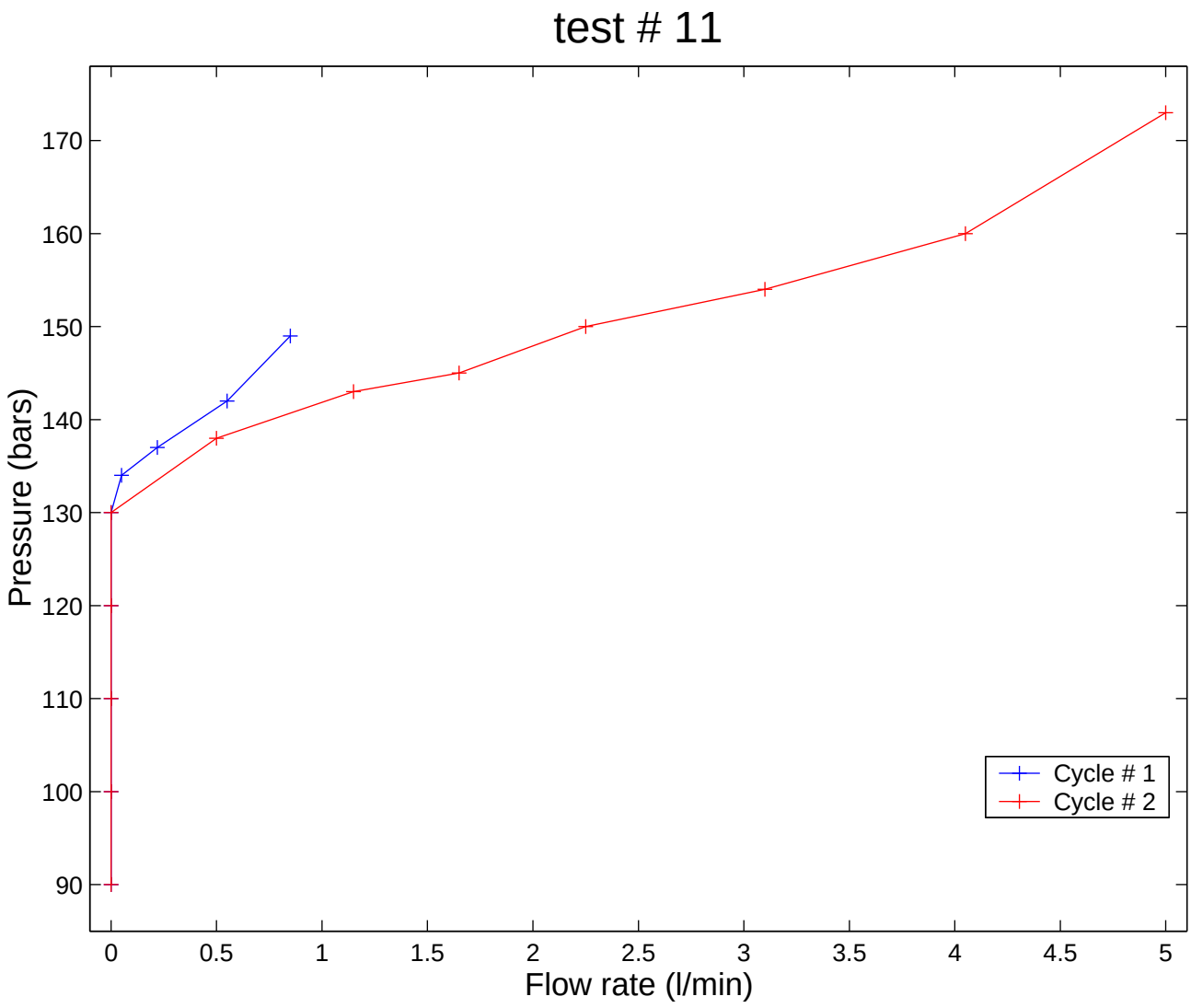
test # 11
Pressure (bars)
170
160
150
140
130
120
110
100
90
0
0.5
1
1.5
2
2.5
3
3.5
4
4.5
5
Flow rate (l/min)
Cycle # 1
Cycle # 2

KLX12A -- Post-frac Log # 11

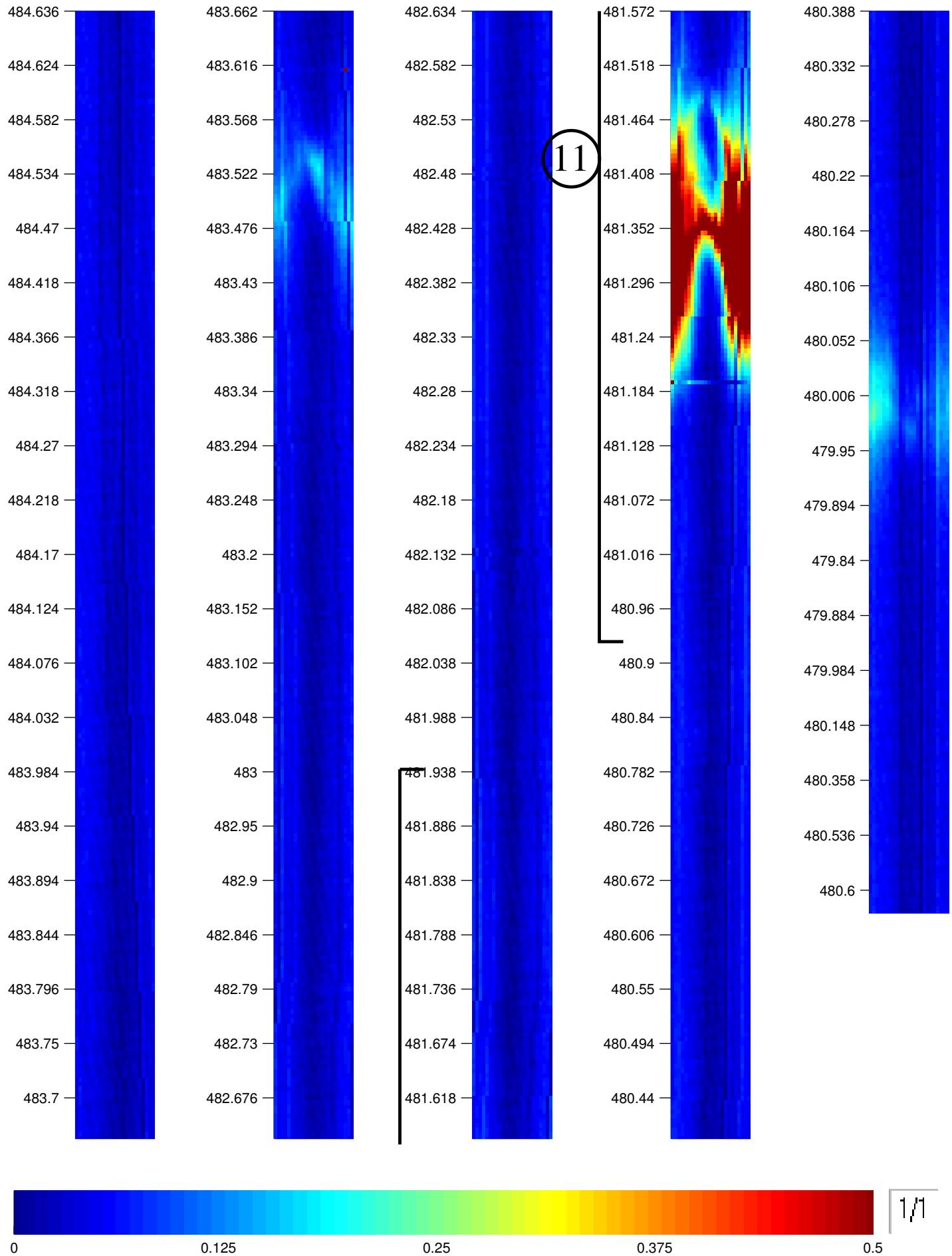

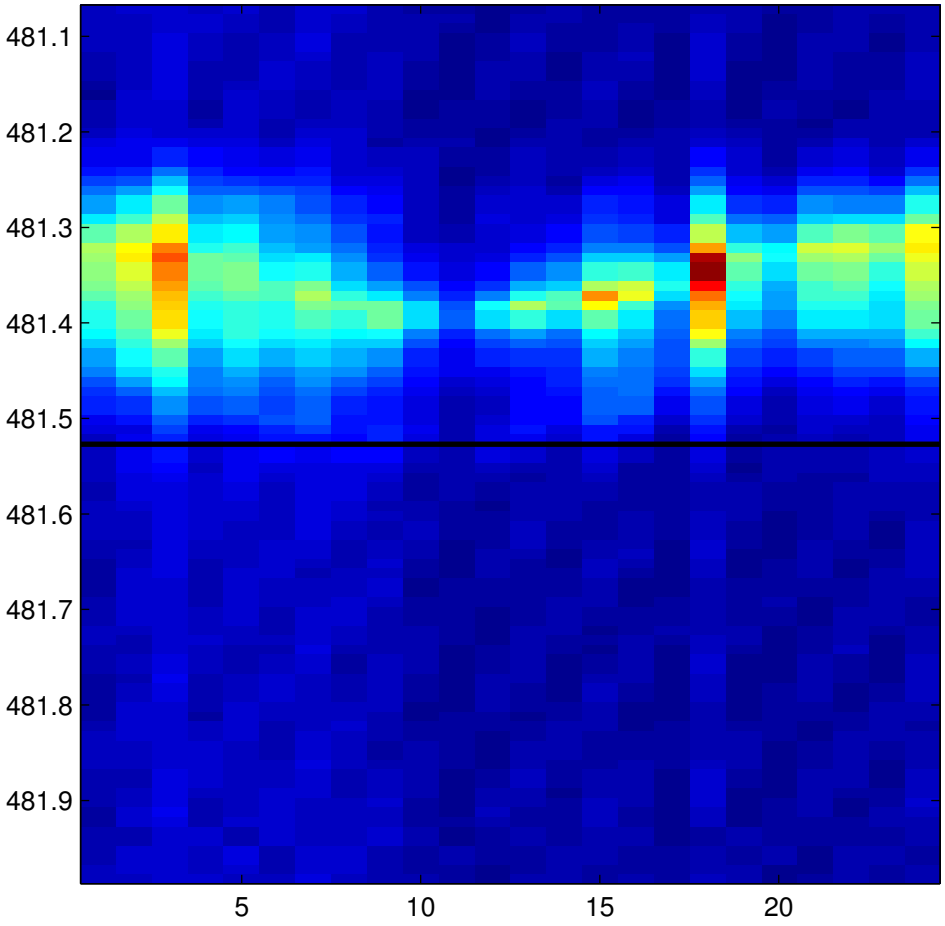

Repère du forage

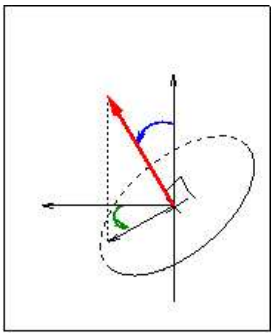

Repère absolu

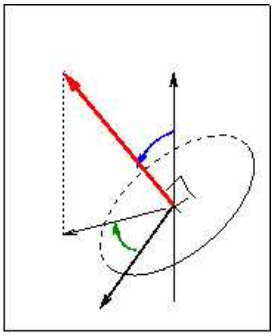

sinusoide visible

Diamètre 7.6 cm

Incidence ° Azimut °

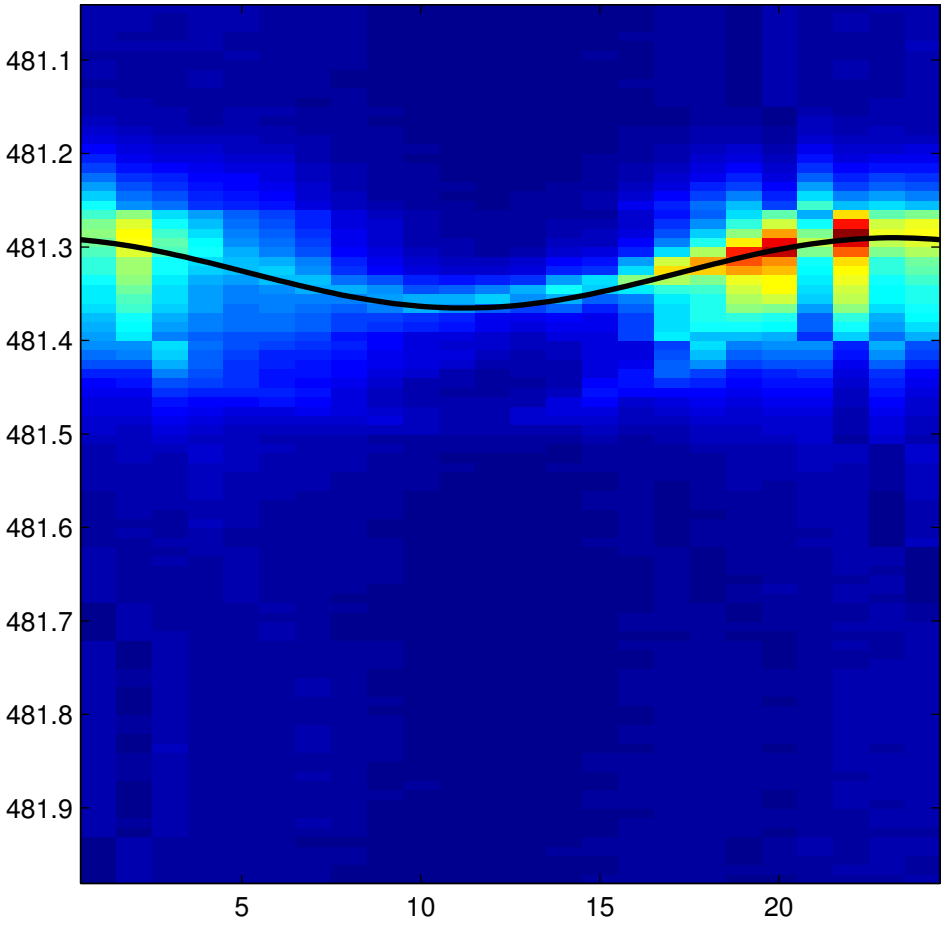

Repère du forage

342

44.679

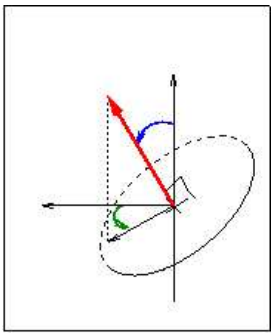

Repère absolu

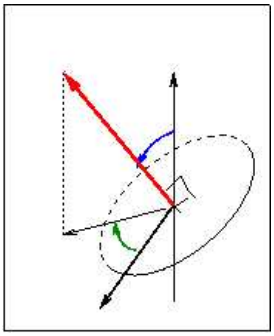

sinusoide visible

Diamètre 7.6 cm

Incidence ° Azimut °

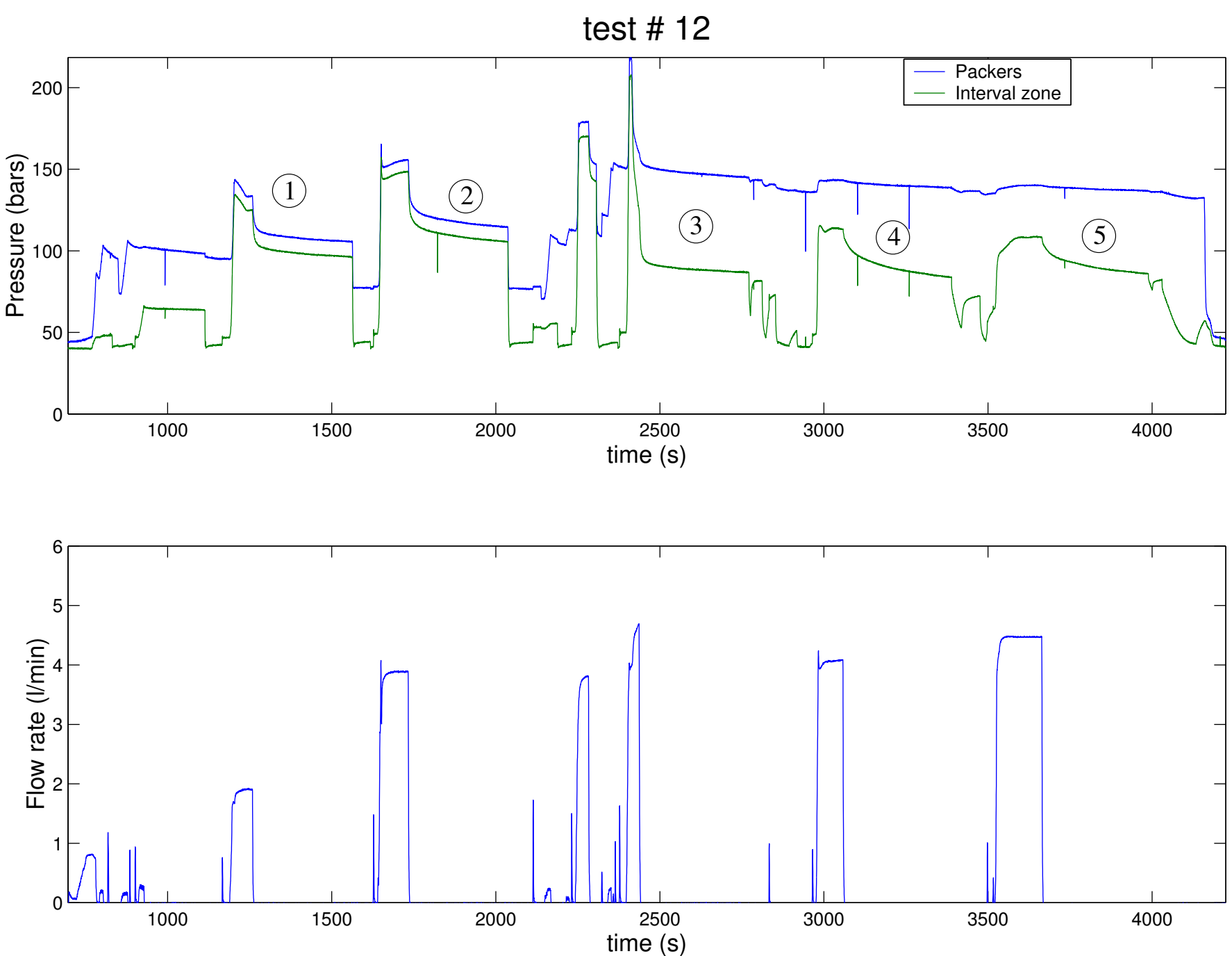
test # 12
Packers
Interval zone
Pressure (bars)
time (s)
1
2
3
4
5
Flow rate (l/min)
time (s)

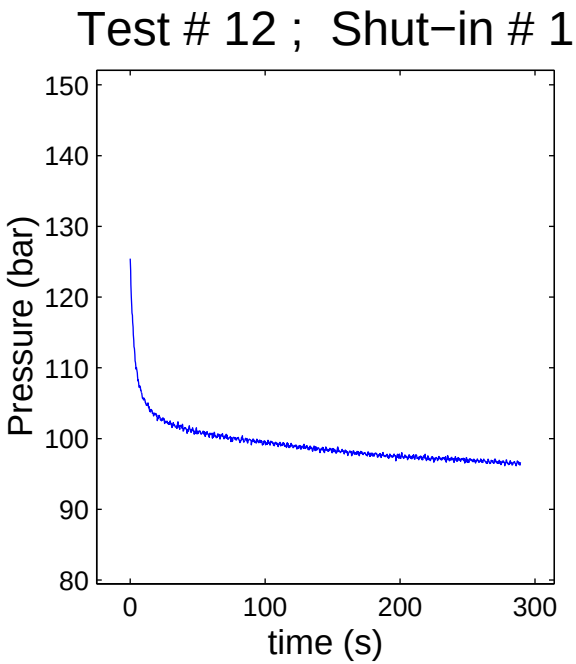
Test # 12 ; Shut−in # 1
Pressure (bar)
time (s)
150
140
130
120
110
100
90
80
0
100
200
300

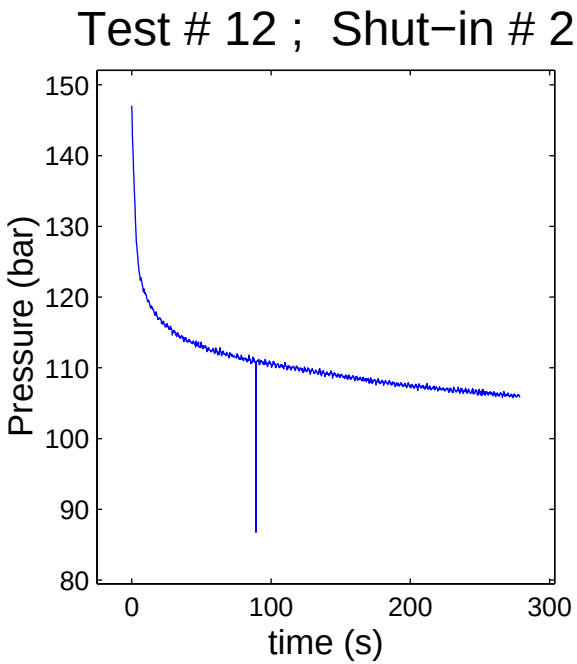
Test # 12 ; Shut−in # 2
Pressure (bar)
time (s)
150
140
130
120
110
100
90
80
0
100
200
300

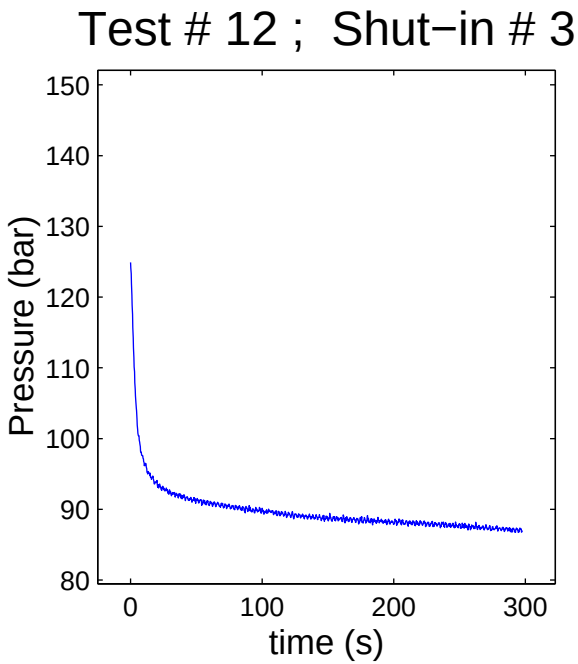
Test # 12 ; Shut−in # 3
Pressure (bar)
time (s)
150
140
130
120
110
100
90
80
0
100
200
300

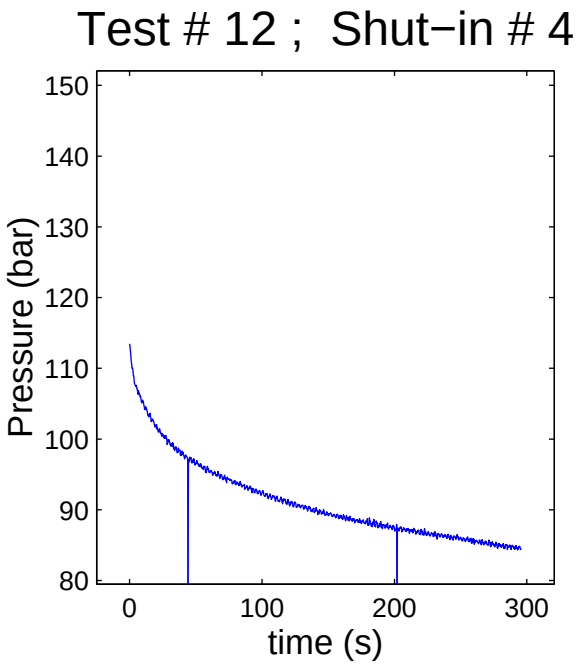
Test # 12 ; Shut−in # 4
Pressure (bar)
time (s)
150
140
130
120
110
100
90
80
0
100
200
300

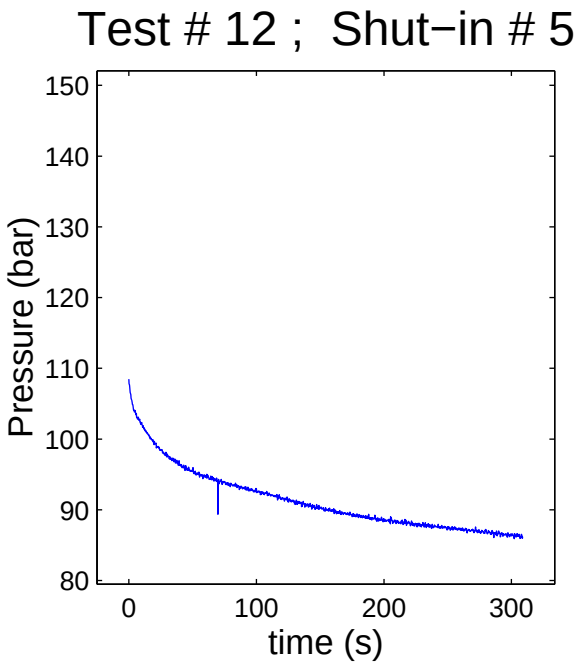
Test # 12 ; Shut−in # 5
Pressure (bar)
time (s)
150
140
130
120
110
100
90
80
0
100
200
300

KLX12A -- Post-frac Log # 12

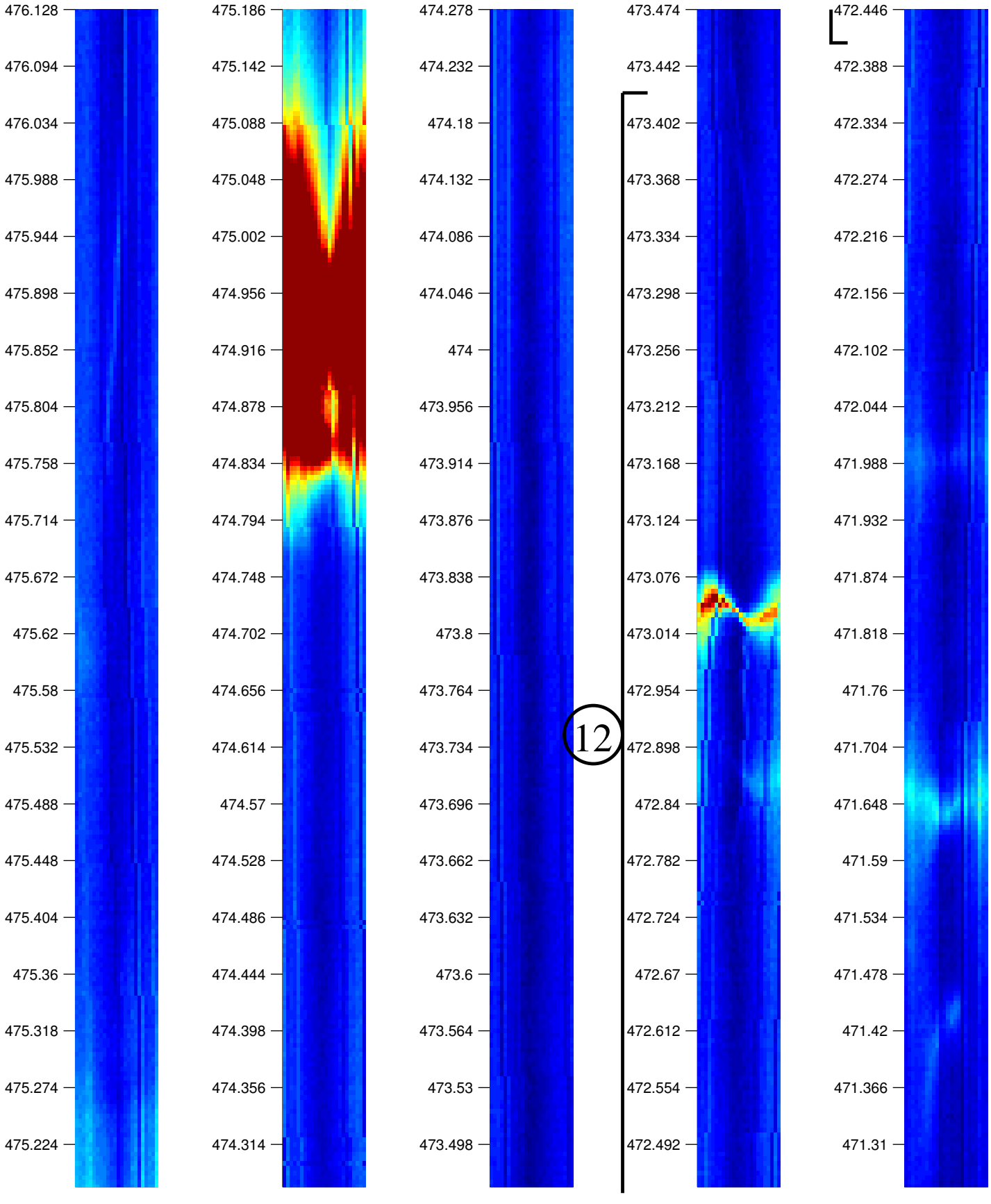

KLX12A -- Post-frac Log # 12

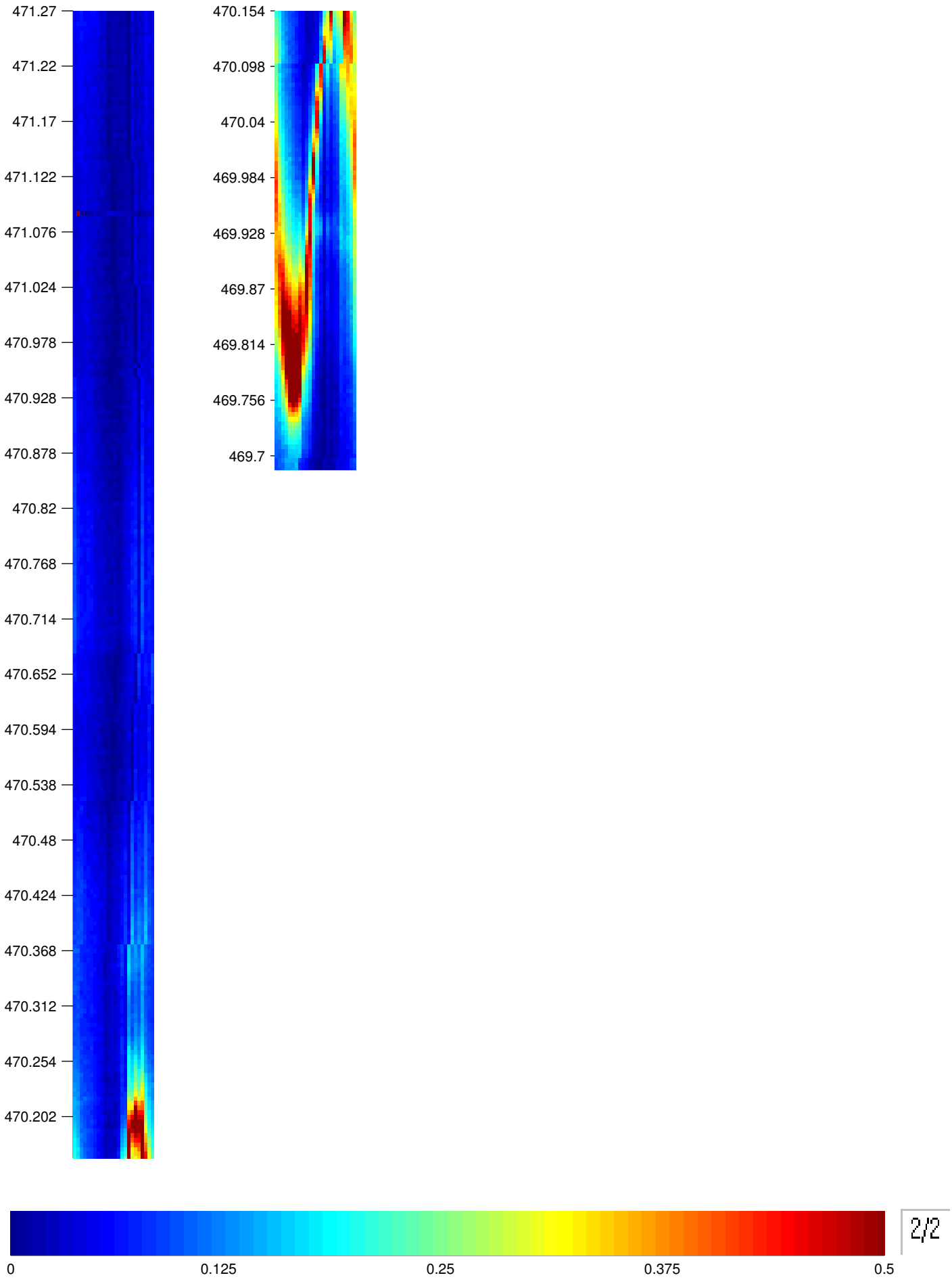

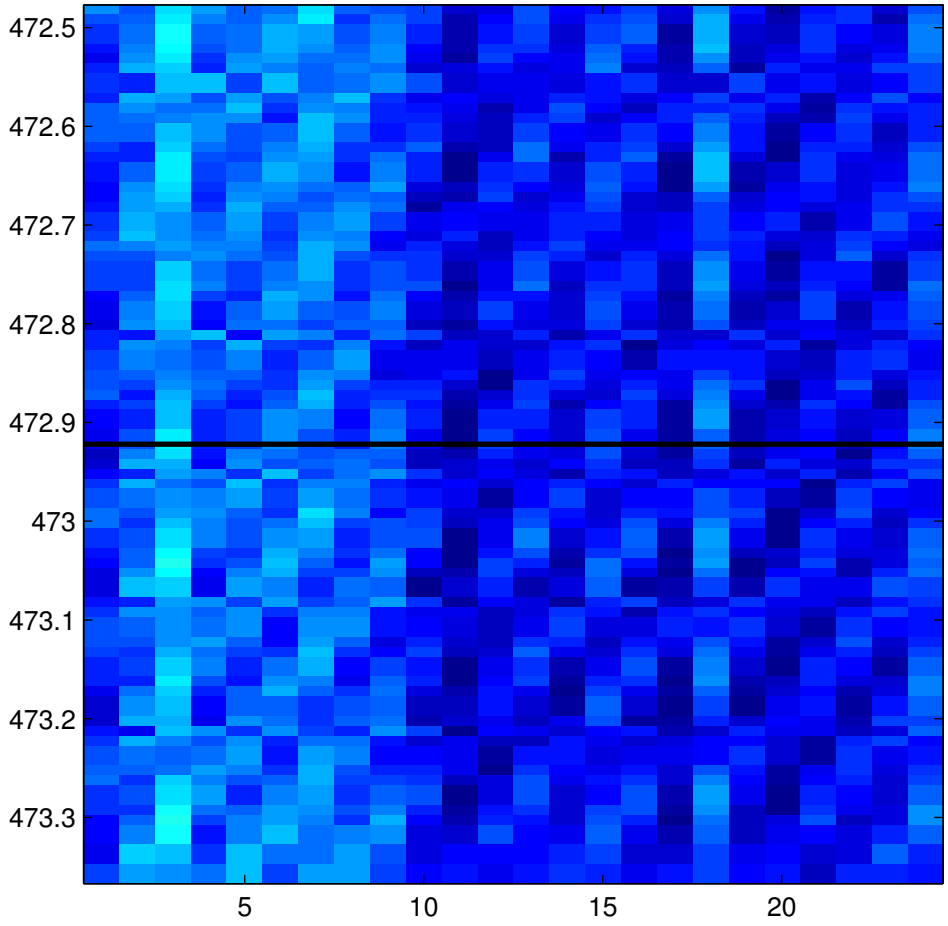

Repère du forage

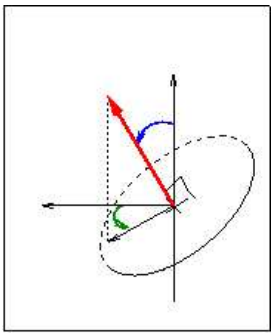

Repère absolu

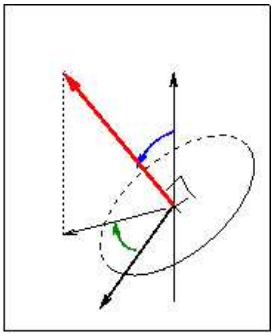

sinusoide visible

Diamètre 7.6 cm

Incidence °

Azimut °

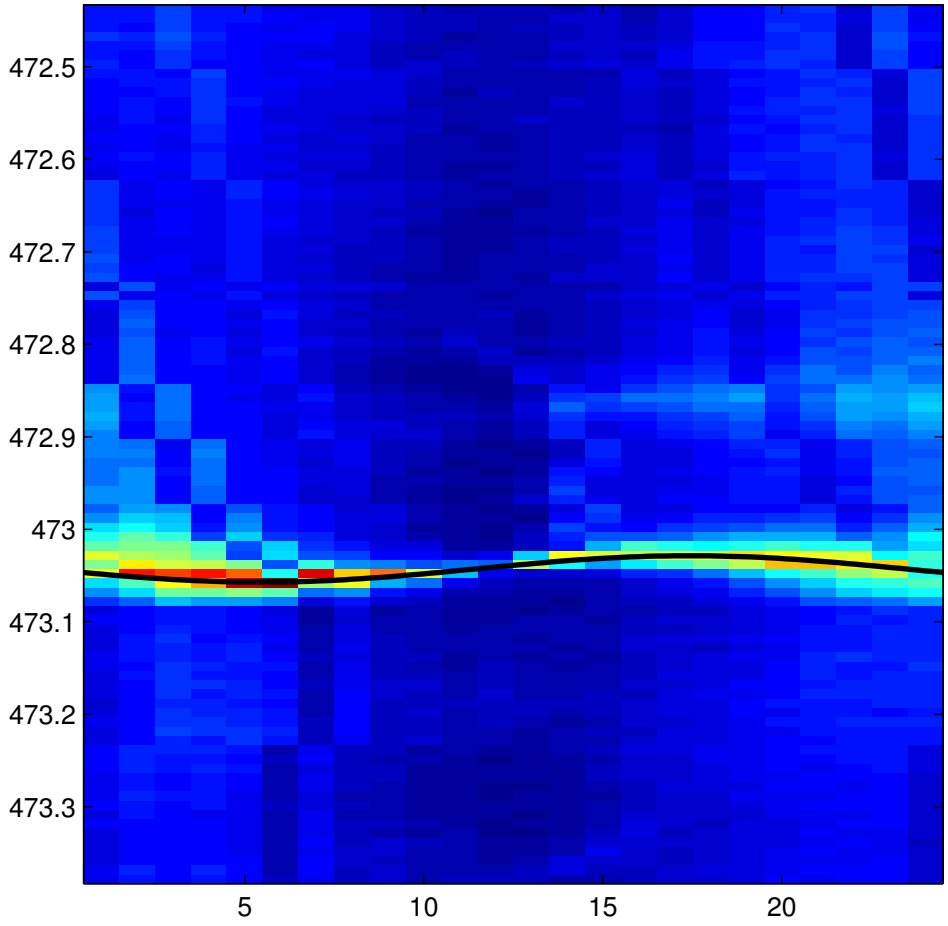

Repère du forage

255.6

20.577

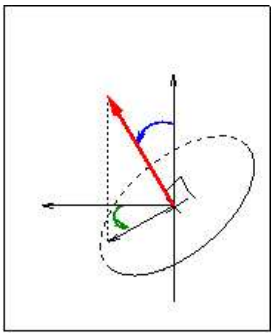

Repère absolu

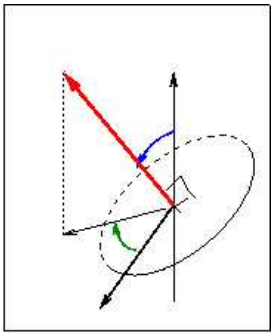

sinusoide visible

Diamètre 7.6 cm

Incidence ° Azimut °

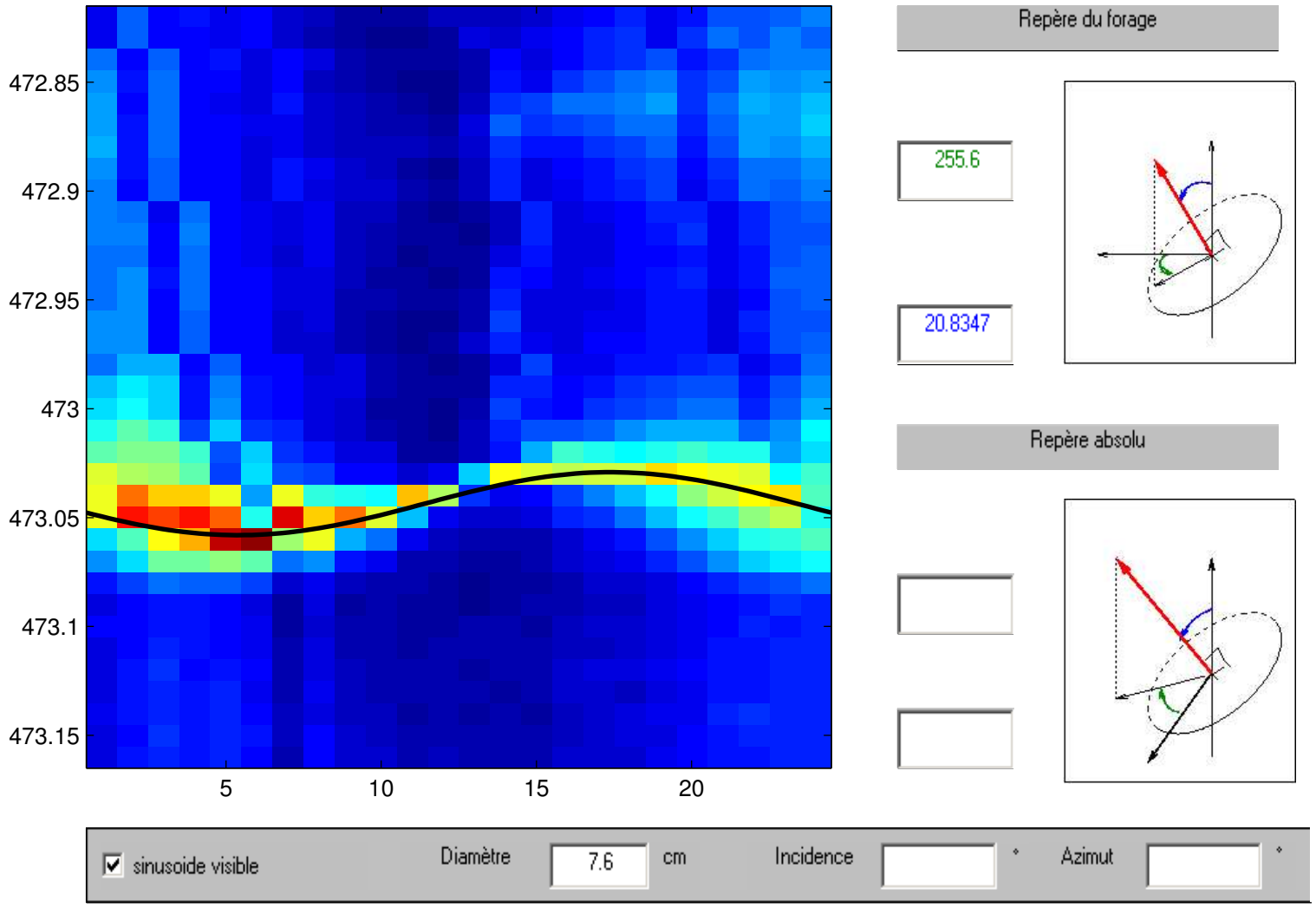
472.85
472.9
472.95
473
473.05
473.1
473.15
5
10
15
20
Repère du forage
255.6
20.8347
Repère absolu
sinusoide visible
Diamètre
7.6
cm
Incidence
°
Azimut
°

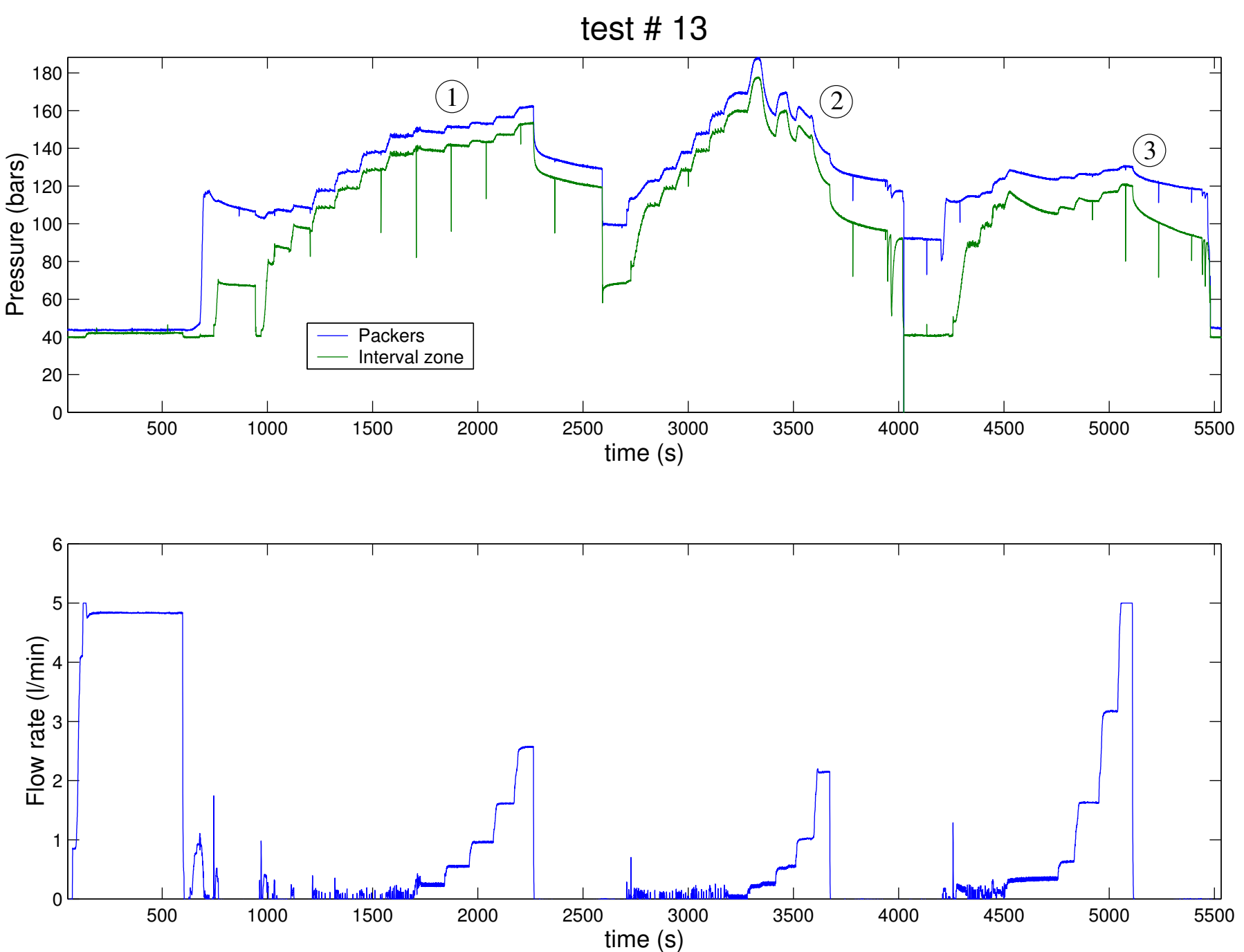
test # 13
Pressure (bars)
time (s)
Packers
Interval zone
1
2
3
Flow rate (l/min)
time (s)

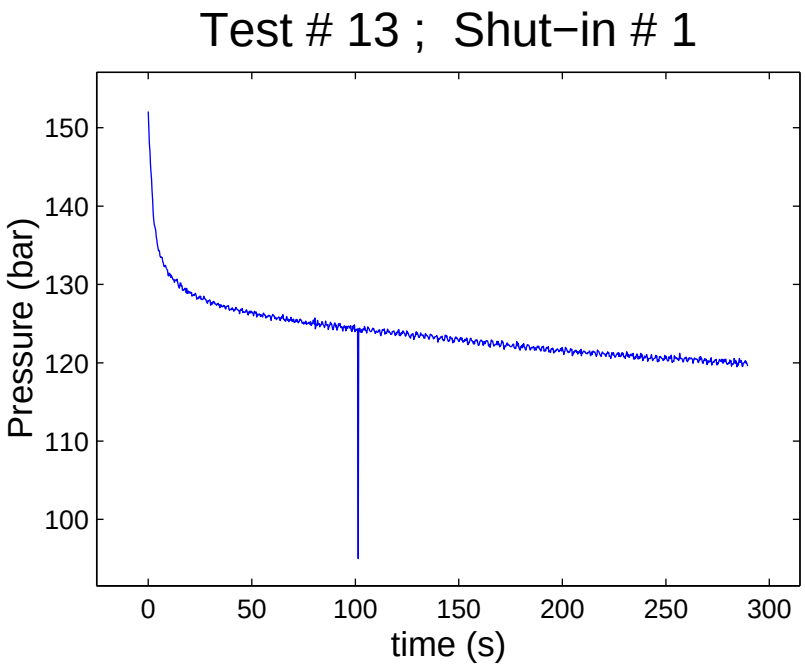
Test # 13 ; Shut−in # 1
Pressure (bar)
150
140
130
120
110
100
0
50
100
150
200
250
300
time (s)

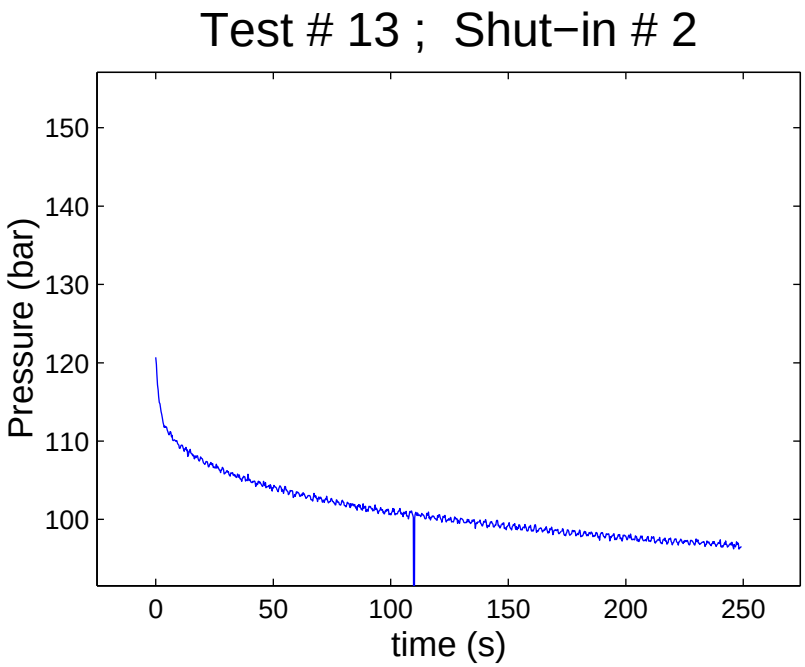
Test # 13 ; Shut−in # 2
Pressure (bar)
150
140
130
120
110
100
0
50
100
150
200
250
time (s)

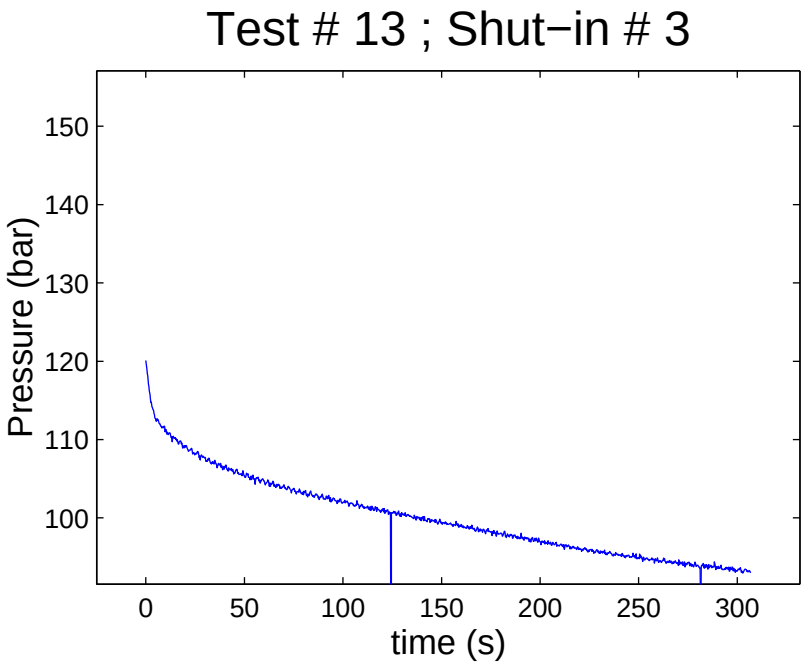
Test # 13 ; Shut−in # 3
Pressure (bar)
150
140
130
120
110
100
0
50
100
150
200
250
300
time (s)

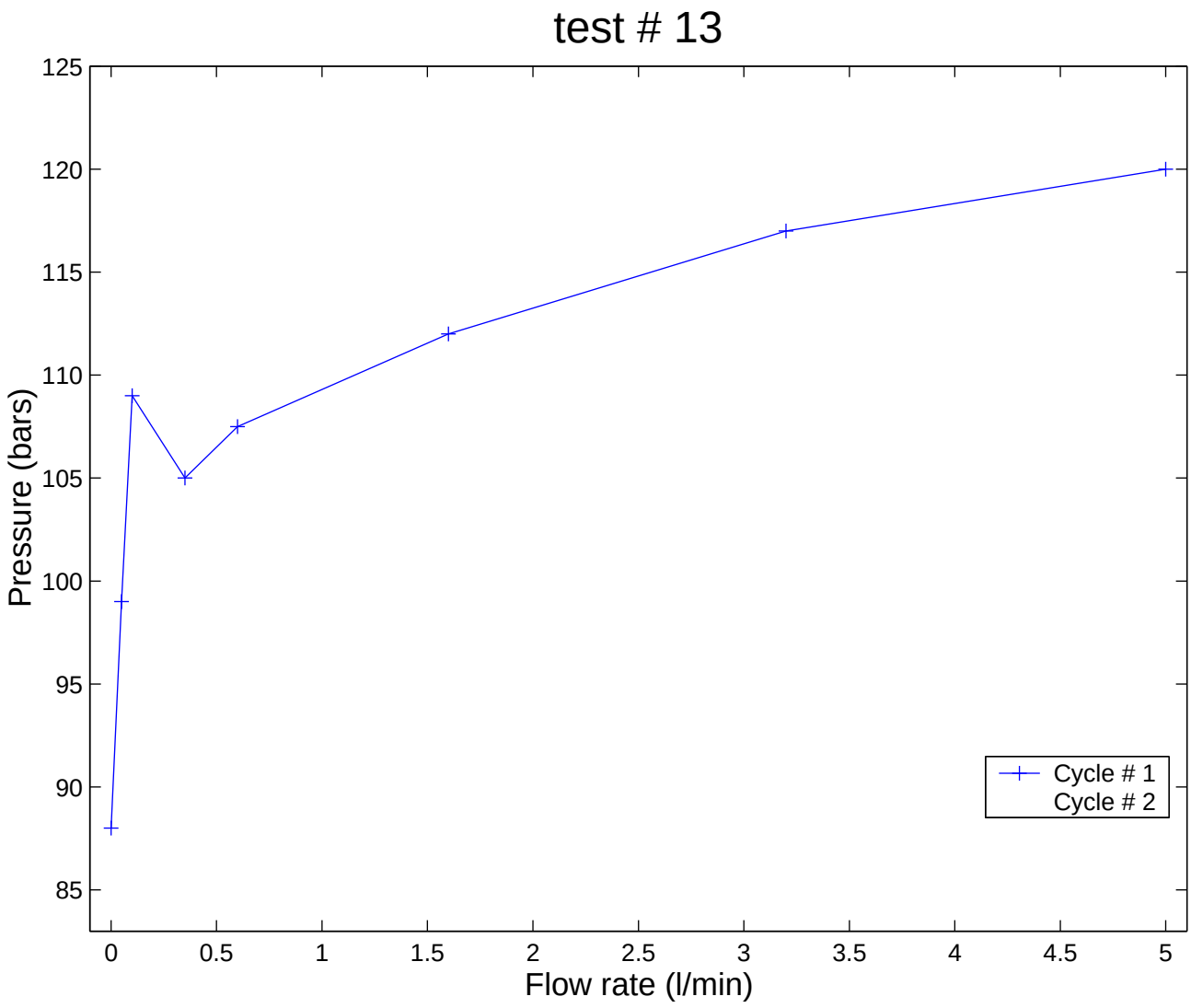
test # 13
Pressure (bars)
125
120
115
110
105
100
95
90
85
0
0.5
1
1.5
2
2.5
3
3.5
4
4.5
5
Flow rate (l/min)
Cycle # 1
Cycle # 2

KLX12A -- Post-frac Log # 13

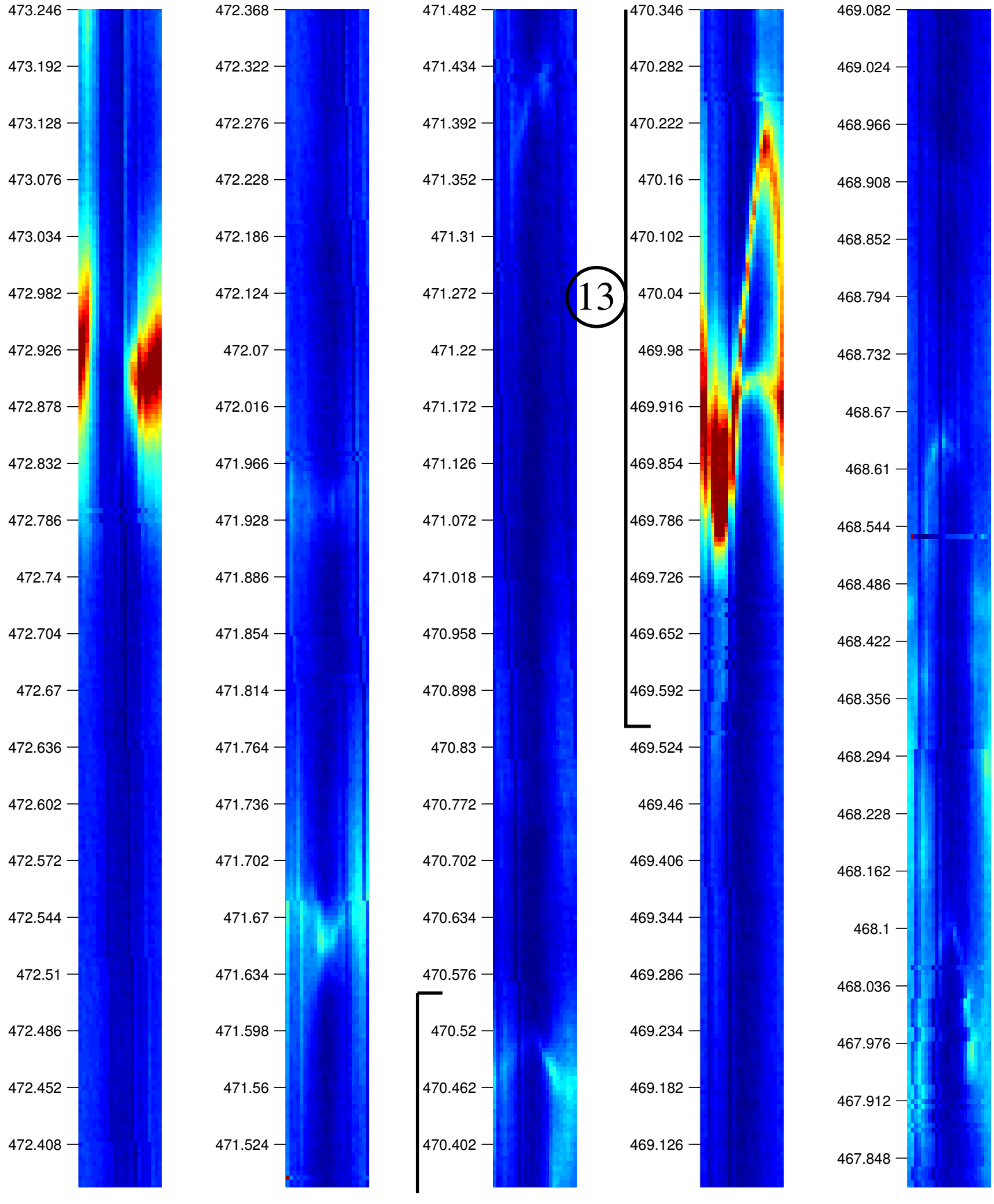

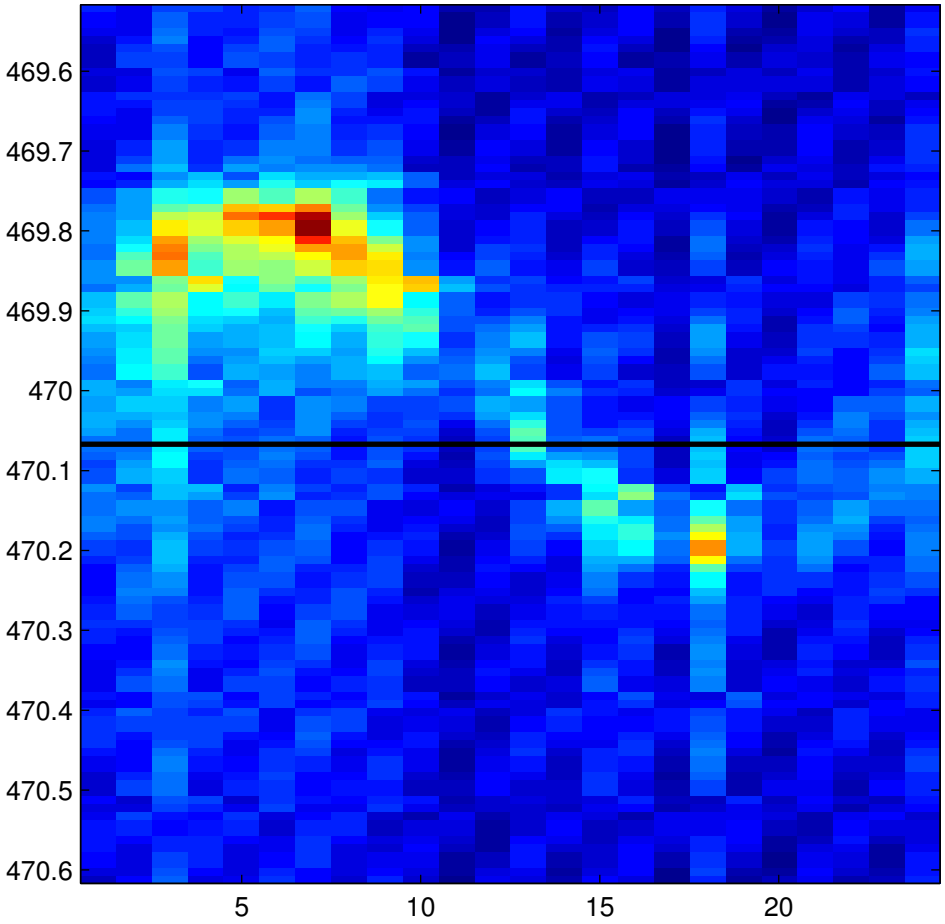

Repère du forage

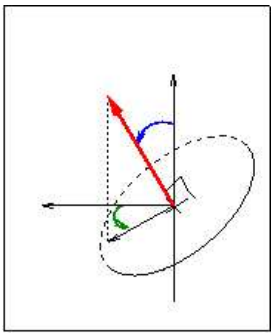

Repère absolu

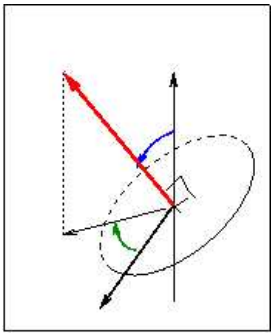

sinusoide visible

Diamètre 7.6 cm

Incidence ° Azimut °

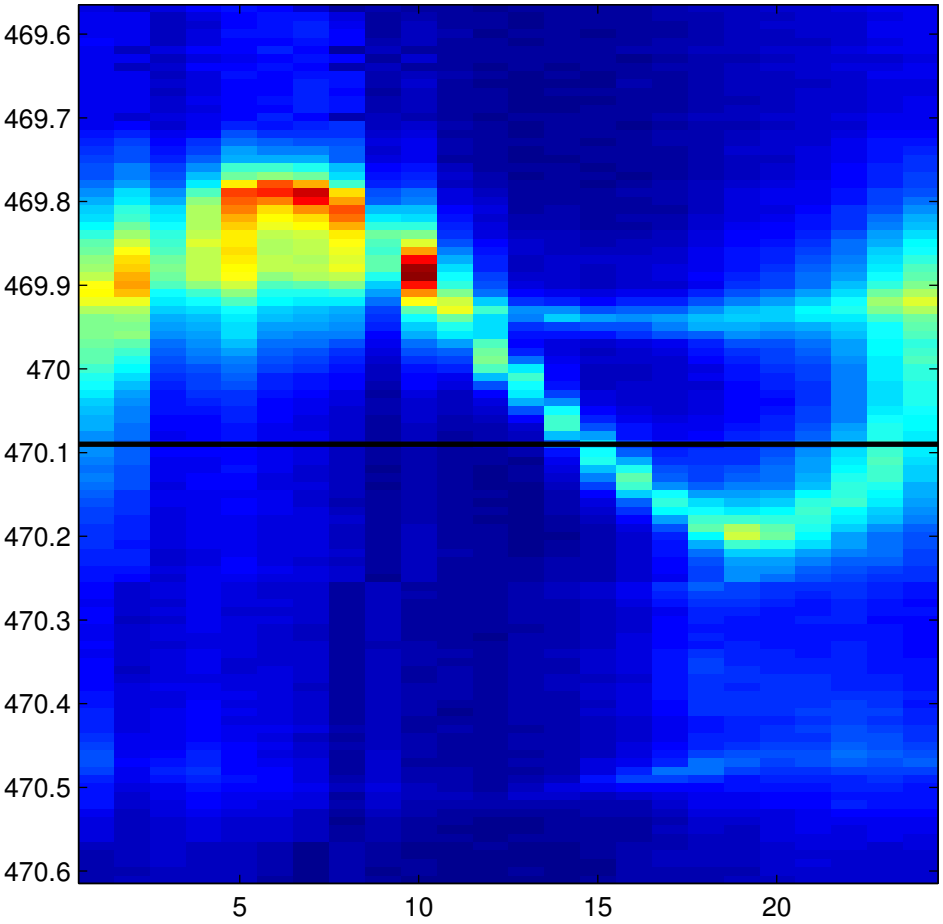

Repère du forage

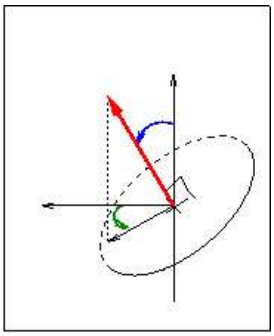

Repère absolu

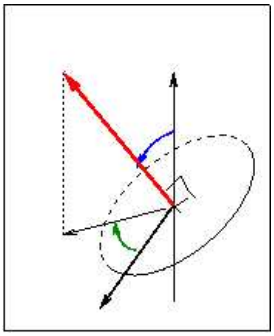

sinusoide visible

Diamètre 7.6 cm

Incidence ° Azimut °

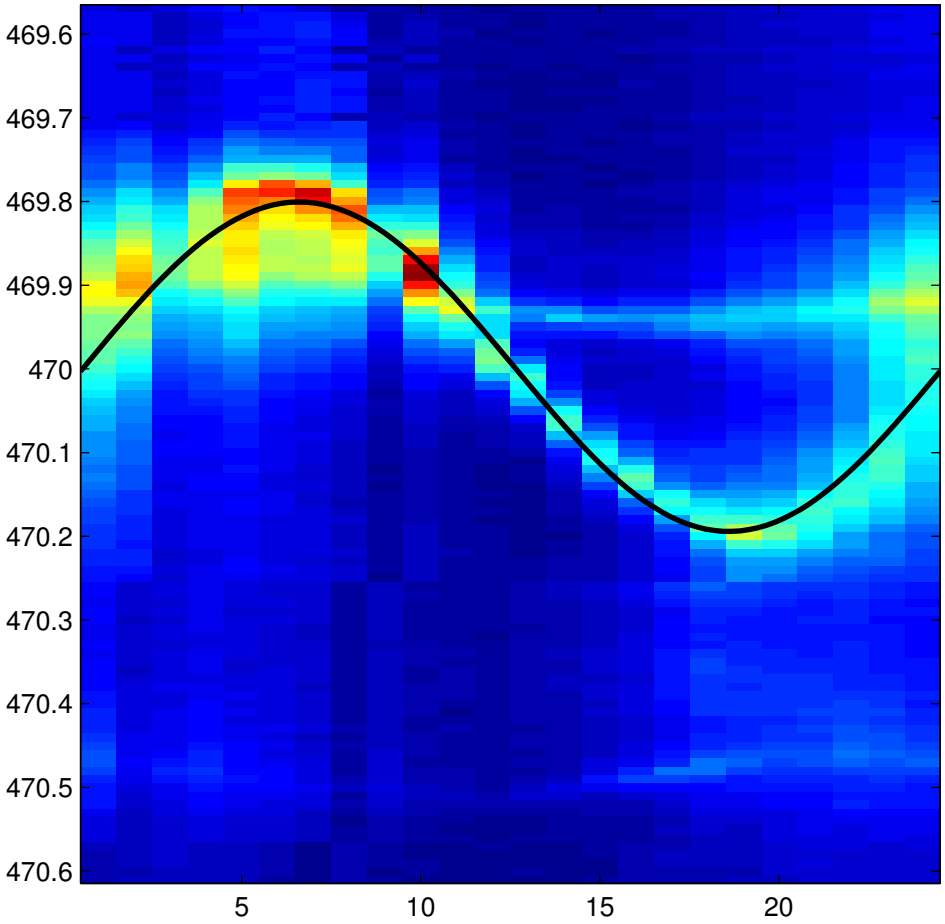

Repère du forage

93.6

79.0714

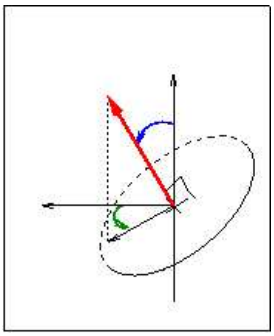

Repère absolu

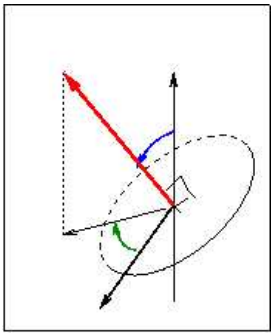

sinusoide visible

Diamètre 7.6 cm

Incidence ° Azimut °

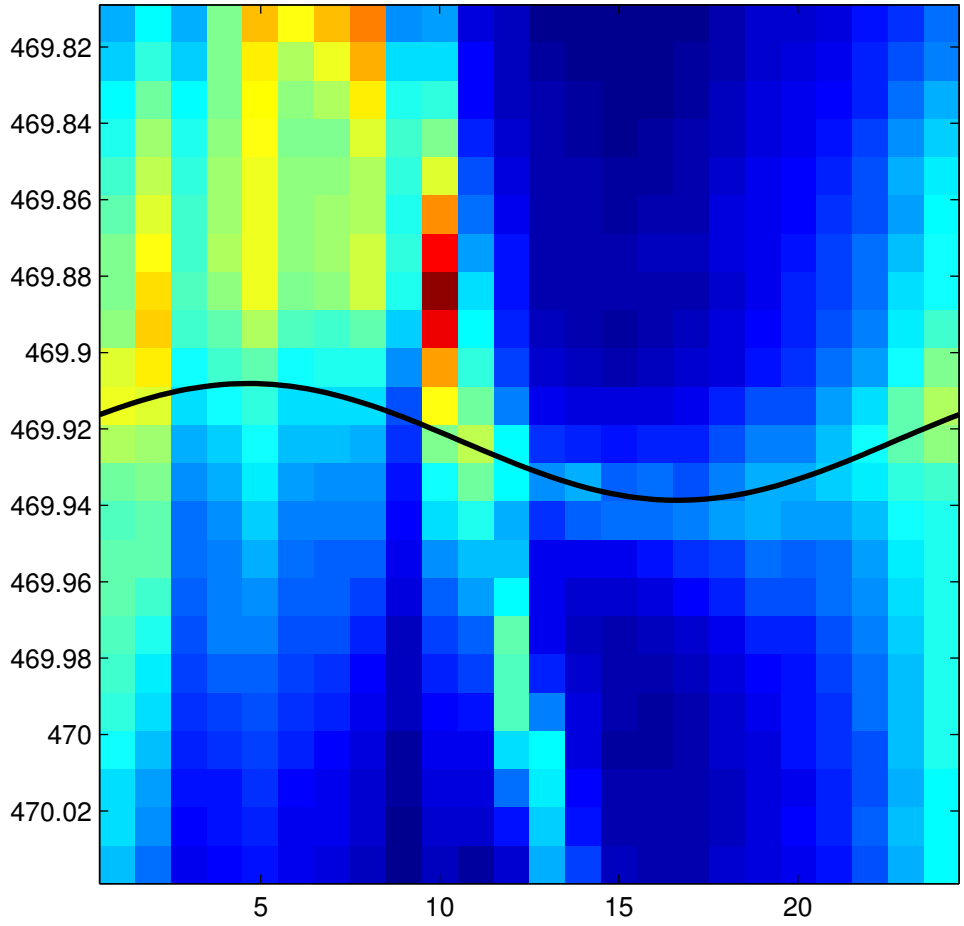

Repère du forage

64.8

21.9108

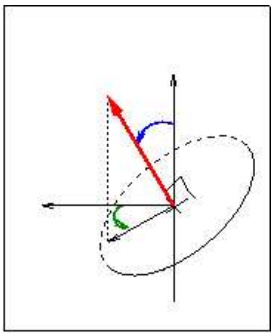

Repère absolu

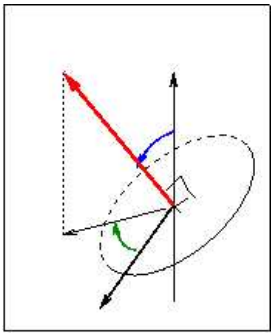

sinusoide visible

Diamètre 7.6 cm

Incidence ° Azimut °

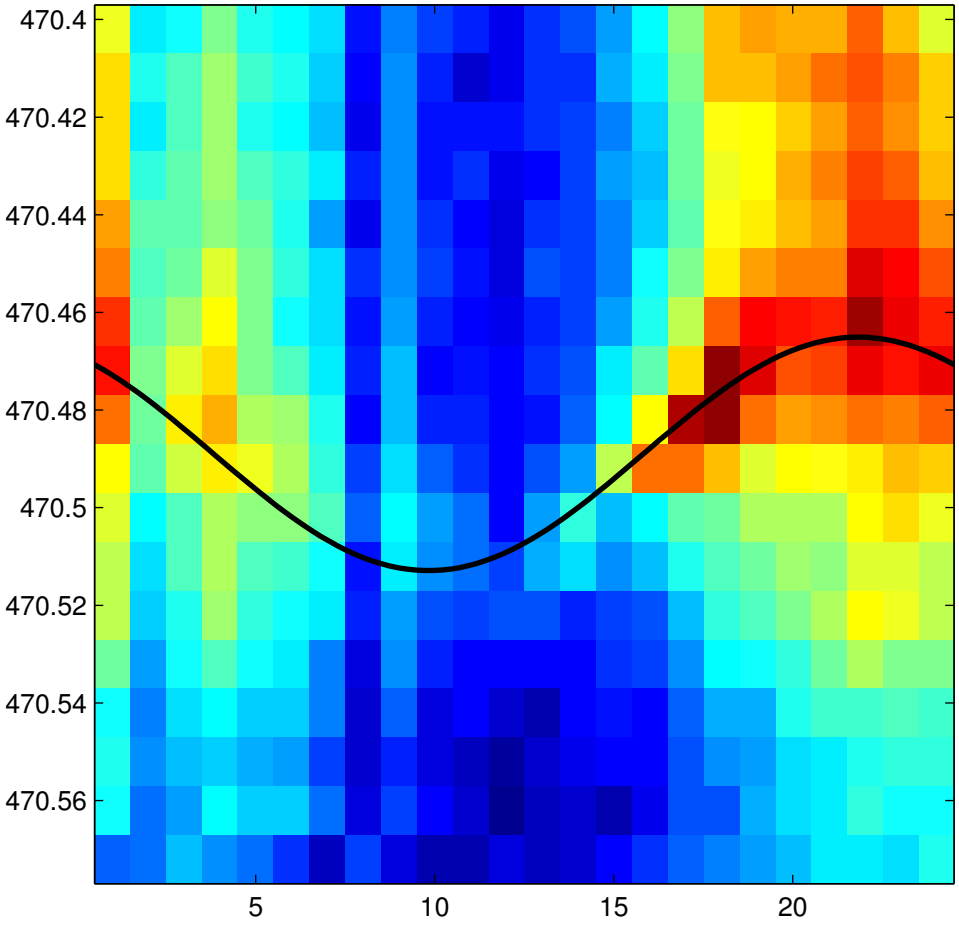

Repère du forage

320.4

32.177

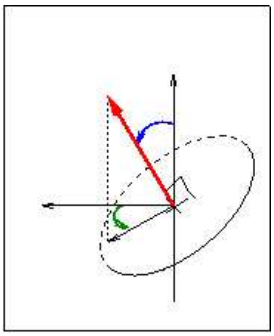

Repère absolu

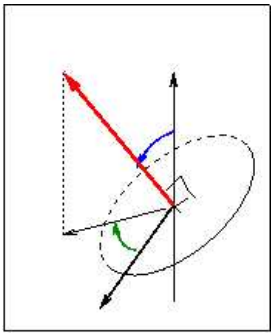

sinusoide visible

Diamètre 7.6 cm

Incidence ° Azimut °

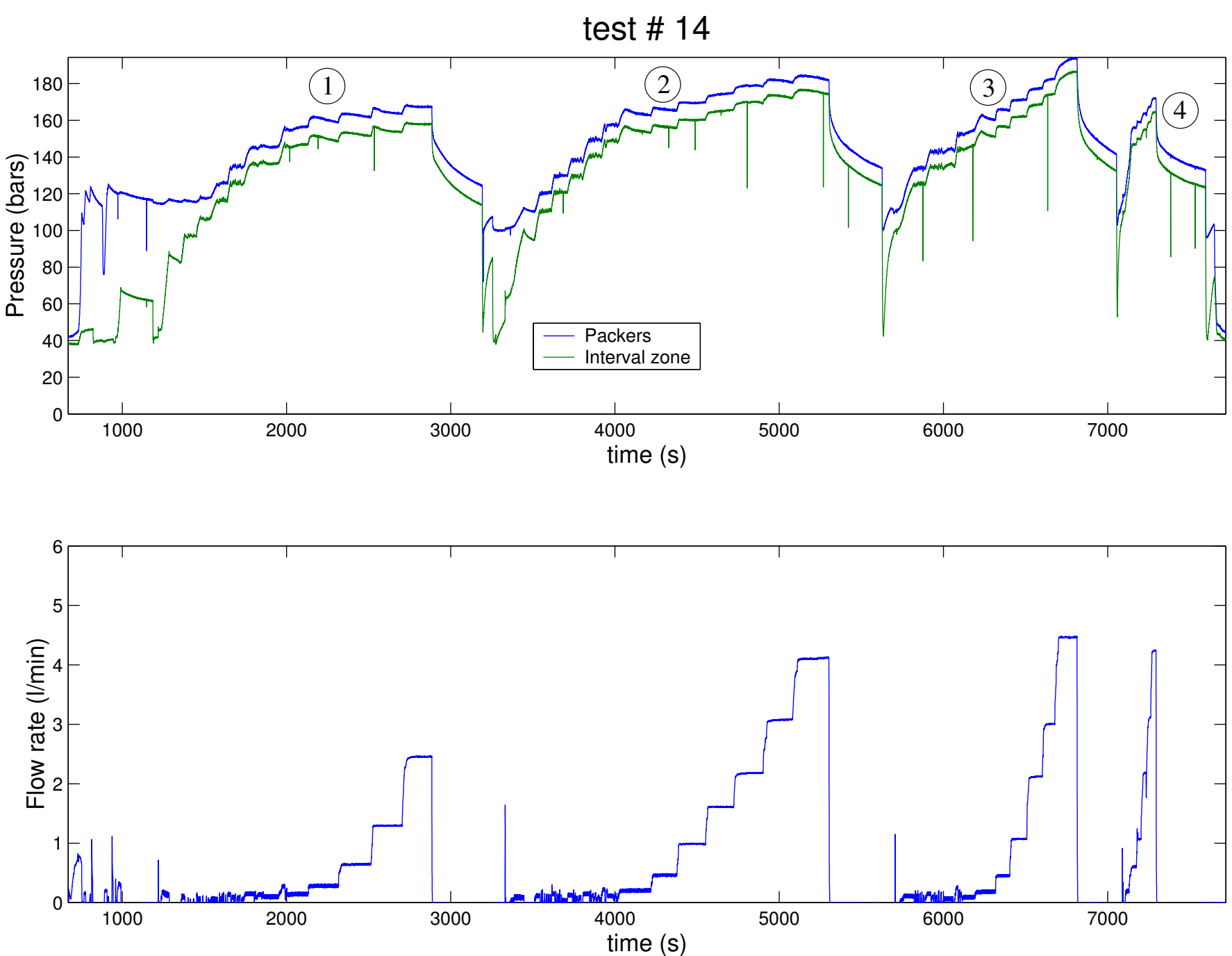
test # 14
Pressure (bars)
time (s)
Packers
Interval zone
1
2
3
4
Flow rate (l/min)
time (s)

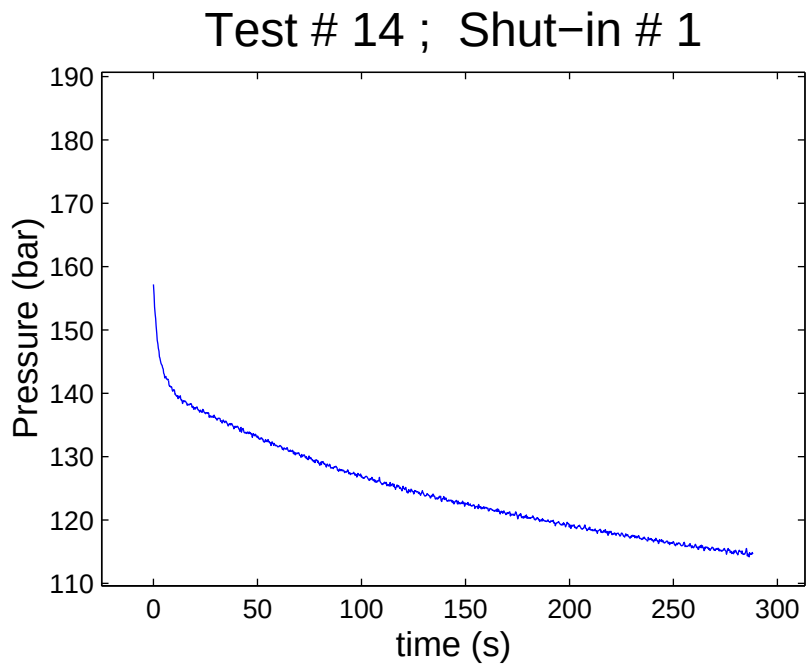
Test # 14 ; Shut−in # 1
Pressure (bar)
time (s)
190
180
170
160
150
140
130
120
110
0
50
100
150
200
250
300

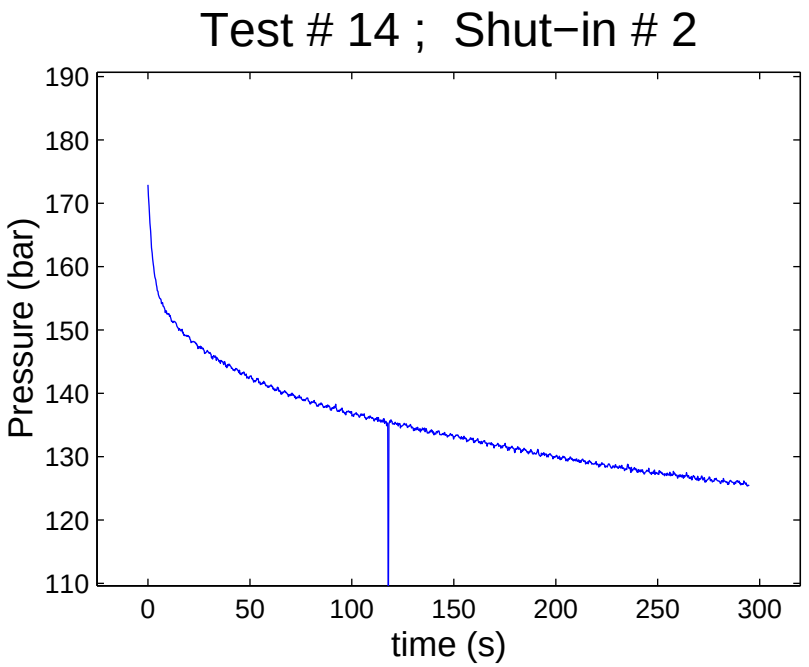
Test # 14 ; Shut−in # 2
Pressure (bar)
time (s)
190
180
170
160
150
140
130
120
110
0
50
100
150
200
250
300

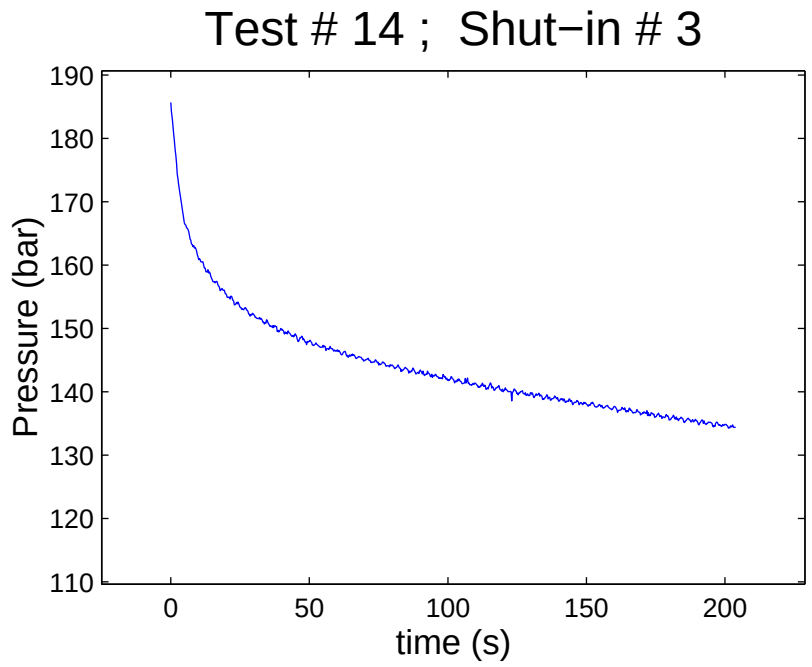
Test # 14 ; Shut−in # 3
Pressure (bar)
time (s)
190
180
170
160
150
140
130
120
110
0
50
100
150
200

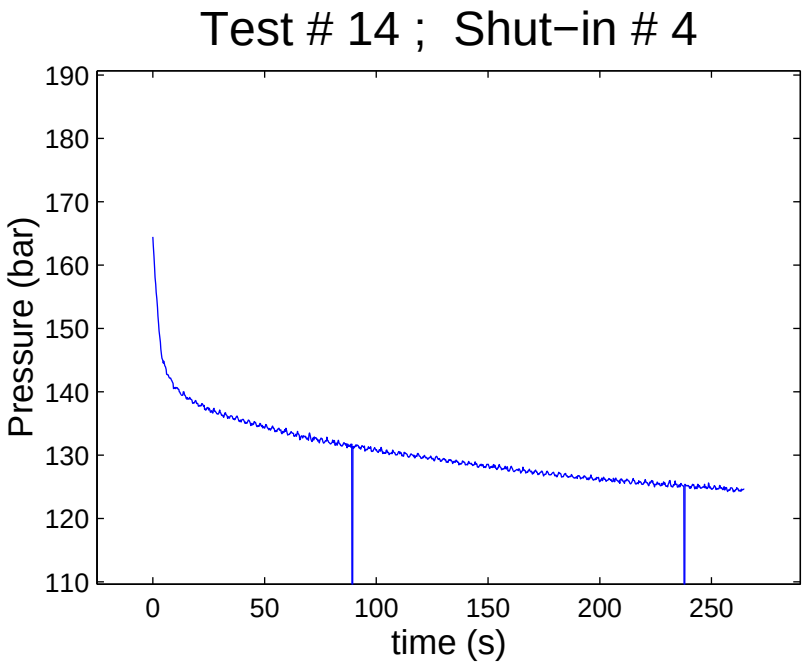
Test # 14 ; Shut−in # 4
Pressure (bar)
time (s)
190
180
170
160
150
140
130
120
110
0
50
100
150
200
250

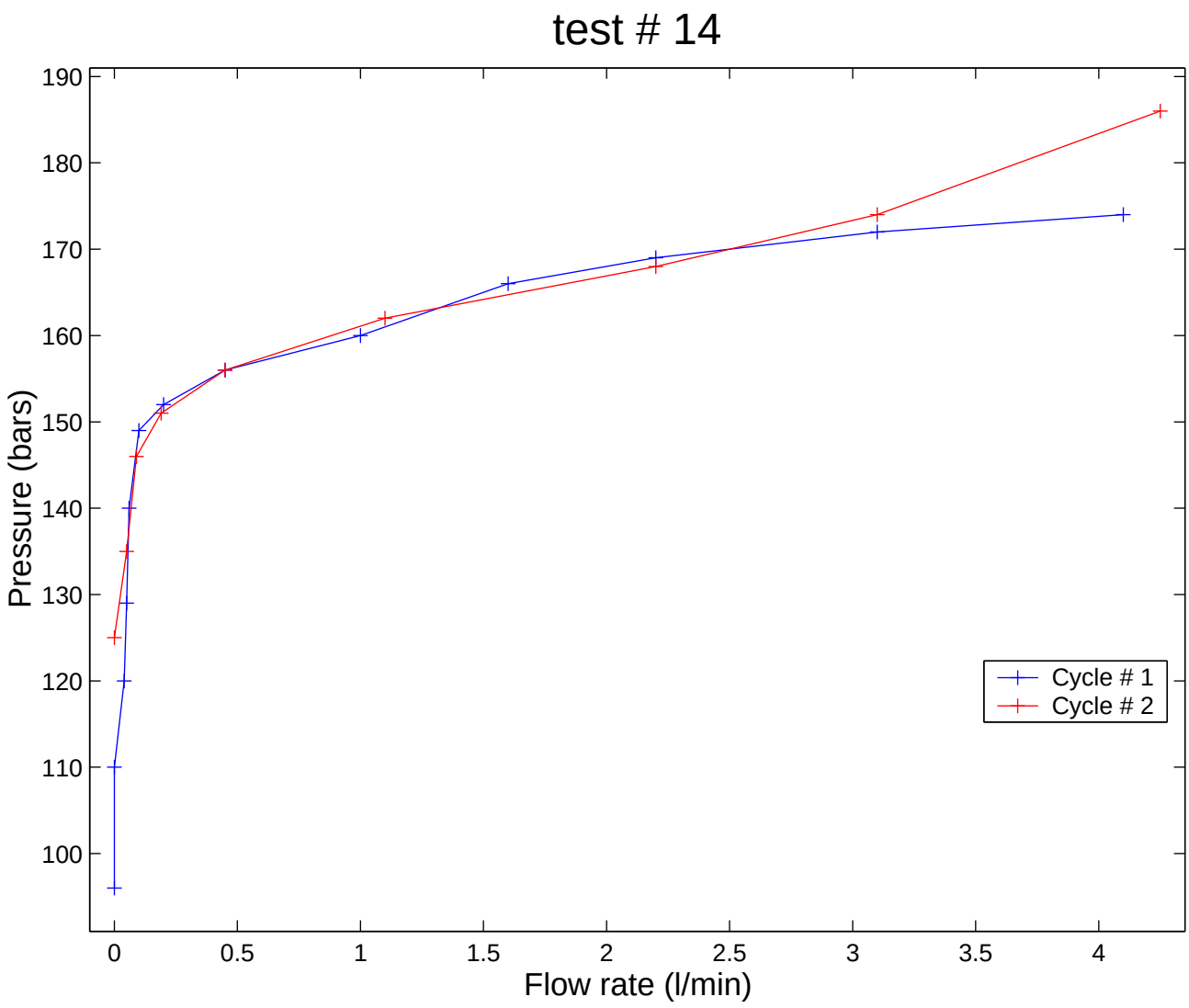
test # 14
Pressure (bars)
190
180
170
160
150
140
130
120
110
100
0
0.5
1
1.5
2
2.5
3
3.5
4
Flow rate (l/min)
Cycle # 1
Cycle # 2

KLX12A -- Post-frac Log # 14

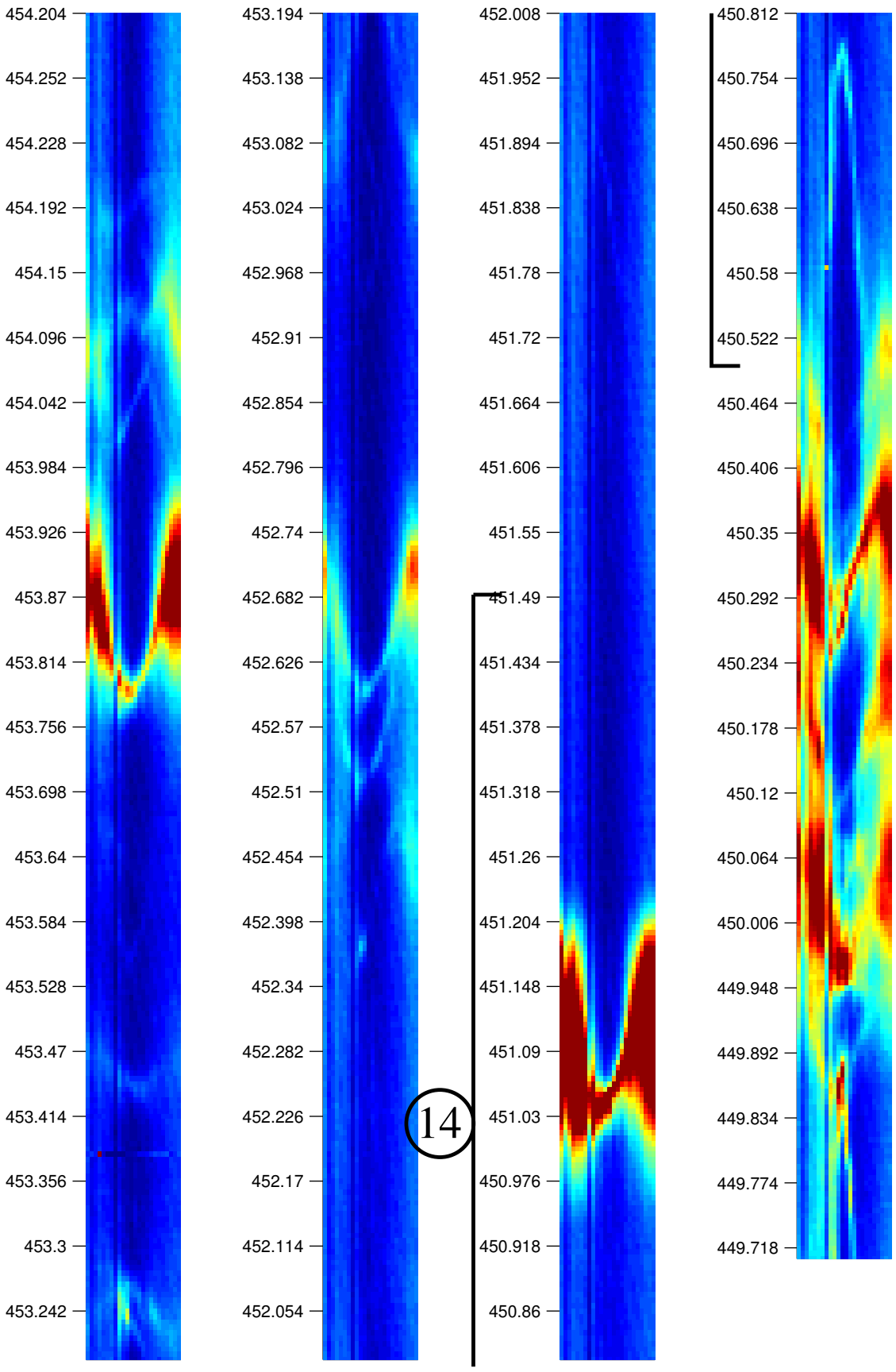

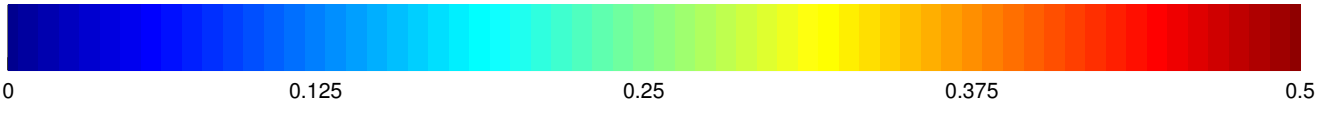

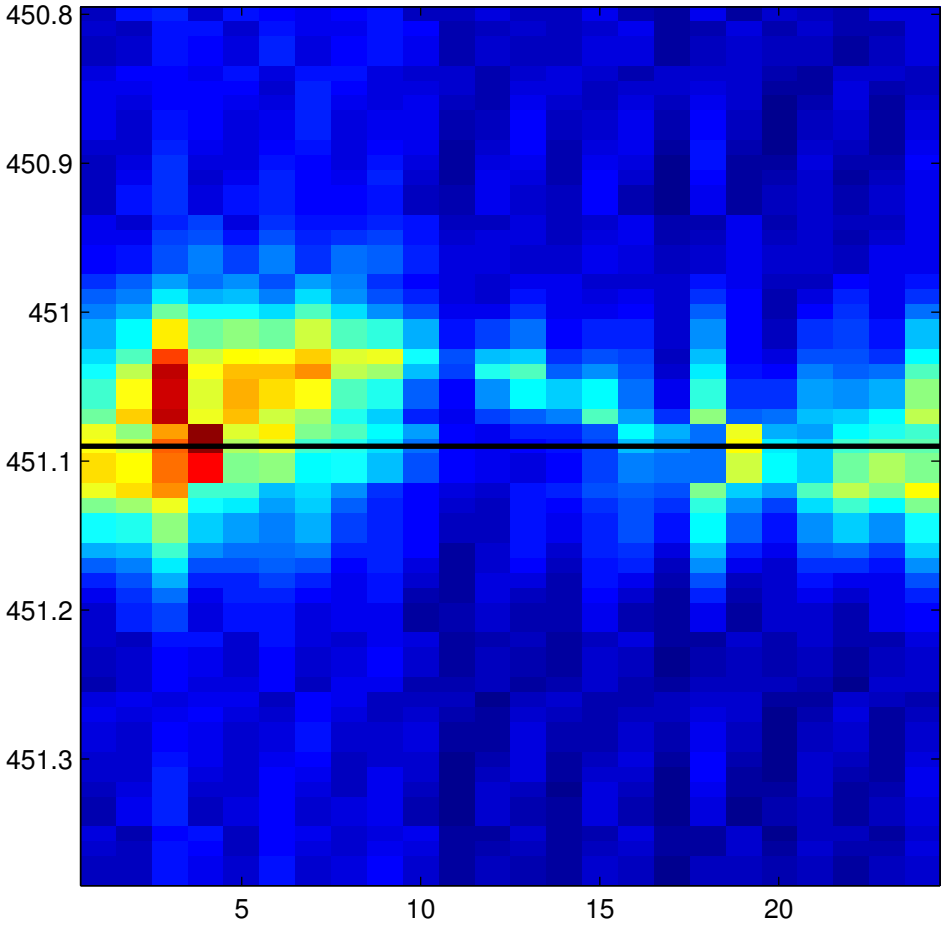

Repère du forage

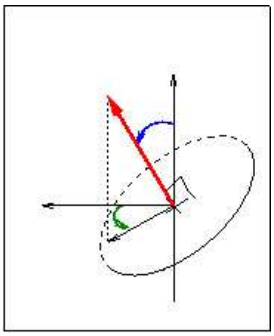

Repère absolu

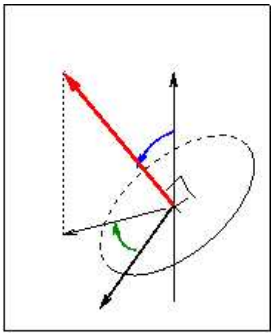

sinusoide visible

Diamètre 7.6 cm

Incidence ° Azimut °

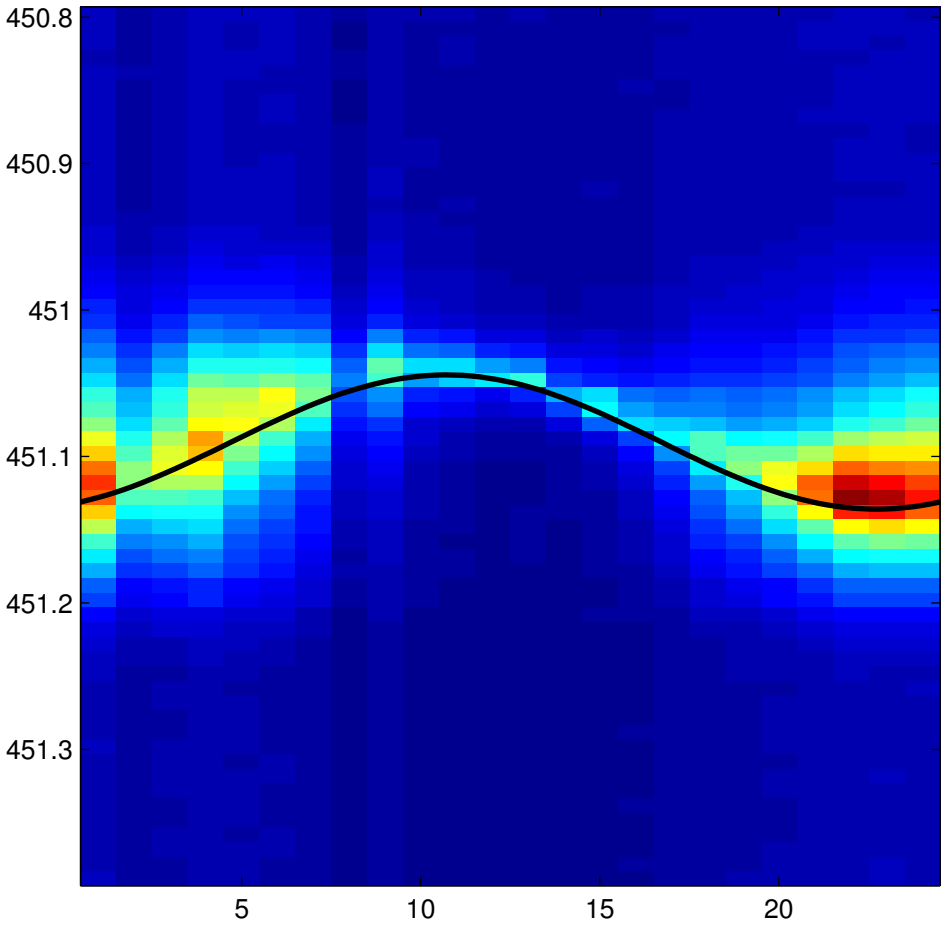

Repère du forage

154.8

50.3276

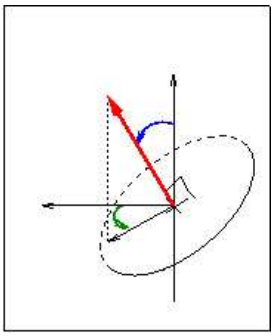

Repère absolu

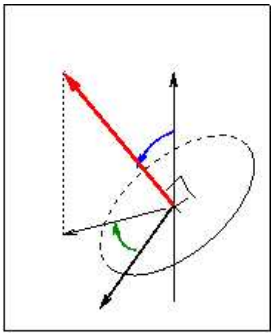

sinusoide visible

Diamètre 7.6 cm

Incidence ° Azimut °

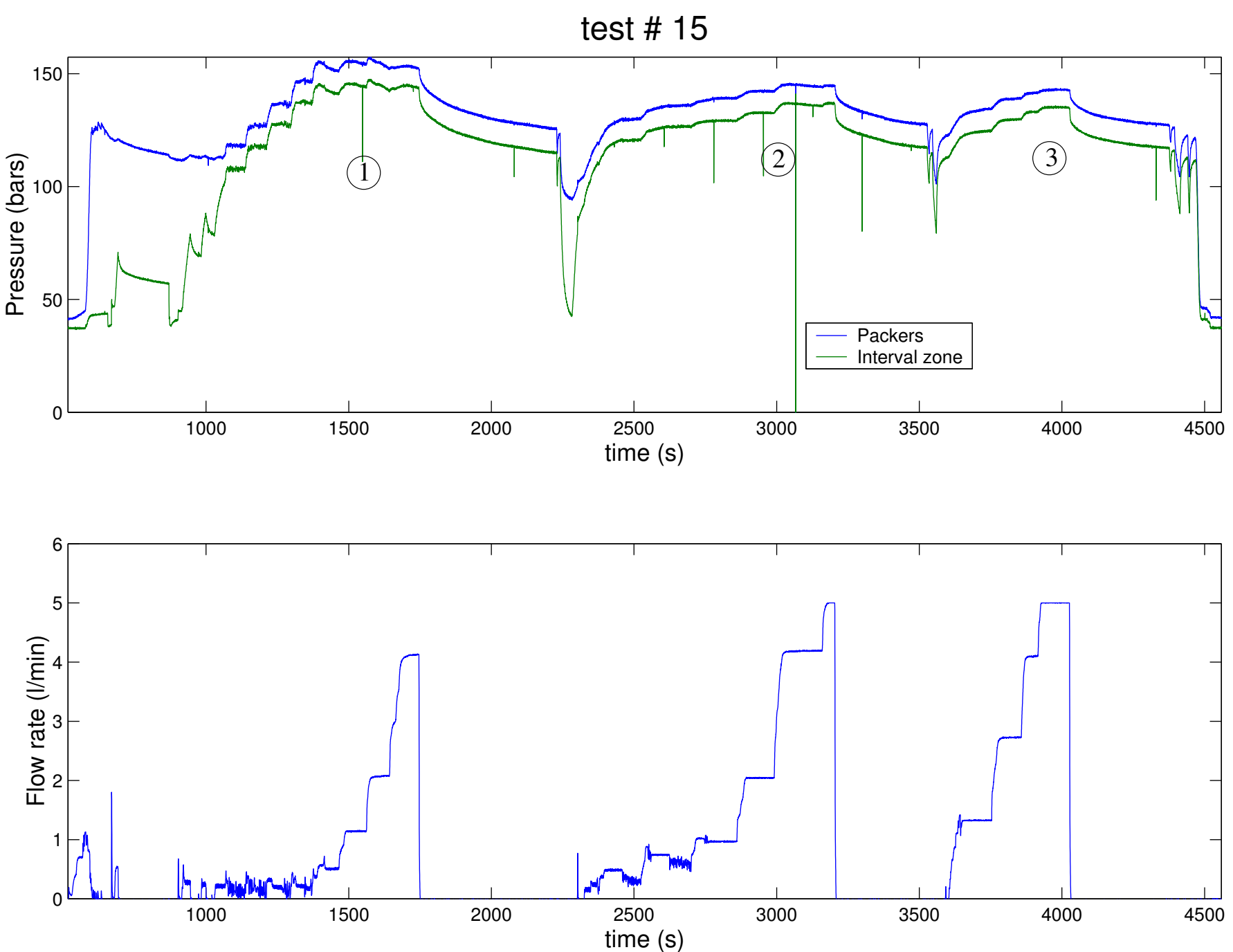
test # 15
Pressure (bars)
150
100
50
0
1
2
3
Packers
Interval zone
1000
1500
2000
2500
3000
3500
4000
4500
time (s)
Flow rate (l/min)
6
5
4
3
2
1
0
1000
1500
2000
2500
3000
3500
4000
4500
time (s)

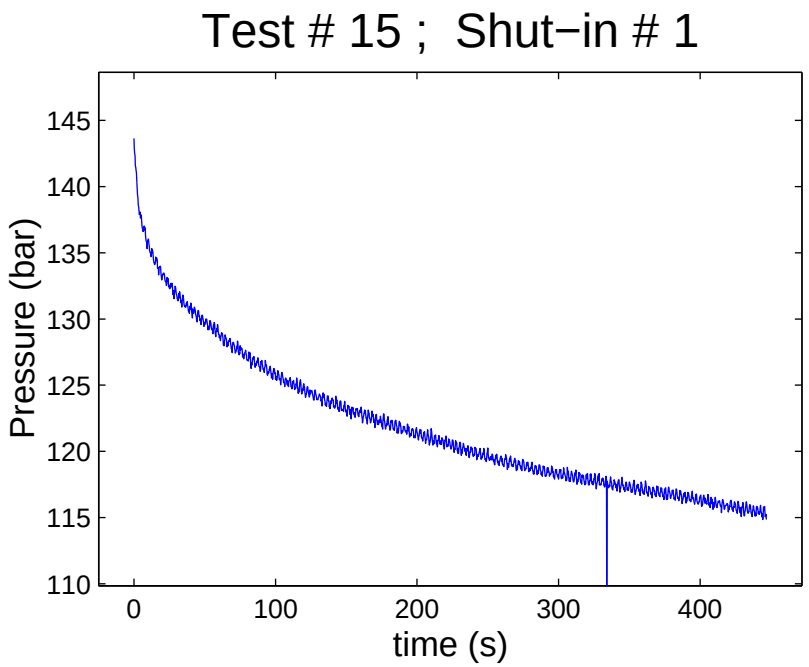
Test # 15 ; Shut−in # 1
Pressure (bar)
time (s)
145
140
135
130
125
120
115
110
0
100
200
300
400

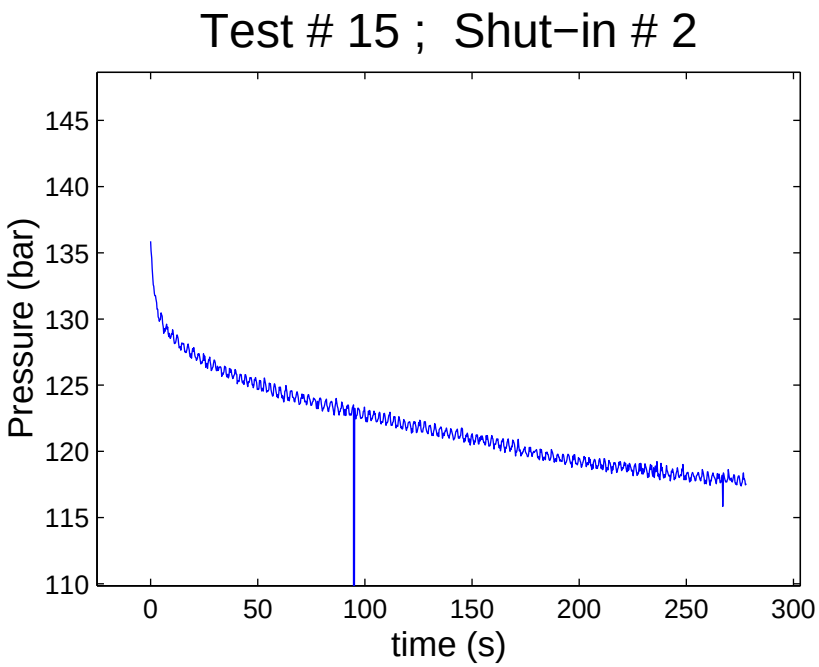
Test # 15 ; Shut−in # 2
Pressure (bar)
time (s)
145
140
135
130
125
120
115
110
0
50
100
150
200
250
300

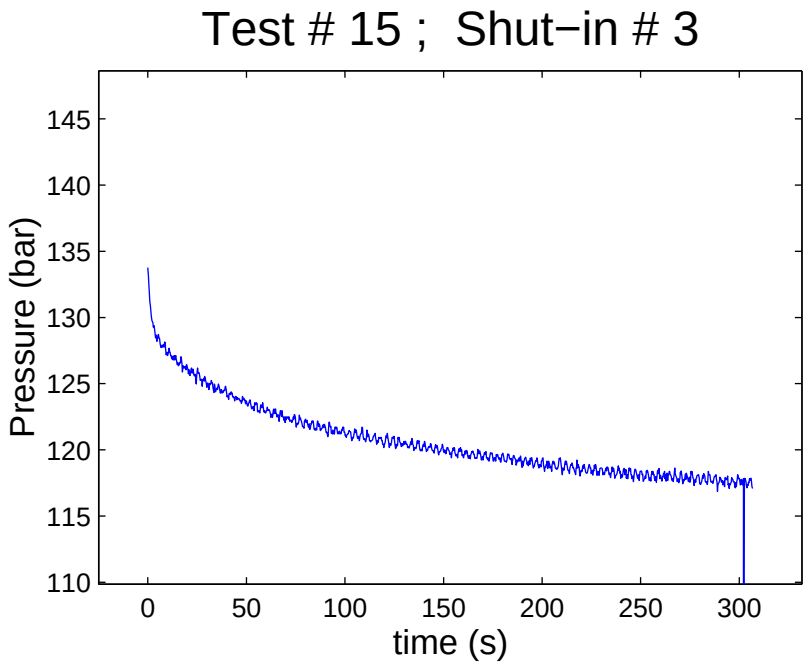
Test # 15 ; Shut−in # 3
Pressure (bar)
time (s)
145
140
135
130
125
120
115
110
0
50
100
150
200
250
300

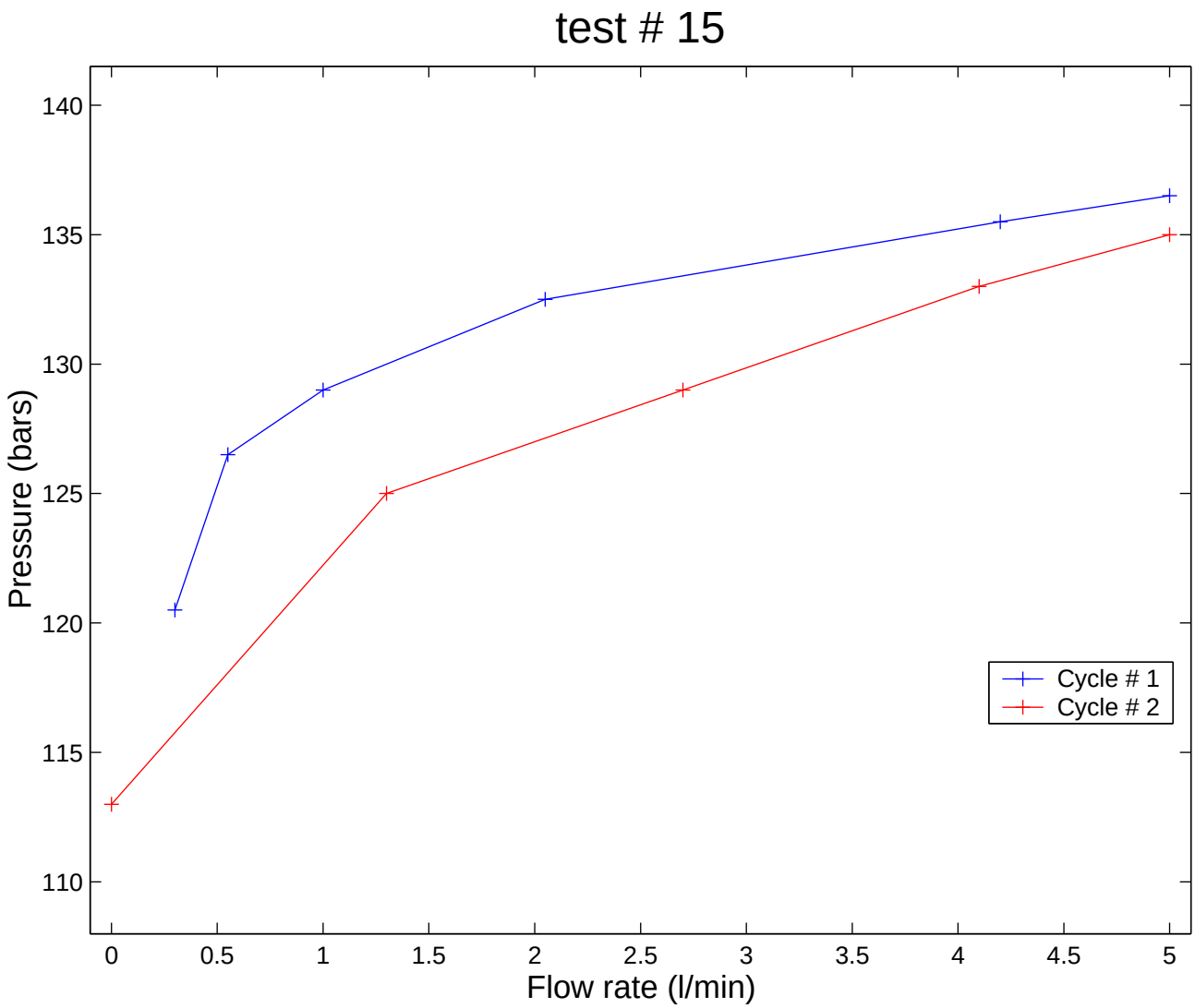
test # 15
Pressure (bars)
140
135
130
125
120
115
110
0
0.5
1
1.5
2
2.5
3
3.5
4
4.5
5
Flow rate (l/min)
Cycle # 1
Cycle # 2

KLX12A -- Post-frac Log # 15

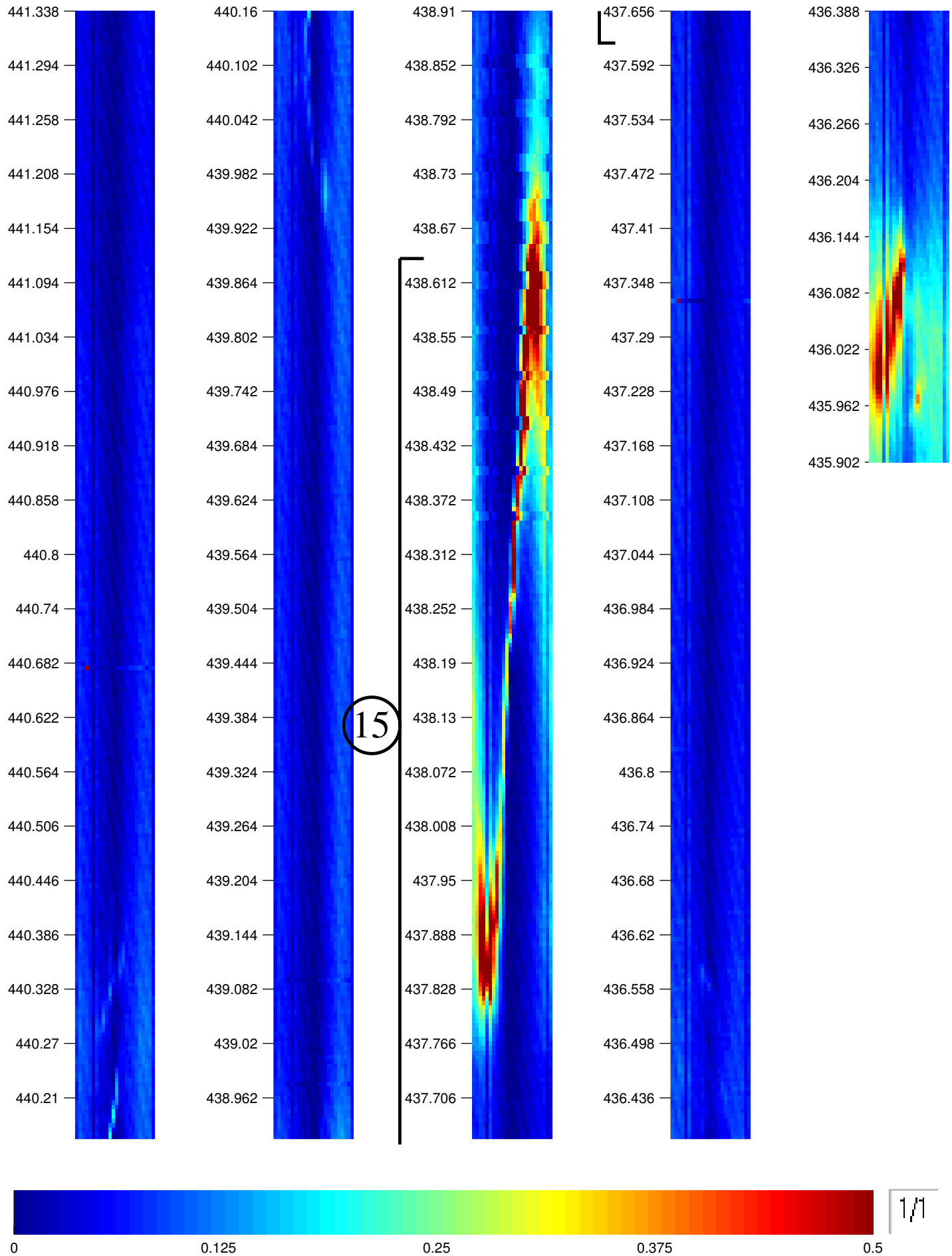

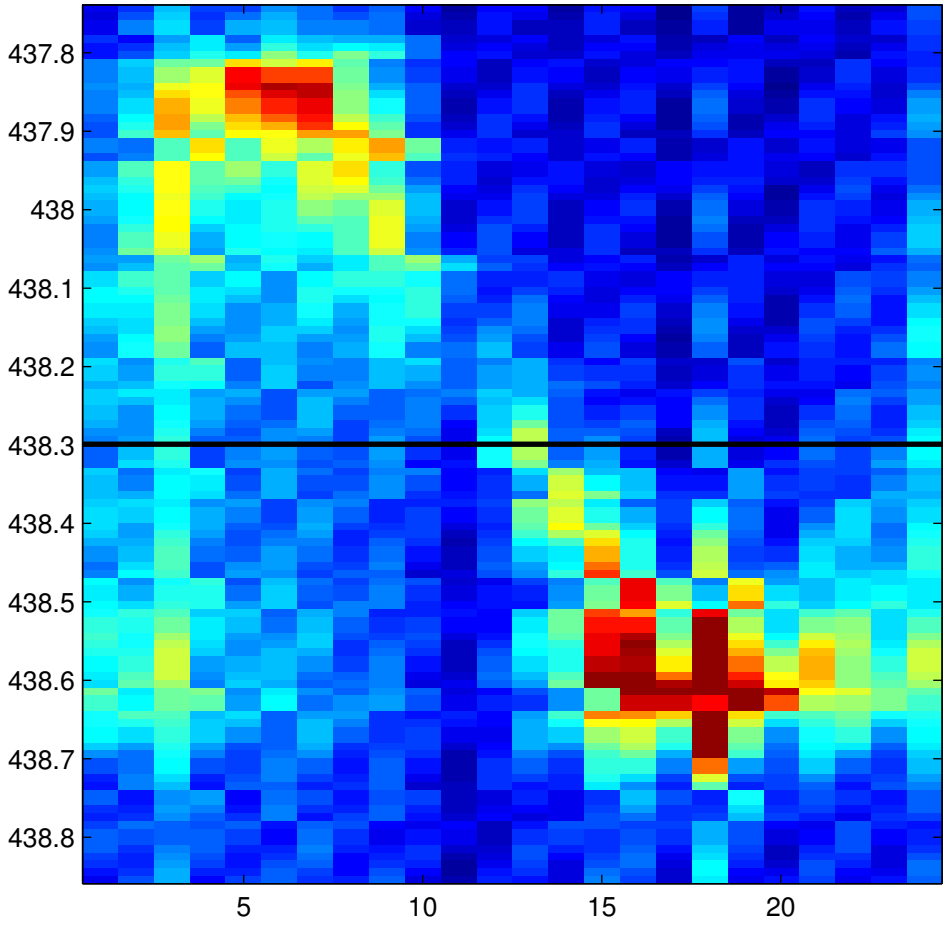

Repère du forage

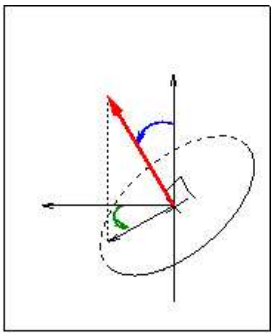

Repère absolu

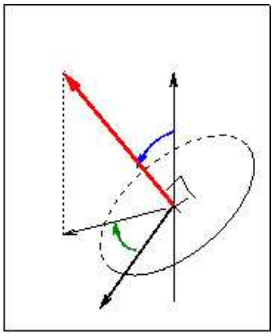

sinusoide visible

Diamètre 7.6 cm

Incidence ° Azimut °

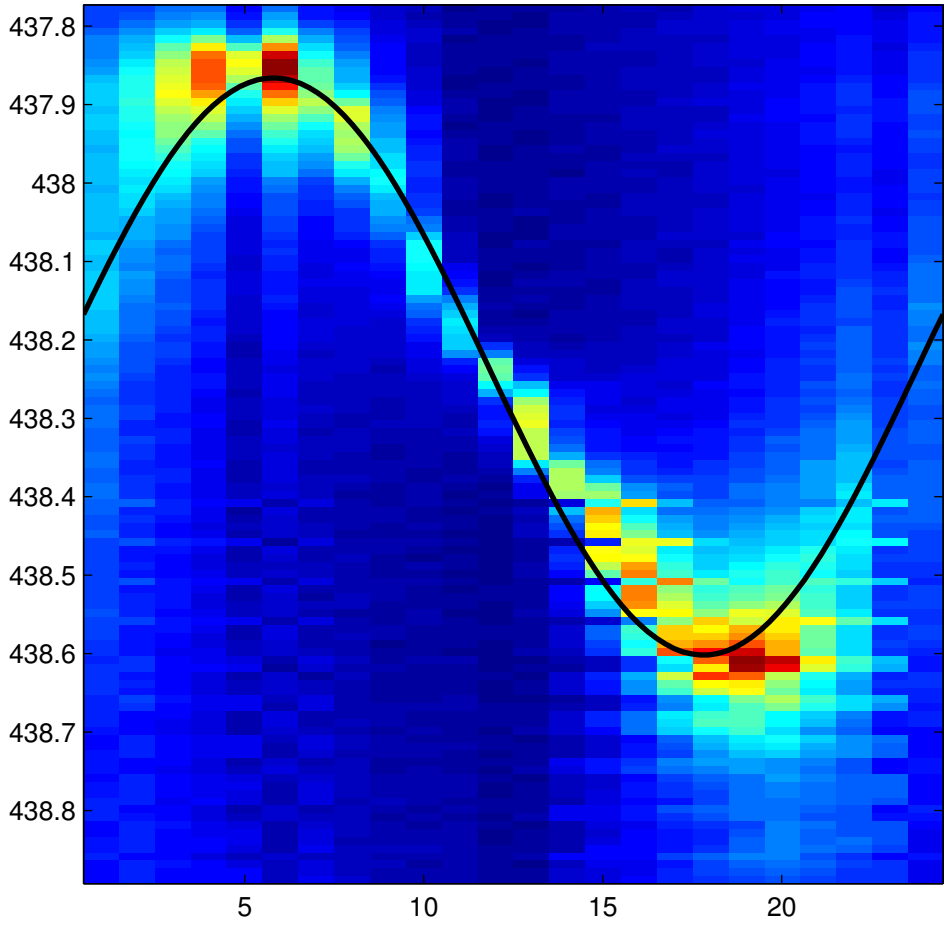

Repère du forage

82.8

84.1011

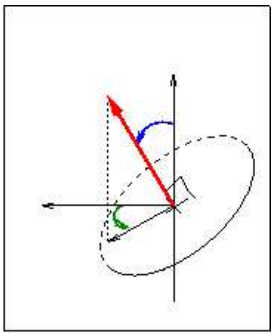

Repère absolu

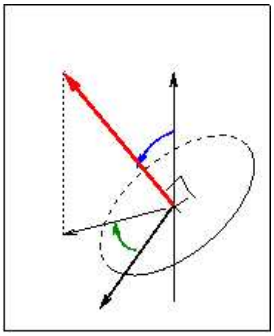

sinusoide visible

Diamètre 7.6 cm

Incidence ° Azimut °

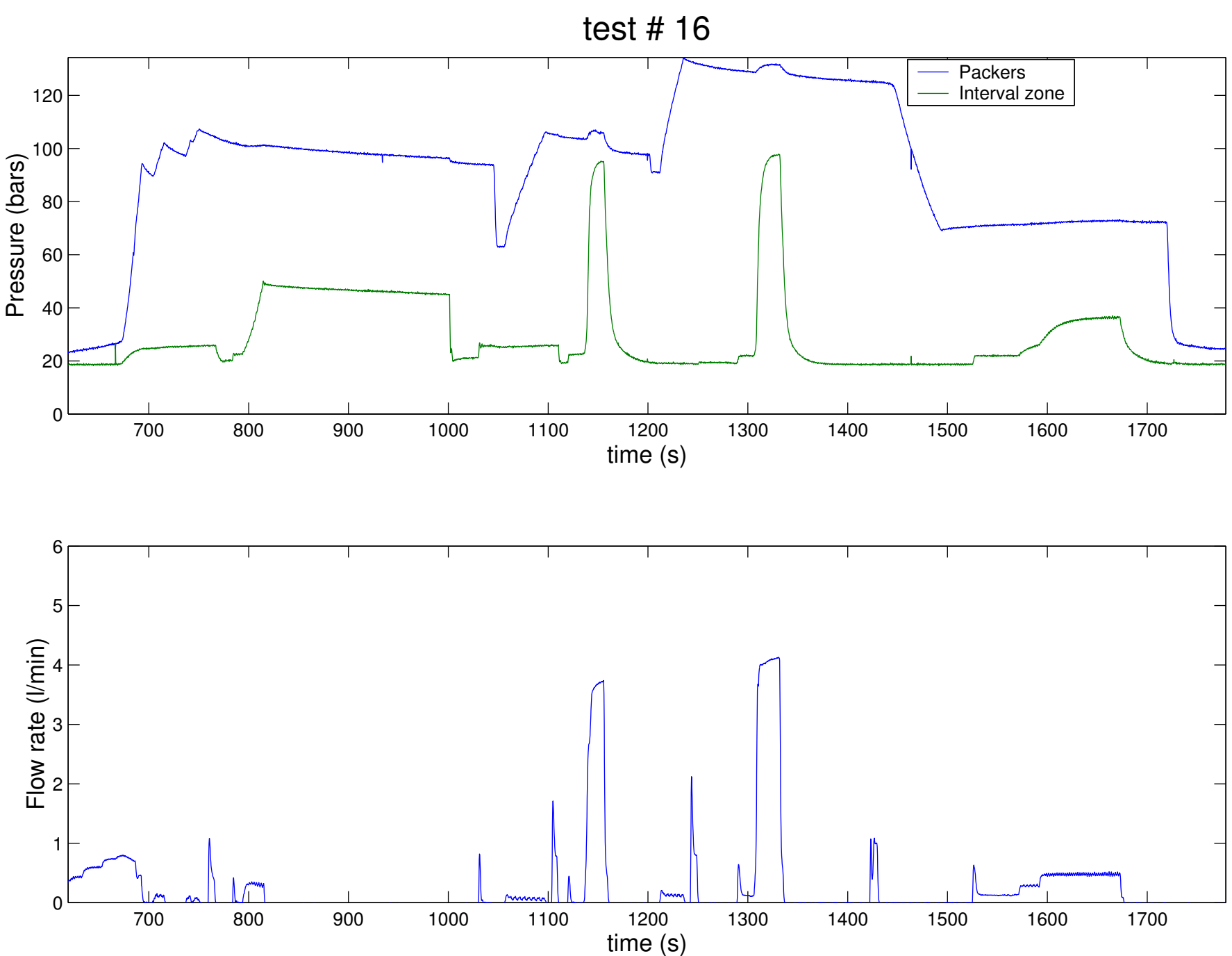
test # 16
Packers
Interval zone
Pressure (bars)
0
20
40
60
80
100
120
700
800
900
1000
1100
1200
1300
1400
1500
1600
1700
time (s)
Flow rate (l/min)
0
1
2
3
4
5
6
700
800
900
1000
1100
1200
1300
1400
1500
1600
1700
time (s)

KLX12A -- Post-frac Log # 16

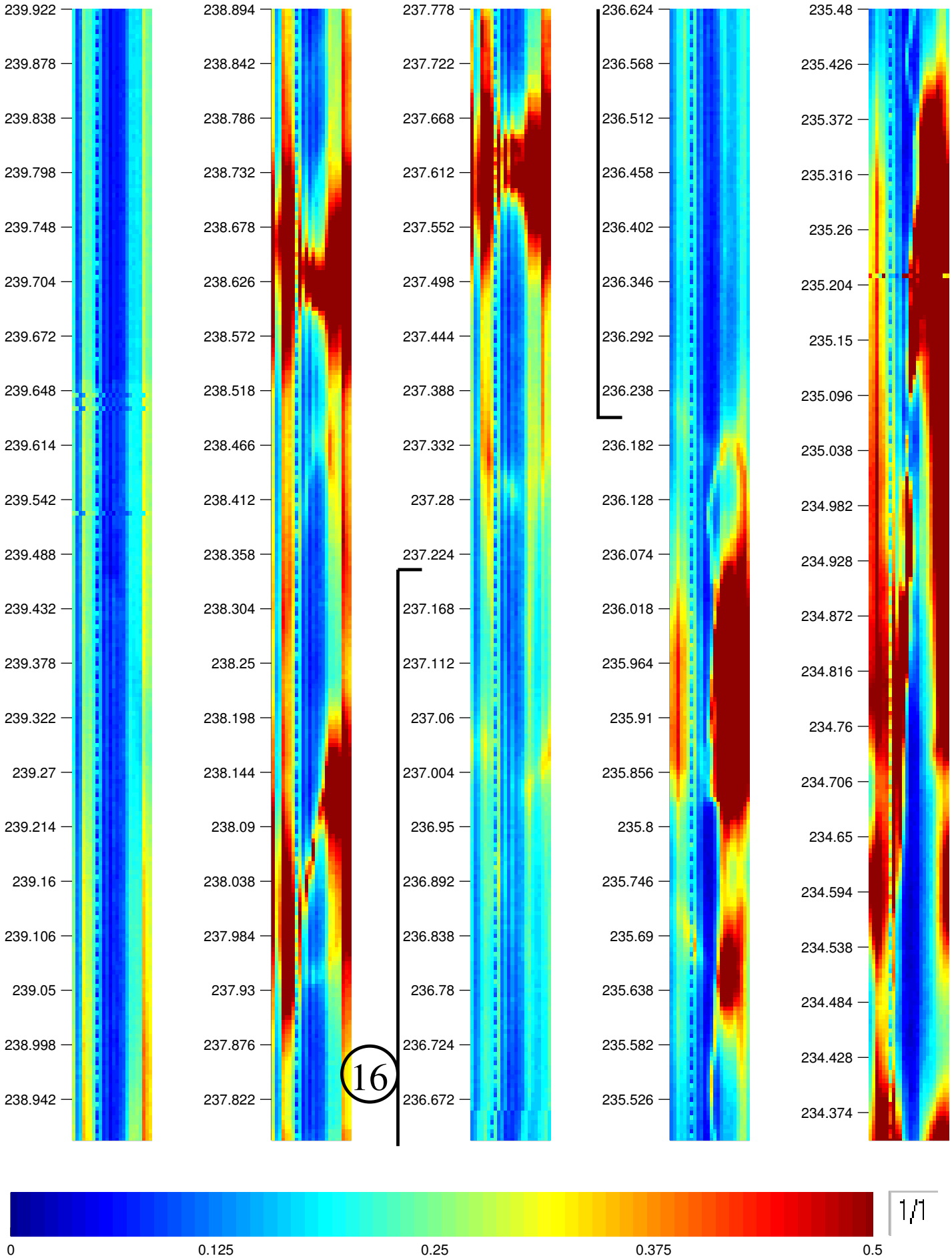

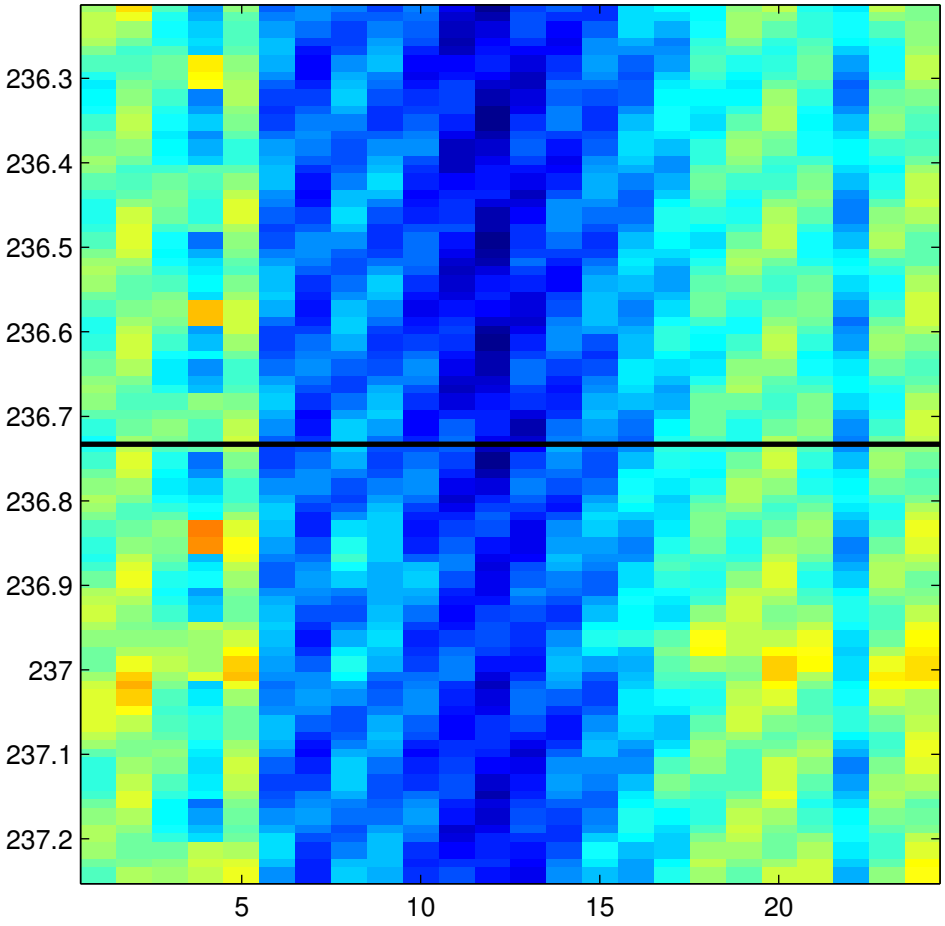

Repère du forage

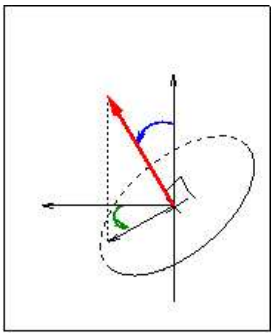

Repère absolu

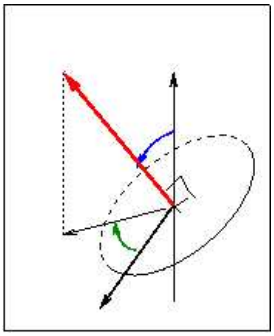

sinusoide visible

Diamètre 7.6 cm

Incidence ° Azimut °

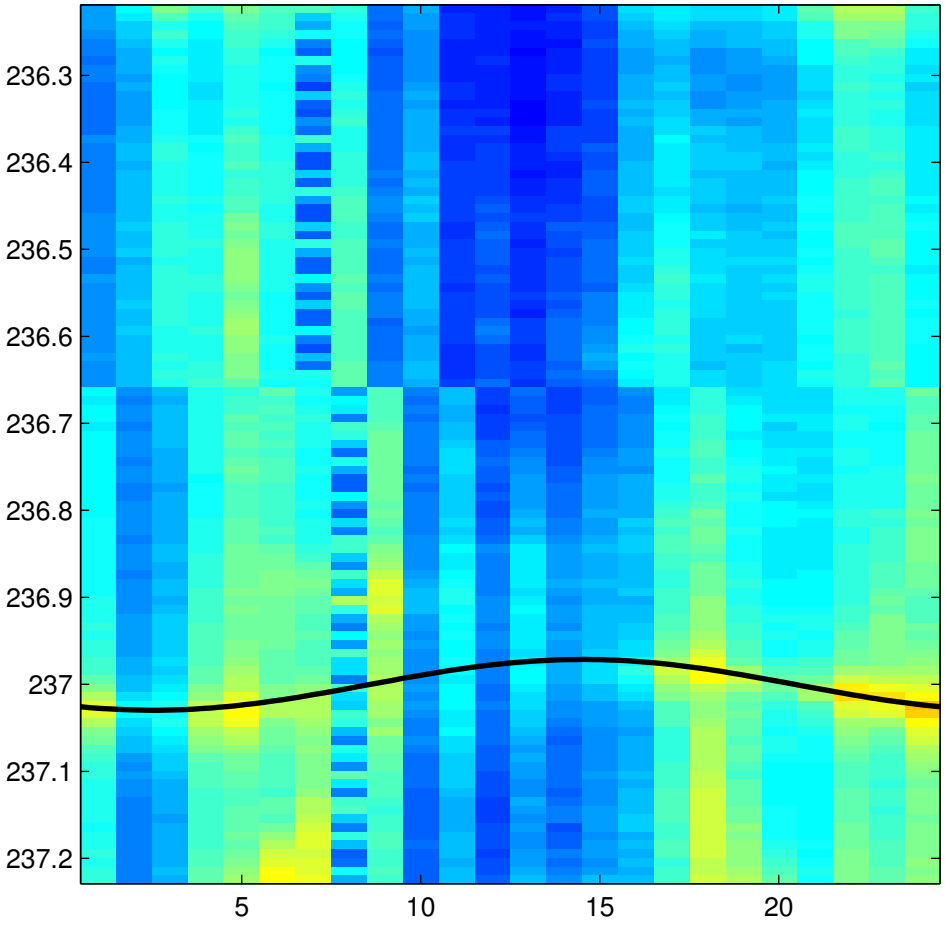

Repère du forage

212.4

37.4987

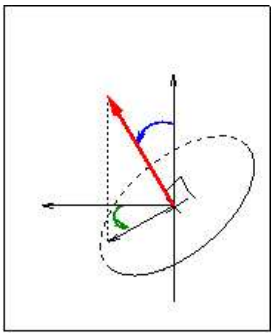

Repère absolu

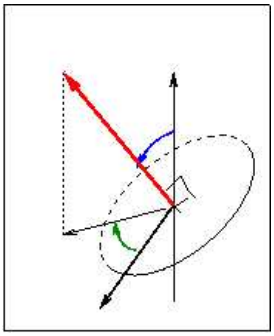

sinusoide visible

Diamètre 7.6 cm

Incidence ° Azimut °

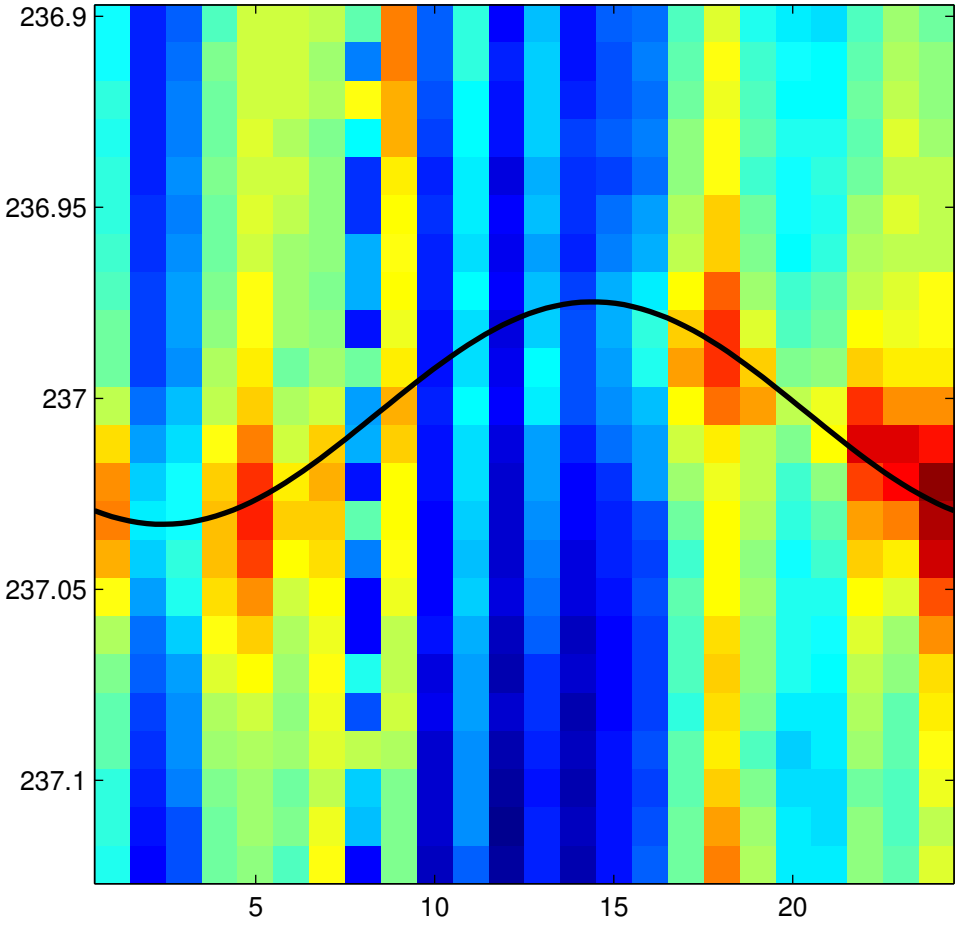

Repère du forage

208.8

37.4584

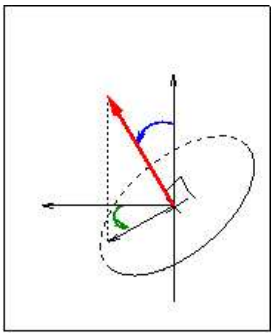

Repère absolu

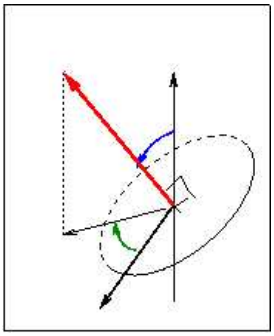

sinusoide visible

Diamètre 7.6 cm

Incidence ° Azimut °

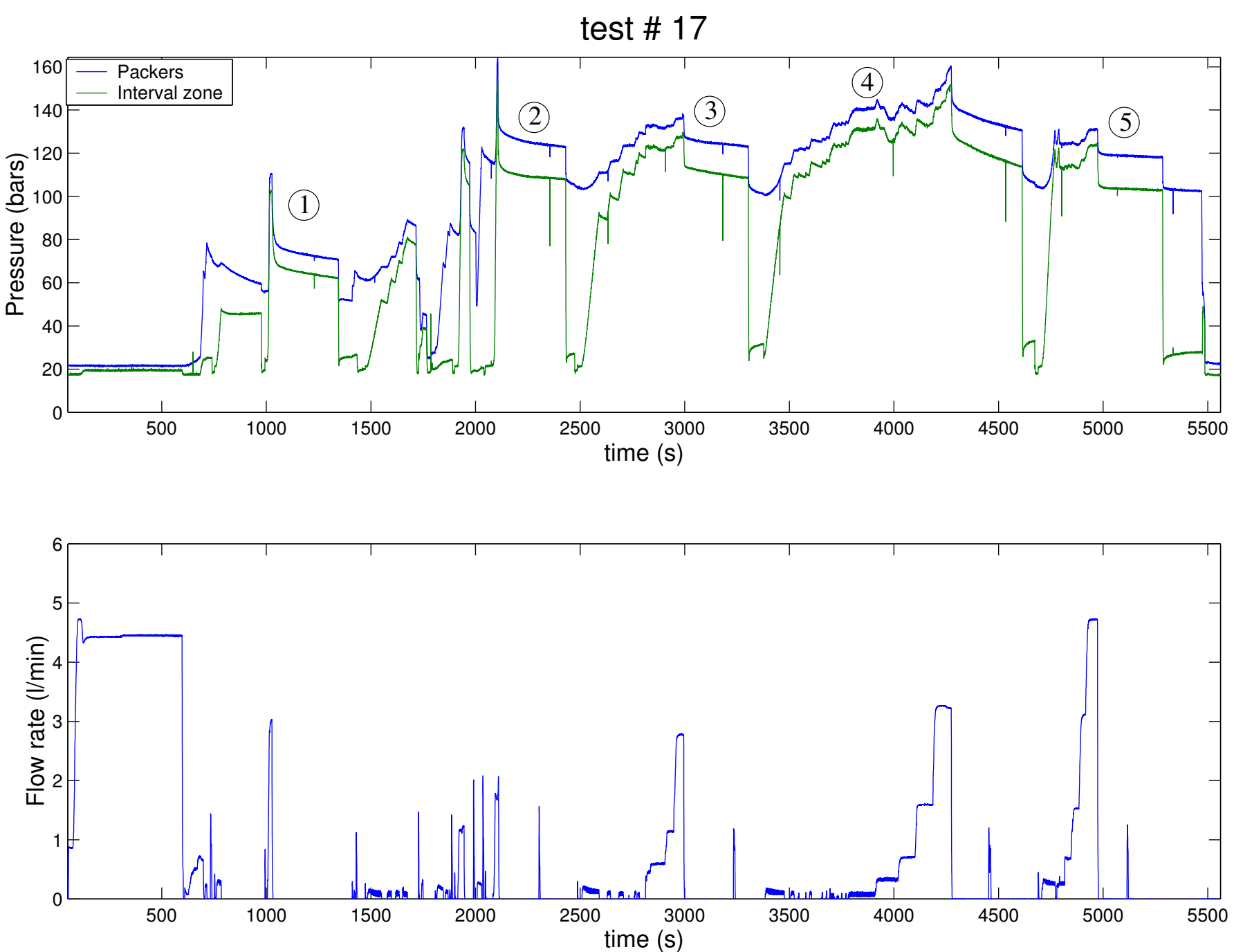
test # 17
Packers
Interval zone
Pressure (bars)
time (s)
1
2
3
4
5
Flow rate (l/min)
time (s)

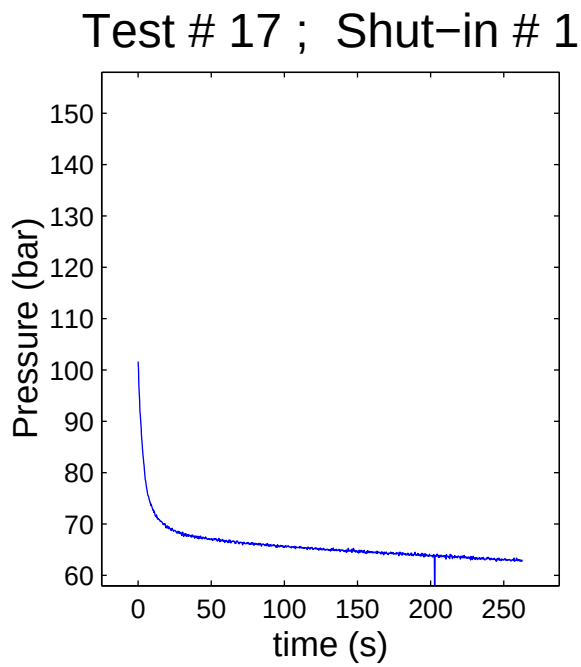
Test # 17 ; Shut−in # 1
Pressure (bar)
time (s)

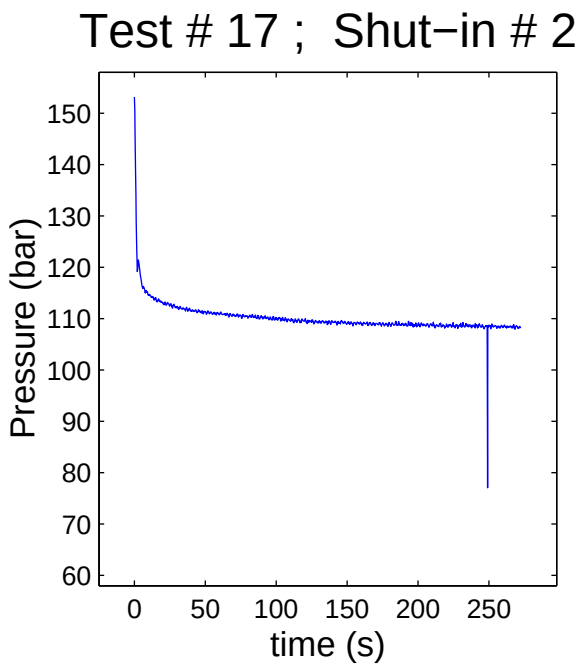
Test # 17 ; Shut−in # 2
Pressure (bar)
time (s)

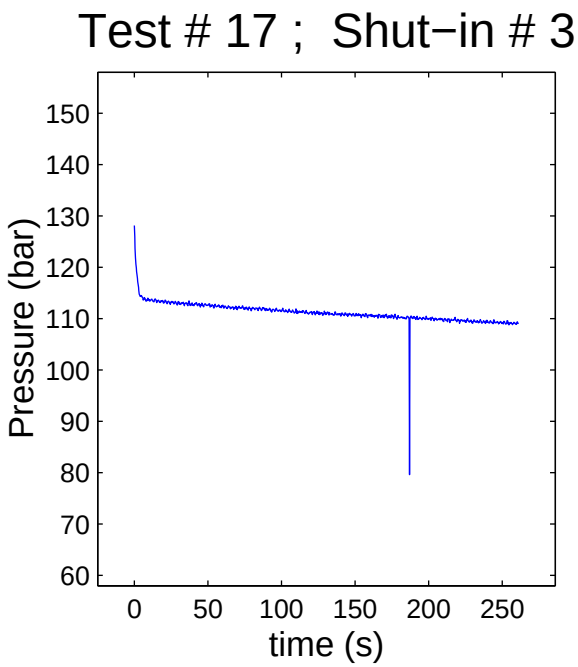
Test # 17 ; Shut−in # 3
Pressure (bar)
time (s)

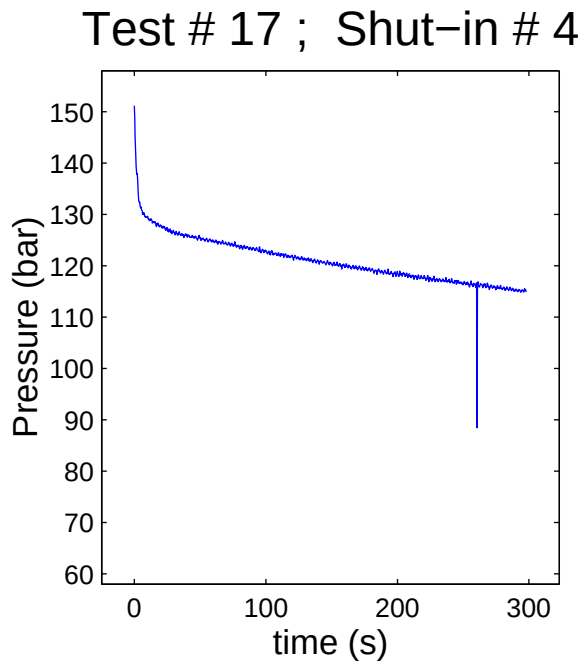
Test # 17 ; Shut−in # 4
Pressure (bar)
time (s)

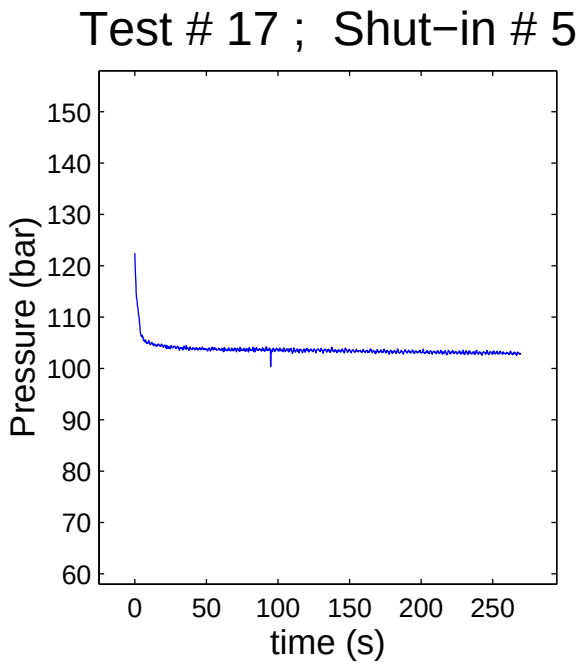
Test # 17 ; Shut−in # 5
Pressure (bar)
time (s)

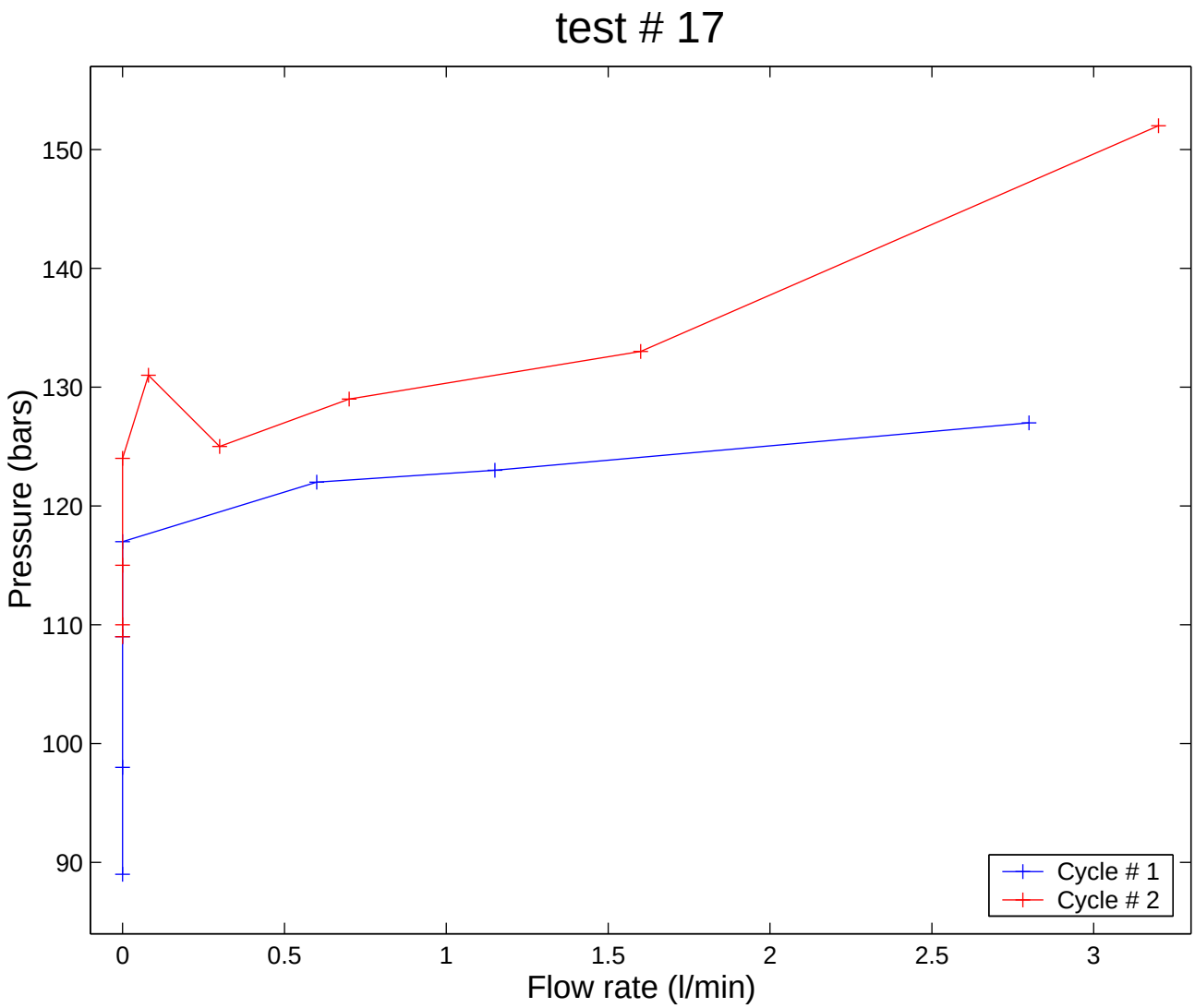
test # 17
Pressure (bars)
150
140
130
120
110
100
90
0
0.5
1
1.5
2
2.5
3
Flow rate (l/min)
Cycle # 1
Cycle # 2

KLX12A -- Post-frac Log # 17

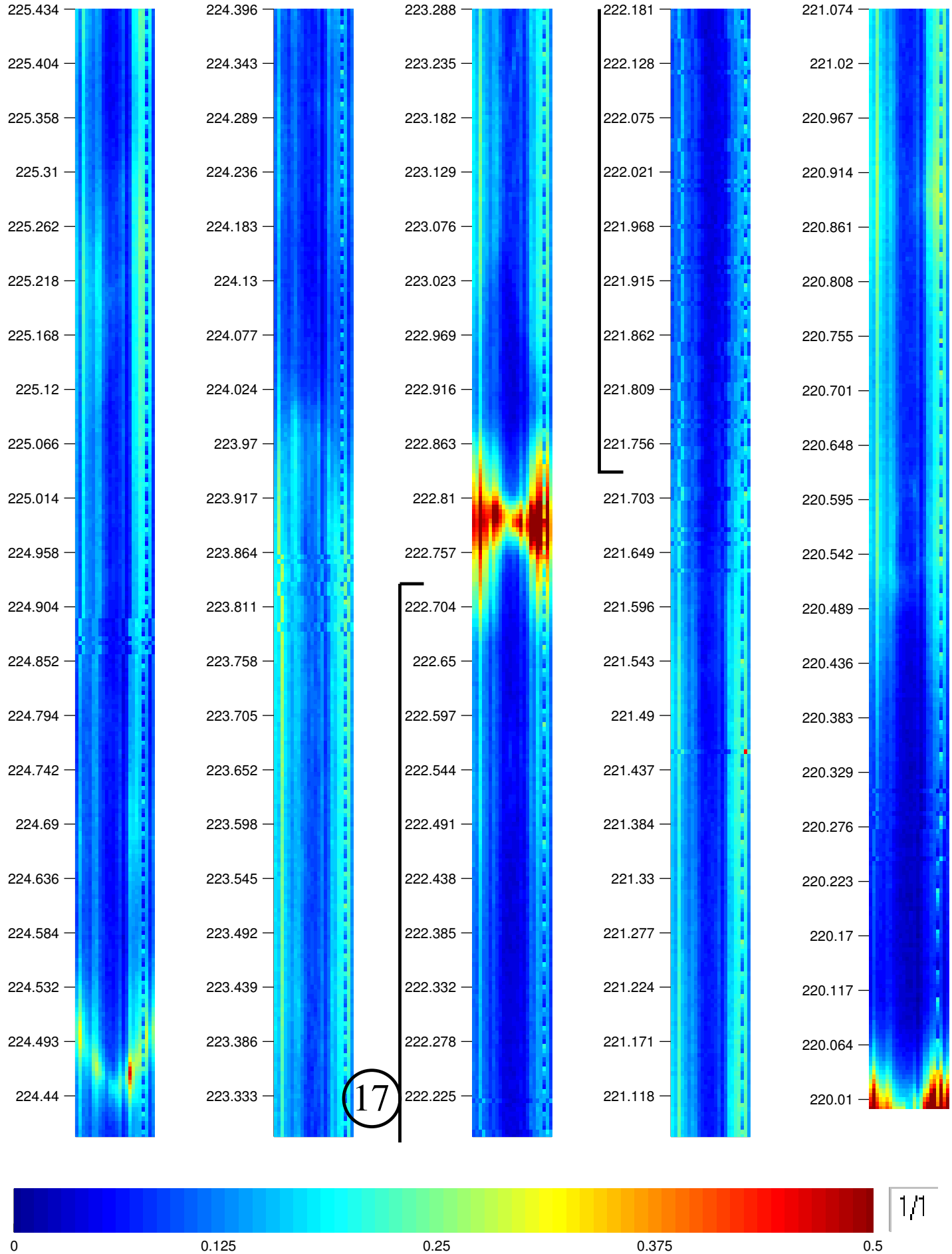

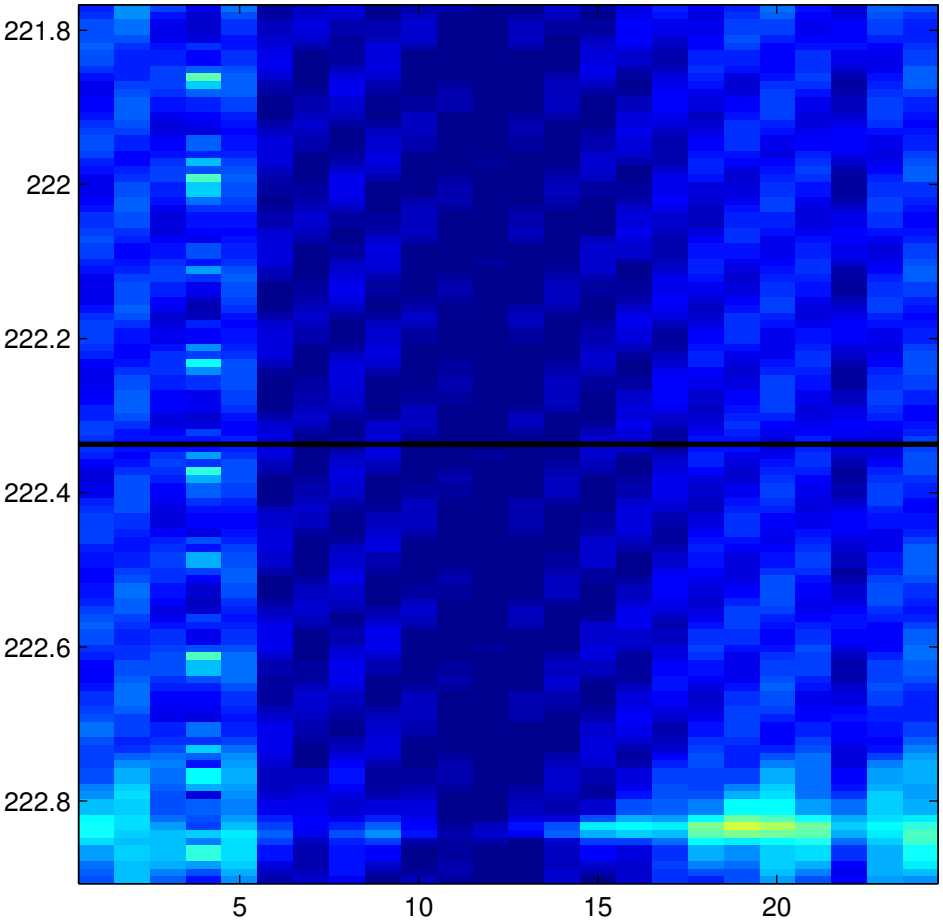

Repère du forage

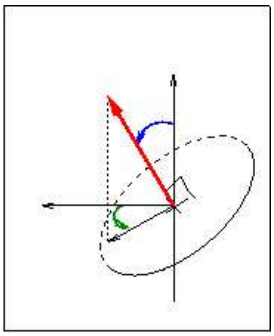

Repère absolu

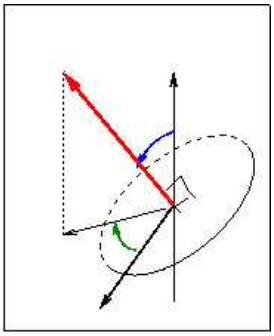

sinusoide visible

Diamètre 7.6 cm

Incidence ° Azimut °

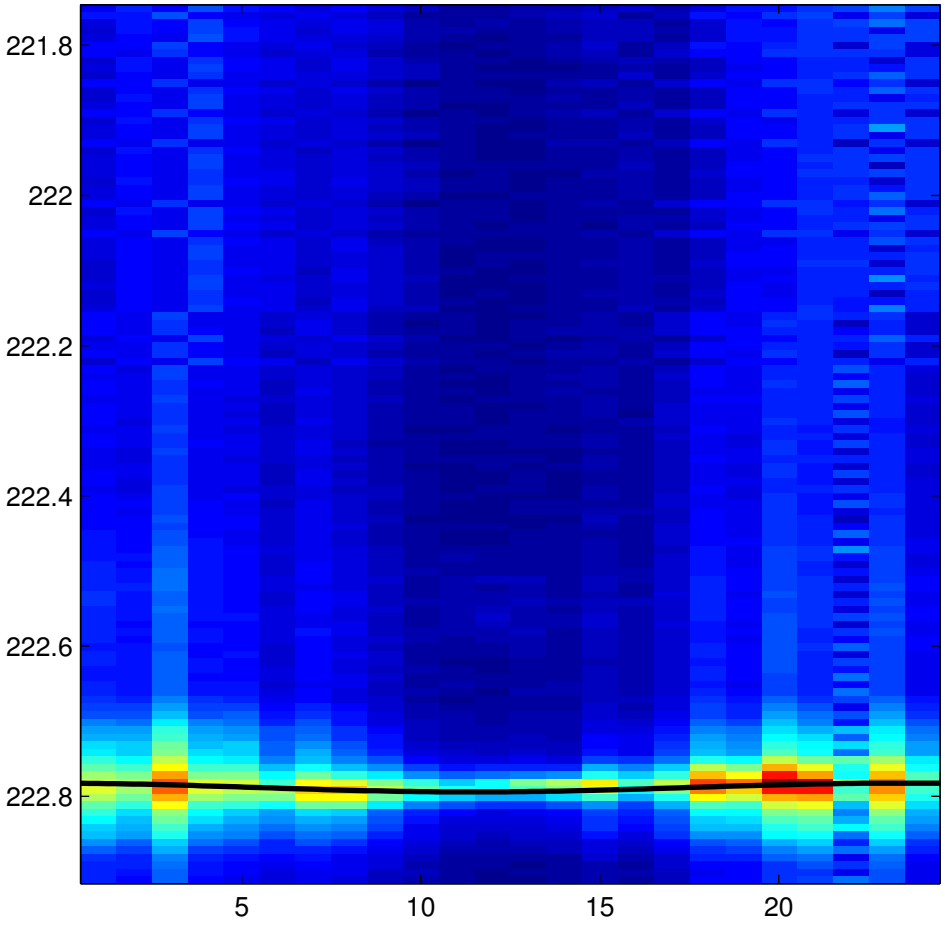

Repère du forage

345.6

8.7913

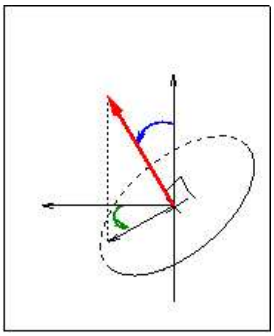

Repère absolu

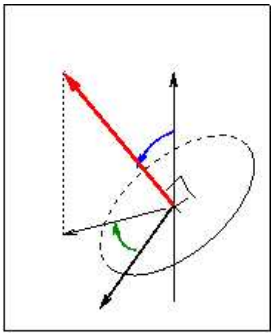

sinusoide visible

Diamètre 7.6 cm

Incidence ° Azimut °

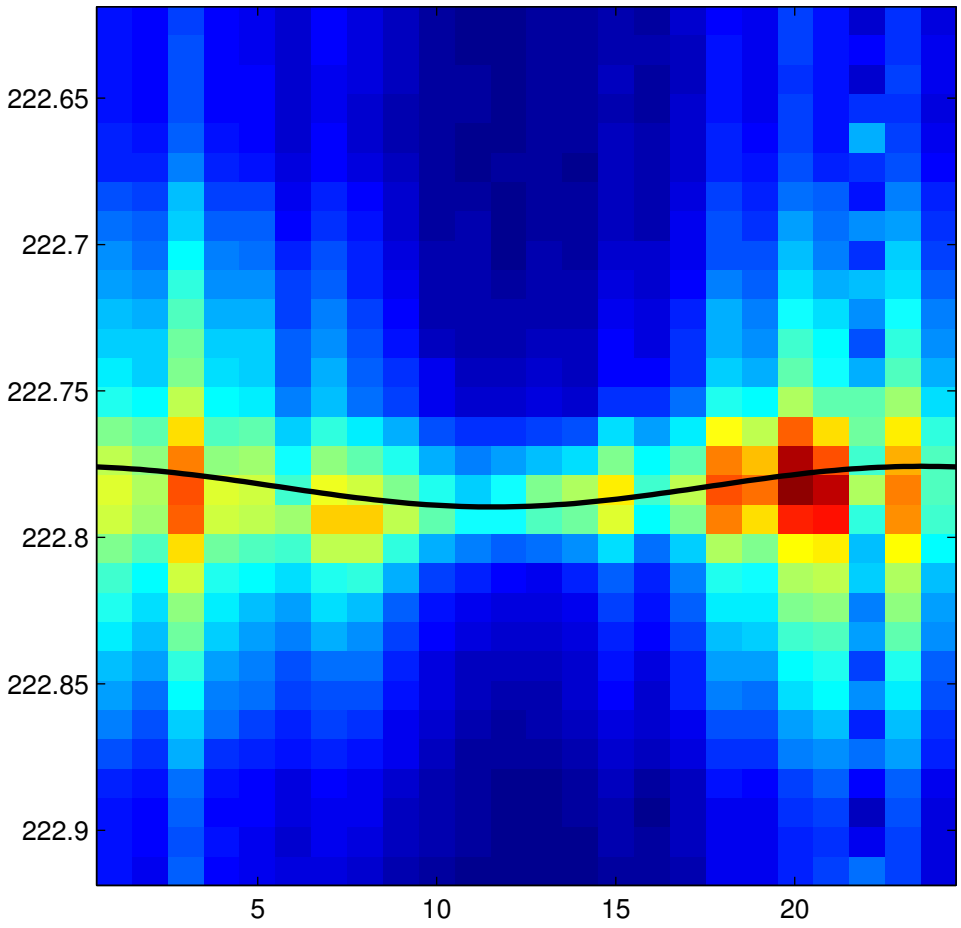

Repère du forage

345.6

10.3375

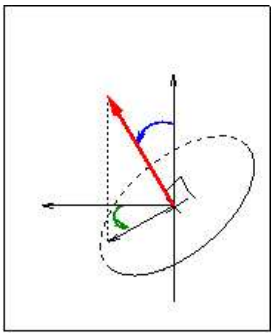

Repère absolu

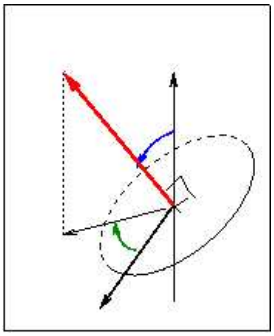

sinusoide visible

Diamètre 7.6 cm

Incidence ° Azimut °

APPENDIX 5

TEST RESULTS FOR BOREHOLE KLX12A

Bh length [m]	Depth [m]	Fract. [No.]	Azimuth, min [^{o}N]	Azimuth, max [^{o}N]	Azimuth, aver [^{o}N]	ε_{Azim} [^{o}]	Std_{Azim} [^{o}]	Dip, min [^{o}]	Dip, max [^{o}]	Dip, aver [^{o}]	ε_{Dip} [^{o}]	Std_{Dip} [^{o}]
590.1	547.0	1	218	243	230	13	6.5	80	91	85	6	3.0
579.4*	536.0	1	43	70	56	14	7.0	26	40	33	7	3.5
		2	271	350	311	40	20.0	5	19	12	7	3.5
		3	45	68	56	12	6.0	81	88	84	4	2.0
574.2*	531.0	1	56	92	74	18	9.0	19	32	25	7	3.5
572.0*	529.0	1	72	98	85	13	6.5	74	80	77	3	1.5
564.4	522.0	1	301	325	313	12	6.0	9	19	14	4	2.0
		2	59	85	72	13	6.5	77	84	80	4	2.0
536.0*	496.0	1	57	88	72	16	8.0	27	43	35	8	4.0
532.0*	491.0	1	80	118	99	19	9.5	25	39	32	7	3.5
		2	58	84	71	13	6.5	77	84	80	4	2.0
529.6*	488.0	1	63	102	82	20	10.0	22	35	28	6	3.0
491.2*	453.0	1	56	83	69	14	7.0	18	29	23	6	3.0
484.6*	446.0	1	291	327	309	18	9.0	19	29	24	5	2.5
		2	38	80	59	21	10.5	25	45	35	10	5.0
481.4*	443.0	1	289	306	298	9	4.5	58	68	63	5	2.5
472.9*	436.0	1	237	259	248	11	5.5	20	29	24	5	2.5
470.0*	433.0	1	31	46	38	7	3.5	75	82	78	3	1.5
		2	330	359	344	15	7.5	28	44	36	8	4.0
		3	272	288	280	8	4.0	43	53	48	5	2.5
451.0*	414.0	1	78	104	91	13	6.5	28	40	34	6	3.0

Bh length [m]	Depth [m]	Fract. [No.]	Azimuth, min [^{o}N]	Azimuth, max [^{o}N]	Azimuth, aver [^{o}N]	ε_{Azim} [^{o}]	Std_{Azim} [^{o}]	Dip, min [^{o}]	Dip, max [^{o}]	Dip, aver [^{o}]	ε_{Dip} [^{o}]	Std_{Dip} [^{o}]
438.1*	402.5	1	27	35	31	4	2.0	85	89	87	2	1.0
236.7	210.0	1	144	228	186	42	21.0	13	40	26	14	7.0
222.2	196.0	1	278	326	302	24	12.0	16	36	26	10	5.0

Note: Bh length and depth correspond to the center of the test section. For stress calculation, the columns containing the average azimuth and dip will be used together with their corresponding standard deviation. Stress data (columns 14 and 15) correspond to the interpretation that will be used for stress calculation. Unambiguous data are marked with "*" in the first column.

			Tangents			Aamodt		Hayashi					Stress data		
Bh length [m]	**Depth [m]**	**Cycle [No.]**	**σ_n, min [Bar]**	**σ_n, inter. [Bar]**	**σ_n, max [Bar]**	**σ_n, min [Bar]**	**σ_n, max [Bar]**	**σ_n, min [Bar]**	**σ_n, max [Bar]**	**Cum. vol. [l]**	**Q-S re-op. [Bar]**	**σ_n [Bar]**	**σ_n [Bar]**	**Std$_{\sigma n}$ [Bar]**	**$\sigma_{v,theory}$ [Bar]**
590.1	547.0	1	108.0	112.5	125.0	108.5	114.5	115.5	122.0	1.9		115.0	125	5.0	142.2
		2	120.5	124.0	132.5	123.5	126.5	125.0	133.0	2.5	135.0	127.0			
		3	98.0	100.5	145.5	98.0	101.5	119.0	140.0	4.8	145.0	114.0			
579.4*	536.0	1	140.5	142.4	154.5	141.5	144.0	143.0	151.5	0.5		145.0	157	1.7	139.4
		2	138.5	140.0	158.0	137.5	142.0	140.5	151.0	1.1		143.0			
		3	137.5	144.5	174.5	141.0	153.0	154.0	166.5	5.2		154.0			
		4	138.0	150.5	169.5	151.5	158.5	162.0	165.5	4.4		159.0			
		5	128.0	146.5	169.5	147.0	158.5	161.0	164.5	3.7		158.0			
574.2*	531.0	1	130.0	135.5	150.0	135.0	140.5	141.5	147.5	4.8		141.0	149	2.7	138.1
		2	139.5	146.5	157.0	150.0	155.0	151.0	154.0	11.5	153.0	152.0			
		3	143.0	148.0	159.5	143.5	157.0	154.5	157.0	11.9	150.0	153.0			
572.0*	529.0	1	149.0	151.0	161.0	150.0	151.5	153.5	161.0	1.6		154.0	151	1.3	137.5
		2	144.5	147.0	157.0	142.5	152.5	148.5	155.5	4.8	158.0	150.0			
		3	143.0	145.5	153.0	147.0	149.0	147.5	152.0	8.2	150.0	149.0			
564.4	522.0	1	129.5	138.5	154.0	142.0	146.5	148.5	150.5	1.7		147.0	147	2.3	135.7
		2	134.0	137.0	154.0	137.0	140.0	138.5	147.5	4.6		141.0			
		3	150.5	151.5	172.0	143.5	151.0	158.5	163.5	8.1		154.0			
536.0*	496.0	1	95.5	96.5	106.0	82.0	99.0	100.5	105.0	2.4		97.0	98	0.7	129.0
		2	91.0	95.0	102.5	96.5	98.5	97.0	101.0	9.3	104.0	98.0			
		3	94.0	96.0	101.0	96.5	98.5	98.0	100.5	13.3	98.0	98.0			

			Tangents			Aamodt		Hayashi					Stress data		
Bh length [m]	**Depth [m]**	**Cycle [No.]**	**σ_n, min [Bar]**	**σ_n, inter. [Bar]**	**σ_n, max [Bar]**	**σ_n, min [Bar]**	**σ_n, max [Bar]**	**σ_n, min [Bar]**	**σ_n, max [Bar]**	**Cum. vol. [l]**	**Q-S re-op. [Bar]**	**σ_n [Bar]**	**σ_n [Bar]**	**$Std_{\sigma n}$ [Bar]**	**$\sigma_{v,theory}$ [Bar]**
532.0*	491.0	1	87.0	96.0	117.0	96.5	105.5	104.5	108.0	2.3		104.0	104	0.7	127.7
		2	75.5	87.0	119.5	92.5	106.5	99.0	112.5	6.9	112.0	103.0			
		3	54.5	59.5	119.5	55.5	75.5	73.0	111.5	7.3	110.0	79.0			
529.6*	488.0	1	84.5	94.0	109.5	98.0	104.0	99.5	99.5	19.9		100.0	104	1.3	126.9
		2	98.0	102.5	111.0	101.5	105.0	110.0	110.0	38.4	100.0	107.0			
		3	98.0	101.0	110.0	102.0	106.0	107.0	108.5	18.4	100.0	106.0			
491.2*	453.0	1	82.5	88.0	110.0	87.5	93.0	94.5	103.5	1.4		95.0	93	1.3	117.8
		2	86.5	88.0	95.0	87.5	88.5	88.0	94.0	5.1		89.0			
		3	91.5	93.0	97.5	93.0	95.0	92.5	97.5	10.7		94.0			
		4	91.5	93.0	99.0	93.0	94.0	93.0	99.0	16.0		95.0			
484.6*	446.0	1	112.0	114.0	127.5	114.5	115.0	115.0	120.0	3.1		116.0	105	5.0	116.0
		2	107.5	108.5	118.0	108.5	109.0	109.0	113.0	4.4		110.0			
		3	86.5	87.0	97.5	86.0	87.5	87.0	94.5	15.4		89.0			
481.4*	443.0	1	127.0	128.0	134.0	128.5	129.0	128.0	130.5	13.9		129.0	138	3.3	115.2
		2	130.0	133.0	141.5	135.0	136.5	133.5	139.0	4.5		136.0			
		3	131.0	138.5	160.0	140.5	145.5	150.5	153.0	15.4		147.0			
		4	136.0	137.0	154.0	136.5	138.0	137.0	146.0	34.3	135.0	139.0			

			Tangents			Aamodt		Hayashi					Stress data		
Bh length [m]	**Depth [m]**	**Cycle [No.]**	**σ_n, min [Bar]**	**σ_n, inter. [Bar]**	**σ_n, max [Bar]**	**σ_n, min [Bar]**	**σ_n, max [Bar]**	**σ_n, min [Bar]**	**σ_n, max [Bar]**	**Cum. vol. [l]**	**Q-S re-op. [Bar]**	**σ_n [Bar]**	**σ_n [Bar]**	**$Std_{\sigma n}$ [Bar]**	**$\sigma_{v,theory}$ [Bar]**
472.9*	436.0	1	99.0	100.5	114.5	101.0	102.0	102.0	109.0	2.1		103.0	97	1.7	113.4
		2	111.5	112.5	134.5	113.0	116.0	117.5	124.5	5.7		118.0			
		3	89.5	90.5	112.5	90.0	91.0	93.5	103.5	5.1		94.0			
		4	89.5	93.5	108.0	93.0	99.5	101.5	106.5	5.4		100.0			
		5	89.5	93.5	104.0	95.5	98.5	96.5	103.0	10.4		98.0			
470.0*	433.0	1	124.5	126.5	141.0	127.5	129.0	127.5	134.5	10.4		130.0	109	1.0	112.6
		2	101.0	103.0	113.5	105.0	108.0	107.0	111.5	5.7		108.0			
		3	100.5	105.0	114.0	107.0	110.0	111.5	112.5	15.8	107.0	110.0			
451.0*	414.0	1	124.0	131.0	147.5	139.5	141.0	139.5	142.5	15.6		141.0	141	1.0	107.6
		2	135.0	140.5	162.5	144.0	149.0	151.0	155.5	40.5	153.0	150.0			
		3	145.0	150.0	173.5	151.5	156.5	157.5	164.5	20.4	153.0	157.0			
		4	133.0	136.5	152.5	137.5	140.0	139.0	143.5	5.6		140.0			
438.1*	402.5	1	119.5	124.5	137.5	124.5	129.5	127.0	136.5	13.2		129.0	127	1.0	104.7
		2	122.5	125.0	130.5	126.5	128.5	125.0	130.0	25.0	128.0	127.0			
		3	120.5	122.5	129.0	123.0	126.0	124.5	128.5	20.6	125.0	125.0			
236.7	210.0	Failed	test										-	-	54.6

			Tangents			Aamodt		Hayashi					Stress data		
Bh length [m]	**Depth [m]**	**Cycle [No.]**	**σ_n, min [Bar]**	**σ_n, inter. [Bar]**	**σ_n, max [Bar]**	**σ_n, min [Bar]**	**σ_n, max [Bar]**	**σ_n, min [Bar]**	**σ_n, max [Bar]**	**Cum. vol. [l]**	**Q-S re-op. [Bar]**	**σ_n [Bar]**	**σ_n [Bar]**	**$Std_{\sigma n}$ [Bar]**	**$\sigma_{v,theory}$ [Bar]**
222.2	196.0	1	66.5	67.5	88.5	67.5	68.5	72.5	79.0	1.0		72.0	115	3.3	51.0
		2	111.0	111.0	132.0	109.5	110.0	111.5	121.5	1.5		113.0			
		3	111.5	113.0	118.5	113.5	113.5	113.0	115.5	4.1	119.0	114.0			
		4	123.0	126.5	138.5	127.5	128.5	128.5	131.5	8.9	125.0	129.0			
		5	104.0	104.0	111.5	104.0	104.0	103.5	108.5	7.7		105.0			

Note: Bh length and depth correspond to the center of the test section. “Tangents” refers to analysis using the method of Enever and Chopra (1989); “Aamodt” refers to analysis using the method of Aamodt and Kuriyagawa (1981); and “Hayashi” refers to analysis using the method of Hayashi and Haimson (1991). Unambiguous data are marked with “*” in the first column.

APPENDIX 6

COMPARISON BETWEEN THE HTPF TOOL AND BOREMAP IN BOREHOLE KLX12A

				HTPF tool				BOREMAP	
Bh length [m]	**Depth [m]**	**Fract. [No.]**	**Test type**	**Azimuth [°N]**	**Std_{Azim} [°]**	**Dip [°]**	**Std_{Dip} [°]**	**Azimuth [°N]**	**Dip [°]**
590.1	547.0	1	HTPF	230^{pe}	6.5^{pe}	85^{pe}	3.0^{pe}	**226**	**86**
579.4	536.0	1	HF	56$^{pe?}$	7.0	33	3.5	18?	33?
		2		311^{pe}	20.0^{pe}	12^{pe}	3.5^{pe}	310	15
		3		56^{i}	6.0^{i}	84^{i}	2.0^{i}		
574.2	531.0	1	HTPF	74^{pe}	9.0^{pe}	25^{pe}	3.5^{pe}	**54**	**32**
572.0	529.0	1	HF	85^{i}	6.5^{i}	77^{i}	1.5^{i}	**-**	**-**
564.4	522.0	1	HF	313^{pe}	6.0^{pe}	14^{pe}	2.0^{pe}	315	21
		2		72^{i}	6.5^{i}	80^{i}	2.0^{i}		
536.0	496.0	1	HTPF	72^{pe}	8.0^{pe}	35^{pe}	4.0^{pe}	**65**	**40**
532.0	491.0	1	HTPF	99^{pe}	9.5^{pe}	32^{pe}	3.5^{pe}	**93**	**34**
		2		71^{i}	6.5^{i}	80^{i}	2.0^{i}		
529.6	488.0	1	HTPF	82^{pe}	10.0^{pe}	28^{pe}	3.0^{pe}	**92**	**36**
491.2	453.0	1	HF	69^{i}	7.0^{i}	23^{i}	3.0^{i}	**-**	**-**
484.6	446.0	1	HTPF	309^{pe}	9.0^{pe}	24^{pe}	2.5^{pe}	**290**	**24**
		2		59^{i}	10.5^{i}	35^{i}	5.0^{i}		
481.4	443.0	1	HTPF	298^{pe}	4.5^{pe}	63^{pe}	2.5^{pe}	**39**	**61**
472.9	436.0	1	HF	248^{i}	5.5^{i}	24^{i}	2.5^{i}	**-**	**-**
470.0	433.0	1	HTPF	38^{pe}	3.5^{pe}	78^{pe}	1.5^{pe}	**56**	**77**
		2		344$^{pe?}$	7.5$^{pe?}$	36$^{pe?}$	4.0$^{pe?}$	339	32
		3		280^{i}	4.0^{i}	48^{i}	2.5^{i}		
451.0	414.0	1	HTPF	91^{pe}	6.5^{pe}	34^{pe}	3.0^{pe}	**93**	**43**

				HTPF tool				BOREMAP	
Bh length [m]	**Depth [m]**	**Fract. [No.]**	**Test type**	**Azimuth [^{o}N]**	**Std$_{Azim}$ [^{o}]**	**Dip [^{o}]**	**Std$_{Dip}$ [^{o}]**	**Azimuth [^{o}N]**	**Dip [^{o}]**
438.1	402.5	1	HTPF	31^{pe}	2.0^{pe}	87^{pe}	1.0^{pe}	**27**	**87**
236.7	210.0	1	HF	186^{i}	21.0^{i}	26^{i}	7.0^{i}	-	-
222.2	196.0	1	HF	302^{pe}	12.0^{pe}	26^{pe}	5.0^{pe}	293	23

Note: Bh length and depth correspond to the center of the test section. “pe” and “i” denote pre-existing and induced fracture, respectively. The fracture intended for testing is marked with bold font in the BOREMAP columns, whereas other pre-existing fractures have normal font. “?” indicates doubtful match. For stress calculation, the columns containing the average azimuth and dip will be used together with their corresponding standard deviation. The HTPF orientations are based on Maxibor well deviation data, whereas the BOREMAP system is based on Flexit well deviation data.

APPENDIX 7

ANALYSIS OF THE EFFECT OF ERRORS IN WELL ORIENTATION

ANALYSIS FOR THE EFFECT OF ERRORS ON FRACTURE ORIENTATION DETERMINATION

Introduction

In the results, all fracture orientation data that will be used for stress calculation is based on borehole deviation measurements of the Maxibor method. After this study was initiated, a decision was taken to up-date SKB´s deviation measurements, entailing that for many boreholes Maxibor measurement will be exchanged to Flexit measurements as the official deviation measurement files in SKB´s database Sicada. In this note, we investigate the consequences on interpreted fracture orientation data when based on the Flexit instead of Maxibor method. The problem is below formulated as influence of errors in the Maxibor data on calculated fracture orientations, where the error is defined as the difference in borehole azimuth and dip between the Flexit and Maxibor data.

Definitions and theory

Let $\hat{I}_i$ be the geographical frame of reference (i = 1 is North, i = 2 is East, and i = 3 is vertical and positive downwards). Let $\hat{I}'_j$ be the frame of reference associated with the borehole (j = 1 is normal to the borehole axis directed toward the Top Of Hole (TOH), j = 2 is horizontal and normal to the borehole axis, and j = 3 is along the borehole axis, positive downwards). The Mosnier tool provides the orientation of fractures in the borehole frame of reference, $\hat{I}'_j$, and all images are oriented with respect to TOH. The azimuth, φ, and inclination, ψ, (angle with respect to vertical direction) of the borehole axis are used to determine the fracture orientation in the geographical frame of reference. Let n be the normal (unit vector) to a fracture plane:

$$n = n_i \hat{I}_i = n'_j \hat{I}'_j = n'_j \left(Q_{jk} \hat{I}_k \right) = \left(Q_{kj}^T n'_j \right) \hat{I}_k \tag{1}$$

where i, j, and k = 1, 2, and 3, and Q_{jk} are the components of $\hat{I}'_j$ in the geographical frame of reference. The components of $\hat{I}'_j$ are :

$$\hat{I}'_1 : \cos\psi \cos\varphi; \cos\psi \sin\varphi; -\sin\psi \tag{2}$$

$$\hat{I}'_2 : -\sin\varphi; \cos\varphi; 0 \tag{3}$$

$$\hat{I}'_3 : \sin\psi \cos\varphi; \sin\psi \sin\varphi; \cos\psi \tag{4}$$

Equations (1) through (4) provide means to evaluate the components of the normal to the fracture plane in the geographical frame of reference.

Errors on the components of the normal n in the geographical frame of reference, as a function of errors on azimuth and incidence of borehole axis, are given by:

$$dn_i = \frac{\partial n_i}{\partial \psi} d\psi + \frac{\partial n_i}{\partial \varphi} d\varphi ; i = 1,2,3 \tag{5}$$

where $d\varphi$ and $d\psi$ are errors on the azimuth and incidence of borehole axis, respectively. Equations (1) through (5) provide means to calculate the influence of errors on borehole geometry on the determination of the fracture dip and azimuth as characterized by the normal

n to the fracture plane, expressed in the geographical frame of reference. This leads to the following equations:

$$dn_1 = \left(-n_1^{'}\sin\psi\cos\varphi + n_3^{'}\cos\psi\cos\varphi\right)d\psi - \left(n_1^{'}\cos\psi\sin\varphi + n_2^{'}\cos\varphi + n_3^{'}\sin\psi\sin\varphi\right)d\varphi \quad (6)$$

$$dn_2 = \left(-n_1^{'}\sin\psi\sin\varphi + n_3^{'}\cos\psi\sin\varphi\right)d\psi + \left(n_1^{'}\cos\psi\cos\varphi - n_2^{'}\sin\varphi + n_3^{'}\sin\psi\cos\varphi\right)d\varphi \quad (7)$$

$$dn_3 = -\left(n_1^{'}\cos\psi + n_3^{'}\sin\psi\right)d\psi \quad (8)$$

Observed differences between the Maxibor and Flexit methods and analysis of effect of errors on borehole inclination

From the locations where tests have been conducted, the most critical zone concerns Tests 10 and 11 around 445 m vertical depth, i.e. 484 m borehole length. At this depth, the error on borehole inclination reaches 4.5 ° and errors on azimuth are of the order of 1°. For all other test locations, the errors are smaller.

For Tests 10 and 11, the uncertainty on fracture orientation determination from the HTPF tool ranges between 5 and 10°, while those on azimuth range between 9 to 21 °. Clearly errors on fracture orientation because of errors on borehole orientation are not significant. However, we pursue the analysis to check the influence of this error on normal stress magnitude. Indeed, it may be recalled that the normal stress is given by:

$$\sigma_n = n_1^2\sigma_{11} + n_2^2\sigma_{22} + n_3^2\sigma_{33} + 2n_1n_2\sigma_{12} + 2n_2n_3\sigma_{23} + 2n_3n_1\sigma_{31} \quad (6)$$

where n_1, n_2 and n_3 are the director cosines for the normal to the fracture plane.

Influence of errors on director cosines of normal to the fracture plane on the normal stress is given by:

$$d\sigma_n = \frac{\partial\sigma_n}{\partial n_1}dn_1 + \frac{\partial\sigma_n}{\partial n_2}dn_2 + \frac{\partial\sigma_n}{\partial n_3}dn_3 \quad (7)$$

From Eq. (7), we conclude that the resulting error is given by:

$$d\sigma_n = 2\left[\begin{matrix}\left(n_1\sigma_{11} + n_2\sigma_{12} + n_3\sigma_{13}\right)dn_1 + \left(n_1\sigma_{21} + n_2\sigma_{22} + n_3\sigma_{23}\right)dn_2 + \\ \left(n_1\sigma_{31} + n_2\sigma_{32} + n_3\sigma_{33}\right)dn_3\end{matrix}\right] \quad (8)$$

This shows that if the errors on the director cosines are 2 or 3 percents, the maximum error to be expected on the normal stress is smaller than 10%. This will have negligible effects on the stress determination. Indeed, it is generally considered that only errors larger than 10° on fracture orientations are worth being corrected.